

# **Ion Effects on Stability of Carbon Nanotubes Dispersions and Complex Formation in Polar Solvents**



Anastasia Romanova

Department of Physics; Scottish Universities Physics Alliance

A thesis presented in partial fulfilment of the requirements for the degree of

*Doctor of Philosophy*

2014

This thesis is the result of the author's original research. It has been composed by the author and has not been previously submitted for examination which has led to award of a degree.

The copyright of this thesis belongs to the author under the terms of the United Kingdom Copyright Acts as qualified by University of Strathclyde Regulation 3.50. Due acknowledgement must always be made of the use of any material contained in, or derived from this thesis.

Signed:

Date:

---

## 0.1 Abstract

The focus of this work is the effects of ions on solute association processes in solution: complex formations of aromatic carboxylic acids with  $\alpha$ -cyclodextrin and bundle formation of carbon nanotubes in their N-methylpyrrolidone based dispersions.

The work has two distinct parts: cation effects and anion effects. In one part we explain experimentally observed difference between effects of sodium and potassium cations on interactions of aromatic carboxylic acids with  $\alpha$ -cyclodextrin. To explain this difference, we propose a molecular mechanism, which we call "competition for the guest". According to this mechanism sodium ions interact with carboxylic group of aromatic carboxylic acid, which prevents the acid from the formation of a complex with cyclodextrin.

Another manifestation of ion effects explored in this work is the impact of ions on the behaviour of benzoic acid at water/vapour interface. As a consequence of ion induced changes in hydration pattern, the molecule changes its orientation at the interface as well as its affinity to the interface. The results of the molecular dynamics simulations are compared to surface sensitive technique of X-ray photoemission spectroscopy.

Another part of the work studies ion effects on the stability of carbon nanotube dispersions in N-methylpyrrolidone. By evidence of spectroscopy and transmission electron microscopy, it was found that inorganic ions significantly reduce stability of carbon nanotubes dispersions in N-methylpyrrolidone. Comparing the results to molecular dynamics simulations it was suggested that the reduction of stability takes place due to the formation of ion depletion areas around carbon nanotubes. These ion depletion areas increase the free energy of the interface between the tube and the salty N-methylpyrrolidone, forcing the carbon nanotubes to associate with each other, forming bundles and larger aggregates.

Overall, this work is devoted to study of ion effects in aqueous and non-aqueous liquid media, using a combination of experimental and computational tools. Here we deepen the understanding of ion effects as a subtle balance of several pairwise interactions, which take place in liquid media containing both solutes and salts.

## 0.2 Acknowledgements

I wish to acknowledge the help provided by the many people who made this thesis possible.

First I would like to acknowledge the support and help of my supervisor, Dr. Maxim V. Fedorov, Professor of Physics and Life Sciences, PhD, DSc, Priv.-Doz. His wide knowledge, logical way of thinking, and patience have been of great value for me.

I would like to thank many teachers from the Ivanovo State University of Chemistry and Technology and the Institute of Solution Chemistry of the Russian Academy of Science Prof. Dr. Yuriy V. Chistyakov, Prof. Dr. Olga V. Lefedova, Dr. Alexander V. Burov, Prof. Dr. Georgiy V. Girichev, Prof. Dr. Alexander I. Maksimov, Prof. Dr. Michael V. Ulitin, Prof. Dr. Elena V. Antina, Dr. Elena L. Gavrilova, Dr. Vladimir B. Sheinin, and others for their deeply interesting lectures in fields of general chemistry, computational chemistry, mathematics, physics, physical chemistry, biochemistry, supramolecular chemistry, etc.

I am indebted to my colleagues Dr. Vladislav Ivanistsev, Dr. Kathleen and Dr. Tom Kirchner, Dr. Nicolaj Georgi, Dr. Ekaterina Ratkova, Dr. Andrey Frolov, Dr. Volodymyr Sergiievskyi, and Roman Saburdjajew for supporting me.

My sincere thanks are due to the official referees, Professor Milo Shaffer, PhD, and Kevin O'Donnell, Professor of Semiconductor Spectroscopy, PhD, for their detailed review, constructive criticism and excellent advice during the preparation of this thesis.

I am very grateful to the Guest Support Service of Max Planck Institute for Mathematics in the Sciences for providing me with an environment where I can do my research without spending much time on practical everyday matters associated with my living in Leipzig (accommodation, visas, etc). I am particularly thankful to our Guest Program Manager, Ms. Heike Rackwitz, who made my movement to the Institute very smooth and well organized. At the beginning of my stay in Leipzig I lived in the comfortable guest house with all necessary facilities (kitchen, furniture, laundry, etc.). I am very grateful to all our secretaries and members of our Library Group (led by Mr. Ingo Brüggemann) and Computer Group (led by Mr. Rainer Kleinrensing) for their daily work to organize our living and working in the Institute: Ms. Heike Rackwitz, Ms. Valeria Hünninger, Ms. Theresa Petsch, Ms. Elke Herrmann, Ms. Katrin Scholz, Ms. Saskia Gutzschebauch, Ms. Gertraude Torkler, Ms. Jana Gregor, Ms. Antje Vandenberg, Ms. Johanna Göpfert, and Ms. Katarzyna Baier. I really appreciate this support as it allows me to fully concentrate on my scientific problems without spending much time on the organization of everyday life.

I would also like to thank secretaries in the University of Strathclyde, who helped us with

the challenging move from Leipzig to Glasgow: Ms. Annette Sinclair, Ms. Lauren Angus, Mr. Timothy Briggs, Ms. Catherine Cheshire, Ms. Lynn Gilmour, Ms. Kayleigh Macaskill, and Ms. Kirsten Munro.

I am deeply thankful to technical staff at the University of Strathclyde, who made a lot of research tasks possible: Mr. John Broadfoot, Mr. David Clark, Mr. Ged Drinkwater, Mr. Ken Gibson, Mr. Andrew Hughes, Mr. Mark Hutcheon, Mr. John Revie, and Mr. Ronnie Weston.

We are grateful for use of the Desmond Molecular Dynamics System, version 2.2, D. E. Shaw Research, New York, NY, 2009, Maestro-Desmond Interoperability Tools, version 2.2, Schrodinger, New York, NY, 2009. Maestro, version 308 9.1, Schrodinger, LLC, New York, NY, 2010. Jaguar, version 309 7.7, Schrodinger, LLC, New York, NY, 2010.

I acknowledge the supercomputing support from the John von Neumann-Institut für Computing (NIC), Juelich Supercomputing Centre (JSC), Forschungszentrum Juelich GmbH, Germany. Project ID: HLZ18. We acknowledge financial support of the HPC-EUROPA2 project (project number: 228398) with the support of the European Commission - Capacities Area - Research Infrastructures. This work was partially supported by Deutsche Forschungsgemeinschaft (DFG) - German Research Foundation, Research Grant FE 1156/2-1 and REA - Research Executive Agency, Grant No. 247500 "BioSol", Programme: FP7-PEOPLE-2009-IRSES. Results were partially obtained using the EPSRC funded ARCHIE-WeSt High Performance Computer ([www.archie-west.ac.uk](http://www.archie-west.ac.uk)). EPSRC grant no. EP/K000586/1. I would like to acknowledge the use of the Chemical Database Service at Daresbury. I am grateful to the Graduate School of Excellence BuildMoNa (funded by the Deutsche Forschungsgemeinschaft) for partial financial support. I would like to thank Scottish Universities Physics Alliance (SUPA) for partial support of this work.

Research carried out in part at the Center for Functional Nanomaterials, Brookhaven National Laboratory, which is supported by the U.S. Department of Energy, Office of Basic Energy Sciences, under Contract No. DE-AC02-98CH10886. I would also like to thank support of the team on the Center for Functional Nanomaterials (CFN) at Brookhaven National Laboratory and especially Dr. Eric Stach, Electron Microscopy Group Leader; Kim Kisslinger, a senior TEM technical staff member; Grace Webster, User Administration and Outreach for their support and guidance.

I owe my deep gratitude to my colleagues for sharing their research and ideas with me and writing common papers: Dr. Irina V. Terekhova who led our collaboration with Institute of Solution Chemistry of the Russian Academy of Sciences (ISC RAS) and other people from the ISC RAS team (Dr. Roman Kumeev, Ekaterina Chibunova); Niklas Ottosson and his colleagues

( J. Söderström, O. Björneholm, G. Öhrwall) who made a joint paper "Molecular Sinkers: X-ray Photoemission and Atomistic Simulations of Benzoic Acid and Benzoate at the Aqueous Solution/Vapor Interface" possible; group of Dr. Alexey Rozhin (Raz N. Arif and Martin Kolar) for my introduction to the field of carbon nanotubes, and Dr. Andrey Frolov for sharing his simulations results on ion interactions with carbon nanotubes in NMP.

# Contents

0.1	Abstract . . . . .	ii
0.2	Acknowledgements . . . . .	iii
	<b>List of Figures</b>	<b>ix</b>
	<b>List of Tables</b>	<b>xi</b>
<b>1</b>	<b>Introduction</b>	<b>1</b>
1.1	Motivations . . . . .	1
1.2	Objectives . . . . .	2
1.3	Ion effects and solvation interfaces . . . . .	4
1.4	Studied systems . . . . .	6
1.4.1	Aromatic carboxylic acids. Benzoic acid . . . . .	6
1.4.2	Cyclodextrins . . . . .	8
1.4.3	Carbon nanotubes . . . . .	11
<b>2</b>	<b>Physical-chemical processes at solvation interfaces</b>	<b>15</b>
2.1	Hydration of simple inorganic ions . . . . .	15
2.1.1	Energetic balance of hydration . . . . .	15
2.1.2	Properties of dynamic equilibrium . . . . .	21
2.2	Hydration of polyatomic species . . . . .	22
2.3	Hydrates and solvates . . . . .	24
2.4	Effects of ions on complex formation of cyclodextrins . . . . .	25
2.4.1	Non-specific effects of ionic strength. . . . .	25
2.4.2	Specific cyclodextrin-ion interactions. Competition for the cyclodextrin cavity. . . . .	26
2.5	Solvation in N-methylpyrrolidone . . . . .	27
2.5.1	Solvation of ions in NMP . . . . .	27

2.5.2	NMP based dispersions of carbon nanotubes . . . . .	29
2.6	Solvation. Solutions and dispersions . . . . .	29
2.7	Chapter conclusions . . . . .	30
<b>3</b>	<b>Experimental methods</b>	<b>32</b>
3.1	Molecular dynamics simulations . . . . .	32
3.1.1	Preparation of a simulation cell . . . . .	34
3.1.2	Solvent models. Explicit and implicit models . . . . .	35
3.1.3	Calculation of forces and Force Fields . . . . .	36
3.1.4	System control . . . . .	39
3.1.5	Software . . . . .	44
3.1.6	Trajectory analysis . . . . .	45
3.2	Determination of stability constants of $\alpha$ -cyclodextrin with aromatic carboxylic acids . . . . .	51
3.2.1	Nuclear magnetic resonance . . . . .	51
3.2.2	Calorimetry . . . . .	56
3.3	Determination of molecular orientation at water/vapour interface . . . . .	58
3.4	Optical absorption spectroscopy of carbon nanotubes . . . . .	61
3.5	Photoluminescence of carbon nanotubes . . . . .	68
3.6	Transmission Electron Microscopy . . . . .	69
<b>4</b>	<b>Cation interactions with carboxylic group</b>	<b>73</b>
4.1	Ion pairing between carboxylate group and sodium and potassium ions . . . . .	73
4.1.1	Simulation details . . . . .	74
4.1.2	Results and analysis . . . . .	75
4.1.3	$\text{Na}^+/\text{K}^+$ specific effects on complex formation. Competition for the guest	78
4.2	Effects of ions and pH on benzoic acid behaviour at water/vapour interface . . . . .	86
4.2.1	Simulation details . . . . .	88
4.2.2	Effects of pH on benzoic acid behaviour at water/vapour interface . . . . .	96
4.2.3	Comparison of $\text{Na}^+$ and $\text{K}^+$ effects on surface affinity of benzoate . . . . .	101
4.3	Chapter conclusions . . . . .	103
<b>5</b>	<b>Effects of ions on stability of carbon nanotubes dispersion</b>	<b>105</b>
5.1	Carbon nanotubes in ternary systems . . . . .	105
5.2	Effects of aqueous impurities on carbon nanotubes dispersion stability . . . . .	108



---

5.2.1	Spectrophotometric titration . . . . .	109
5.2.2	Transmission electron microscopy . . . . .	112
5.3	Effects of iodide and bromide . . . . .	113
5.3.1	Spectrophotometric titration and photoluminescence control . . . . .	113
5.3.2	Transmission electron microscopy . . . . .	121
5.4	Chapter conclusions . . . . .	129
<b>6</b>	<b>Conclusions</b>	<b>131</b>
<b>7</b>	<b>Future work</b>	<b>133</b>
<b>8</b>	<b>Bibliography</b>	<b>135</b>
<b>A</b>	<b>Experimental details</b>	<b>157</b>
A.1	Force field parameters . . . . .	157
A.2	Equipment characteristics . . . . .	160
<b>B</b>	<b>Example of a spectrum correction</b>	<b>161</b>
<b>C</b>	<b>List of Peer-Reviewed Journal Papers</b>	<b>167</b>
<b>D</b>	<b>Contributions to the work</b>	<b>168</b>
	<b>Glossary</b>	<b>170</b>

# List of Figures

1.1	Schematic representation of interactions in ternary systems . . . . .	5
1.2	Structure of benzoic acid . . . . .	6
1.3	Structure of $\alpha$ -cyclodextrin . . . . .	9
1.4	Carbon nanotubes chiralities definition . . . . .	12
1.5	Structure of N-methylpyrrolidone. . . . .	14
2.1	Collins volcano. Criteria of direct ion pair formation in a solution . . . . .	19
2.2	Energetic criteria of ion classification into kosmotropes and chaotropes . . . . .	20
2.3	Hydration shells of a complex ion . . . . .	24
2.4	Solvation of ions in NMP . . . . .	28
3.1	Representation of inter- and intramolecular interactions . . . . .	37
3.2	A typical bulk simulation cell . . . . .	42
3.3	A typical simulation cell with a slab geometry . . . . .	43
3.4	Definitions of hydration shells from $g(r)$ . . . . .	47
3.5	Partial $^1\text{H}$ NMR spectra of $\alpha$ -CD-ACA systems . . . . .	54
3.6	C1s photoelectron spectra of BAH/BA $^-$ . . . . .	59
3.7	Origin of the CNT chirality-specific spectra . . . . .	64
3.8	Typical UV-Vis-NIR spectrum of CNTs . . . . .	65
3.9	Example of soot induced background absorption in the carbon nanotube spectrum	66
3.10	Example of a spectral congestion . . . . .	67
4.1	Water and ions distributions near the carboxylate group of benzoate . . . . .	76
4.2	Water and ions distributions near the carboxylic group of nicotinic acid . . . . .	77
4.3	Scheme of equilibriums in the system ACA- $\alpha$ -CD-K $^+$ . . . . .	80
4.4	Scheme of equilibriums in the system ACA- $\alpha$ -CD-Na $^+$ . . . . .	81
4.5	Hydration strength effects on the complex formation . . . . .	85

4.6	Simulation cell for simulations of benzoic acid/benzoates at the water/vapour interface . . . . .	89
4.7	Definitions of angles used for characterisation of surface orientation of benzoic acid . . . . .	90
4.8	Free energy profile of benzoic acid along water slab . . . . .	93
4.9	Benzoic acid orientation under concentration limit . . . . .	95
4.10	BAH and BANa surface density changes during equilibration . . . . .	96
4.11	BAH/BA <sup>-</sup> behavior at the water-vapour interface . . . . .	98
4.12	Pictorial representation of hydrophobic/hydrophilic areas of BAH/BA <sup>-</sup> . . . . .	100
4.13	Angle distribution of BAK at the surface layer . . . . .	102
4.14	Density profiles of BANa and BAK . . . . .	103
5.1	Spectrophotometric titration of NMP based dispersions of carbon nanotubes with water . . . . .	110
5.2	Characteristic transmission electron microscopy images of CNT-NMP dispersion with water content in the dispersion 4% <sub>wt</sub> . . . . .	113
5.3	Spectrophotometric titration of CNT-NMP dispersion with NaBr . . . . .	115
5.4	Spectrophotometric titration of CNT-NMP dispersion with NaI . . . . .	116
5.5	Photoluminescence evidence of CNT bundle formation in the presence of NaI . . . . .	118
5.6	Pictorial representation of ion depletion from CNT surface . . . . .	120
5.7	TEM image of a typical structure formed by NaBr . . . . .	122
5.8	TEM images of typical structures formed by NaI . . . . .	123
5.9	TEM image of typical structures observed in reference CNT-NMP dispersion . . . . .	125
5.10	TEM micrographs of CNT-NMP dispersion after addition of 0.1 mM of NaBr . . . . .	126
5.11	TEM micrographs of CNT-NMP dispersion after addition of 0.1 mM of NaI . . . . .	126
5.12	Pictorial representation of CNT crystallosolvates . . . . .	128
B.1	Original and zero-corrected spectrum of pure NMP . . . . .	163
B.2	Uncorrected spectrum of pure CNT-NMP dispersion . . . . .	164
B.3	Corrected spectrum of CNTs in CNT-NMP dispersion . . . . .	165
B.4	Example of linear baseline subtraction (energy domain) . . . . .	166

# List of Tables

2.1	Solubility of benzoic acid and benzoates in different solvents . . . . .	23
3.1	Representation of a molecular structure in molecular dynamics . . . . .	35
3.2	Stability constants of $\alpha$ -CD complexes with benzoate and nicotinic acid obtained from $^1\text{H}$ NMR . . . . .	53
3.3	Thermodynamic characteristics of complex formation of $\alpha$ -CD with nicotinic acid in water and in aqueous solutions of NaCl and KCl . . . . .	58
4.1	Hydration energies of ACAs in different ionization state . . . . .	84
4.2	Concentration ratios of benzoic acid in different phases . . . . .	94
5.1	Semi-quantitative analysis of characteristics of CNT bundles obtained with TEM	127
A.1	Force field parameters for pH-orientational dependency . . . . .	158
A.2	Force field parameters for CD-ACA simulations . . . . .	158
A.3	JEOL JEM 1400 characteristics . . . . .	160

# 1

## Introduction

### 1.1 Motivations

Solutions and solvents make important parts in many industrial and laboratory practices. Solvents and co-solvents may help control many processes, including processes of association, e.g. complex formation, surface segregation and bundle formation. Unfortunately, understanding of the mechanisms of solvent-solute interactions is far from complete. Moreover, ternary systems, which include solvent, co-solvent or salt and a solute, are even less studied. These ternary systems may present a cheap but powerful mechanism of controlling association processes in a solution. This is why it is important to increase our understanding of interactions in ternary systems solvent-salt-solute. Effects in such systems are often denoted as ion effects.

At the moment, ion effects are conventionally separated into specific and non-specific ion effects. It is important to note, however, that this separation is not quite strict: observable and measurable ion effects originate from a balance between multiple mutual interactions between ions, solvents and solutes. A small change in any part of this balance is capable of provoking dramatic changes in the observable ion effects. This is why it is very important to understand molecular level details of how solvent molecules and ions interact with solutes at solvation interfaces. This area received a significant attention during the last decades. However, despite an extensive research in the area of ion effects, we still lack knowledge on how microscopic behaviour of ions manifests itself on a macroscopic scale. This is why it is important to study the phenomena of ion effects from both, microscopic and macroscopic points of view.

## 1.2 Objectives

The main objective of this work is to study mechanisms of ion effects in aqueous and non-aqueous liquid media using a combination of experimental and computational tools. Here we deepen the understanding of ion effects as a subtle balance of several pairwise interactions, which take place in liquid media containing solutes and salts simultaneously.

Understanding of multiple mutual interaction in ternary systems solvent-salt-solute attracts a lot of attention during the last decades. This subject has a wide variety of applications in such areas as drug solubility control, water purification, aggregation of nano particles, etc. In this work we focus on ion effects on solute association processes in solution: bundle formation of carbon nanotubes in their N-methylpyrrolidone based dispersions and complex formation of aromatic carboxylic acids with  $\alpha$ -cyclodextrin in aqueous solutions.

Carbon nanotubes are one of the most promising materials for industrial applications due to their unique mechanical, electrical and optical properties. Complexes of aromatic carboxylic acids with  $\alpha$ -cyclodextrin are important for the pharmaceutical industry as they are used to increase drug bioavailability and decrease the toxicity. These complexes are also important for their scientific value as *simple model systems* of small molecules' interactions with proteins, enzymes and membranes.

We have chosen to study ion effects on complex formation in aqueous solutions because this would best represent physiological conditions. On the other hand, it is impossible to disperse carbon nanotubes in water without any surfactant. This is why, to eliminate surfactant effects in our research we studied carbon nanotubes dispersions in N-methylpyrrolidone. This solvent is capable of dispersing significant amount of nanotubes without any surfactants. Another advantage of N-methylpyrrolidone is its relatively low toxicity and low vapour pressure, which additionally reduces risks of intoxication via vapour. Moreover, studies of aqueous and non-aqueous polar media allowed us to gain broader overview of the nature of ion effects on association processes in liquid media. To gain molecular insights into the effects of ions on association processes, we use a combination of experimental techniques (UV-vis-NIR spectroscopy, transmission electron microscopy, photoluminescence spectroscopy) and computational tools (molecular dynamics). We also compare our simulation findings on some of the investigated systems with experimental results of our colleagues in Uppsala University (X-ray photoemission spectroscopy) and in the Russian Academy of Sciences (nuclear magnetic resonance and calorimetry).

In one part of this work, we study how sodium and potassium ions affect interactions of aromatic carboxylic acids with  $\alpha$ -cyclodextrin. According to nuclear magnetic resonance and

calorimetric studies, presence of sodium ions in a solution reduces effectively the binding constant of benzoic and nicotinic acids with  $\alpha$ -cyclodextrin. Unlike the presence of sodium, presence of potassium ions affects the binding constant only insignificantly within the error limits. To explain the difference in sodium and potassium effects we propose a molecular mechanism, based on results of our molecular dynamics simulations. According to this mechanism, sodium ions form a stable ion pair with benzoate or nicotinate anions, which reduces the effective concentration of the acid, available for binding with  $\alpha$ -cyclodextrin.

To gain a deeper understanding of the origins of ion effects on aromatic carboxylic acid interactions with  $\alpha$ -cyclodextrin, we study ion effects on benzoic acid interactions with a water/vapour (hydrophobic-hydrophilic) interface using molecular dynamics simulations and compare our findings to X-ray photoemission spectroscopy. It was found that the nature of ions dramatically affects the hydration pattern of benzoic acid. As a result of ion-induced changes in hydration pattern, the molecule changes its orientation at the interface as well as its affinity to the interface. Neutral molecules of benzoic acid tend to lie flat on the surface and show high surface affinity. Unlike neutral acid, benzoates tend to stay perpendicular to the water-vapour interface. Surface affinity of benzoates is significantly reduced, compared to neutral acid.

Another area discussed in this work, is the study of ion effects on the stability of carbon nanotubes dispersion in N-methylpyrrolidone. N-methylpyrrolidone, unlike water and many other solvents, is capable of dispersing significant amounts of carbon nanotubes without any dispersing agents. This advantage of N-methylpyrrolidone allows to study ion effects on carbon nanotubes associations more in details, because it allows to avoid the necessity to account for ion-surfactant interactions. We found that inorganic ions significantly reduce stability of carbon nanotubes dispersions in N-methylpyrrolidone. To gain molecular level details of the processes taking place upon salt addition to carbon nanotubes dispersion, spectroscopic observations are complimented with transmission electron microscopy and compared to results of molecular dynamics simulations. We suggest, that reduction of the dispersion stability originates in formation of ion depletion areas around the carbon nanotubes. Formation of the depletion areas, according to Kirkwood-Buff theory leads to an increase of free energy of the interface between the carbon nanotube and the salty N-methylpyrrolidone. This, in turn, forces carbon nanotubes to associate with each other, forming bundles and large aggregates.

### 1.3 Ion effects and solvation interfaces

Ionic compounds are widely spread in nature. Many of them are well soluble in polar solvents e.g. water. As an ionic compound is dissolved in water, or another polar solvent, it dissociates. Dissociation leads to formation of ionic solutions. Ionic solutions possess different properties, compared to the pure solvent. Ionic solutions, unlike pure solvents, are wide spread in nature and play an important role in geological, technological and biochemical processes. This is why ionic solutions attract much attention during recent decades.

First systematic studies of ion effects in solutions in the modern science were performed in the late 19<sup>th</sup> century by Franz Hofmeister [1] (translation of the original papers in German). He showed that stability of protein solutions is greatly affected by presence of salts. He also found that different salts make different effects on the stability of a protein solution. Later research developed Hofmeister's ideas, and these days ion and salt effects went far beyond the area of protein precipitation. Studies of ion effects embrace surface activity [2, 3, 4], bubble coalescence and foam stability [5, 6], nanotubes dispersion stability [7, 8, 9, 10], complex formation [11], etc.

As research on ion effects progresses, it brings more understanding of the complex nature of ion effects on different kinds of the processes. It is known, that ion effects arise as interplay of several forces at solvation interface and depend on mutual interactions solvent-solvent, solvent-ion and, if present, solvent-solute.<sup>1</sup>

It is important to note that the original research of F. Hofmeister was dedicated to *salt* effects on stability of protein solutions rather than ion effects. Although salts dissociate into ions and form ionic solutions upon dissolution, there is a significant differences between terms "salt effects" and "ion effects". Ion effects suggest consideration of ions apart from each other, i.e. cations act separately from anions. Although this approach gives us some level of understanding of many ion-related phenomena [12], it does not explain several other important manifestations of salt effects, e.g. surface activity changes [2, 3], foam formation and bubble coalescence [13, 14, 15]. These cases require employing the term "salt effects", which highlights a complex nature of the phenomenon. These cases are a good example to illustrate the nature of ion effects as *interplay* of several forces at solvation interfaces.

The solvation interface is a molecular level interface between solvent and solute. The solvation interface corresponds to a solvent accessible surface area of the solute. Depending on

---

<sup>1</sup>Generally, a term "solute" denotes any dissolved compound. However, in this work we separate terms "ions" and "solutes", denoting by the term "solute" only the main solute: carbon nanotubes, benzoic acid, etc.



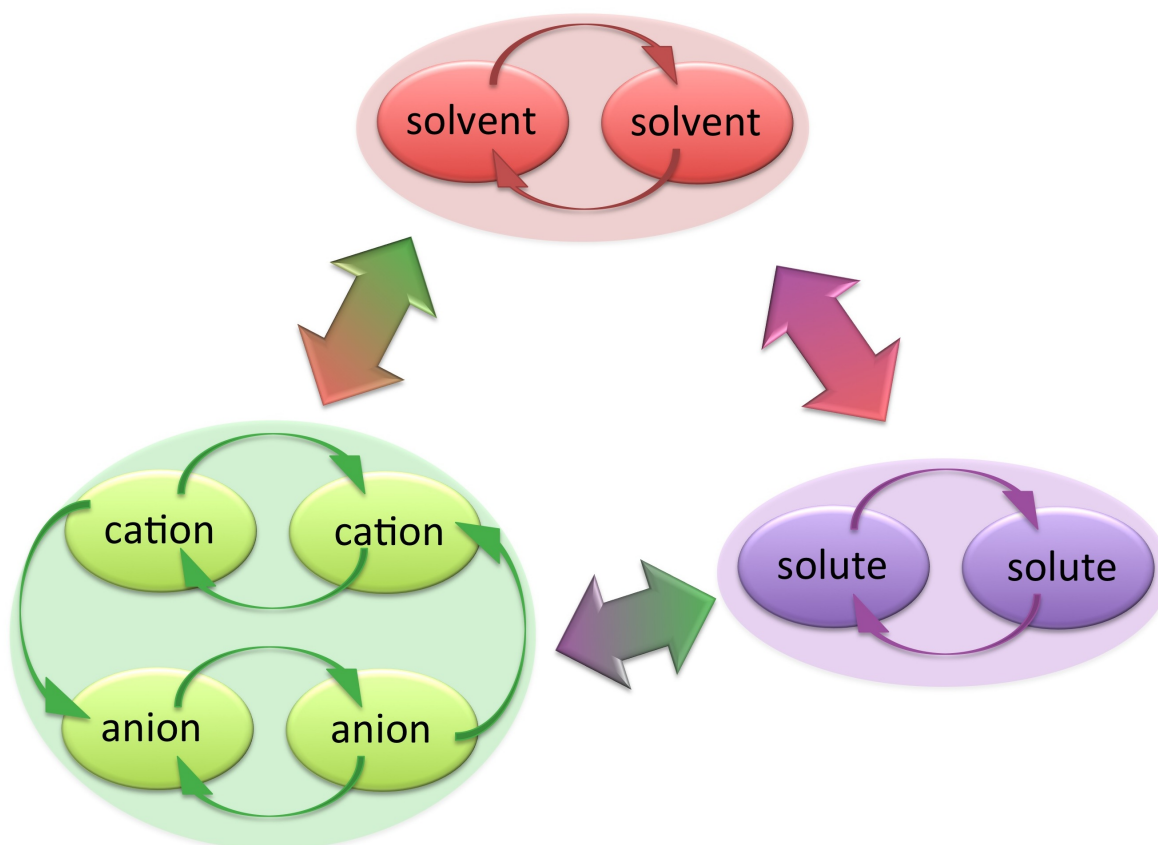


**Figure 1.1** – Schematic representation of interactions in ternary systems. The scheme presumes, that the solute is not ionizable. Ion effects is a complex phenomena, which originates in mutual interactions between ions, solute and solvent molecules. These interactions are shown with arrows.

the size of the solute, area of the solvation interface may vary from a few squared nanometers for small molecules to thousands of squared nanometers for large solutes, such as carbon nanotubes of proteins. Solvation interface always introduces perturbation to the structure of the bulk solvent. The extent and character of this perturbation depends on molecular interactions between solvent molecules and solute molecules. Depending on the nature of these interactions, one may distinguish solvophobic and solvophilic solutes. Interactions of solute and solvent molecules are energetically favourable in the case of *solvophilic* solute (positive solvation), whereas unfavourable interactions between solvent and solute molecules make the solute *solvophobic* (negative solvation).

Solvophobicity or solvophilicity of a solute in a particular solvent depends on three factors: *i*) interaction energy between solute particles; *ii*) interaction energy between solvent molecules; and *iii*) interaction energy between solvent molecules and solute particles. If interactions between solute particles and solvent molecules are more favorable compared to interactions between the same molecular species (solute-solute or solvent-solvent), than the solvation is positive. And

the other way around, the solvation is negative, when interactions between same molecular species are more energetically favourable compared to interactions between solvent and solute molecules.

Introduction of salts (ions) into a solution changes the balance of interactions between solute and solvent. Ions in the solution interact both with solvent molecules and with solute species. As a result, overall balance of forces includes mutual interactions between solute, solvent and ions, as well as interactions between particles of the same kind (solute-solute, solvent-solvent, ion-ion). The balance of forces in a triple system non-ionizable solute-salt-solvent is represented in the figure 1.1. As one can see from the figure 1.1, ion effects is a complex phenomena which includes, among others, ion-ion interaction. This is why it is important to consider "salt effects" when talking about "ion effects". As ion effects have several different inputs, their manifestations may be controlled by changing any of the pairwise interactions (denoted with arrows in figure 1.1). Unfortunately, the contemporary theoretical knowledge how to fine-tune ion effects is not well developed. This is why it is impossible to precisely forecast effects of a particular salt on a particular system. This is why this work attempts to further develop understanding of how ion effects work in several highly demanded systems: benzoic acid at water-vapor interface, complex formations of  $\alpha$ -cyclodextrin with aromatic carboxylic acids and stability of carbon nanotube dispersion in N-methylpyrrolidine.

## 1.4 Studied systems

### 1.4.1 Aromatic carboxylic acids. Benzoic acid

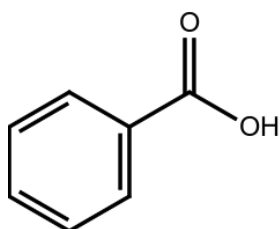


**Figure 1.2** – Structure of benzoic acid.

Benzoic acid (BAH,  $C_6H_5COOH$ , figure 1.2) is a carboxylic derivative of benzene and an elementary representative (first member of homologous series) of aromatic carboxylic acids (ACAs). Many ACAs possess biological and pharmacological activities. For example niacin (vitamin PP, nicotinic acid), aspirin (2-acetoxybenzoic acid), *o*-aminobenzoic acid (*in vivo* synthesis precursor of amino acid tryptophan) and *p*-aminobenzoic acid (*in vivo* synthesis precursor of vitamin folic acid) belong to aromatic carboxylic acids. Non-substituted benzoic acid has several important industrial applications. It is actively used as a food preservative and antibacterial agent [16, 17, 18, 19]. Benzoic acid as well as its derivatives are also commonly used in the organic synthesis of other chemicals, such as phenols, benzoate plasticizers, drugs

etc [20, 21, 22]. The main disadvantage of benzoic acid and its derivatives is their ability to cause some irritation effects (e.g., flushing, hepatotoxicity) [23, 24]. Wide use of benzoic acid requires deep understanding of variety of aspects of benzoic acid behaviour. It is important to understand the behaviour of benzoic acid at interfaces for catalysis, environmental chemistry, food and agricultural industries [18, 20, 21, 25, 26, 27, 28, 29, 30, 31].

Adsorption of benzoic acid at different interfaces has been intensively studied by different experimental and modelling techniques [32, 33, 34, 4]. In several studies it has been shown that the pH level of aqueous benzoic acid solutions (and, hence, the degree of dissociation of the acid) strongly influences its adsorption at interfaces. For example, Ishikawa *et al.* [35] investigated the adsorption of aromatic carboxylic acids into low-density polyethylene films as a function of pH. They showed that the adsorption level of benzoic acid to the film increased with decreasing of pH. Studies of benzoic acid orientation without considering directly its ionization state suggest that the aromatic ring of the benzoate anion is preferentially oriented perpendicular to the water-electrode interface [36]. These two findings reveal, that, in principle, it should be possible to control extent of surface adsorption of benzoic acid, as well as, possibly, its orientation, by changing the pH level of the solution.

Taking into account the above mentioned pH dependent properties of benzoic acid, as well as its structural features, one could conclude, that benzoic acid is a valuable object to study molecular level details of ion effects. The reasons for this are as follows. Benzoic acid is rigid and amphiphilic molecule, i.e. it has hydrophilic and hydrophobic parts (carboxylic ionisable group and benzene ring, correspondingly). As the pH level of the solution increases, carboxylic group ionises and gains a negative charge on it. This charged carboxylate group increases hydrophilicity of the hydrophilic part of benzoic acid molecule, which, in turn, shifts the balance between hydrophobic and hydrophilic parts of benzoic acid molecule in understandable and controllable way. The fact that benzoic acid is a relatively rigid molecule adds more control into the changing of the hydration balance. This change in balance between hydrophobic and hydrophilic parts of benzoic acid molecule is capable of inducing differences in the pattern of the benzoic acid interaction with water, which, it turn, may affect the acid orientation at surfaces as well as surface adsorption. Ionization of benzoic acid molecule is the most powerful tool to change the molecule's interactions with water. On the other hand, as we know from the previous section, addition of ions may change interactions of the solute (benzoic acid) with the solvent. This, in turn, may lead to changes in surface adsorption, though, less significantly compare to ionization.

Molecular-scale study of the behavior of benzoic acid at aqueous solution/vapor interface has

fundamental importance for understanding the molecule's environmental effects, its transport and adsorption properties in technological processes and its photo- and biodegradation in natural and industrial environments, etc. [26, 27, 29, 31, 33, 37, 38, 39, 40, 41, 42, 43]. Overall, the molecular mechanisms of interface adsorption of benzoic acids are still poorly understood. The main reason for this gap in our knowledge is the difficulty to obtain direct molecular-scale information about benzoic acid at interfaces, which is a challenge both for experiments and theory. To fill parts of this gap, and obtain a molecular-scale picture of the behaviour of both neutral benzoic acid and benzoate anion at the aqueous solution/vapour interface, this work presents a combined experimental and theoretical study using X-ray photoelectron spectroscopy complemented by fully atomistic molecular simulations.

As it has been mentioned previously, behavior of benzoic acid and its derivatives in the bulk is just as important as their behavior at interfaces. Knowing ion effects on behavior of aromatic carboxylic acids in the bulk is important, because of the following. As they have large hydrophobic part, these acids are capable to aggregate in a solution and participate in reaction of complex formation. The later is used in the pharmaceutical industry to increase solubility of these poorly soluble molecules. As it is known from the discussion above, ions may affect interactions between solute and solvent molecules, which, in turn, may affect processes of complex formations in the solutions. This is why this work suggests a molecular mechanism of ion effects on complex formation of some aromatic carboxylic acids.

### 1.4.2 Cyclodextrins

Cyclodextrins are a family of cyclic oligosaccharides, constructed with D-(+) glucopyranose units attached by  $\alpha$ -(1, 4) glucosidic bonds. The family of cyclodextrins contains three non-substituted compounds:  $\alpha$ -cyclodextrin (six sugar residues),  $\beta$ -cyclodextrin (seven sugar residues),  $\gamma$ -cyclodextrin (eight sugar residues) and their many derivatives. Non-substituted  $\alpha$ -,  $\beta$ - and  $\gamma$ -cyclodextrins are conventionally devoted as *native cyclodextrins*. Figure 1.3 represents structural formula of  $\alpha$ -cyclodextrin (panel 1.3a) and its 3D molecular view (panel 1.3b). As glucopyranose is not aromatic molecule, its rings are not plain. This non-planarity of glucose rings result in one rim of cyclodextrin slightly wider compare to another one.

Cyclodextrins are known for more than a century [44]. Due to their structure cyclodextrins have relatively hydrophilic outer surface and relatively hydrophobic (lipophilic) central (inner) cavity (see fig. 1.3). The conformation of cyclodextrins is quite rigid, however it allows some limited flexibility. Limited conformational flexibility of cyclodextrins and combination

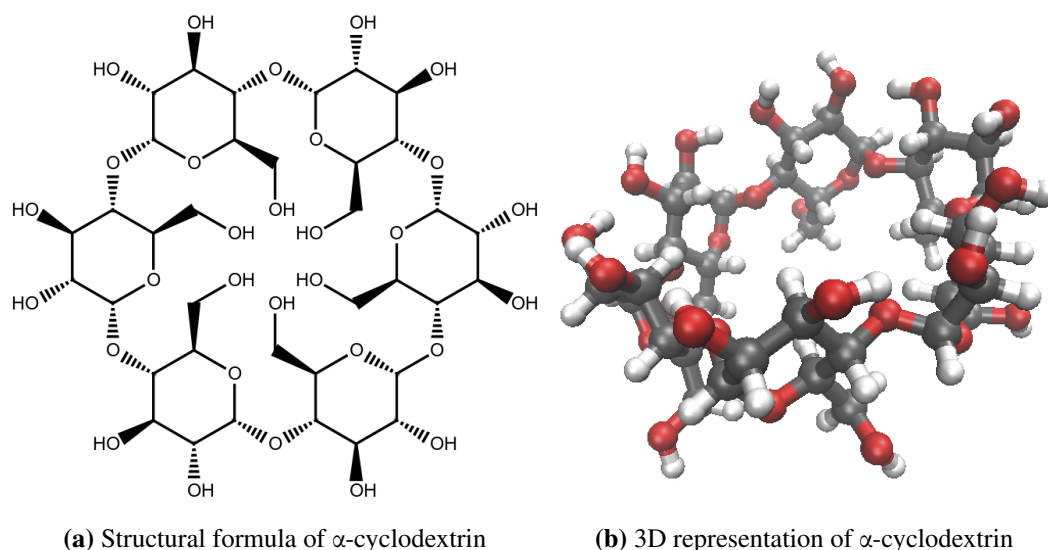


**Figure 1.3** – Structure of  $\alpha$ -cyclodextrin. As glucopyranose is not an aromatic molecule, its rings are not plain. This non-planarity of glucose rings results in one rim of cyclodextrin slightly wider compare to another one. The 3D structure shows presence of wider and narrower rim in cyclodextrin, as well as internal cavity. Comparison of structural formula with 3D representation reveals, that internal cavity is weakly polar and relatively hydrophobic; the external area of cyclodextrin is more hydrophilic. Combination of hydrophobic internal cavity with hydrophilic external areas allows cyclodextrins to accommodate poorly soluble compounds, e.g. drug-like molecules, which effectively increases solubility of the guest molecules.

of hydrophilic outer and hydrophobic inner surfaces allows cyclodextrin to form inclusion complexes with a variety of small hydrophobic molecules, particularly, drug and drug-like molecules. In these complexes cyclodextrin acts as a host accommodating a small molecule, which is often denoted as guest molecule. This is why complexes of cyclodextrins with small molecules are often denoted as guest-host complexes.

Formation of guest-host complexes is a very important property of cyclodextrins. Formation of these complexes leads to increase of solubility of a guest molecule and provides a prolonged drug release of small poorly soluble drug-like molecules. Increased solubility and prolonged drug release, in turn, increase biological availability, stability, and prevents some side effects [45, 46]. Although many details of mechanisms of complex formation are unknown, it is well established, that cyclodextrins and their complexes with drug-molecules have very low toxicity to animals [47]. Substitution of hydroxyl groups (R – OH) to larger groups, e.g. hydroxypropyl, is capable of increasing positive effects of cyclodextrins complex formation with drug-molecules, as well as further decreasing of low cyclodextrins toxicity. This is why cyclodextrins are valuable compounds for the pharmaceutical industry: at the moment, more that thirty commercial drugs

in the market contain cyclodextrins in their formulations [45, 46]. Unfortunately, although CDs are actively used in drug formulation to increase drug solubility, small attention was paid to the effects of biological aqueous environments on the CD complex formation. Previous discussion and some experimental evidence suggest that the biologically relevant salts can make significant effects on biomolecules [48, 49, 50], and, therefore, they should be also considered in the host-guest binding.

In addition to their high practical importance cyclodextrins represent a simple and rigid model for studies of enzyme reactions [51]. Indeed, the inner cavity of different cyclodextrins, just like inner cavities of many enzymes, have different size, which results in stereo-selectivity of the CD complex formation. In other words, cyclodextrins are capable to form stable complexes only with those small molecules, which fit well into the cyclodextrin cavity. Too large molecules are not able to form the complex as it induces sterical clashes between atoms of the guest-molecule and cyclodextrin. Too small molecules do not have sterical possibility to interact with all atoms of the cyclodextrin cavity, which weakens the binding. The inner cavity of cyclodextrins, like inner cavity of enzymes, possesses limited flexibility and is weakly polar and relatively hydrophobic. A molecule of cyclodextrin is, like a protein molecule, quite large compared to the guest molecule. This is why the analysis of guest-host complex formation plays an important role in studies of enzymatic activity. As cyclodextrins molecules are used as a model to study enzyme reactions, it is very important to understand how ions affect the process of complex formation of cyclodextrin with different molecules.

Fortunately, guest-host complexes represent a particular case of association processes in liquid solutions. They are a good simple model to study ion effects on association processes in solutions. The reasons for this are as follows. Smallest of cyclodextrins,  $\alpha$ -cyclodextrin, is capable of forming stable complexes with benzoic acid and its derivatives. As it was discussed in section 1.4.1, benzoic acid is a great model to study ion effects as it is ionizable and rigid. Therefore, we may study complex formation of benzoic acid with  $\alpha$ -cyclodextrin without the need to account for conformational changes of the guest molecule.

This means (see section 1.4.1) that we can fine-tune interactions of the guest molecule with the solvent without a necessity to account for different types of conformer energies. At the same time, cyclodextrin itself does not change its ionization state over a large interval of pH levels, which means that we can describe fully changes in the process of complex formation to changes in the guest molecule interactions with the liquid media. At the same time it is known that  $\alpha$ -cyclodextrin does not bind with simple mono-atomic cations like sodium or potassium [52], which creates a possibility to raise the pH level (with sodium or potassium hydroxides) to

high values without a risk of blocking the cyclodextrin reacting ability.

To summarize, combination of cyclodextrin structural and ionization properties makes it an ideal model for study of ion effects on association process (complex formation): cyclodextrins are relatively rigid; they form complexes with aromatic carboxylic acids; they do not ionize in wide interval of pH.

### 1.4.3 Carbon nanotubes

Carbon forms several allotropes. The most widely known allotropes of carbon are diamond and graphite. Diamond and graphite represent an ideal example of how mechanical, electrical and optical property of a substance depend on its structure: both diamond and graphite are built solely of carbon. The only difference between the two materials is their crystal structure, which determines different physical properties of diamond and graphite. Carbon also has another allotropes, which are less known compare to diamond and graphite. Starting from the second half of the 20<sup>th</sup> century, as available analytical methods became developed enough to register structures of a few nanometres size, several nano-sized modifications of carbon were found: fullerenes [53], which include spherical (buckminsterfullerene or "buckyballs") and elongated cylindrical species ("nanotubes", [54]), graphene [55], etc.

Properties of these nano-sized allotropes of carbon are significantly different from bulk materials. These allotropes are also significantly different from each other, but all these structures are often denoted as carbon nanomaterials. This family of materials attracts significant attention last decades. Just as other carbon nanomaterials, carbon nanotubes (CNTs) attract much of attention these days due to their unique mechanical, electronic and optical properties. Conventionally, one could describe structure of CNTs as a graphene sheet seamlessly rolled into a cylinder. Depending on the number of graphene sheets rolled together into a carbon nanotube, it is common to classify CNTs as single walled (one rolled graphene sheet) and multiwalled (two or more parallel graphene sheets rolled). Typical diameter of SWCNTs is just a few nanometers, at the same time, their typical length reaches micrometers, and in some cases it goes up to centimetres [56, 57, 58] which makes CNT ratio length-to-diameter extremely high. This alone is important for design of nanowires and nanofibres.

All carbon nanotubes possess honey-comb structure made of many fused benzene rings.<sup>2</sup>

---

<sup>2</sup>As benzene rings are fused, amount of hydrogen atoms per one carbon atom reduces, as valencies of carbon atoms become occupied with other carbon atoms. Compare C<sub>6</sub>H<sub>6</sub> for benzene (one ring), C<sub>10</sub>H<sub>8</sub> for naphthalene (2 fused benzene rings), C<sub>14</sub>H<sub>10</sub> for phenantrene (three fused benzene rings), and so on.

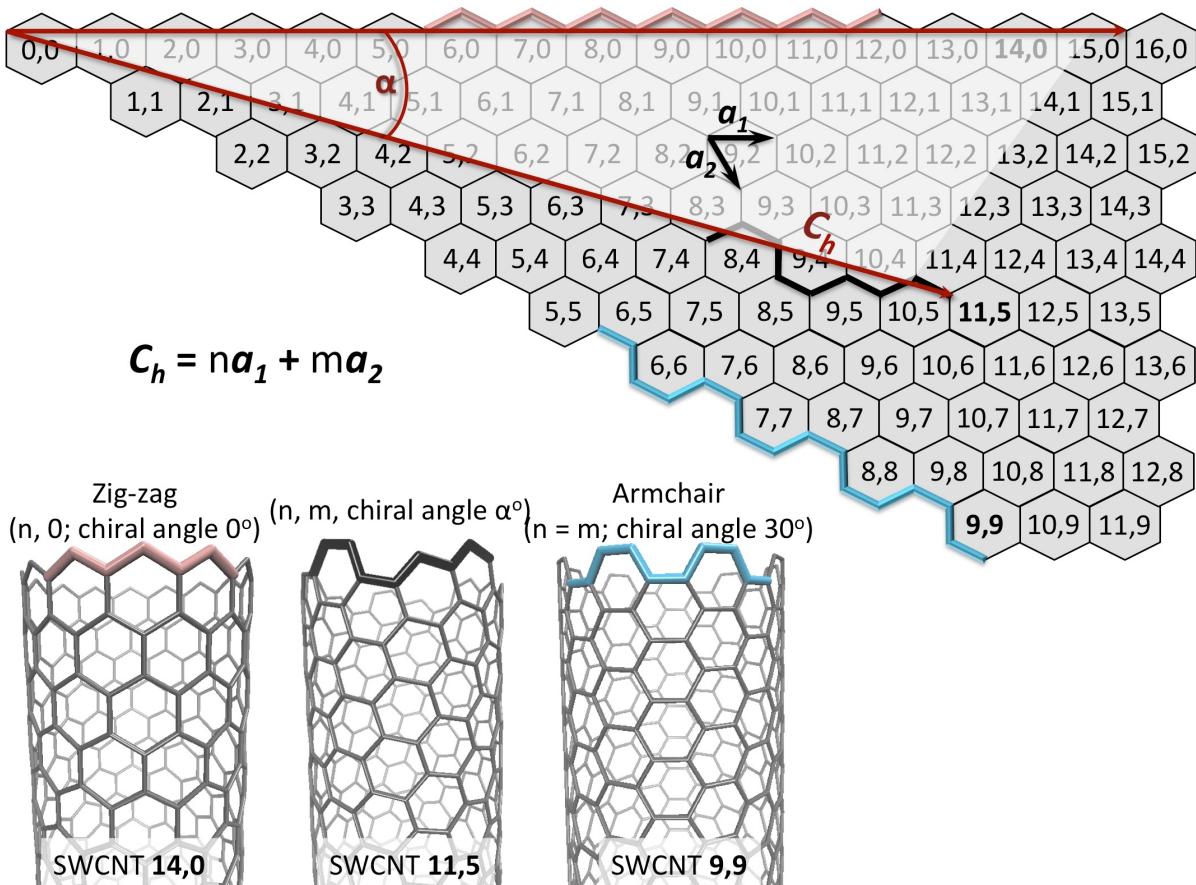


**Figure 1.4** – Carbon nanotubes chiralities definition. Carbon nanotubes may be represented as a graphene sheet seamlessly wrapped into tubular shape, therefore, carbon nanotubes may be described with vectors of hexagonal lattice. Chirality is defined as a sum of lattice vectors with coefficients (n, m) ( $a_1$  and  $a_2$ ). Chirality is an important characteristic of CNTs as it defines optical and electrical properties of CNT, as well as their diameters.

The orientation of the honey-comb pattern along the tube axis varies depending on the directions of rolling of the graphene sheet. Different type of the honey-comb pattern orientation in carbon nanotubes are usually referred as "chirality". Figure 1.4 describes how different ways of rolling the graphene sheet result in different chiralities. Chirality (length of the chiral vector and angle  $\alpha$ ) of a nanotube describes the tube's diameter (see fig. 1.4). Nanotubes of different chiralities have significantly different properties. Such armchair CNTs possess high conductivity and usually addressed as metallic. Other CNTs are semiconducting with variable band gaps depending on the chirality.

Electrical properties of CNTs depend on their chirality. For metallic nanotubes carrying capacities are higher compare to copper or gold [59]. Therefore CNTs can be effectively used as nanowires or as details of single-electron transistors [60]. CNTs have already found applications as conducting components in polymer composites [61], they also could be used as electrodes in



supercapacitors and lithium batteries. Semiconducting CNTs exhibit higher electron mobility compare to silicon. Thermal conductivity of CNTs are one of the highest registered conductivities for known materials. CNTs show a specific optical and fluorescence respond. At the same time they are transparent in visible and infra-red regions which allows their potential usage in displays, solar cells, electroluminiscent lightning, etc. [59].

Unfortunately, despite many possible applications, there are a few significant issues, which prevent wide practical applications of CNTs: *i*) there are no reliable method of reproducible synthesis of CNTs with predefined chirality and purity; and *ii*) there is no cheap and reliable technique of purification of carbon nanotubes. Absence of cheap and reliable technique to purify carbon nanotubes has its origins in poor solubility of nanotubes; additionally, inability to obtain a stable dispersion of CNTs with reproducible CNTs concentration makes many technological processes more complicated or impossible. Carbon nanotubes are very solvophobic materials [62, 63, 64, 65], which means that obtaining a stable dispersion or solution of them is rather complicated. Pristine CNTs cannot be dissolved in water and require additional surface modification (covalent or non-covalent functionalization) to disperse them in aqueous solutions [61, 66]. This is why research of how to effectively disperse carbon nanotubes is very intensive over last decades.

The work on dispersing of carbon nanotubes can be separated into two main parts: functionalization of CNT surface (covalent surface modification) and dispersing of pristine carbon nanotubes with different surface active compounds and surfactants (non-covalent surface modification). Covalent modification of CNT surface means chemical attachment of hydrophilic groups, e.g. carboxylates or sulphur groups, to carbons of the CNT. This modification is capable of making carbon nanotubes well soluble in water. Unfortunately, this technique significantly compromises unique CNT properties. Non-covalent functionalization of CNTs means using of different surfactants. Although non-covalent functionalization affects properties of CNTs less compare to covalent functionalization of CNT surface, it still has some drawbacks.

Some organic solvents disperse relatively high amounts of non-modified CNTs, which allows one to avoid drawbacks of CNT surface modifications, which opens up new avenues for CNT applications in many areas of nanotechnology [63]. The employment of organic solvents may be particularly important for electronic applications of carbon nanomaterials dispersions (e.g. in photonics and optoelectronics) where it is important to keep the surface of the nanotubes free of chemical or physical modification to minimize changes in their electronic properties [67, 68]. Preparation of CNT dispersions is an important step in CNT bundle engineering. The bundle engineering is very important in ultrafast photonics and bio-medical applications [67, 69, 70].

Theoretically, controllable bundle formation may be achieved by dispersing CNTs, followed by a controllable aggregation. Unfortunately, this process is very difficult to control by standard methods [71]. Controllable bundle formation may be achieved through several consequent steps: *i*) debundling of as-prepared carbon nanotubes followed by a purification, if needed; *ii*) controllable change of the media parameters in such way, that bundles with particular properties are formed (e.g. only metallic tubes in the bundles or tubes of particular chirality). This is why to gain the required level of control on the nanotubes dispersion, intensive research concentrates on area of solvent engineering.

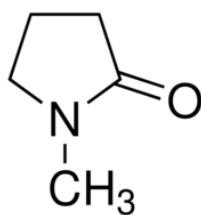


**Figure 1.5** – Structure of N-methylpyrrolidone.

Despite active research in the area of solvent engineering for CNT dispersions, the main physical-chemical mechanisms of solvent effects on CNTs have not been sufficiently explored. Even less studied have been the effects of other dispersion components, e.g. salt. However, as one may conclude from the discussion above, salts may have significant effects on dispersion stability [72]. Moreover, by varying salt concentration, one may introduce a controllable shift in the media properties, which is an important step on the way to controllable bundle formation. It has been shown recently that salts can regulate dispersing properties of surfactants in aqueous solutions [7, 8]. Unfortunately, in the multi-component CNT-surfactant aqueous dispersions, the ion effects on CNTs interfere with ion-surfactant interactions. This is why it is important to understand whether salts make any effects on CNT dispersions which do not contain surfactants.

N-methylpyrrolidone (NMP) (see figure 1.5) is a promising solvent for making stable dispersions of pristine CNTs [63, 73, 74]. Despite its high polarity (the dipole moment of NMP is 4.1 D), many inorganic salts are poorly soluble in NMP. However, there is a general pattern of inorganic salt solubility in NMP: salt solubility increases with increase of ionic radii of the ion, which compose the salt. Such, solubility of sodium iodide in NMP reaches ~0.2 M [75] compared to poorly soluble sodium chloride [76]. This is why in our research on ion effects on stability of CNT dispersions in NMP we used salts with large anions: sodium iodide and sodium bromide. This allows one to understand salt effects on stability of CNT-NMP dispersions without interference from surfactants.

## 2

# Physical-chemical processes at solvation interfaces

Solvation is a complex phenomenon, which lies at the interface between chemistry and physics. The phenomenon occurs as a subtle balance of several forces acting in a solution. This balance is dynamic, which means that acting on any of the involved forces may easily alter it. This ease of altering represents a powerful mechanism to control variety of processes in a solution, including surface behaviour, complex formation, and dispersion stability. Unfortunately, we do not fully understand the mechanisms, which allow deliberate changing of the properties of solvation. This prevents many prospective applications of this powerful tool to control variety of processes in a solution.

## 2.1 Hydration of simple inorganic ions

### 2.1.1 Energetic balance of hydration

Hydration<sup>1</sup> of simple inorganic ions is the case of solvation, best documented in the literature, including variety of textbooks. Simple ions are formed upon dissolution and dissociation of salts, acids, and bases, which are made up of simple anions and simple cations. Examples of these compounds are NaBr, HCl, KOH, CaBr<sub>2</sub>, H<sub>2</sub>S, etc. Some of these compounds are strong electrolytes in water,<sup>2</sup> which means that they dissociate completely in aqueous solutions. Other

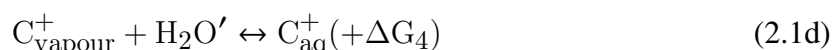
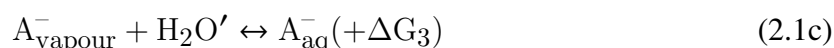
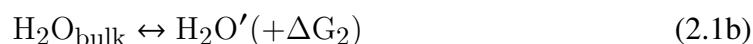
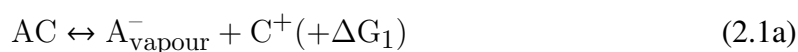
---

<sup>1</sup>Conventionally, the term "hydration" replaces the term "solvation" if the solvent is water.

<sup>2</sup>Note, that the same compound may show weak electrolyte properties or not dissociate in other solvents. The power of electrolyte is a mutual characteristic of the solute and the solvent.

compounds dissociate in water only partially (weak electrolytes). In other words, solutions of strong electrolytes consist solely of ions up to saturation (degree of dissociation is close to unity);<sup>3</sup> while solution of weak electrolytes consist partially of ions and partially of non-dissociated molecules (degree of dissociation is significantly less than unity). For simplicity let us consider a solution of a strong electrolyte.

Dissolution of a strong electrolyte may be approximated with the following steps: *i*) full destruction of the crystal structure of the compound with formation of ions in gaseous phase, which may be compared to sublimation coupled with ionization; *ii*) reorganization of solvent molecules in order to accommodate the solute; and *iii*) solvation of the ions from the gaseous phase. These processes may be schematically represented with the equations 2.1:



where AC is a compound, which consists of anions  $A^-$  and cations  $C^+$ ;  $H_2O_{\text{bulk}}$  is the water with undisturbed structure (bulk water);  $H_2O'$  is the water with a structure, reorganized in order to accommodate the solute. Although it is clear, that upon real dissolution no sublimation is required to dissolve a compound in water, this representation makes it easier to understand the energetic balance of the whole dissolution process.

Each of the stages in the equations 2.1 may be characterized with a change of free energy ( $\Delta G$ ). The negative free energy means that the process is spontaneous, and the other way around, a positive change in free energy means that the process is not spontaneous and does not take place unless some external energy is applied (e.g. heat or ultrasound).  $\Delta G$  in turn, consists of two contributions: enthalpic ( $\Delta H$ ) and entropic ( $\Delta S$ ):

$$\Delta G = \Delta H - T\Delta S.$$

Enthalpy (H) is a measure of the total energy of a thermodynamic system at constant pressure. The negative change of the enthalpy means that the system loses the energy and the process is

---

<sup>3</sup>As one may conclude from the further reading, the assumption that solutions of strong electrolytes consist solely of ions is not quite correct. In fact, concentration of ionic pairs and even larger clusters slowly increase with increase of the electrolyte concentration. However, the assumption of full dissociation works well for most of cases in analytical chemistry.

exothermic (the system heats up). The positive enthalpy change means that system takes some heat from the environment (the system cools down). Generally, the *negative enthalpy favours a process*.

Another contribution to the free energy of a process is entropy ( $\Delta S$ ). Entropy is a measure of the number of ways in which a system may be arranged, a measure of "disorder":

$$S = k_B \ln \Omega,$$

where  $k_B$  is the Boltzmann constant; and  $\Omega$  is the number of microstates available for the system (the ways, how the system may be arranged on the micro level). According to the second law of thermodynamics, entropy of a closed system tends to maximum. This means that the *positive entropy favours a process*. Let us now come back to theoretical stages of dissolution in more details.

**Destruction of the crystal structure with formation of gaseous ions.** It is important to note, that some electrolytes are gases under normal conditions (e.g. HCl). In this case some energy is required for dissociation of molecules into ions. The process of formation of gaseous ions from crystals or gaseous molecules always requires external energetic input ( $\Delta G > 0$ ) and it is endothermic. The value of the heat effect depends on the binding energy in the electrolyte molecule or crystal energy. On the other hand, the enthalpy of this process is always positive, as the number of particles in the system increases.

**Reorganization of bulk water structure and solvation of ions.** The bulk water has a dynamic short-range ice-like order. To accommodate an ion this structure of water needs to be modified. First of all, some cavities should be introduced to the water structure. Size of these cavities should correspond to the size of ions. This process is energetically not favorable. After the ion was placed into the cavity, water molecules in the direct contacts with the ion should be reoriented in a way to best interact with it. As water molecules are polar molecules, they need to orient their dipoles such a way, that negative partial charges are oriented towards cations, while positive partial charges are oriented towards anions. This interaction is favorable due to Coulomb attraction. It is also suggested, that chemical forces are involved in the process, including charge transfer from the ion to water molecule [50]. At the same time, excessive number of like-charged dipoles in the same volume of space makes this structure unfavorable due to Coulomb repulsion. Therefore, a balance of the chemical and Coulomb attraction and repulsion defines the final orientation of water molecules near the ion as well as a number of water molecules affected

by the ion. This modified orientation of water molecules near the ion is often denoted as the hydration shell of the ion. The number of affected water molecules is denoted as hydration (sometimes, coordinate) number. **Formation of hydration shell** may be accompanied by either positive or negative enthalpic and entropic contributions, depending on the nature of the ion.

As one may conclude from the discussion above, these three steps of dissolution may introduce different energetic inputs to the dissolution process. This means, that the resulting  $\Delta H$  and  $\Delta S$  of the process, and, as a consequence,  $\Delta G$  may be different.<sup>4</sup> The change of the enthalpy of solvation is negative for those compounds, for which the energy required for the ionization of the compound and/or destruction of its crystal structure is less, compared to the energy gain upon hydration.<sup>5</sup> Examples of these compounds are HCl (-74.84 kJ/mol), KF (-17.73 kJ/mol), NaI (-7.53 kJ/mol). If the energy gain from hydration is less compared to the energy required for ionization and/or crystal structure destruction, then the enthalpy of hydration is negative. Examples of compounds with negative hydration enthalpy are NaCl (3.88 kJ/mol), KBr (19.87 kJ/mol) and KCl (17.22 kJ/mol). Processes with negative enthalpy are usually denoted as enthalpy driven, while processes with positive enthalpy are entropy driven. Entropy of gas dissolution (e.g. HCl) is always negative; therefore, gas dissolution is always an enthalpy driven process. Unlike dissolution of gases, dissolution of crystals is always accompanied with positive entropy, and often with positive enthalpy (excluding bases and acids). This is why, dissolution of salts is often entropy driven.

Like salts ions possess free energy of hydration, which may be represented with enthalpic and entropic contributions. These characteristics are important due to two reasons: *i*) one may calculate unknown energies of hydration of any salt; and *ii*) based on the difference of enthalpies of solvation between ions one may suggest the preferential pattern of its behaviour in a solution.

In real solutions, unlike in the ideal solution, ions do not behave independently from one another. In principle, there are two theoretical possibilities for counterions of a salt to behave in a solution: forming a direct contact pair and forming water-separated contact pairs (see fig. 2.1). Collins and his co-authors [50] suggested a qualitative criterion for prediction, whether oppositely charged ions form preferentially a direct contact pair in water or, on the contrary, water-separated ion pair. They suggested to separate ions into chaotropes and kosmotropes according to the difference of water entropy in the direct proximity of the ion and in the water bulk (see fig. 2.2). If entropy of water molecules in the direct proximity of an ion is higher than in the bulk (bottom part in the figure 2.2), then this ion is denoted as structure-breaking

---

<sup>4</sup> $\Delta G$  of ideal solution formation is equal to zero.

<sup>5</sup>Source of the data on enthalpy of solvation is [77].

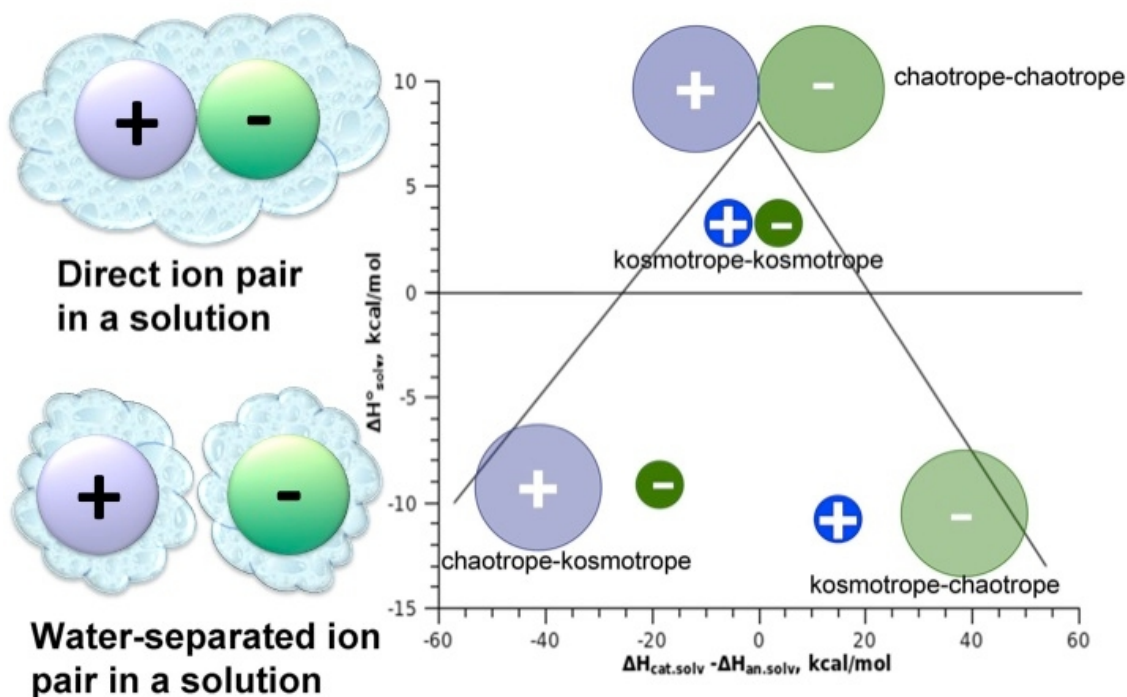


**Figure 2.1** – Collins volcano. A schematic representation of the experimental law of Water Matching Affinities: the ions tend to form direct contact pairs in the solution when the hydration energies of anions and cations are close to each other. On the contrary, when the hydration energies of ions are significantly different, ions tend to form water-separated ion pairs. Adapted from [50].

or chaotrope. Kosmotropes, on the other hand, bind water molecules strongly, and, as a result, entropy of water molecules in the direct contact with a kosmotrope ion is lower compared to the bulk water. As one can see in the figure 2.2, ability of an ion to bind a water molecule is in a direct dependency of the ion size and charge. In other words, small ions with high surface charge density tend to bind water stronger compared to larger ions with lower surface charge density. Strength of interaction of ions between each other, as well strength of water interactions with the ions, defines, whether counter-ions tend to form direct contact pairs in a solution, or, oppositely, tend to stay water separated.

Ions tend to form direct contact pairs in aqueous solutions if hydration energy of the salt is positive and the value of hydration energy of the cation is similar to the hydration energy of the anion. This takes place in two cases. First, case takes place when a salt consists of two small ions, i.e. both, the salt cation and salt anion are small and have high surface charge density (e.g. LiCl). In this case the ions are strongly hydrated, however, due to high charge density on their surface and small water accessible area, water can not screen their charge efficiently. Positive

and negative charges interact directly, according to the Coulomb law. The second case takes place when a the salt contains both large anion and large cation, both with low surface charge density (e.g. CsI). In this case the charge density on the ion surface is not sufficient to form a dense hydration shell around the ion. The ion stays partially hydrated and its charge is not efficiently screened. As in the first case, anion and cation interact with each other according to the Coulomb law. These cases are represented in the upper part of the figure 2.1.

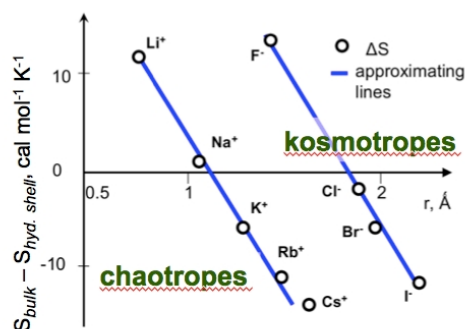


**Figure 2.2** – Energetic criteria of ion classification into kosmotropes and chaotropes. Adapted from [50].

Hydration shells of small and large ions are structurally different. As small ions possess large surface charge, they effectively orient water dipoles around them, i.e. they increase water ordering in the close proximity from themselves. Because of the ability of small ions to increase water molecules structural ordering these ions are denoted as "kosmotropes" or "order makers". Large ions, on the contrary, are not capable to effectively orient and structure water molecules. Moreover, large ions introduce a perturbation to the bulk water structure, often making water molecules more mobile compared to the bulk water. This is why large ions are denoted as "chaotropes" or "order breakers". Employing this terminology, one may say, that two chaotropes or two kosmotropes are likely to form a direct ion pair in a solution. On the contrary, a mixture of a chaotrope and a kosmotrope is likely to stay apart in a solution, forming a water-separated ion pair.

Although the idea of a connection between surface charge of an ion and its hydration shell explains why some ions tend to stay in direct contact in a solution and some ions prefer to stay water separated, it does not explain, why thermodynamic characteristics of interactions of water molecules with cations are different from thermodynamic characteristics of water with anions (see fig. 2.2). In order to explain this one needs to consider molecular details differences in the structure of hydration shells. The authors of the work [78] discovered, that solvation patterns

If anion and cation have noticeably different strength of hydration (one is kosmotrope, the other is chaotrope), then the ions tend to form solvent separated pairs. This situation occurs when a salt contains one small and one large ion, when the surface charge density for the counter-ions differs significantly. In this case the large ion cannot compete with the water molecules from the thick hydration shell of the small ion for a direct interaction. However, the ions interact with each other through the hydration shell(s) (lower part of the figure 2.1).



of anions differ from solvation patterns of cations at molecular level. This is due to different orientation of water dipoles around the ions.

### 2.1.2 Properties of dynamic equilibrium

The discussion above represents solutions as a static system in a "frozen" equilibrium state. This way of understanding systems in equilibrium corresponds well to our every-day experience with physical objects. Indeed, if a pen falls on the floor from a table (the pen decreases its potential energy), it stays there unless someone picks it up and puts it back on the table (some external energy is applied). Unlike physical systems, equilibria in chemical systems, including solutions, are dynamic. Continuing the analogy with the pen imagine that the pen never stays exactly where you put it on the table. It always bounces around the table. It may also eventually fall down from the table, which reduces the pen's potential energy. On the floor the pen continues to bounce. The pen may eventually jump high enough and land on the table. However, as the potential energy of the pen on the floor is lower compared to the energy on the table, the pen stays on the floor longer than on the table. If one averages the pen's position, one may find that the pen is effectively somewhere between the floor and the table. At the same time, the pen spends only a short while at the point of its average position and moves around all the time. This example with the abnormal pen would be the best to describe a dynamic chemical equilibrium in a solution.

A dynamic equilibrium in a solution means that, although we may detect water molecules in the direct contact with the ion, and may even record their characteristics, we see only an averaged picture of the solvation. To gain more understanding of the solvation process, one needs to consider dynamic and kinetic of the equilibrium as well as thermodynamic (static) properties of a solution. Dynamic properties of a solution include residence time of one particle in the direct contact with another. The residence time of water molecules near an ion in aqueous solution is usually around several picoseconds. The residence time of water molecules near variety of ions is usually in a good agreement with entropic data: positive entropy corresponds to residence times of water near the ion being shorter compare to the bulk water, and the other way around, larger residence time of water near an ion correspond to negative change in the entropy upon hydration.

Another important consequence of dynamic equilibrium is existence of multiple different ways to arrange the system. This is usually denoted as kinetic stability and thermodynamic stability. Continuing the analogy with the pen, let us imagine that someone puts several books

on the edge of the table when the pen is on it. In order to fall to the floor, the pen needs to jump higher than the height of the book; in other words, it needs to increase its energy to overcome the potential barrier (books). All jumps of the pen, which are lower than the height of the books, will be insignificant and will not allow the pen to leave the table. This reduces the probability of a pen falling to the floor, although does not completely rule it out. If the pen is on the floor, it may still jump back to the table, although in this case it will need to spend more energy. This makes the change “table-floor” less probable in both directions. In other words, introduction of a potential barrier between two states of the system reduces the probability of transfer between these two states; the system is preserved in one of the states. The higher the barrier, the less probable is the transition. This preservation of a system has an important consequence: *the system may be caught in thermodynamically unstable state* if a potential barrier is introduced. This phenomenon is denoted as kinetic equilibrium. An example of a system in kinetic equilibrium is benzene, which is thermodynamically not stable and slowly degrades. Another example of kinetically stable systems are colloidal dispersions. The issue of kinetic stability of dispersions is an important issue for this work and will be discussed farther in this chapter.

## 2.2 Hydration of polyatomic species

A polyatomic ion is any ion, which contains more than one atom. Polyatomic ions may be inorganic (e.g.  $\text{SO}_4^{2-}$ ,  $\text{ClO}_4^-$ ,  $\text{NH}_4^+$ , etc.) and organic (compounds, which contain ionized group, e.g. amino-groups, carboxylic groups, sulphated organic compounds, etc). Polyatomic ions are usually larger compared to simple ions. On the other hand, the charge is often localized at relatively small group of the atoms, which may create a significant charge density in this group.

A significant difference between organic ions and inorganic ions is presence of hydrophobic areas in organic ions. The hydrophobic areas are capable of altering a hydration pattern of the charged group. This makes hydration of organic ions more complicated compared to hydration of simple spherically symmetric ions, which has been reviewed in the previous section. Hydration of polyatomic ions is less explored in comparison to hydration of simple ions. For example, it is known, that dissolution may lead to a conformational change [79] in the flexible solutes. This may require inclusion of an additional equilibrium into the energetic balance of dissolution. This additional energetic balance should describe the energetic difference between two conformers of the compound.

A significant challenge in accurate description of hydration of organic ions is the need to account for contradicting energetic inputs from hydrophobic and hydrophilic parts of the ion.

**Table 2.1** – Solubility (M) of benzoic acid and benzoates in different solvents at 20°C [80]. As one may see from the data, solubility of benzoic acid increases as polarity of the solvent decreases. This is due to increasing efficiency of interactions between the acid and a solvent.

	Solubility, M
water	0.03
Ethanol	2.55
Methanol	2.84
THF	3.37

Importance of these contradicting inputs may be well demonstrated with changes of solubility of benzoic acid in different solvents (table 2.1).

Benzoic acid (fig. 1.2) is a good example to get insights into hydration/solvation pattern of organic ions. The acid has large hydrophobic benzoic ring and relatively small hydrophilic polar carboxylic group. This means, that if we change a solvent in such a way, that its molecules interact more efficiently with the benzene ring of the benzoic acid, the acid solubility should increase. The extent of this solubility increase depends on the efficiency of benzoate-solvent molecules interactions. This trend becomes clear when analysing data on solubility of benzoic acid in different solvents (see table 2.1). Although solubility data for non-aqueous solutions are restricted, the trend of increased benzoic acid solubility with decrease of the polarity of the solvents can be seen from the table 2.1. This well corresponds with the increase in efficiency of interactions between large benzoic ring of benzoic acid and molecules of less polar solvents.

Another important phenomenon in hydration of benzoic acid/benzoates is that its hydration shell is not spherical. There are two reasons for this: *i*) the molecule itself is not spherically symmetric, which restricts free movement of water molecules around the carboxylic group; and *ii*) the hydration shell around the carboxylic group is disturbed with hydrophobic benzoic ring of the molecule. Water molecules avoid the area in the direct vicinity of benzene ring. On the contrary, water molecules form hydration shell around hydrophilic carboxylic/carboxylate group of the molecule. As formation of hydration shell is energetically favourable, the density of water molecules here is higher, compared to the water density in the bulk. The area of increased water density (1.5 times of the bulk density and higher) is represented in figure 2.3. As one can see from the figure 2.3, hydration shell of the hydrophilic carboxylic/carboxylate group of benzoate is not spherically symmetric and has a complicated layered structure.

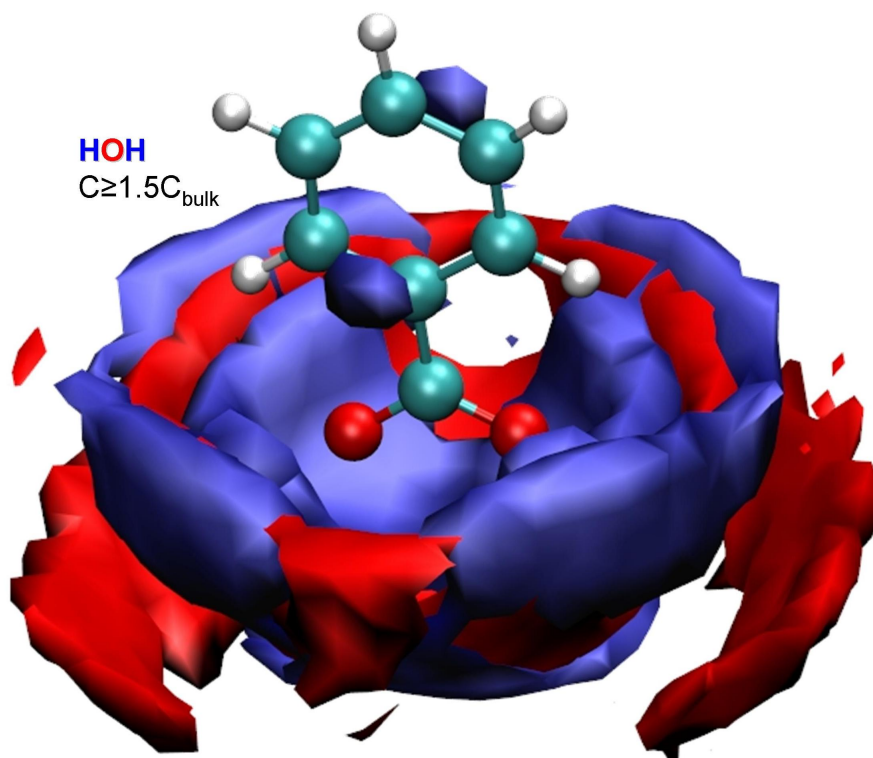


**Figure 2.3** – Hydration shells of a complex ion. An example of a hydration shells of a complex ion ( $-\text{COO}^-$ ). Blue areas represent positions of hydrogen atoms; red areas represent positions of oxygen atoms. The figure represents areas, where number water density exceeds the density of bulk water 1.5 times or more, which approximately corresponds to the first and second hydration shells.

## 2.3 Hydrates and solvates

As it was discussed previously, water molecules in the direct contact with an ion possess dynamic and energetic properties different from those of water molecules in the bulk. The binding between an ion and water molecules may have different strength. If strength of the binding cation-anion is weaker than cation-water and/or anion-water, than the compound forms crystallohydrates upon evaporation of water from the solution with some water molecules remaining in the structure of the solute. This remaining water is usually included into the crystal structure of the salt in stoichiometric ratio (mostly inorganic salts, e.g.  $\text{CuSO}_4 \cdot 5\text{H}_2\text{O}$ ). In other cases, the solvation shell could conserve its liquid-like state (e.g. non-crystalline proteins). In the present study we will not distinguish between these two types of solvent residues around a solute in a solid state.

A common feature of amorphous remaining solvation water and crystallohydrates is that in both cases this residual water usually does not evaporate under normal conditions. Thus in the case of  $\text{CuSO}_4 \cdot 5\text{H}_2\text{O}$  the crystallohydrate is stable until  $105^\circ\text{C}$ . At  $105^\circ\text{C}$  only two water molecules leave the salt crystals and the salt exists as  $\text{CuSO}_4 \cdot 3\text{H}_2\text{O}$  until the temperature of

150°C. Within the temperature range of 150 – 250°C copper sulphate exists as monohydrate. In other words, transfer of the crystalhydrate water molecule into vapor state requires significantly higher energy compared to evaporation of the bulk water, which boils at 100°C. Higher energy of transfer of water molecules from direct proximity of ions into vapour compared to bulk water molecules originates from energy gain which the system gets upon hydration.

Some solutes are capable of preserving water molecules from their solvation shells without forming crystals. The origins of the forces which prevent water molecules from evaporation from amorphous solid are analogues to the forces, which keep water molecules in crystal structure of salts. Proteins are an example of a solute which does not form a definite crystal structure, but preserves readily water molecules from its hydration shell from evaporation.

Similarly to water, other solvents also may remain attached to a solute upon evaporation of the bulk solvent. Thus the authors of [81] found, that fullerenes form solvates of composition 1:2 with toluene, bromobenzene and o-xylene. As carbon nanotubes are closely related to fullerenes, they could also form solvates, provided that interactions between the tubes and the solvent are strong enough to prevent the solvent molecules from evaporation.

## 2.4 Effects of ions on complex formation of cyclodextrins

As it was discussed earlier, ions introduce a perturbation to a system solute-solvent. One of the possible effects is ion effects on guest-host complex formation. An important representative of guest-host complex formation is complex formation between drug-like molecules and cyclodextrins. It is common to separate these interactions into non-specific (effects of ionic strength) and specific.

### 2.4.1 Non-specific effects of ionic strength.

Non-specific ion effects are usually denoted as effects of ionic strength. These effects are the most basic type of effects. They affect structure of hydration shell of the solutes. Reorganisation of hydration/solvation shells of solutes is always involved in the process of complex formation. Participation of hydration shells of solutes in the process of complex formation may be summarized in the following steps: *i*) reorganisation of the hydration shell of the guest molecule with removal of water molecules, which interfere with the complex formation; *ii*) similar reorganisation of hydration shell of the host molecule with removal of water molecules, which interfere with the binding to the guest molecule; and *iii*) formation of hydration shell of the newly composed

complex.

As ions may significantly affect the structure of water, they *indirectly* affect the process of complex formation, e.g. via restructuring of hydration shells. As energy of complex formation is usually low, the ion-induced changes in behaviour of hydration shells may significantly affect the measured stability constant. It is important to note here the difference between the thermodynamic equilibrium constant and the equilibrium constant measured at certain conditions.

The true thermodynamic equilibrium constant *does not* depend on any parameters of the solutions (ionic strength, pH, buffers) and represents the affinity of two species to each other. These constants are rarely measured in practice. Usually stability constants are measured at the fixed pH level of the solution, in presence of buffers or salts to keep the ionic strength constant. Stability constants measured at particular parameters of a solution are denoted as apparent or conditional constants. Apparent constants always depend on the solution parameters and can change significantly with a change of conditions, e.g. from one pH to another, or from one ionic strength to another. As apparent constants depend on the solution parameters, they may be significantly affected by indirect ion effects. These indirect ion effects on the binding constant of cyclodextrins with a guest molecule have been demonstrated in work [82].

Indirect ion effect is often associated with an *increase* of the binding constant. It can be explained by the following. Guest molecules, which bind to cyclodextrins often have large hydrophobic part. Hydration of this part is usually unfavourable. Upon addition of salt the unfavourable interaction between water molecules and the hydrophobic part of a molecule becomes even less favourable. This, in turn, decreases solubility of the organic molecule, followed by aggregation or precipitation in order to reduce contacts between ionic solution and the guest molecule. Formation of a guest-host complex also reduces effectively interactions between the guest molecules and its hydration shell, which makes the process energetically more favourable compare to pure water (example may be found in work [83]).

#### **2.4.2 Specific cyclodextrin-ion interactions. Competition for the cyclodextrin cavity.**

Additionally to indirect effects, ions are capable of interacting more specifically with cyclodextrins and form complexes. Unlike non-specific ion effects, competition for the cyclodextrin cavity always leads to a significant decrease of the binding constant CD-organic guest molecule. As a rule, cations do not bind with cyclodextrins, while large anions are capable of forming quite stable complexes. Smaller anions, e.g. chloride, do not bind to the cyclodextrin cavity or this

interactions has very low ( $\sim 1$ ) binding constant. This interaction between the anion and the cyclodextrin competes with interactions between cyclodextrin and guest molecule, which, in turn, may lead to a significant drop in the binding constant between cyclodextrin and the guest molecule.

## 2.5 Solvation in N-methylpyrrolidone

Any liquid may be a solvent. Structure and properties of different liquids vary significantly from one solvent to another. This creates vast variety of different ways to solvate the same solute. Despite the differences in structures of solvents, the pattern of the process of solvation is quite general for all solvents and solutes, irrespective of chemical physical nature of solvents and solutes (see above). This difference in the chemical nature results in the fact that details of the solvation pattern as well as energies of solvation may change significantly depending on the solute and/or solvent. Such, solvent molecules with long flexible alkane chain may undergo a significant conformational change in order to maximize energetic gain of the solvation. On the other hand, just like water, solvent molecules in the direct proximity of an ion interact and repel each other, which prevents large number of solvent molecules from being in the direct contact with an ion or solute. The number of molecules in the direct contact with the ion or solute is usually denoted as solvation (or coordination) number. Like in water, ordering of the coordinated solvent molecules is different compared to the bulk solvent and these molecules are denoted as solvation shell. Solvation in organic solvents is usually less studied than solvation in water. Some aspects of solvation of inorganic ions in NMP were explored in the work [10].

### 2.5.1 Solvation of ions in NMP

Solvation in non-aqueous solutions is studied in less details compared to aqueous solutions. The work [10] studies the molecular pattern of inorganic ion solvation in NMP with molecular dynamics simulations. According to these simulations, ions dissolved in NMP have distinct solvation shells (see fig. 2.4). These distinct solvation shells originate in electrostatic charge-dipole interactions (the dipole moment of NMP is about 4.1 Debye). As one may see from the figure 2.4 both of the ion-NMP radial distribution functions show a peak (at  $r = 0.42$  and  $r = 0.55$  nm for  $\text{Na}^+$  and  $\text{I}^-$  respectively), followed by a hollow (at  $r = 0.50$  and  $r = 0.70$  nm for  $\text{Na}^+$  and  $\text{I}^-$  respectively), indicating formation of the first solvation shells around the ions.

The structures of the solvation shells of the ions are different: the negatively charged NMP

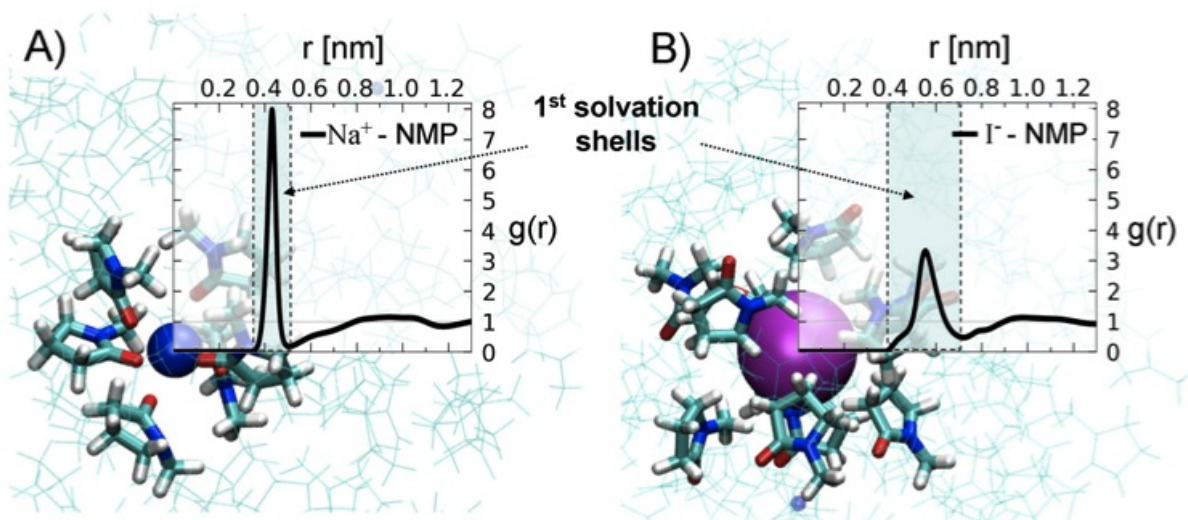


**Figure 2.4** – Solvation of ions in NMP. Ion-NMP (center of mass) radial distribution functions,  $g(r)$ , in NaI-NMP solution combined with corresponding simulation snapshots: (A) sodium ion (shown as a blue sphere), (B) iodide ion (shown as a magenta sphere). The highly noticeable peaks on the  $g(r)$  functions indicate distinct solvation shells around the ions. In the simulation snapshots the NMP molecules in the first solvation shell around the ions are represented by thick sticks. The oxygen atoms in these molecules are coloured in red, nitrogen in blue, carbons in cyan and hydrogen in white. Other NMP molecules are shown with thin cyan lines. Reproduced from [10].

oxygen atoms are strongly attracted to the positively charged sodium ions (see the snapshot illustrating typical configuration of the NMP molecules around this ion in Fig. 2.4A); from another side, the oxygen atoms are oriented outwards from the negatively charged iodide ions (see the molecular snapshot on Fig. 2.4B). In general, similar to the mechanisms of ion solvation in water [84, 85, 78] there is a strong asymmetry in sodium and iodide ions solvation in NMP. As illustrated by the high peak on  $\text{Na}^+$ -NMP  $g(r)$  (Fig. 2.4), the sodium ion solvation shell is very dense because the ion is relatively small and, consequently, has a large surface charge density [50].

The authors of the work [10] observe in their molecular dynamics simulations that ions, dissolved in NMP have distinct solvation shells (see Fig. 2.4). That was expectable, because NMP is a very polar solvent (the dipole moment is about 4.1 Debye) and, therefore, the NMP molecules interact strongly with the dissolved ions due to their electrostatic charge-dipole interactions. The boundaries of the ion solvation shell were estimated as the region with non-zero ion-NMP radial distribution function ending at the first distinct minimum on the corresponding function. Interestingly, despite high polarity of NMP molecules, the second solvation shell is absent for both ions (sodium and iodide).



### 2.5.2 NMP based dispersions of carbon nanotubes

The chemical nature of carbon nanotubes is quite inert. As a result, the surface of carbon nanotubes does not readily participate in interactions with a solvent, which makes carbon nanotubes very solvophobic. Despite solvophobicity of CNTs, their relatively stable dispersions may be obtained in a variety of organic solvents as well as in water. Aqueous dispersions of carbon nanotubes are always stabilized with some surfactants, as water alone is not capable to disperse CNTs. Dispersions of carbon nanotubes in some organic solvents may be obtained without the help of surfactants.

N-methylpyrrolidone (NMP) is one of organic solvents, belongs to the class of dipolar aprotic solvents which includes also dimethylformamide, dimethylacetamide and dimethylsulfoxide. Its structure is shown in the figure 1.5. NMP is one of a few solvents which are capable of dispersing carbon nanotubes in relatively high concentrations (up to 15 mg/ml) without any surfactants. The NMP-based carbon nanotube dispersions are stable in time and show some properties of real solutions [86], e.g. establishment of a dynamic equilibrium between bundles and single tubes in the solution. The dispersion of CNTs in NMP is stable for at least several weeks. Some studies reveal even a few signs, that CNT-NMP dispersions are, in fact, real solutions [87].

The possibility of preparation of stable dispersions of carbon nanotubes is an important condition for studying ion effects on association processes in carbon nanotubes dispersions. As it was described previously, ion effects originate in interplay of different forces, acting on the solute in a solution. As we increase the number of solutes in a solution, we increase the number of mutual interactions between the solutes (see fig. 1.1). The authors of the works [88, 89] demonstrated that salts significantly affect stability and composition of surfactant-based aqueous dispersions of carbon nanotubes. These results, however, may not be interpreted in a unique way and need consideration of interactions between ions and surfactants as well as *ion induced changes* in the following mutual interactions: surfactant-tube, surfactant-water and water-tube (introduction of another complex unit into the scheme in the figure 1.1). Surfactant-free NMP based dispersion of carbon nanotubes represents a great possibility to directly study ion effects on stability of carbon nanotubes dispersion.

## 2.6 Solvation. Solutions and dispersions

A solution is a system in thermodynamic equilibrium, therefore, it is stable in time. However, many multicomponent liquid systems are not stable over long periods of time, in other words,

these systems possess only kinetic stability. These kinetically stable systems are denoted as "colloidal dispersions", or to make it shorter "dispersions". Dispersions are different from solutions mainly in terms of the size of the dissolved/dispersed particles. Conventionally, the border between solutions and dispersions is defined at 1 nm: if particles of a dissolved substance are smaller than 1 nm, than they form a solution; if particles are larger than 1 nm, than they form a dispersion. The border between solutions and dispersions is quite artificial. On the other hand, 1 nm is an approximate border, above which the destabilizing gravity forces start to overcome the stabilizing Brownian motion acting on the dissolved/dispersed substance. This, in turn, leads to a gradual decrease of a solution/dispersion stability with an increase of a particle size of a dissolved/dispersed substance.

Although with an increase of the particle size of a dissolved/dispersed substance, the balance between the Brownian motion and gravity changes dramatically, other forces, acting on the dissolved/dispersed substance, do not change significantly: a dispersed substance may participate in hydrogen bonding, van der Waals and electrostatic interactions, etc. just as a dissolved substance does. This allows one to apply a term "solvation" and connected terminology to describe molecular level details of interactions in dispersions.

## 2.7 Chapter conclusions

A solution is a complex dynamic system, where dissolved particles are in equilibrium with solvent. This equilibrium is strongly affected by introduction of another solute into the solution, e.g. ions. Ions form real solutions in water and some other organic solvents, e.g. NMP. Ions strongly affect structure of water in their solvation shells. These changes, in turn, may dramatically affect other processes in a solution, e.g. processes of association.

A real solution is a thermodynamically stable system in a dynamic equilibrium. This leads to two main consequences: *i*) real solution is stable for an infinitely long period of time; and *ii*) processes associated with dissolution (e.g. solute dissociation, appearance and solvation of new solvation interfaces) happen constantly in a solution just like the processes, associated with separation of solution components (precipitation). Real solution may exist only if particles of the dissolved compound are smaller than  $\sim 1$  nm. If the particles of the dissolved compound are larger than 1 nm, the gravity forces acting on them usually outbalance solvation forces and the dispersion aggregates and precipitates, which results in gradual separation (degradation) of dispersions. This is usually referred as kinetic stability of dispersions. Although dispersions are only kinetically stable, it is possible to apply thermodynamic laws to them.

In this work we focus on ion effects on association processes in liquid solutions and dispersions. We consider ion effects on complex formation between aromatic carboxylic acids and  $\alpha$ -cyclodextrin in aqueous solutions and effects of ions on stability of carbon nanotubes dispersions in N-methylpyrrolidone.

# 3

## Experimental methods

Liquid media is a very dynamic media, i.e. molecules are not statically fixed in a predefined positions. Instead, they are in the constant Brownian motion: they hit each other as well as the molecules of vessel walls, as they move, they exchange energies, change their movement velocities and directions. Therefore, one should not think about liquids as about motionless and static systems. On the other hand, static *simplified models* offer a convenient way to represent the pattern of solvation. This is why in this work we actively employ simplified static models to explain the *general pattern* of solvation.

There are two approaches to study solvation pattern at the molecular level: computer simulations and modern experimental techniques. Both approaches represent significant challenges in terms of standardisation and characterisation of the obtained results as well as separation of representative results from artefacts. Therefore, it is very important to understand parameters and functions employed to characterize a solution. In this work we combined both the laboratory and computer experiments to gain as much information about the molecular level details of processes at solvation interface as possible. The description of the experimental techniques used in this work, is presented below: the computer experiment is represented mostly with classical molecular dynamics simulations (MD) while variety of laboratory experimental techniques are used.

### 3.1 Molecular dynamics simulations

Classical molecular dynamics simulations is a technique for computing the equilibrium and transport properties of a many-particle system, where the dynamics of particles obeys the laws of classical mechanics. Classical mechanics is an appropriate approximation for a wide variety of

systems, including liquid solutions and solid state systems, which do not require consideration of translational or rotational motions of light atoms or molecules (e.g. He, H<sub>2</sub>, D<sub>2</sub>) or vibrational motion at high frequencies  $\nu$ , so that  $h\nu > k_B T$ . As MD simulations do not consider quantum effects, they are much cheaper compare to quantum simulations. This is why MD simulations can be used for modelling of larger systems (tens to millions of particles) which makes MD a powerful tool to simulate molecular level details of processes at the solvation interfaces.

In order to compute properties of a many particle system, each particle in the system should be characterized with coordinates, velocities, and accelerations as a function of time. To obtain coordinates, velocity and accelerations as a function of time, one needs to integrate the equations of particles motion. For this one needs to construct a Lagrangian depending on positions of all particles:

$$L(x, \dot{x}, t) = \sum_{i=1}^{3N} \frac{1}{2} m_i \dot{x}_i^2 - U(x, t),$$

where  $U$  is the potential energy of the system;  $x_i$  is the spatial coordinate of a particle in the system;  $N$  is the number of particles in the system;  $x = \{x_1, \dots, x_{3N}\}$  is the vector of all the particle coordinates in the system (each particle has 3 coordinates in the real space);  $\dot{x}_i$  is the velocity vector component;  $\dot{x}$  is the vector of all particle velocity components in the system;  $m_i$  is the mass of the particle;  $t$  is time.

The equations of particle motion can be written as:

$$\frac{d}{dt} \frac{\partial L}{\partial \dot{x}_i} - \frac{\partial L}{\partial x_i} = 0, (i = 1, \dots, 3N),$$

or equivalently:

$$\left\{ \begin{array}{l} m_1 \ddot{x}_1 = -\frac{\partial U(x_1, \dots, x_{3N})}{\partial x_1} \\ m_2 \ddot{x}_2 = -\frac{\partial U(x_1, \dots, x_{3N})}{\partial x_2} \\ \dots \dots \dots \\ m_{3N} \ddot{x}_{3N} = -\frac{\partial U(x_1, \dots, x_{3N})}{\partial x_{3N}}, \end{array} \right. \quad (3.1)$$

where  $-\frac{\partial U(x_1, \dots, x_{3N})}{\partial x_i} = F$  is the force vector component acting on the particle with  $x_i$  spatial coordinate;  $\ddot{x}_i$  is the acceleration vector component.

Molecular dynamics solves the equations of motion 3.1 to obtain  $x(t)$  and  $\dot{x}(t)$  which is sufficient for full mechanical description of a system at every time step ( $t$ ). The system of equations of motion does not have an analytical solution for more than two particles ("many body

problem"). That is why one has to employ numerical methods and utilize significant computer resources to obtain a solution for a system of reasonable size.

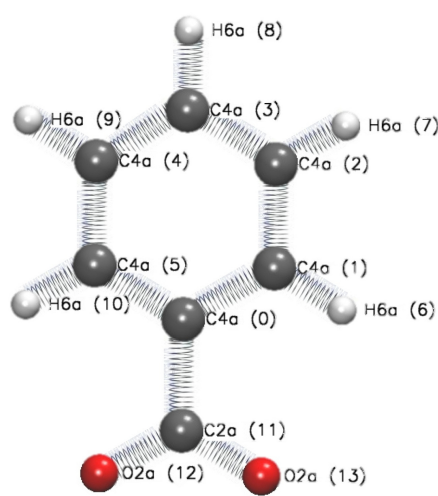
### 3.1.1 Preparation of a simulation cell

Initial coordinates and velocities are generated during the construction of the simulation cell. Construction of the simulation cell in MD simulations is very similar to a laboratory experiment. The reasons for this similarity are as follows. First of all, one needs to design an experiment. To do this, one needs to understand, which property one would like to measure. Having this in mind, one needs to prepare a simulation cell (sample), bring it to a certain temperature and sustain the temperature (thermostat), and sometimes a certain pressure (barostat). Further one needs to *measure* a property and evaluate statistical errors in the measurements. If quality of measurement and error values turn out to be satisfactory, the experiment could be stopped. Otherwise, one needs to prolong the measurements until their quality reaches the appropriate level. The precision of MD simulations may be evaluated using the known algorithm [90].

Let us now follow a typical procedure of preparation of a structure for MD simulations. First of all, one needs to define a solute molecule(s) position. Let us use sodium benzoate as an example. Now one needs to locate all atoms of a benzoate anion (see table 3.1). Afterwards, one needs to assign atomic parameters to each atom, describe covalent bonds in the molecule and potentials, which govern bonded atoms interactions (see fig. 3.1). A consistent set of atomic parameters, used in a simulation can be addressed as a force field. As the same chemical element may show different kinds of interactions with other species (e.g. aromatic carbon atom and carbon atom in a hydroxylate group), one needs to distinguish types of atoms of the same element (e.g. atoms C4a and C2a in table 3.1). Another important feature of a structure for an MD simulations is the necessity to distinguish between atoms of the same type, as they may be placed differently in the molecule (e.g. atoms C4a in the table 3.1). To satisfy this requirement one should use atomic indexing (see the column "index" in the table 3.1).

When the main solute molecule is in place, one needs to solvate it. To solvate a solute in MD simulations means to immerse the model of a solute into a model of a solvent. Solvent models may be explicit or implicit. The number of solvent molecules is limited by the system size and the solvent density at the temperature of simulations. One should take care to avoid sterical clashes between solvent molecules and solute molecule(s). At this stage the system has a negative charge, as benzoate anion is negatively charged while solvent molecules are neutral. To neutralize the system one random solvent molecule should be replaced with a cation ( $\text{Na}^+$ ).

**Table 3.1** – Representation of a molecular structure in molecular dynamics. The table includes description of each atom in the solute. It also distinguishes between different atom types of the same element (e.g. C4a and C2a), as well as between different atoms of the same atom type (indexes).



atom name	index	x	y	z
C4a	0	0.088	-0.001	-0.000
C4a	1	0.018	0.122	0.000
C4a	2	-0.123	0.123	0.000
C4a	3	-0.195	0.002	0.000
C4a	4	-0.125	-0.121	0.000
C4a	5	0.016	-0.122	0.000
H6a	6	0.074	0.214	0.000
H6a	7	-0.176	0.217	0.000
H6a	8	-0.303	0.003	0.000
H6a	9	-0.180	-0.214	0.000
H6a	10	0.070	-0.215	-0.000
C2a	11	0.239	-0.002	-0.000
O2a	12	0.298	-0.113	-0.000
O2a	13	0.300	0.107	0.000

This replacement neutralises the system as a whole. As the last step in the preparation algorithm one should randomly assign velocities to each particle in accordance with Maxwell distribution for the given temperature.

### 3.1.2 Solvent models. Explicit and implicit models

Employing of one of the solvent models is essential in simulations of processes at solvation interface. All solvent models may be divided into explicit and implicit solvent models. Explicit solvent models explicitly treat every molecule of the solvent. On the contrary, implicit solvents models represent solvent as a continuous medium with a dielectric constant of a real solvent. Both explicit and implicit solvent models have their own strong and weak sides. Explicit solvent models are computationally more expensive compared to implicit models as they require inclusion of large amount of particles in the simulations. On the other hand, explicit solvent models are capable of reproducing granularity, viscosity and other molecular level details of solvent behaviour at solvation interface. Most importantly for this study, implicit solvent models

are not capable of reproducing structures of solvation shells and solvation interfaces. Therefore, it is crucial to use explicit solvent models for studying of ion effects at solvation interfaces.

In this work we performed molecular dynamics simulations with explicit water model TIP4P [91, 92]. This model proves to describe correctly structural and thermodynamical properties of the real water. Combination of a solvent model and a solute model is denoted as a molecular dynamics system or a cell or a box.

### 3.1.3 Calculation of forces and Force Fields

One can see from the equations 3.1 that it is not sufficient to know spacial positions of all particles in the system. One also needs to know potential energy of the system. The most direct and general way to obtain potential energy of a system is to solve the Schrödinger equation. In this case we would need to take into account each nuclei and each electron separately, which would result in a huge amount of particles, and, as a result, would lead to enormous computational expenses. This is why *Ab initio* simulation of a system of a typical MD size is not feasible at present. Therefore, MD approximates atoms or groups of atoms as molecular sites. In fully atomistic MD each atom is represented as a separate molecular site, making terms "molecular site" and "atom" synonymous.

Approximation of atoms and groups of atoms as a molecular site reduces amount of calculations significantly, which makes acceptable the costs of simulations of systems of reasonable size ( $10^4$ – $10^5$  particles). On the other hand, this approach presents a new challenge: we can not deduct potential energy of the system as in *ab initio* simulations. To eliminate this drawback we need to describe effective potentials, which govern interactions between all possible molecular sites (see fig. 3.1). The effective parameters for the inter-atomic potential should be parametrized by fitting against experimental data or data from high level quantum simulations. A complete set of effective parameters is often referred as a force field. Molecular interactions can be classified into intramolecular (or bonded) and intermolecular (or non-bonded), such that  $U = U_{\text{bon}} + U_{\text{nb}}$ . Bonded interactions are the interactions between the atoms in the same molecule if the atoms are separated by one or two covalent bonds (e.g. atoms 1 and 2 and 1 and 3 in the figure 3.1). If there are three or more covalent bonds separating interacting atoms (e.g. atoms 1 and 4 in the figure 3.1), those interactions are usually addressed as 1-4 interactions.

It is common to represent a potential energy of bonded interactions ( $U_{\text{bon}}$ ) of a system as a sum of the following terms: *stretching*, *bending* and *dihedral* terms (see fig. 3.1). A covalent bond between two atoms is described with a stretching term, which usually has a harmonic form.



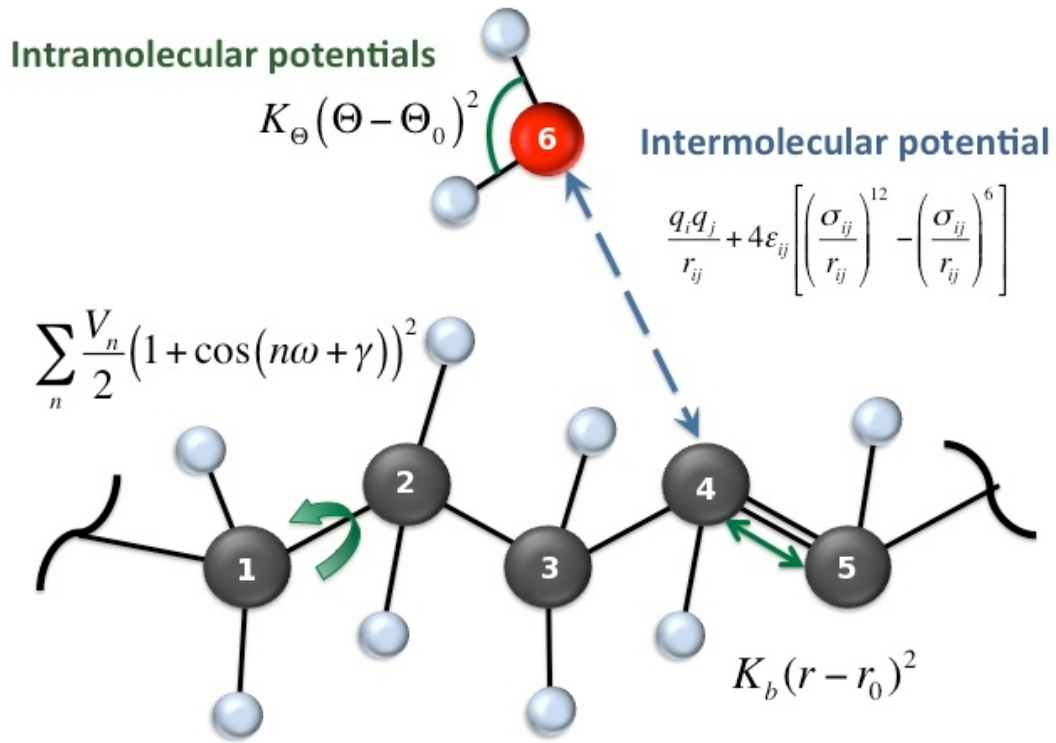


**Figure 3.1** – Representation of inter- and intramolecular interactions. Interactions in a typical molecular dynamics system are divided into intramolecular and intermolecular. Intermolecular interactions are represented with stretching, bending and dihedral terms. Adapted from [93].

The angle between two bonds is described with bending term, which is usually described with a harmonic potential as well. Dihedral term describes rotation of two molecular groups relatively to each other. This term is usually represented via the Fourier series. Combining all three terms together one can formulate an expression for the intermolecular part of the potential energy of the system in the following way:

$$U_{\text{intra}} = \sum_{N_{\text{bonds}}} k_b (r - r_0)^2 + \sum_{N_{\text{angles}}} k_{\Theta} (\Theta - \Theta_0)^2 + \sum_{N_{\text{dihedrals}}} \sum_n \frac{V_n}{2} (1 + \cos(n\varphi + \gamma)),$$

where  $k_b$  and  $k_{\Theta}$  are stretching and bending force constants respectively;  $r_0$  and  $\Theta_0$  are equilibrium values of the bond length and angle respectively;  $V_n$  are the Fourier series coefficients;  $\gamma$  is the cosine phase. All these parameters should be parametrized against the experimental data or data from high level quantum simulations.

It is common to subdivide non-bonded interactions into the van der Waals and Coulomb interactions. The Lennard-Jones (LJ) potential usually represents the van der Waals interactions.

Therefore, one can write the expression for the potential energy of non-bonded interactions as

$$U_{\text{nb}} = \sum_{N_{\text{nb}}} \left\{ 4\epsilon_{ij} \left[ \left( \frac{\sigma_{ij}}{r_{ij}} \right)^{12} - \left( \frac{\sigma_{ij}}{r_{ij}} \right)^6 \right] + \frac{q_i q_j}{r_{ij}} \right\} \quad (3.2)$$

Here the term in squared braces describes van der Waals interactions with LJ potential; the term  $\frac{q_i q_j}{r_{ij}}$  describes Coulomb interactions. Intermolecular interactions in MD are usually approximated to be pair-wise additive. Therefore, if a system contains  $N$  particles, complexity of energy calculations is proportional to  $N^2$ .

As one can see from the LJ part of the equation 3.2 van der Waals forces decay rapidly with increase of inter-particle distance (proportional to  $r^{-6}$ ). To put it differently, these forces can be classified as *short-range forces*. As these interactions decay within a few atomic distances, it is reasonable to evaluate them only for small distances between particles. Therefore, to save the computational power, one can introduce the cut-off distance ( $R_{\text{cut}}$ ) for the LJ potential without loss of accuracy of MD calculations.

Introduction of the cut-off distance is one of the techniques, used to make the MD simulations less computationally expensive. There are also other techniques available to increase speed of MD simulations by making calculation of short range interactions more efficient. One of the most effective techniques is a technique named cell lists. In this technique the initial simulation cell (and all its copies) are divided into smaller subcells with the edge length slightly greater than  $R_{\text{cut}}$ . All particles located within a subcell are listed and the list is stored in the memory. Further one needs to evaluate short-range interactions between particles within the interparticle distance less than  $R_{\text{cut}}$ . We assume that particles do not move significantly within a small time interval (a few integration steps). That is how we know all potential neighbouring particles for a few simulations steps and we do not need to check every particle in the system whether it is within the  $R_{\text{cut}}$  distance to the particle of interest. The procedure employed in the cell lists method reduces the complexity of evaluation of short-range interactions for large systems from  $O(N^2)$  to  $O(N)$ . In turn, the Coulomb interactions decay slowly (proportional to  $r^{-1}$ ) and therefore these interactions are considered as *long-range* interactions. In this case a simple cut-off technique leads to a significant artefacts. Instead, there are several techniques available to speed up evaluation of long-range interactions (Ewald summation, P3M, PMM). The most popular of them is the Ewald summation method.

**Ewald summation method in 3D and 2D periodic boundary conditions.** The main idea of Ewald summation method is as follows. Let us consider a system of point charges being

infinitely replicated in all three directions. We make an assumption that our liquid has a crystal-like structure with the original simulation cell being the unit cell of the lattice. The Coulomb interaction energy is then the sum of interaction energies between the charges of the original cell and all the charges of the lattice.

Simulations with 3D periodicity imitate systems, which are uniform in all three directions, i.e. uniform liquids, gases and solids. However, there is a variety of systems with interfacial layers which can not be described with 3D periodicity: surfactant in interfacial layer, pores, liquid-vacuum interactions are just a few examples of this type of systems which are periodic in only two directions. In the case of a system with 2D periodicity, it does not have any physical sense to calculate the electrostatic interactions in all three dimensions. This is why one should use specially designed 2D techniques to evaluate electrostatic interactions in these systems.

There are several techniques to compute long-range interactions in systems with 2D periodicity. The most straightforward solution is to use the same approach as for the 3D Ewald summation but restrict the summation to vectors in  $x$  and  $y$  directions only. In this case the energy should be calculated as

$$U_{\text{Coul}} = \frac{1}{2} \sum_{i,j=1}^N \sum_{\mathbf{n}} \frac{q_i q_j}{|\mathbf{r}_{ij} + \mathbf{n}|},$$

where the summation over  $\mathbf{n} = (L_x n_x, L_y n_y, 0)$  indicates that periodicity is only imposed in the  $x$  and  $y$  directions. This equation is inconvenient from a computational point of view. Unlike the three dimensional case, the double sum over the particles in the Fourier part of this equation can not be expressed in terms of the square of a single sum. This makes the calculation significantly more expensive than the three-dimensional counterpart. Several methods have been developed to increase the efficiency of evaluation of Ewald sum for 2D periodic systems.

The most obvious way to simulate interfaces is to add a slab of vacuum between the periodic images (see fig. 3.3). However, this approach presents the following challenge. Even a slab, which is four times the distance between the charges, does not give us the correct limiting behaviour. This is because a periodically repeated slab behaves like a stack of parallel plate capacitors. Yeh and Berkowitz introduced a correction which improves the limiting behaviour in the limit of an infinitely thin slab [94, 95].

### 3.1.4 System control

From the point of view of statistical mechanics, MD system is a particle ensemble. There are three particle ensembles in statistical thermodynamics: microcanonical ensemble (constant  $N$ ,

V, E), canonical ensemble (constant N, V, T) and grand canonical ensemble (constant  $\mu$ , V, T). However, there are possibilities to modify those ensembles in the MD simulations, for example, a canonical ensemble with a constant pressure (NPT), a canonical ensemble with a constant pressure and area (NPAT), a canonical ensemble with a constant pressure and surface tension ( $NP\gamma T$ ). Sustaining constant parameters requires employment of additional techniques, e.g. thermostats for keeping the "temperature" of the simulations constant.

### Thermostat and barostat

Molecular dynamics simulations were designed to be performed on an ensemble of particles which has constant total energy. Unfortunately, this approach has two major drawbacks: *i*) gradual accumulation of numerical errors leads to a drift in total energy; and *ii*) constant energy of the ensemble complicates comparison of the simulation results to the experimental ones, as experimental results often correspond to isothermal-isobaric or isothermal ensemble (constant temperature and pressure or only constant temperature).

The idea of involving different kinds of thermostats and barostats into molecular dynamics simulations was introduced to resolve the problems with numerical errors as well as comparison with practical experiments. One of the most established methods to keep temperature and pressure constant in the simulations is to scale kinetic energies of the system and the distance between particles correspondingly [96]. In 1984 Berendsen *et al.* [96] proposed one of the most popular these days algorithms of temperature and pressure corrections. The main idea of the algorithm is to introduce so called weak coupling between the system and the bath of the proper temperature and pressure by introducing a global stochastic coupling into the modified Langevin equation. Berendsen thermostat represents a form of velocity scaling thermostats. Unfortunately, velocity-scaling thermostats have a serious artefact, denoted as flying ice cube effect.

The flying ice cube phenomenon is an artefact of molecular dynamics simulations, caused by a thermostat. For the first time it was described in the work [97]. The authors observed an effect of rearrangement of kinetic energy of the system, when the kinetic energy from motions with high frequency was transferred to motions with low frequency due to intrinsic inconsistencies of scaling approach. This behavior of a system contravenes to a principle of equipartition of energy, which requires an equal distribution of kinetic energy between all degrees of freedom in the system. Moreover, this allows some unphysical artefacts, e.g. restriction of atom and group of atoms vibrations and appearance of a centrifugal force due to increased kinetic energy of the center of mass of the system, which is capable to affect the structure of flexible molecules.

Harvey [97] suggests three primary methods of removing the artifacts, connected to the flying ice cube phenomenon: *i*) substitution of the rescaling velocities to reassigning velocities; *ii*) periodic removal of motion of center of mass; and *iii*) modification of the currently used algorithms of the velocities rescaling in such a way, that the rescaling would be done with regards to the time averaged kinetic energy instead of instantaneous kinetic energies in the original approach. The suggestion to remove periodically motion of the center of mass is implemented into several molecular dynamic simulation software, including that of Gromacs [98].

### **Periodic boundary conditions**

MD simulations usually deal with systems of  $10^4$ – $10^5$  particle size. A small droplet of water falling from a 1 mm wide glass pipette tip contains roughly  $10^{21}$  water molecules. By comparing these two numbers ( $10^5$  and  $10^{21}$ ) one can easily understand that results obtained with a typical MD simulation can not be directly transferred to real bulk systems. On the other hand, a direct simulation of a small droplet is not feasible. To avoid this contradiction and be able to simulate bulk solutions one should employ periodic boundary conditions (PBC).

The PBC technique works in the following way. We create 24 images of the initial simulation cell (see fig. 3.2) and surround the initial cell with its copies in 3D. Particles in each cell copy repeat the motions of particles in the original cell. In other words, if one particle leaves the initial cell at the top boundary, than its copy leaves the cell copy below and enters the original cell from the bottom. As a result, the number of particles remains the same and the cell is closed on itself. It effectively simulates an infinite bulk media. The PBC work also for the energy and force calculations for particles interacting via the short-range potentials. In other words, the short-range potential accounts all the particles within its cut-off distance, even those particles which belong to the copy of the original cell.

Although PBC are very useful in simulation of an infinite bulk solutions, they are not helpful in simulations of systems at macrointerfaces. In this case one needs to create a surface (interface) in the simulations. However, one can not completely skip PBC because the real surfaces have a geometry which differs significantly from a geometry of a simulation cell. Molecular dynamics simulations solve this problem with 2D periodic boundary conditions. In both cases periodic boundary conditions are applied to the systems, however, the initial cells' structures differ. An example of 2D periodic boundary conditions is represented in the figure 3.3.

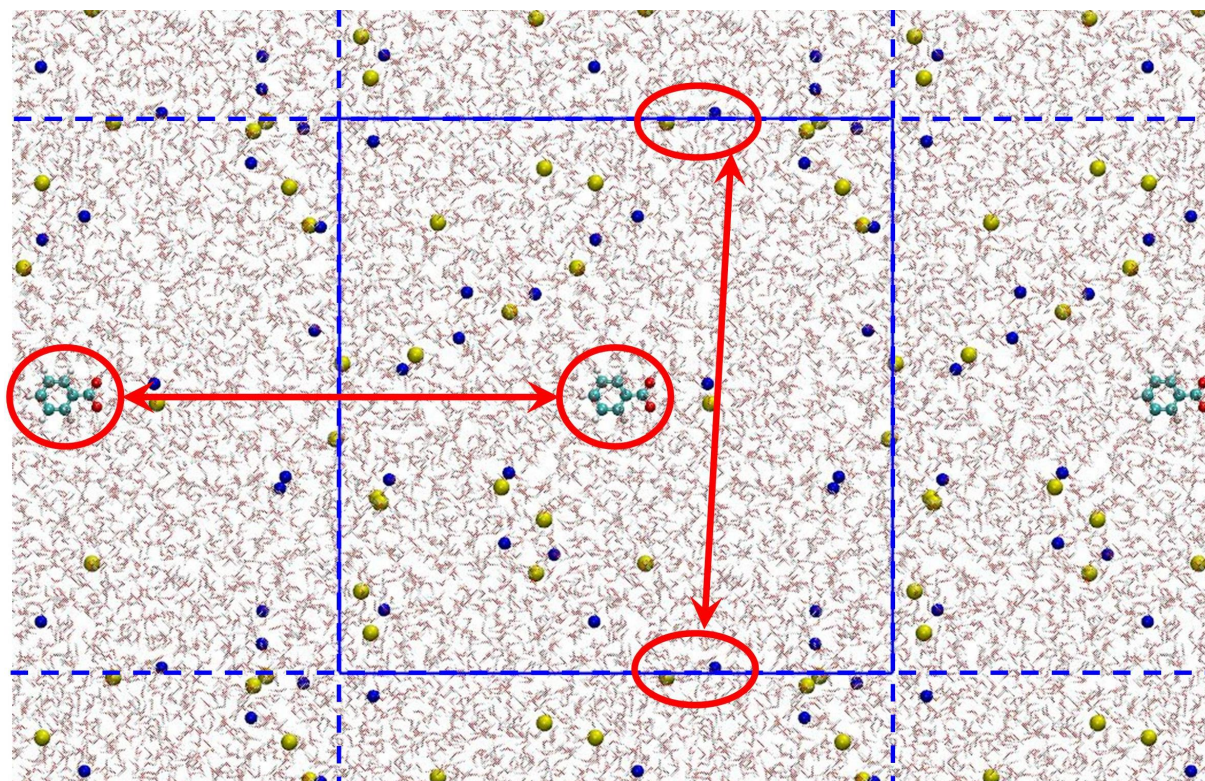


**Figure 3.2** – A typical bulk simulation cell. The whole cell with every particle in it is repeated in all directions. As a result, when a particle leaves the cell, its copy image comes to the cell from the opposite side. This prevents the system from "blowing up" and mimics bulk solution.

### Choice of simulation cell size

Molecular dynamics simulations are capable of simulating a reasonably large system. Nevertheless the typical size of a molecular dynamic simulation system is far below any macroscopic systems. This is why it is very important to select wisely the *smallest possible* simulation box, so that it would correctly represent behaviour on the bulk keeping the simulation costs at minimum.

There are several criteria to consider when choosing dimensions of the simulation box: long range interactions, structures of solvation shells, intrinsic features of the solute, and properties, which should be measured. Let us briefly go through these criteria.

**The solute structure** plays the most important role when it comes to defying the simulation system size. The very first thing to consider when choosing the simulation system size is that the solute of interest has to fit inside the box. In the case of large periodic molecules, e.g. graphene, it is important to fit the elementary cell of the molecule into the simulation system. In the case of periodic molecules it is important to properly address their periodic nature. Ability of a simulation software to handle periodic molecules in this case is a very important issue in the choice of a software.

**Short range interactions** are represented with hydration/solvation shells. When constructing

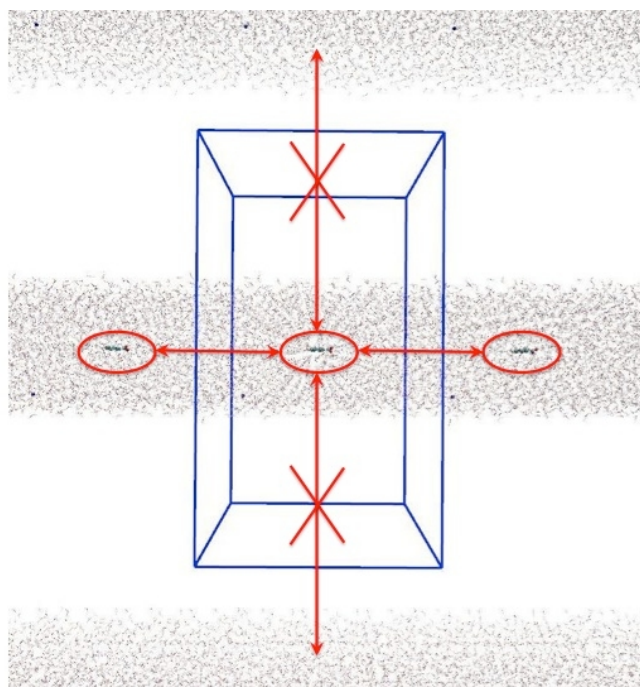


**Figure 3.3** – A typical simulation cell with a slab geometry. Although the whole system is repeated in all directions, the liquid phases are separated in one direction by a slab of vacuum or a solid object. In this case interactions take place only within the slab of liquid. This creates a phase separation and, as a result, the simulations mimic interface solution-vapour or solution-solid.

a simulation cell, it is important to take into account that hydration shells of a solute do not interfere with hydration shells of the solute's copy in the neighbouring copy of the simulation shell. In other words, it is important that the simulation box is large enough to fit all solvation shells of the solute inside. The work [78] shows that perturbations, caused by immersion of a spherical solute in water, spread for up to  $\sim 1$  nm.

**Measured properties** play an important role in the size and shape of a simulation cell. The simulation cell should be large enough to allow a sufficient sampling, allow free rotation of a solute, allow enough of distance for pulling simulations, etc. A researcher should consider the volume and/or linear dimensions of the cell, which would allow to measure the property of interest. As a short example one could bring simulations with pulling of an ion towards a solute. In this case the simulation cell should be large enough to comply with the following criteria: *i*) the simulation cell should allow a sufficient separation of the ion and the solute at the beginning of the simulation to prevent interactions between the ion and the solute; *ii*) the ion should not interact with a copy of the solute in the simulation cell copy.

**Electrostatic interactions** of the solute should not include interactions with a copy of the solute. One may estimate this with the Bjerrum length. The Bjerrum length is a separation at which the electrostatic interaction between two elementary charges is comparable with thermal

fluctuations. The Bjerrum length may be calculated according to the following formula:

$$\lambda_B = \frac{e^2}{4\pi\epsilon_0\epsilon_r k_B T},$$

where  $e$  is an elementary charge;  $\epsilon_0$  and  $\epsilon_r$  is vacuum and media dielectric constant correspondingly;  $k_B$  is the Boltzman constant;  $T$  is the temperature in Kelvins. The Bjerrum length in water is about 0,7 nm at 300K.

### **Salt concentration in simulations**

Concentrations of salts in simulations of ternary systems solvent-salt-solute is a very important issue. Indeed, when studying ion effects on solvation interfaces one needs to be sure, that the observed pattern of ion behaviour is not an artifact of insufficient sampling. Particularly, this problem is very important to biologically related systems, as physiological concentrations of ions are low.

As in some circumstances one can not increase ion concentrations in simulations, it is very important to increase duration of the simulations to gain the same quality of sampling. The work [85] shows dependence of simulation convergence time on salts concentration. Sodium salts of fluoride, chloride, bromide and iodide at concentrations 0.2, 0.5, 1.0 and 2.0M were used in the simulations. The criteria of convergence of the simulations was an efficiency of ions sampling the simulation box. The study reveals that lower ion concentrations need more time to sample the box, and convergence for higher concentrations is achieved much earlier. The lowest concentration of 0.2M required about 10 ns of simulation time to effectively sample the box. These estimates may be used as a guideline while estimating a duration of simulations. However, it seems to be important to additionally check the convergence of the simulations for significantly different systems, e.g. systems at interfaces.

### **3.1.5 Software**

MD simulations require extensive numerical calculations which are not feasible without a dedicated software and a significant CPU time. A typical MD software contains about a million lines of code. Therefore, a mature MD software can not be designed and developed within a short period of time. Because of that, MD simulations are usually performed with an established software, which is suitable in the best way for a researcher, simulation tasks and the allocated computer resources. Today there is a significant number of various well developed MD codes. To name a few one could mention Desmond [99, 100, 101], Gromacs [98], LAMMPS [102, 103],



Amber [104], etc. All MD software have the same theoretical background. The differences arise in the details of the theory implementation and analysis options. This work employed Desmond and Gromacs MD simulation packages. Let us now consider advantages and disadvantages of each of them.

**Gromacs** (GRONingen MACHine for Chemical Simulations) was created at the Biophysical Chemistry department of the University of Groningen (the Netherlands). The code is free, and therefore it is maintained by a large community. One of the most significant advantages of the package is its flexibility: Gromacs allows users to use variable force fields and atom parameters, including user-defined. The software may run in parallel as well as in serial. Parallel execution of Gromacs requires MPI (Message Passing Interface) or threads. A significant advantage of Gromacs for the present work is its ability to simulate systems with interfaces (slab geometry). Unfortunately, there is no convenient and automated way to assign molecular parameters to a system. To fill this gap we used another MD software - Desmond: molecular parameters (topology), obtained with Desmond, were automatically transferred into Gromacs topology files with a home-made script.

**Desmond** was created and maintained by D. E. Shaw Research. This may be obtained free-of-charge for academic and non-profit uses, however the code is not free. Desmond is capable of working with several force field types and automatically assigns corresponding parameters to every atom of a system. In comparison with Gromacs, Desmond uses computer time and storage facilities more efficiently: it is approximately 3-5 times faster than Gromacs, while the generated trajectory takes approximately three times less storage. These advantages are possible due to novel parallel algorithms and numerical techniques implemented into the package. The main disadvantage of the package is directly connected to its sophisticated parallelization technique: the package can not be easily adapted to non-standard queue-algorithms in high performance computer centres. The crucial for this work disadvantage of the Desmond package is its inability to simulate systems in slab geometry as well as insufficient flexibility of the simulation control.

### 3.1.6 Trajectory analysis

A set of sequential frames is the direct result of any molecular dynamics simulations. These frames do not present any understandable by humans information by themselves. In order to get a useful and understandable information from an MD simulation one needs to define, which characteristics one would like to obtain, and then specifically process the MD trajectory to obtain these characteristics. There is a wide variety of molecular scale properties, which may be

measured with MD simulation: radial distribution function, potential of mean force, molecular orientations, density profiles, energy landscape along the reaction coordinate, etc. Let us look at these characteristics more in details.

### **Radial distribution function. Pair correlation function**

The radial distribution function (RDF) is an important property characterizing the structure of condensed systems. This function can be obtained both in practical (for example, X-ray or neutron scattering) and computer experiments (for example, MD simulations). The RDF for distribution of the A-particles around the the B-particle is defined with the following expression:

$$\rho_A \int g_{BA}(r) 4\pi r^2 dr = N_A - 1,$$

where  $\rho_A$  is the number density of the A-particles;  $N_A$  is the number of particles A in the sample;  $r$  is the distance between the particles B and A. The function shows the ensemble average of the relative density profile of the A-particles at the certain distance  $r$  from the B-particle.

The radial distribution function  $g_{AB}(r)$  for a liquid homogeneous system is equal to pair correlation function [105]. This function describes probability to find the B-particle at the given distance from A-particle. A "particle" in this case is a material point which coincides with the center of the real particle, or, alternatively, could be a center of mass of a set of particles, e.g. a center of mass of benzoic acid. The  $g(r)$  function is used efficiently to describe hydration shells and preferential positioning of one particles with respect to other ones. Let us consider  $g(r)$  of an ion in water as an example (figure 3.4).

As one can see from the figure 3.4, one can split the represented  $g(r)$  into four distinct regions. The first region lasts from 0 to the sum of interacting particles radii (in our case it is a sum of the ion radius and water molecule radius). This region describes the possibility to find interacting particles inside each other. Intuitively, particles can not penetrate through each others "surfaces" and, as a result, probability of this "interaction" is 0.

The second region at the  $g(r)$  is the region which describes direct contacts between two particles. It is limited with the first minimum on the  $g(r)$  (around 1.5). If one of the particles under consideration is a water molecule (like at the represented  $g(r)$ ) then this region corresponds to the first hydration shell of the other particle (in our case – ion). The water density in the first hydration shell of hydrophilic species is higher than in the water bulk, heat movement of water molecules in the first hydration shell is slowed down compared to the bulk water. The first hydration shell is limited by the first minimum at the  $g(r)$ . The region, following the region of

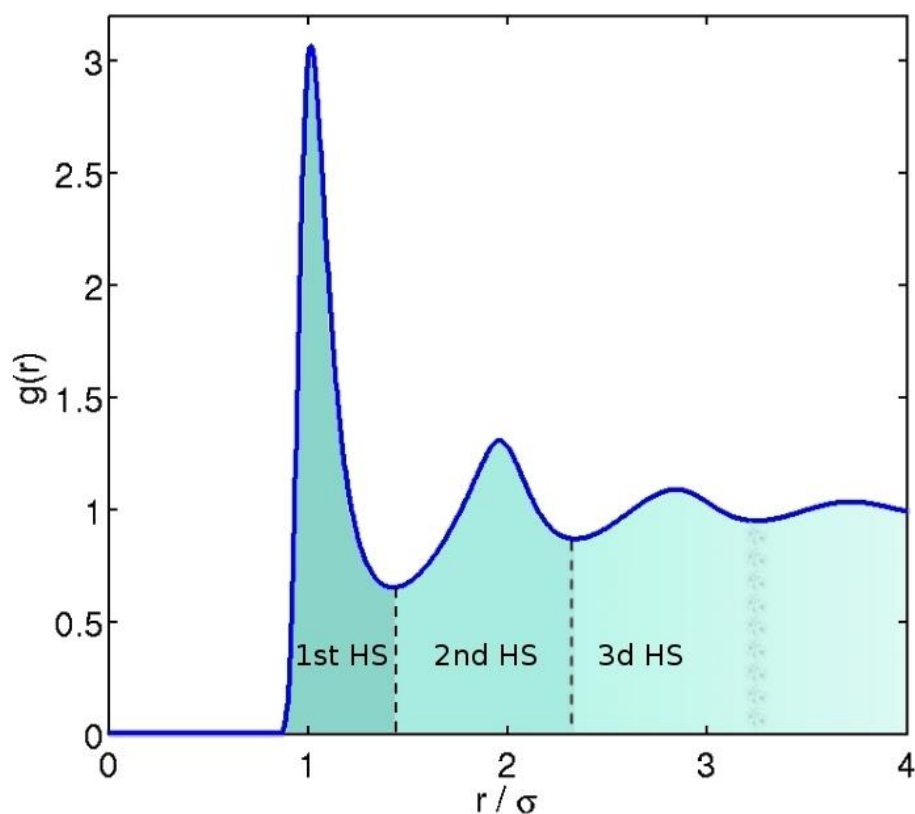


**Figure 3.4** – Definitions of hydration shells from  $g(r)$ . The distance is given in the diameters of a water molecule. As one can see, the first peak of the  $g(r)$  is the highest one and is narrower, compared to the second and third peaks, because the water molecules of the first hydration shell have the strongest binding to the solute or the ion.

the first hydration shell, describes the second hydration shell.

The third area on  $g(r)$  is the second maximum, which represents the second hydration shell. The second hydration shell is not all the times well distinguished from the bulk. The separation between the first and the second hydration shells is a well distinguished minimum on  $g(r)$ . Although diffuse and less stable the second hydration shell is still could be distinguished from the bulk water. The second hydration shell may be followed by the third hydration shell or, alternatively, by bulk water.

If the hydration strength is high, it is possible to distinguish the third hydration shell from the bulk water. However, it is even more diffuse and "bulk-like" than the second hydration shell. The separation between the second and the third hydration shells is less pronounced than the separation between the first and the second hydration shells. The region of the third hydration shell smoothly transfers into the bulk water region. Although some  $g(r)$  oscillations around bulk density are still possible, they are not usually considered as hydration shells of higher order. As  $g(r)$  is one of the most convenient tools of description of solvation shell, this work employs

massively  $g(r)$  to study ion effects at solvation interfaces.

### Density (concentration) profiles

**2D density profile.**  $g(r)$  is a convenient tool to describe particles distributions around a selected particle. Unfortunately,  $g(r)$  does not describe effectively the distribution of molecules in solutions at macrointerfaces. As analysis of molecular distribution near an interface is crucial for understanding of the molecular level details of the interfacial processes, a function, similar to  $g(r)$  may be applied to systems at macrointerfaces. This function describes density profile along the simulation cell, i.e. it operates with absolute coordinates along one of the axes (often, Z axis) instead of radial distances from a given particle. Density functions usually are not useful for description of bulk properties, as they converge to a bulk density in a direct proximity from the interface.

Usually, the property of interest is density deviations near the interface compared to a constant bulk density. Theoretical bulk density is the density of particles when they are absolutely randomly distributed in the volume. The analogue of the theoretical density on the macro-level is an analytical concentration of the solute under ideal mixing. Therefore, density deviations near the interface may be compared with macro-concentration deviations at the interfacial layer. These deviations are useful in description of the surface affinity of a substance. This is why this work employs density profiles in the part, concerning behaviour of benzoic acid and its salts at the water/vapour interface.

**3D density areas.** Transferring the idea of 2D density profiles to 3D, one could obtain density distributions around a particle or a group of particles. In this case, the density changes should be obtained in every small space volume, which gives a researcher a valuable information, showing density distribution in a way, similar to the image human brain acquires in every-day life. This is why these distributions are more intuitively understandable, compared to the spherical  $g(r)$ . In the case of a simple ion 3D density distribution of water repeats the shape of the ion and is close to spherical shape. This may be equally well understood with the radial  $g(r)$  and with 2D density distribution. However, the shape of a hydration shell can be very complicated when we consider a group of connected particles (a molecule or a multiatomic ion). This is when 3D density distributions are more convenient in description of solvation shells compared to radial  $g(r)$ . A hydration shell of carboxylic group is a good example of the sophisticated 3D  $g(r)$  (fig. 2.3).

### Potential of mean force

The potential of mean force (PMF) is an effective description of an energy profile of a chemical process. It can be defined in different ways. In this work we used two definitions of the PMF to obtain it from MD simulations: *i*) as effective potential acting between two particles *i* and *j* in the condensed phase and *ii*) as the *n*-particle correlation function. Let us first consider a homogeneous system containing *N* spherically symmetric particles in the volume *V* with the temperature *T* (NVT-ensemble).

One way to represent potential of mean force is the **effective potential acting between two particles *i* and *j* in the condensed phase**. Let us consider two molecules (*i* and *j*) in a gas phase, where we may neglect interactions of these two molecules with all other molecules. The interaction between the two molecules results in forces acting on these two molecules. As the force is a negative gradient of the interaction potential, it results in acceleration of particles. In other words, the particle *i* produces force on the particle *j* and vice versa.

Now we may employ the same scheme for the liquid phase. Let us consider the same particles *i* and *j* at distance *r* in an ensemble of *N* molecules. Now the forces acting on *i* and *j* are not only the result of mutual interactions of *i* and *j* but also include interactions of *i* and *j* molecules with all other molecules in the ensemble. In other words, the molecules *i* and *j* interact with each other via modified (compare to gas phase) potential. This potential includes an average influence of all particles in the ensemble. This modified potential is called "potential of mean force".

$$\overrightarrow{-\text{grad}}_j \text{PMF}(\mathbf{r}_{ij}, \Omega_{ij}) = \frac{\int \dots \int \exp(-\beta U) (-\overrightarrow{\text{grad}}_j U) d\mathbf{r}_3 \dots d\mathbf{r}_N d\Omega_3 \dots d\Omega_N}{\int \dots \int \exp(-\beta U) d\mathbf{r}_1 \dots d\mathbf{r}_N d\Omega_1 \dots d\Omega_N},$$

where  $\beta$  is the inverse temperature ( $\beta = (k_B T)^{-1}$ ); *U* is the potential energy of the system;  $\overrightarrow{\text{grad}}_j$  is gradient operator on the position of particle *j*, the denominator is the configuration integral of the system ( $Z_{\text{conf}}$ ).

Thus we can define PMF as a potential that gives mean force acting on the particle *j*. We can calculate PMF with this definition and using MD simulations with *N* particles. On each integration step we choose two molecules (*i* and *j*), fix the distance *r* between them and store forces acting on the molecule *j*. Then we repeat the procedure for a sufficient number of MD integration time steps. Finally we calculate the average all the stored forces. We repeat this procedure following a required trajectory of particle *i* approaching the particle *j*. The length step in this procedure is determined with the required precision. Knowing the averaged force at each distance step between *i* and *j* we can construct the whole PMF. We can use the same

methodology to calculate the PMF as a function of any spatial coordinate (e.g. angles) and even as a combination of spacial coordinates of one or several particles.

Another way to define PMF is **via the n-particle correlation function**. In this case the PMF between two non-spherical particles in one-component homogeneous system in the NVT-ensemble can be defined as:

$$\text{PMF}(\mathbf{r}_{ij}, \Omega_{ij}) = -k_B T \ln g(\mathbf{r}_{ij}, \Omega_{ij}),$$

where  $g(\mathbf{r}_{ij}, \Omega_{ij})$  is the molecular pair correlation function,  $\mathbf{r}_{ij} = \{x_{ij}, y_{ij}, z_{ij}\}$  and  $\Omega_{ij} = \{\varphi_{ij}, \vartheta_{ij}, \psi_{ij}\}$  are the radius-vector between  $i^{\text{th}}$  and  $j^{\text{th}}$  molecules (e.g. between their centres of masses) and the relative orientations of the  $i^{\text{th}}$  and  $j^{\text{th}}$  molecules.

The PMF can also be defined through a thermodynamic cycle. According to this definition the PMF is the work involved in moving two (or more) selected particles from the infinite separation to the final configuration in a condensed phase. For a homogeneous system, containing  $N$  spherically symmetric particles in the volume  $V$  with the temperature  $T$  (NVT-ensemble), the two particle PMF is  $\text{PMF}(r) = A(r) - A(\infty)$ , where  $A$  is the Helmholtz energy. This definition allows us to consider the PMF as a **measurement of the free energy along the reaction coordinate**.

### Molecular orientations

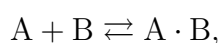
Molecular orientation is an important property which characterises behaviour of solutions at macrointerfaces. Molecular dynamics simulations offer an opportunity to record orientation of solute and solvent molecules at the interface. To do this, one needs to select two or more orientation vectors (e.g. surface of a water slab and main axis of a benzene ring). Next, one should record the angle between the two vectors and store this value. This procedure should be done for every molecule of interest over the whole period of simulation under interest. Afterwards, the results should be averaged over time. As a result, one obtains an averaged value of the angle, which, in the above example, describes the angle, at which the benzene's main molecular axis is tilted towards the water surface. It is important to note here that the obtained angle is *preferential* orientation, which describes a general pattern of molecular orientations and does not need to be represented in every frame of the MD simulation. It should not be considered as the only possible orientation, as a solution is a dynamic system. The liquid system stays dynamic even though its molecules can have some preferential orientations. In this work we employed description of orientation of benzoic acid at the water/vapour interface with two vectors. More details about

this may be found in the chapter 4.

Both computational and practical experiments can provide information, concerning interactions at molecular level. Combination of both practical and computational experiments can bring new insights into understanding of processes at the molecular solvation interfaces. Here we describe theoretical background of some of the practical experimental techniques, we used in this work.

## 3.2 Determination of stability constants of $\alpha$ -cyclodextrin with aromatic carboxylic acids

Stability constants describe the interactions between different species. If the complex is formed according to the reaction



stability constant may be found from equilibrium concentrations of the complex and the reagents in the solution:

$$K_{\text{eq}} = \frac{[A \cdot B]}{[A][B]},$$

where  $K$  is the stability constant;  $[A \cdot B]$  is the equilibrium concentration of the complex  $A \cdot B$ ;  $[A]$  and  $[B]$  are equilibrium concentrations of the reagents  $A$  and  $B$  correspondingly. This direct approach may be employed if reagents and products concentrations may be determined authentically with some analytical method, which is not always possible. When authentic determination of the concentrations is not possible, other techniques may be employed, e.g. nuclear magnetic resonance and calorimetry.<sup>1</sup>

### 3.2.1 Nuclear magnetic resonance

Nuclear magnetic resonance is a spectroscopic technique which makes use of electromagnetic radiation with frequencies  $\sim 10^8$  Hz (radio frequencies range of electromagnetic spectrum). The basic principle underlying nuclear magnetic resonance is quantization of spin energy levels created by an external magnetic field on nuclei with a half-integral spin quantum number ( $^1\text{H}$  and  $^{13}\text{C}$  are the most commonly studied nuclei). It is important to note here that in the

---

<sup>1</sup>The work on determination of stability constants of cyclodextrin complexes has been done in the Russian Academy of Sciences by the group of Dr. Irina V. Terekhova.

absence of external magnetic field, the energy levels are degenerated (not distinguishable) and no spectroscopic transitions can be observed.

Energy difference between energy levels quantized with radio frequency is extremely small and depends on the quantizing energy as  $\Delta E = h\nu$ , where  $h$  is the Planck constant and  $\nu$  is the quantizing radio frequency. As a result of very small energy difference between quantized energy levels, both levels are almost equally populated at room temperature. Therefore, when nuclei are irradiated both emission and absorption occur (the system is in resonance). However, there is a small excess of nuclei in the lower energy level (a few nuclei per million). These nuclei absorb energy which results in net absorption at the resonance frequency. As the number of signalling nuclei is low, the NMR signals are much weaker, compare to UV-vis-NIR spectroscopy. Further, the equilibrium ground state populations are re-established by the excited nuclei relaxing to the lower energy level. The whole process normally takes just a few seconds in liquids and solutions.

For nuclei of each element the spin angular momentum ( $I$ ) is connected to the magnetic moment ( $\mu$ ) with gyromagnetic ratio  $\mu = \gamma I$ , where  $\gamma$  is the proportionality constant. The magnitude of the resonance frequency ( $\nu$ ) and hence  $\Delta E$  is directly proportional to the strength of the applied magnetic field ( $B_0$ ) with the relation  $\nu = B_0(\frac{\gamma}{2\pi})$ . The resonance frequency of the nuclei of one element is sufficiently different from those of others. This enables spectra of different elements to be recorded independently. A very important characteristic of the NMR spectra is that the exact location of the NMR peak for each nucleus depends on the chemical environment of this nucleus. The resonance frequency of the particular NMR-active nuclei shows small variations due to different chemical environments. These variations are known as chemical shifts and they are the source of structural information which one obtains from the NMR. Changes in chemical shifts ( $\Delta\delta$ ) are successfully used to study variety of association processes, e.g. complex formation. Particularly, this work uses results, obtained by  $^1\text{H}$  NMR studies of complex formation of  $\alpha$ -cyclodextrin with different aromatic benzoic acids.

The experimental results on cyclodextrin binding with aromatic carboxylic acids were obtained by our collaborators in the Russian Academy of Science. Stability constants of the complexes ( $K$ ) were evaluated from the concentration dependences of the chemical shifts ( $\Delta\delta$ ) by the nonlinear curve fitting procedure [106]. Values of  $K$  are presented in table 3.2.

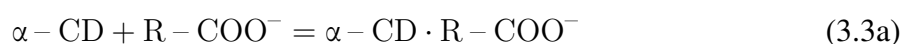
According to the literature, benzoate anion and zwitterion of nicotinic acid form inclusion complexes with cyclodextrin with the composition 1:1 in both cases [106, 107, 108, 109, 110]. Therefore, all thermodynamic properties, considered herein and reported in the tables 3.2 and



**Table 3.2** – Stability constants of  $\alpha$ -CD complexes with benzoate and nicotinic acid in aqueous solutions containing  $\text{Na}^+$  and  $\text{K}^+$  ions at 298.15K, obtained from  $^1\text{H}$  NMR. Reproduced from [11]. Data were obtained by our collaborators in the Russian Academy of Sciences.

complex	solution	K, kg/mol
$\alpha$ -CD/benzoate	0.03M KOH	$19.1 \pm 1.5$
	0.03M NaOH	$17.5 \pm 1.6$
	0.03M KOH + 0.2M KCl	$18.9 \pm 1.6$
	0.03M KOH + 0.2M NaCl	$16.0 \pm 0.6$
	0.03M NaOH + 0.2M NaCl	$17.2 \pm 2.0$
$\alpha$ -CD/nicotonic acid	$\text{H}_2\text{O}$	$27.0 \pm 0.4$
	0.2M KCl	$26.1 \pm 0.6$
	0.2M NaCl	$23.5 \pm 0.7$

3.3, are ascribed to the 1:1 binding process:



$$K = \frac{[\alpha\text{-CD} \cdot \text{R-COO}^-]}{[\alpha\text{-CD}][\text{R-COO}^-]} \quad (3.3b)$$

The  $^1\text{H}$  NMR spectra of  $\alpha$ -CD alone and in the presence of the acids under study were measured and analyzed (figure 3.5). It was obtained that addition of the nicotinic acid induced the considerable upfield shift of the signal of interior proton H3. The downfield shift for H5 was visible, but the magnitude of  $\Delta\delta$  is smaller in comparison with that for H3 proton. The same influence of benzoate on  $^1\text{H}$  NMR spectrum of  $\alpha$ -CD was observed, although the shifts of H3 and H5 are not so pronounced as in the case of nicotinic acid (figure 3.5). This is due to lower binding affinity of  $\alpha$ -CD to benzoic acid anions. The shifts of the  $\alpha$ -CD interior protons indicate the formation of an inclusion complex where the benzoate molecule enters the cavity from the wider rim. The absence of change in the chemical shift for H6 proton additionally proves this binding mode.

The  $^1\text{H}$  NMR spectra of nicotinic acid have been considered earlier [106, 109], and it has been shown that the signals of the protons, located near  $\text{R-COO}^-$  group, are significantly shifted upon complex formation with  $\alpha$ -CD, while the changes for another proton of its aromatic ring have not been observed. These results were interpreted in terms of preferential inclusion of carboxylate group into  $\alpha$ -CD cavity in comparison with the pyridine ring carrying the positively charged

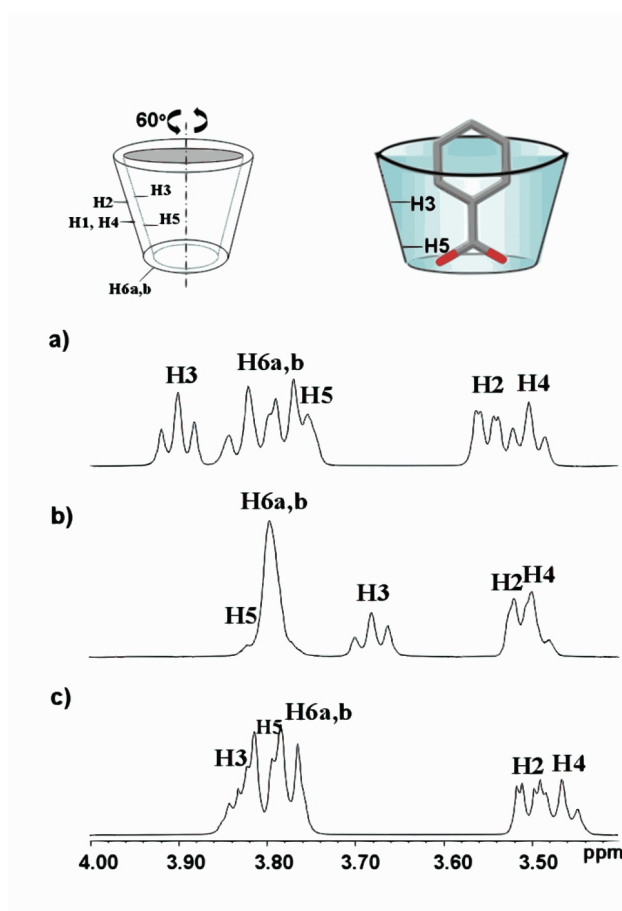


**Figure 3.5** – Partial  $^1\text{H}$  NMR spectra of  $\alpha$ -CD aqueous solution (0.005 mol/kg) at 298.15 K: (a)  $\alpha$ -CD; (b)  $\alpha$ -CD in the presence of nicotinic acid (0.04 mol/kg); (c)  $\alpha$ -CD in the presence of benzoic acid (0.04 mol/kg). The insets on the top show the positions of the hydrogen atoms (left) and the binding mode (right) of the ACAs. Reproduced from [11]. Data were obtained by our collaborators in the Russian Academy of Sciences.

NH<sup>+</sup> group. The revealed binding mode of nicotinic acid is consistent with that described in the literature for complex formation of  $\alpha$ -CD with benzoic acid and benzoate in aqueous solution [111, 112, 113] as well as in the solid state [114]. In the crystalline  $\alpha$ -CD/benzoic acid complex, the guest molecule is packed tightly in the host ring, and the carboxyphenyl group is located inside the cavity [114]. Bergeron with coauthors [111] showed by means of NMR technique that in aqueous solution of both benzoic acid and benzoate are inserted into the macrocyclic cavity by the carboxyl group first, although the benzoate penetration is more random. The orientation of the carboxylate in the  $\alpha$ -CD cavity has been demonstrated by Simova and Schneider [112] on the basis of <sup>1</sup>H and <sup>13</sup>C NMR measurements. The sizable complexation-induced shifts for H3 (-0.45 ppm) and H5 (-0.18 ppm) protons of HP- $\beta$ -CD obtained for binding with benzoic acid are consistent with the deep insertion. In contrast to benzoic acid, values of  $\Delta_c\delta$  for benzoate complexation are considerably lower, and they are equal to -0.18 and 0.04 ppm, respectively, for H3 and H5 protons. The authors discussed the possible location of R – COO<sup>-</sup> inside the cavity and assumed also the probability of random inclusion. Inclusion complexes of  $\alpha$ -CD with benzoate are substantially less stable than with benzoic acid [111, 114, 115]. This fact also confirms that the carboxylic group enters the cavity. Ionization of this group dramatically decreases its affinity to hydrophobic cavity because of the high polarity and strong hydration of –COO<sup>-</sup> in the aqueous medium.

The stability constants of  $\alpha$ -CD complexes with benzoate and nicotinic acid, obtained from <sup>1</sup>H NMR, are presented in the table 3.2. The data are in good agreement with the literature,  $K = 11.2 \text{ M}^{-1}$  [113],  $12.3 \text{ M}^{-1}$  [116],  $13 \text{ M}^{-1}$  [115]. As can be seen from table 3.2, the presence of Na<sup>+</sup> decreases the binding affinity of  $\alpha$ -CD to the carboxylic acids over bulk water and KCl solutions (nicotinic acid) or solutions with only K<sup>+</sup> cations (benzoate). Moreover, in the case of the nicotinic acid solutions, there is no practical difference between ACA-CD binding constants in the neat water solution and the solutions containing K<sup>+</sup> ions.

As it was mentioned previously, the literature describes two manifestations of ion effects on the cyclodextrin complex formation: *i*) indirect effect of ionic strength, which results in *increased* binding constant in the salty solution compared to pure water; and *ii*) "competition for the host", which arises from the fact, that large weakly hydrated anions, e.g. ClO<sub>4</sub><sup>-</sup> are capable of formation of complexes with cyclodextrins. Once the complex anion-cyclodextrin is formed, the effective concentration of the free cyclodextrins falls, which, in turn, prevents partially formation of complexes between the guest organic molecule and the cyclodextrin. Competition for the host reduces significantly binding constants. However, this effect may not explain the detected reduction of binding constants between benzoates and nicotinic acid, as chlorides used in the

experiment do not form complexes with cyclodextrins [83].

### 3.2.2 Calorimetry

Calorimetry is the measurement of the heat flow which occurs in a process [117]. This method was first introduced more than two centuries ago. These days it is a well established and highly precise tool to measure thermodynamic properties of various processes: dilution, chemical reaction, complex formation, etc. Calorimetry measures heat, which a system or a process transfers/absorbs to/from the surrounding. Theory connects this measured heat with other thermodynamic properties of a system, e.g. thermodynamic binding constant.

The theoretical basics of calorimetry lie in the law of conservation of energy, i.e. total amount of energy in an isolated system remains constant over time. In the formulation of the first law of thermodynamics the law of conservation of energy says that the energy of an isolated system is constant. This means that the change of internal energy of a closed system ( $\Delta U$ ) consists of the work which had been done on the system ( $w$ ) and the energy of heat added to the system ( $q$ ):

$$\Delta U = q + w.$$

Here the positive value of heat ( $q$ ) is connected to increase of the temperature. The volume of liquid systems does not change, and as a result, no work is done. This allows one to omit the work from the equation for internal energy. For an infinitesimal change:

$$dU = dq_V = C_V dT,$$

where  $C_V$ , is the heat capacity at constant volume. Heat added to raise the temperature at a constant pressure is given as

$$dH = dq_P = C_P dT.$$

When a change occurs with the transfer of heat from the system to the surroundings at a constant pressure it is referred to as exothermic and the enthalpy of the system decreases ( $\Delta H$  is negative). If the system takes in heat from the surroundings the process is endothermic ( $\Delta H$  is positive).

Unfortunately, one can not determine whether changes in the system are spontaneous if one knows only the heat which accompanies the process. The second law of thermodynamic introduces entropy ( $S$ ), which serves as a measure of disorder in a system. According to this law the entropy of an isolated system can not decrease. However, as we usually deal with non-isolated system, the criterion of increasing entropy as a requirement for spontaneous process does not hold true. The third law of thermodynamics introduces free energy ( $G$ ) which combines enthalpy

(H) and the entropy (S) and represents a convenient criterion of possibility of a spontaneous process:

$$G = H - TS$$

The free energy change ( $\Delta G = \Delta H - T\Delta S$ ) serves as a good indicator of the state of a process. Negative value of the free energy indicates that a process is spontaneous and vice versa, positive free energy indicates that the process can not run spontaneously. The larger the absolute value of the free energy is, the farther the system is from its equilibrium state. If  $\Delta G = 0$ , then the system is in equilibrium.

It is very important to highlight here that the third law of thermodynamics connects the free energy of a process with the equilibrium constant. Under standard conditions,  $\Delta G^\circ$  is related to the equilibrium constant ( $K_{eq}$ ):

$$\Delta G^\circ = -RT \ln K_{eq}$$

In principle, all reactions may be written as equilibrium processes. However, some equilibria are shifted almost completely to the side of product formation, which means that the reagents are almost fully transferred into the products. Other equilibria are shifted towards reagents, which means reagents dominate in the reaction mixture and only minor amount of them is transferred into products.

The table 3.3 shows the main results of calorimetric measurements of  $\alpha$ -CD complexation with nicotinic acid. This table presents the obtained values of stability constants as well as the enthalpy and entropy changes for  $\alpha$ -CD/nicotinic acid complex formation in different solutions. It is evident from table the 3.3 that formation of inclusion complexes between  $\alpha$ -CD and nicotinic acid is thermodynamically favorable. High negative enthalpy changes upon complex formation are mainly caused by the prevalence of attractive intermolecular interactions (van der Waals interactions and hydrogen bonding) over the penalty for desolvation of the  $\alpha$ -CD cavity. The negative  $\Delta_c S$  values are attributed to losses in rotational and translational freedom of solutes upon complexation. It was also assumed that the possibility of hydrogen bonding between the protonated nitrogen of nicotinic acid and hydroxyls surrounding the wider rim of the  $\alpha$ -CD cavity. This suggestion is based on the comparative analysis of enthalpy and entropy changes obtained for  $\alpha$ -CD complexation with nicotinic acid (table 3.3) and benzoate ( $\Delta_c H = -16.3 \pm 1.3$  kJ/mol and  $T\Delta_c S = -10.5 \pm 1.4$  kJ/mol) [110]. Comparing these values, we can conclude that  $\Delta_c H$  and  $\Delta_c S$  are more negative for nicotinic acid complexation than for benzoate.

Different effects of NaCl and KCl on the enthalpy and entropy parameters were observed. As follows from the table 3.3, the presence of KCl has only a slight influence on the  $\Delta_c H$  and

**Table 3.3** – Thermodynamics of complex formation of  $\alpha$ -CD with nicotinic acid in water and in aqueous solutions of NaCl and KCl at 298.15 K obtained from calorimetry. Reproduced from [11]. Data obtained by our collaborators in the Russian Academy of Science.

complex	K, kg/mol	$\Delta_c G$ , kJ/mol	$\Delta_c H$ , kJ/mol	$T\Delta_c S$ , kJ/mol
$\alpha$ -CD/nicotonic acid (H <sub>2</sub> O)	27 $\pm$ 4	-8.2	-25.2 $\pm$ 0.3	-17.0
$\alpha$ -CD/nicotonic acid (0.2M KCl)	30 $\pm$ 5	-8.4	-24.0 $\pm$ 0.3	-15.6
$\alpha$ -CD/nicotonic acid (0.2M NaCl)	19 $\pm$ 4	-7.3	-29.3 $\pm$ 0.4	-22.0

$\Delta_c S$  values. In particular, complex formation in KCl solution is less exothermic and slightly enhances disorder in the system. The difference in the binding constants for pure water and KCl solution is within the error limits. On the contrary, addition of NaCl results in a significant decrease of the apparent binding constant K (also called complex stability constant) and more negative values of  $\Delta_c H$  and  $\Delta_c S$ .

Calorimetric studies, like <sup>1</sup>H NMR studies, reveal a decrease in the binding constant in the presence of sodium chloride. By means of calorimetry one may assign the reduction of the binding constant to a decrease in the entropic contribution to the  $\delta G$  of the process. This reduction of the entropic contribution is strong enough that it outweighs a slightly more negative enthalpy of the process. This pattern of ion effects was not described before in the literature. MD simulations, represented in the chapter 4, help understand the effect at the molecular level.

### 3.3 Determination of molecular orientation at water/vapour interface

Few spectroscopic techniques are available to study the orientation of molecules and molecular ions at the aqueous solution surface. The X-ray photoelectron spectroscopy (XPS), preferably in combination with tunable synchrotron radiation, is ideally suited to quantify the relative abundance of atoms in chemically inequivalent binding environments near a free surface. Therefore, the XPS has become a standard tool in surface science for studies of the chemical state, coverage and orientation of adsorbates on solid surfaces [118, 119]. However, until recently, it has not been possible to perform photoemission studies of aqueous solutions due to their high vapor pressures. This problem was solved by the development of the liquid-jet technique [120].

The X-ray photoemission spectroscopy experiments were performed in Sweden by our

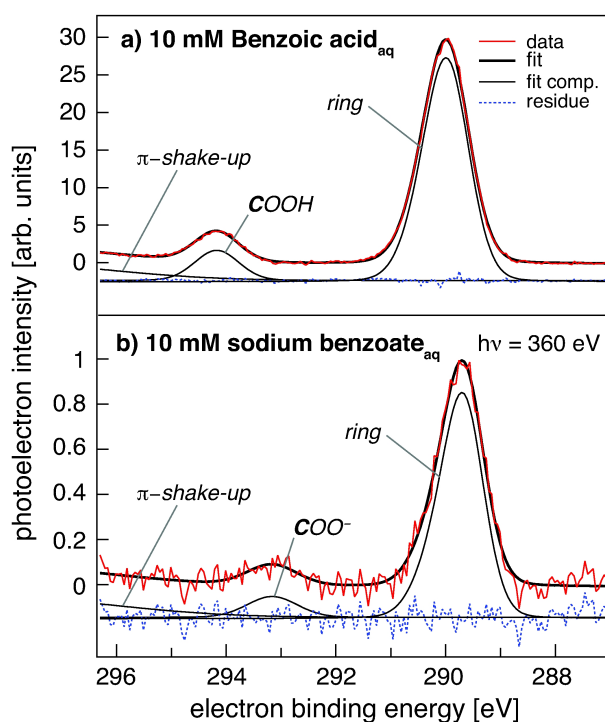


**Figure 3.6** – C1s photoelectron spectra of a) 10 mM benzoic acid and b) 10 mM sodium benzoate in aqueous solution taken at 360 eV photon energy. Each spectrum clearly separates contributions from the carboxylic/carboxylate carbons and aromatic ring carbons. Since the spectra are highly surface sensitive, deviations from the stoichiometric signal intensity proportions are indicative of preferential surface orientations. Reproduced from [121]. Results obtained by our collaborators in Sweden.

collaborators (see ref. [121]). The figures 3.6a and b show the C1s photoelectron spectra of 10 mM aqueous benzoic acid and 10 mM sodium benzoate, respectively. Both spectra were recorded at 360 eV excitation energy. The resulting photoelectron kinetic energies of 65-70 eV lie near the minimum of the photoelectron inelastic mean free path function ( $<1$  nm), making these measurements highly surface sensitive [118, 122]. Each spectrum was fitted with an appropriate number of Voigt functions, using a least-square approach. The Lorentzian lifetime widths were fixed for all lines while the respective Gaussian widths were free to vary. The resulting fits are shown in each panel as a solid line, superimposed on the experimental data, while the individual components are given as thinner lines, rising from the residue (blue dashed line). In order to improve visual clarity, a linear background has been subtracted from each spectrum.

The C1s spectra of both benzoic acid (figure 3.6a) and benzoate (figure 3.6b) can be decomposed into two main regions; that of the carboxylic/carboxylate carbons at higher binding energy (BE), and a more intense feature at lower energy, arising from core-emission of the aromatic ring. At the high-energy tail, the onset of an additional broad feature is observed: we attribute this to shake-ups of the aromatic  $\pi$ -system, which has been thoroughly studied in the gas phase

[123, 124]. The shift of the carboxylic line of about 4 eV, relative to the ring carbons, enables a reliable quantification of the respective peak intensities from BAH and  $\text{BA}^-$ , which is crucial in the current experiment, as we are interested in the molecular orientation as a function of protonation state.

The carboxylic C1s line of BAH, shown in the figure 3.6a, is found at 294.2 eV BE, while emission from the carboxylate carbons of  $\text{BA}^-$  is shifted to lower BEs by  $\sim 1.1$  eV relative to the acid form. While the aromatic ring of BAH and  $\text{BA}^-$  contains four types of chemically inequivalent carbons (1st, *ortho*-, *meta*- and *para*-) the binding energy shifts between these spectral features are obviously too small to allow a reliable separation. The whole ring feature of BAH can indeed be well fitted with a single Voigt function, centered at  $\sim 290.0$  eV, while the fit improves slightly if an additional weak feature is added on the high-BE side (at 290.4 eV). For  $\text{BA}^-$  the ring carbons BEs are less affected by the deprotonation than that of carboxylic group, as can be expected given that they are farther away from the de-protonated site; the peak is centered around 289.7 eV. Since we do not want to attribute the present decomposition of the ring features any definite physical significance, and, given that we are interested primarily in the intensity ratio between the ring and carboxylic/carboxylate PE features, we show the resulting fit of the ring structure as one single component in the figure 3.6 a and b.

As can be seen in the figure 3.6 the ring carbon C1s signal from the BAH solution is approximately a factor 30 stronger than that from the equimolar solution of sodium benzoate. Based on this observation alone, it was concluded that the undissociated benzoic acid has a significantly higher surface affinity compared to its conjugate base form. We also note that this is the reason behind the marked difference in signal-to-noise ratios in the spectra of BAH and  $\text{BA}^-$ .

What do these photoelectron spectra tell us about the preferential orientation of BAH and  $\text{BA}^-$  at the water/vapour interface? To address this issue, we will focus on the C1s spectral intensity distributions. Note that if the molecules were totally randomly oriented, or lying totally flat on the surface, we would expect to retrieve the stoichiometric proportions, i.e. 6:1. For benzoic acid the ring/carboxylic PE ratio is instead found to be  $7.86 \pm 0.01$ , according to the fits shown in the figure 3.6. This value significantly increases for sodium benzoate; the ring/carboxylate PE ratio is now instead  $10.1 \pm 0.7$ . Hence, the experimental results are indicative of a preferential surface orientation, less for BAH but quite pronounced for  $\text{BA}^-$ . Since BAH is heavily surface enriched, the ring/carboxylic PE intensities ratio of  $7.86 \pm 0.01$  suggests that the BAH molecules are lying nearly flat at the water/air interface, with a certain tendency for the carboxylic group to orient into the solution phase. However, for  $\text{BA}^-$  the ring/carboxylate PE ratio is about 70% higher than what would have been expected from simple stoichiometric considerations. This indicates



that the interfacial benzoate anions are strongly oriented in the surface layer, with the aromatic rings pointing out toward the gas phase while the carboxylate groups are sticking into the water.

Combination of results from photoemission and fully atomistic molecular dynamics simulations has a great potential, as photoelectron distributions can be calculated from simulated density profiles, employing simple attenuation models. Hence, the validity of the simulations can be evaluated and the comparison with the photoemission experiments can yield substantial information about the orientation and distribution of different solutes at the aqueous solution/vapor interface.

### 3.4 Optical absorption spectroscopy of carbon nanotubes

The optical absorption spectroscopy is a branch of the optical spectroscopy, which analyses the energy of photons absorbed from incident light by a molecule or molecular aggregate undergoing transition from a lower to a higher energy state. This transition occurs if the energy of the photon ( $E = h\nu = \frac{hc}{\lambda}$ ) matches the energy required for the electronic transition. This is why transitions between close energy levels are activated with lower energy photons with longer wavelengths, and other way around, transitions between distant energy levels require photons with higher energies and shorter wavelengths. This tight binding between the energy of the upcoming photon and the energy required for a transition between energy levels in a molecule or molecular aggregate, combined with the possibility to control the photon energies, makes the core of spectroscopy. As molecules of different compositions possess different electronic structures, qualitative determination of different compounds is possible with spectroscopy.

In addition to the authentic qualitative determination, spectroscopy offers a possibility to quantitatively determine concentrations in mixtures. The origin of qualitative analysis in spectroscopy originates in the following. Energy transition in a substance has probabilistic nature. Some transitions have zero probability (forbidden transitions), while other transitions have non-zero probability (allowed transitions). The probability of allowed transition is characteristic for this transition, and defines partially the measurable intensity of absorption. This probability does not depend on the concentration of the chromophore in the substance or mixture. In other words, for the given chromophore concentration, the intensity of the absorption at the given wavelength is constant, and it changes when the concentration changes. The other factor which controls intensity of the absorption is the path length of the beam (controlled by a researcher). The law connecting the measured intensity of absorbance with the concentration of a chromophore in the mixture is called Lambert-Beer law.

Mathematically the Lambert-Beer law may be written as

$$-dI = \sigma[X]dx,$$

where  $dI$  stands for the decrease in intensity, which occurs for an increase in path length  $dx$ ;  $\sigma$  is the constant of proportionality, which depends on the identity of the chromophore and the energy of the upcoming photons;  $[X]$  is a concentration, measured in either molecular counts or in moles per litre. Although this expression provides a direct connection between the concentration of the chromophore and the intensity of absorption, it is not very convenient to use. To obtain a more convenient expression, one should rearrange the expression and integrate it over the full path length (from 0 to  $l$ ) along with absorbance:

$$\int_{I_0}^I \frac{dI}{I} = -\sigma[X] \int_0^l dx,$$

$$\ln\left(\frac{I}{I_0}\right) = -\sigma[X]l,$$

i.e. the Lambert-Beer law for the intensity,  $I$ , of transmitted radiation is

$$I = I_0 \exp(-\sigma[X]l).$$

The constant of proportionality  $\sigma$  is called an absorption coefficient or extinction coefficient, and it is directly connected to the probability of the transition. Traditionally, to make the Lambert-Beer law more convenient to use without a computer, the form of extinction coefficient was changed to  $\varepsilon = \frac{\sigma}{\ln 10}$ . This changes the form of the Lambert-Beer law:

$$\log \frac{I}{I_0} = -\varepsilon[X]l,$$

denoting the negative logarithm of the ratio of transmitted intensity to the incident intensity (transmittance) as absorbance (or optical density), one may obtain a linear form of Lambert-Beer law:

$$A = \varepsilon[X]l, \tag{3.4}$$

where  $A$  is the optical density. This form of the Lambert-Beer law is widely used in analytical quantitative analysis of variable mixtures in liquids and gases.<sup>2</sup> The extinction coefficient ( $\varepsilon$ ) is an intrinsic characteristic of a compound at given wavelength in the particular solvent. Unfortunately, it changes significantly from one solvent to another.

---

<sup>2</sup>Although many solutions obey Lambert-Beer law, there are some exclusions. Such, highly concentrated solutions usually deviate from the Lambert-Beer law.

The Lambert-Beer law allows us to use absorption spectroscopy as a powerful analytical tool. However, determination of the correct optical density at a given wavelength may be a challenge. There are several sources of losses of light between the beam emitter and the beam detector: light absorption by air, cell material and solvent light absorption, light reflections and scattering. In some cases, a significant widening of absorption maxima may occur, e.g. upon formation of aggregates. The widening of the absorption maxima leads to an incorrect determination of the extinction coefficient at the given wavelength. Some of error sources can not be controlled or eliminated, but they can interfere with the sample spectrum. Other deviations may even provide a significant source of information about the sample.

Absorption spectra are additive, if no chemical interactions take place in the mixture. Since the absorption spectra are additive, one can consider the spectrum of an empty cell or a cell with a solvent as a reference (reference spectrum). Therefore, one obtains a pure sample spectrum by subtraction of the reference spectrum from the sample spectrum. Another important consequence of the additivity of absorption spectra is that one may decompose a spectrum of a mixture into spectra of its components, which allows to analyse each species separately. This approach is widely used in analytical chemistry, including analysis of carbon nanotubes.

Carbon nanotubes, just as other molecules, absorb light with the photon energy, which matches a transition between ground state energy level and an excited state energy level. This transition is represented schematically in the figure 3.7. As the distance between these energy level is different for different nanotubes chiralities, single wall carbon nanotubes have a distinct optical absorption for each chirality. The SWCNTs absorption range is roughly 300-1300 nm. This region covers the NIR, visible and UV light, therefore, absorption spectroscopy of SWCNTs is the UV-Vis-NIR spectroscopy. A typical UV-Vis-NIR spectrum of CNTs with broad chiralities distribution is shown in the figure 3.8.

Unfortunately, unlike many other materials, optical absorption spectroscopy of carbon nanotubes presents several significant challenges: a baseline of a complicated nature, congestion of the spectrum due to poor chiral purity, overlapping input of soot, etc. A complex nature of the carbon nanotube spectra, particularly, multiple inputs into the baseline, have been discussed in the literature [126, 127, 128].

A characteristic feature of the carbon nanotube spectra is a pronounced baseline with significantly increasing intensity towards the shorter wavelengths range. This baseline has several inputs, i.e. light scattering, contribution from amorphous carbon, contributions from metallic carbon nanotubes, and some other. Let us go through these contributions more in details.

**Amorphous carbon impurities (soot)** is a common carbon nanotubes contaminant [129].

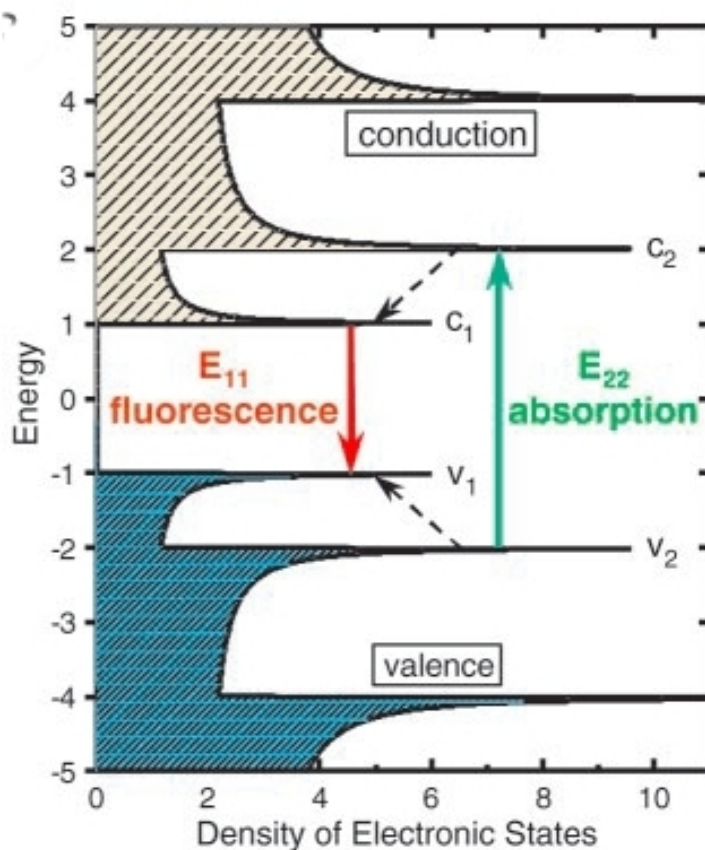


**Figure 3.7** – Origin of CNT the chirality-specific spectra. Schematic density of electronic states for a single nanotube structure. Solid arrows depict the optical excitation and emission transitions of interest; dashed arrows denote non-radiative relaxation of the electron (in the conduction band) and hole (in the valence band) before emission. The exact value of energy, required for the transitions, depends on the tube chirality. Reproduced from [125].

The spectrum of amorphous carbon has been described previously [130] and is known to show strong absorption in the ultraviolet region (with a peak at around 220 nm). The work [128] shows, that the shape of the background, associated with soot in a dispersion may be different, but in all cases it induces elevation of the baseline, more pronounced at shorter wavelengths. The elevation of the baseline, caused by soot, is proportional to the soot concentration in the sample. Naumov and co-workers [128] suggest to estimate the soot contribution to the baseline with the three-parameter exponential function  $A = a(y_0 + \exp(-b\lambda))$ , where  $a$ ,  $y_0$  and  $b$  are fitting parameters. The fitting function was proposed based on absorption spectra of two types of carbon soot. The parameter  $a$  is in linear proportion to the soot concentration, while  $y_0$  and  $b$  depend on the soot itself and may not be assigned authentically. Unfortunately, absence of a robust algorithm to remove of soot contribution from the carbon nanotubes dispersions baseline makes it more a matter of conjecture. Unfortunately, contribution of soot into the baseline is not

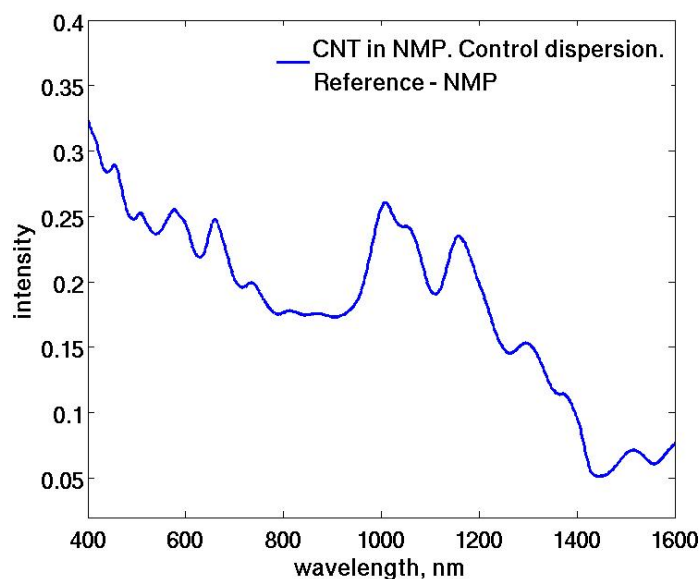


**Figure 3.8** – Typical UV-Vis-NIR spectrum of carbon nanotubes with wide chiralities distribution. The nanotubes sample is N-methylpyrrolidone based dispersion of carbon nanotubes, obtained from SWeNT Inc (SWeNT CG100, Lot # 000-0012, CoMoCat). Each peak corresponds to a certain nanotube chirality, however, there are several peaks interfering with each other. General ascend of the spectrum in shorter wavelengths is due to the presence of metallic nanotubes as well as soot in the sample.

the only one contribution.

**Aggregation** of nanotubes affects the peak-to-valley ratio of the carbon nanotube spectra as well as height of the baseline [128]. Upon aggregation of the tubes the spectrum undergoes significant changes. The background elevates in the whole wavelengths interval, however the elevation in the longer wavelengths region is somewhat higher compared to the shorter wavelengths region. The ratio peak-to-valley intensity reduces upon aggregation. However, the degree of this reduction depends on the wavelength and chirality distribution in the sample. As parameter peak-to-valley ratio is widely used for estimation of sample purity (e.g. [129]), this parameter may serve to estimate a cumulative quality of the dispersion, including purity and amount of aggregates.

**Light scattering** is a non-specific effect. There are two types of scattering, which may be applicable to the carbon nanotubes dispersions: the Rayleigh scattering and the Tyndal scattering. The Rayleigh scattering occurs when light is scattered by particles, smaller than the wavelength of the incident light. Roughly, the Rayleigh scattering is observed in the systems with the particle sizes less than  $\sim 40$  nm. Partially, this effect on the baseline may be compensated by subtracting the spectrum of a pure solvent from the sample spectrum. Unfortunately, in the case of carbon

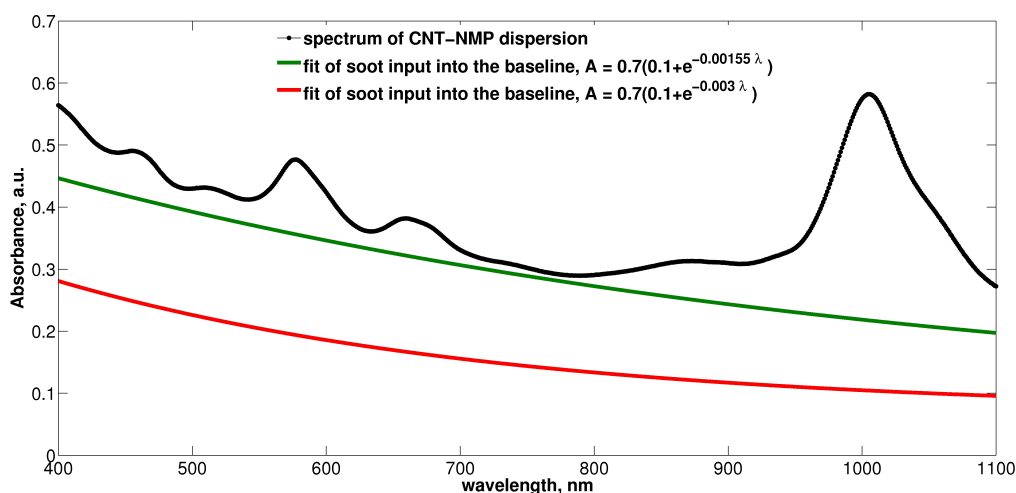


**Figure 3.9** – Example of soot induced background absorption in the carbon nanotube spectrum. The model of soot absorption is from [128]. The model has three parameters, two of which may not be authentically determined (see more details in the text). The two fitting models, represented in the figure, differ only by one parameter ( $b = 0.00155$  and  $b = 0.003$ ). Still, the difference between the models is significant and would result in different outcome of the baseline subtraction. CNT sample: Sigma-Aldrich 704148 CNTs (CoMoCat), enriched with chirality 6,5 (>50%) in N-methylpyrrolidone.

nanotubes dispersions this standard technique does not work, as the contribution from the Tyndal scattering significantly overweights the Rayleigh scattering and can not be simply subtracted as spectrum of a pure solvent. The Tyndal scattering, unlike the Rayleigh scattering, is the major type of scattering observed in colloidal systems. This type of scattering depends on the particle size distribution as well as on the light wavelength.

**Spectral congestion** of spectra of carbon nanotubes is one of major obstacles on the way to define authentically concentrations carbon nanotubes in a dispersion. Indeed, at the moment single-chirality carbon nanotube samples may not be commercially purchased and make a subject of separate scientific papers, e.g. [131, 132, 133]. This is why, despite significant work, which has been done in the field of reliable determination of extinction coefficients of carbon nanotubes of different chiralities (e.g. [134]), the routine analysis of carbon nanotubes chiralities in a mixture still represents a significant challenge and require modelling.

Different carbon nanotubes chiralities have different characteristic absorbance maxima, multiple chiralities in the mixture interfere with each other. This interference results in elevation of the baseline as well as in broadening of the absorption peaks. This phenomenon is known as spectral congestion. It seems useful to step aside from the carbon nanotubes dispersion, to

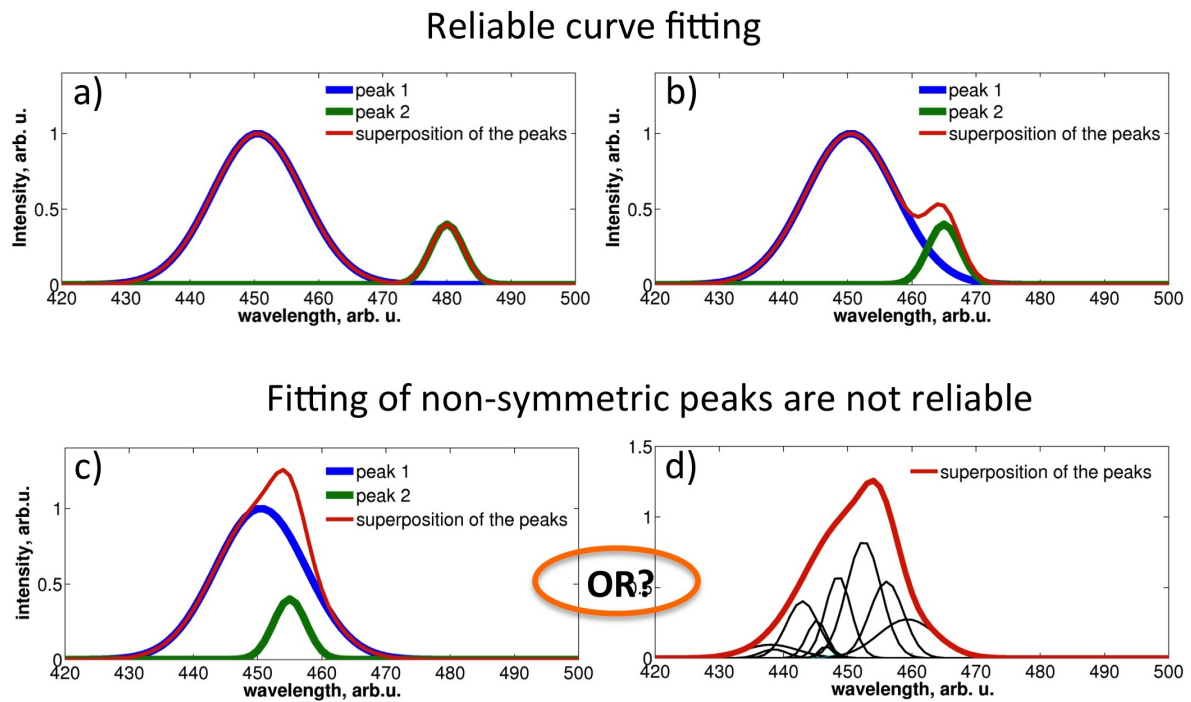


**Figure 3.10** – Example of a spectral congestion. Physical meaning to features of a spectra may be assigned if only each feature is well distinguished from other features (panels a) and b)). If features are not well distinguished, it is impossible to assign a unique set of fitting parameters to the feature (panels c) and d)). Comparing panels c) and d) one may see, that identical curve (red curve) may be fitted in two different ways. In fact, fitting of a curve without distinct features always requires modelling of the features, which make up the curve.

address the subject of spectral congestion from an easier point. The figure 3.10 represents several possibilities to fit a curve with Gaussian functions. Panels a) and b) (fig. 3.10) correspond to a curve, which may be fitted reliably with two Gaussian functions. The most important feature of the curve is that the curve in both cases has two distinct maxima. Assigning a Gaussian to each maximum allows a reliable fit, which may be assigned a physical meaning.

Panels c) and d) (fig. 3.10), unlike panels a) and b), represent a case, when it is impossible to fit the curve reliably. Indeed, as one may see from the figures the curve has a non-symmetric shape, which suggests that the maximum has a complex nature. Unfortunately, in this case it is impossible to fit the maximum with one unique set of Gaussian functions. In fact, both sets of functions (represented in the panel c) and in the panel d)) fit *the same curve* perfectly. This example is an illustration of the fact, that any Gaussian may be represented with a linear combination of Gaussians.<sup>3</sup>

<sup>3</sup>Ideal spectral peak may be represented with a Gaussian.

In the case of carbon nanotubes mixtures optical absorbance spectra represents a superposition of several spectra of different chiralities. Most of the individual carbon nanotube features may not be directly extracted from a spectra fitting. A lot of modelling has to be employed in order to decompose a typical carbon nanotube absorbance spectrum into absorbance spectra of its components. Unfortunately, the number of unknown variable in this modelling is higher than the amount of known parameters. This leads to large uncertainty in the fitting results as well as absence of unique answer on the question "which chirality composition corresponds to this absorption spectrum".

It is possible to overcome this difficulty, provided, that exact positions of peaks of carbon nanotubes of different chiralities are known. The position of the peaks may be obtained experimentally by measuring single nanotube, e.g. [134], or by a combination of experimental and theoretical tools, e.g. [135]. Thanks to these studies it is possible to decompose effectively spectra of surfactant-based aqueous dispersions. Unfortunately, this does not hold true for non-aqueous dispersions of carbon nanotubes. In general case, replacement of a solvent may lead to significant changes in positions of absorption peaks, as well as of the extinction coefficient. This is why at present it is not possible to fit authentically the spectrum of carbon nanotubes in non-aqueous solvent.

Fortunately, authors of the papers [59, 126] suggest the method to remove baseline, which is not tightly bonded to a solvent. They suggest to transfer the baseline of the carbon nanotubes spectrum into the energy domain ( $nm$  to  $eV$ ). This transfer makes the baseline linear, which allows to subtract it easily, based on intensities in the deepest minima of the spectrum. This baseline subtraction enhances the quality of the absorption spectra by removing light scattering contribution and soot contribution, allowing better determination of the maxima of the main chirality of the sample. Unfortunately, this procedure also removes partially background information, associated with the CNT spectra congestion, bundling etc. This is why it is important to represent base-line corrected spectra as well as original spectra.

### 3.5 Photoluminescence of carbon nanotubes

Band-gap photoluminescence is a precise analytical tool to analyse composition of carbon nanotubes dispersion. Depending on their chirality, CNTs have characteristic excitation and emission energy (see fig. 3.7). This allows a precise assignation of each intensity maximum to presence of a CNT of particular chirality.

Although precise, photoluminescence spectroscopy is not capable to detect large bundles



(more than three tubes per bundle). The method also does not detect metallic CNTs and some semiconducting chiralities show only weak luminescence. Additionally, once a metallic CNT gets attached to a semiconducting CNT, it quenches the luminescence of that semiconducting tube, because metallic tubes disturb electronic properties of semiconducting CNTs in the joint bundle.

As CNT bundles are not photoluminescence active, preparation of a photoluminescence active dispersion requires a technique, which insures that only minor fraction of CNTs are in bundles. Usually a dispersion of CNTs which contains only single CNTs and small bundles can be prepared as follows. A mixture of CNTs and of an organic solvent or a solvent with a surfactant undergoes ultrasonification for a few hours. Afterwards the dispersion undergoes ultracentrifugation (minimum 100 000g) to ensure that all medium and large bundles are precipitated and the supernatant contains only small bundles and single CNTs.

Photoluminescence, combined with optical absorbance spectroscopy (before and after ultracentrifugation), allows to estimate amount of CNTs in large bundles as well as the bundle composition.

### 3.6 Transmission Electron Microscopy

Electron microscopy<sup>4</sup> is a relatively new and actively developing technique. In 1932 Knoll and Ruska introduced an idea of electron lenses and were the first to demonstrated images, obtained on an electron microscope. An electron microscope surpassed the resolution of light microscope within a year after the original publication. Regular production of commercial transmission electron microscopes started just seven years later, in 1939. Since then, the electron microscopy has received a significant development and these days it is an important technique in wide area of material science.

The general principle of operation of a transmission electron microscope is very similar to an operational principle of a visible-light microscope, which uses photons as a source of radiation. Both electron and photons have dual wave-particle nature and some other similarities. Both types of a microscope "enlarge" microscopic features up to a resolution  $>0.1-0.2$  mm (resolution of a human eye). In both types of microscopes the "enlargement" is possible due to a system of lenses (optical or electron). Despite some differences light optics is a close relative to electron

---

<sup>4</sup>The material of this section is mainly based on the book *Transmission Electron Microscopy: a Textbook for Material Science* [136].

optics. However, as electrons and photons are different particles, visible-light microscopy and electron microscopy also differ from each other in some aspects.

Visible light radiation at about 550 nm may resolve features of 300 nm size in a visible-light microscope. By reducing the radiation wavelength one increases the resolution. Electrons may have much shorter wavelengths compared to a visible light. Thus at 100keV the wavelength of an electron is about 0.004 nm, which is below the atomic size. This theoretical possibility to resolve the atomic and subatomic details of materials structure originally inspired the research in the field of electron microscopy. The major obstacle in the development of electron microscopes, nearing the theoretical resolution, is a severe spherical and chromatic aberration of electron lenses. At the moment the available quality of electron lenses allows one to resolve features at the angstrom level, which is above the theoretically reachable resolution of a transmission electron microscope.

Transmission electron microscopy, as any other technique, has several important limitations: *i)* sampling; *ii)* artifacts of a specimen preparation; *iii)* interpreting 3D structure in 2D images; and *iv)* damage of the specimen with the electron beam.

Sampling of a specimen with transmission electron microscope is very poor. This is a direct consequence of a high resolution of the instrument. As an example, one could cite the fact that only about 0.6 mm<sup>2</sup> of surfaces have been described with electron microscopy over the last 70 years [136]. This is why it is very important to follow two basic rules when performing an electron microscopy research. First, one needs to supplement an electron microscopy study with a better sampling technique (e.g. optical absorption spectroscopy, which accompanies the electron microscopy studies in this work); and second, one needs to take care that the sample represents the bulk of the material. There are several techniques available which are capable of producing a representative and at the same time an electron transparent film: electrolytic thinning, mechanical thinning, producing a thin solution film, followed by evaporation of a solvent. A comprehensive guide to sample preparation could be found at [137] and in the two-volume book [138].

Interpreting 3D structure in 2D is particularly challenging in transmission electron microscopy. Indeed, the techniques shows not only topology of a surface, but represents the whole volume of a sample. Unfortunately, the information about different slices of the sample volume overlap on the resulting 2D image, formed on a screen, film or a camera sensor. The same phenomenon may occur in the macro world, for example, when photographing against a sunset, when one would see an additive silhouette of all objects between the camera and the sun. In the real world, however, it is easy to understand the real nature of the objects behind this artifact.

This is often not the case at the micro- and nanolevel, as we are unfamiliar with the real nature of the objects. The transmission electron microscopy technique has no depth sensitivity, in other words, the information which is represented on the micrographs is averaged through the thickness of the sample.

Transmission electron microscopy operates by means of powerful electron beams. This always introduces a damage to a specimen. The extent of the damage depends significantly on the specimen nature, exposure time, intensity of the electron source and energy of the electron beam. Organic samples are more vulnerable to the beam damage compared to inorganic substances. Inorganic specimen may be significantly damaged with the electrons. To reduce the electron damage, one may reduce the exposure time, intensity of the electron source or the energy of the electron beam.

Atomic scale resolution of electron microscopes made them irreplaceable part of the nanoparticle characterization process. There are many types of electron microscopy today: transmission, scanning, reflection, etc. Electron microscopy is an important instrument of material science and nanotechnology, particularly, it is an important tool in studies of carbon nanotubes. Transmission electron microscopy has been one of the major tools to study carbon nanotubes since they were discovered [54].

Studies of carbon nanotubes dispersion often involve the following technique of sample preparation. A droplet of the carbon nanotubes dispersion is placed on an amorphous carbon film attached to a metal grid, followed by drying or freezing. This specimen is studied in the electron microscope. As this work deals with ion effects on carbon nanotubes association processes in a dispersion, it is important to discuss this technique more in details here. The main advantage of this technique is its relative simplicity. Indeed, it is reasonable to assume, that a dispersion is quite uniform throughout its volume and concentration fluctuations do not deviate significantly from the analytical concentrations. If the deviations occur, they should be attributed to a physical chemical process and may not be considered random. This property of a dispersion allows one to prepare a specimen, which represents well the bulk. Unfortunately, benefits of this technique are conjugated closely with its drawbacks.

The technique employs placing a droplet of the dispersion onto an amorphous carbon film attached to a metal grid. The procedures of preparation of this carbon film are similar to the procedures of preparation of carbon nanotubes: the carbon is placed onto a plastic matrix by arc-evaporation method. This is why new clean thin carbon films may contain multi-walled carbon nanotubes [139, 140] as well as hydrocarbon contamination [141]. There are several suggestions of how one may exclude studies of the carbonaceous and hydrocarbon contaminations of the

films: *i*) use grids with no support films; and *ii*) use non-carbon support films, e.g. SiO<sub>x</sub>; *iii*) as hydrocarbon contaminations may be mixed up easily with salt, reference studies should include imaging of salt-free dispersions.

The disadvantage of grids with no support films are significant. The grid itself is not transparent for electrons. As a result, only the material, which spans through the grid holes may be studied. Standard grids available commercially vary between 200 and 600 mesh.<sup>5</sup> The grid hole size in 400 mesh is  $\sim 42\mu\text{m}$ , which means that many carbon nanotubes would simply penetrate through the grid. This dramatically reduces the amount of material available for studies.

The silica coating may be unstable, which makes this way of excluding the carbonaceous contamination also not convenient. Another disadvantage of silica coating is its higher electron density compared to carbon. This means, that due to low contrast of carbon nanotubes, they may be simply lost on the silica support film.

Fortunately for this work, the probability to find single walled carbon nanotube on a nominally empty carbon film is low. Moreover, the amount of carbon nanotubes in the sample is quite high. These two factors allowed to use carbon support films in the study.

---

<sup>5</sup>The number in the mesh size of a grid defines the number of holes per inch of the grid. The larger number, the more holes fit into the inch, the smaller is the size of each hole.

# 4

## **Cation interactions with carboxylic group. Cation effects on behaviour of benzoic acid at interface and binding constants with $\alpha$ -cyclodextrin**

### **4.1 Ion pairing between carboxylate group and sodium and potassium ions**

The chapters 1 and 2 show that ions are capable of altering interactions in a system solute-solvent. Although the salt effects are studied intensively in the protein [142, 143, 144, 145, 146, 147] and colloidal sciences [148, 149], they are not sufficiently explored in surface chemistry of benzoic acid as well as in CD chemistry. The current understanding of ion effects on cyclodextrin binding with small molecules is represented in the section 2.4. This understanding does not explain the experimental results, described in details in the section 3.2. Summarizing these experimental results, sodium ion reduces effectively the binding constant between  $\alpha$ -cyclodextrin and benzoic or nicotinic acids. These results may not be explained from the current point of view regarding ion effects on the guest-host complexes stability. The effects of ionic strength should be excluded

because the increase of the binding constant, which is characteristic for this type of ion effects, is not observed. Another known ion effect, such as competition for the host, manifests itself with a reduction of the binding constant. This type of ion effects could not explain the observed experimental results because it manifests itself only in the case of large, polarizable anions, e.g.  $\text{ClO}_4^-$ .

On the other hand, it is known that cations can interact selectively with charged molecules or ions via ionic pairing. This effect of ion pair formation may play a significant role in the mechanisms of host-guest complexation. If affinity of sodium ions to the carboxylate group exceeds the affinity of potassium ions to this acidic group, it may explain the observed difference in the salts effects on stability of complexes. Molecular dynamics simulations is a convenient tool to study ion pairing in a solution. This is why in this work molecular dynamics was used for studies of ion pairing between carboxylic group of benzoic or nicotinic acids with sodium or potassium ions.

#### 4.1.1 Simulation details

Fully atomistic molecular dynamics (MD) simulations of separate salt and bulk water solutions of benzoic acid, nicotinic acid, and  $\alpha$ -CD were performed with the Desmond 2.2 package [99]. In salt solutions the concentration of NaCl or KCl was constant and equal to 0.3M for all simulations. In the simulations we used the TIP4P model for water [91, 150] and the OPLSAA force field [151, 152, 153, 154, 155, 156, 157, 158] for ions and organic compounds. The force field parameters were assigned automatically with Desmond standard algorithm. We used the RESPA integration algorithm with two integration time steps: the integration time step for the short-range interactions was 2 fs, and the time step for the long-range interactions was 6 fs. To treat the the long-range electrostatic interactions we used the smooth particle mesh Ewald method [159] with the cutoff radius of 9 Å.

In every simulation the solutes (benzoate anion or zwitterion of nicotinic acid) were placed in a periodic cubic cell of size 5X5X5 nm<sup>3</sup>. Next, 21 ion pairs ( $\text{Na}^+\text{Cl}^-$  or  $\text{K}^+\text{Cl}^-$ ) were placed randomly in the cell volume excluding the solute volume (in the case of benzoate we placed an extra sodium cation into the cell to neutralize the system). Afterwards water molecules were added in the simulation cell; water molecules overlapping with any solute atom or any ion were removed. The final amount of water molecule was 3791 for every system except for the  $\alpha$ -CD solutions (in this case, there were 3753 water molecules in the box, as CD has a larger excluded volume). We used the molecular structures of benzoic acid, nicotinic acid, and  $\alpha$ -CD obtained

from the Cambridge Structural Database [160]. During the simulations, the positions of carbon atoms were restrained harmonically to their original positions in space. These restraints should not influence the density distribution functions, discussed in this work because the functions operate with relative positions of the atoms. The restraints were introduced for the sake of convenience of the 3D distribution functions calculations.

Simulations were carried out in two stages for all systems. During the first stage the systems were equilibrated in the NPT ensemble for 2 ns. The simulation temperature was 300K and the pressure was 1 atm, which were kept constant using the Berendsen thermostat and barostat with the relaxation times of 1 and 2 ps correspondingly. Before the equilibration the potential energy of every system was minimized, using the standard relaxation procedure [99] to avoid sterical clashes between the atoms.

Next, productive simulations in the NVT ensemble were performed at the constant  $T = 300\text{K}$ , using the Berendsen thermostat with the relaxation time equal to 1 ps. To collect sufficient statistics of ion pairing we simulated all systems for 130 ns.

#### 4.1.2 Results and analysis

Radial distribution functions and 3D distributions were calculated with VMD 1.8.7 [161] using the following VMD plug-ins: Radial Distribution Function and VolMap respectively [161]. The mesh size for the 3D density distributions was  $0.5 \text{ \AA}$ . The 3D distributions for ions were smoothed with the Gaussian window method [161] to remove noise (the width of the window was set equal to the van der Waals radii of the ions).

Similar to the works [162, 85], the potential of mean force (in  $k_B T$  units) was calculated as the negative natural logarithm of the corresponding radial distribution function  $g(r)$  (see also sec. 3.1.6). The figure 4.1 shows the calculated potentials of mean force and the 3D density distributions of ions and water molecules around the carboxylate groups of the benzoate molecule. We plot the PMFs curves in  $k_B T$  units ( $\text{PMF}/(k_B T)$ ) to show the scale of the effects as compared to the energy of temperature fluctuations  $k_B T$ .

The potential of mean force functions (PMF) exhibit a short distance minimum corresponding to the direct ion pairing, while the less pronounced second minimum corresponds to the solvent-separated ion pairing. The depths of the second minimum are around  $0.3\text{--}1.0 k_B T$ , which means that the energies of the solvent-separated ion pairs are within the range of the energy of thermal fluctuations. Because of the low energies of the solvent-separated ion pairs, we assume that their effects on the  $\alpha$ -CD-ACA complex formation are rather weak, and therefore in the discussion of

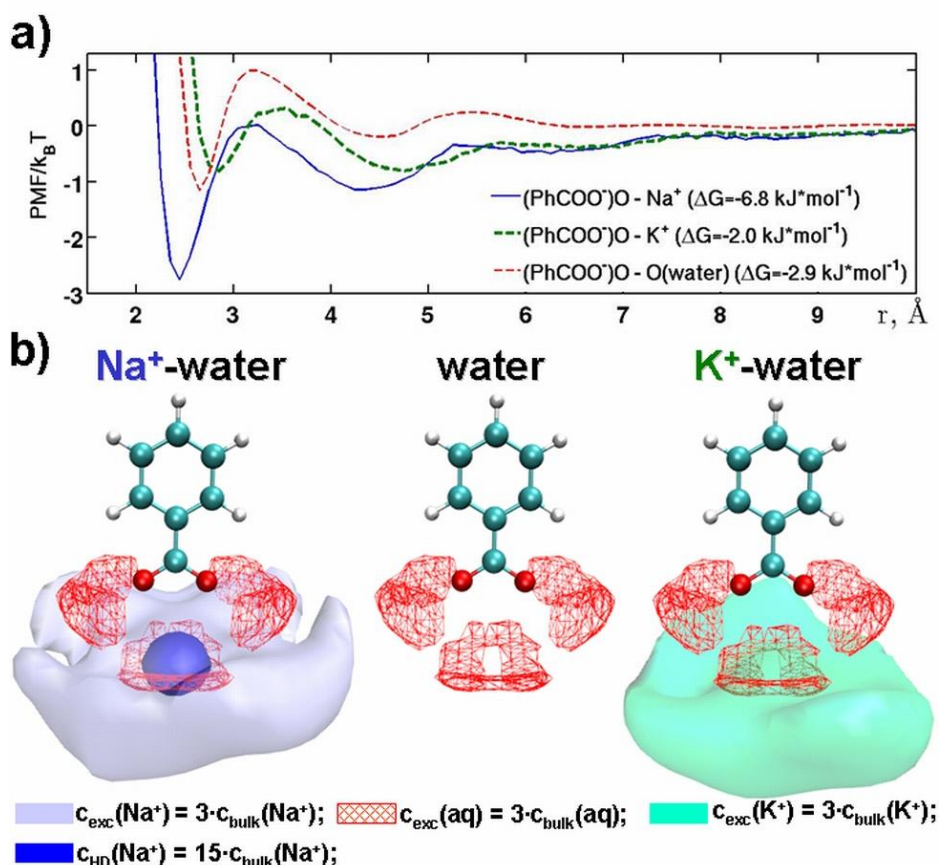


**Figure 4.1** – Water and ions distributions near the carboxylate group of benzoate. (a) Potentials of mean force (PMF) between the carboxyl oxygen of benzoate acid and Na<sup>+</sup>, K<sup>+</sup>, and water. The values of the free energies of formation direct contact pairs ( $\Delta G$ ) between the species are given in brackets. The solid blue line is the (PhCOO<sup>-</sup>)O – Na<sup>+</sup> PMF; the bold dashed green line is the (PhCOO<sup>-</sup>)O – K<sup>+</sup> PMF; the dashed red line is the (PhCOO<sup>-</sup>)O – O (water) PMF. (b) Water and ions isoconcentration surfaces around the carboxylate group of benzoate. The red mesh as well as the light blue and green surfaces are isosurfaces of local particle concentrations that are 3 times higher than the bulk concentrations of water ( $c_{\text{bulk}}(\text{water})$ ), Na<sup>+</sup> ( $c_{\text{bulk}}(\text{Na}^+)$ ), and K<sup>+</sup> ( $c_{\text{bulk}}(\text{K}^+)$ ), correspondingly. The dark blue surface is the isosurface of local Na<sup>+</sup> ion concentration that is 15 times higher than the Na<sup>+</sup> concentration in the bulk. Bulk concentrations are:  $c_{\text{bulk}}(\text{Na}^+) = c_{\text{bulk}}(\text{K}^+) = 0.3 \text{ M}$  ( $1.84 \cdot 10^4$  particles per  $\text{Å}^3$ );  $c_{\text{bulk}}(\text{water}) = 55.4 \text{ M}$  ( $3.33 \cdot 10^2$  particles per  $\text{Å}^3$ ).

the experimental results, we will mainly focus on the effects of direct ion pairing.

Using the PMFs, we obtained the free energies of formation of direct contact pairs ( $\Delta G$ ) between the molecular species as the minimum values of the corresponding PMFs. For the  $\Delta G$  calculations we used the standard definition of PMF ( $\text{PMF}(r) = -k_B T \ln(g(r))$ ) [85].

One can see from figures 4.1 and 4.2 that, as compared to K<sup>+</sup>, the distribution of Na<sup>+</sup> around R – COO<sup>-</sup> is much more dense. This tendency is the same for both acids. Thus Na<sup>+</sup>



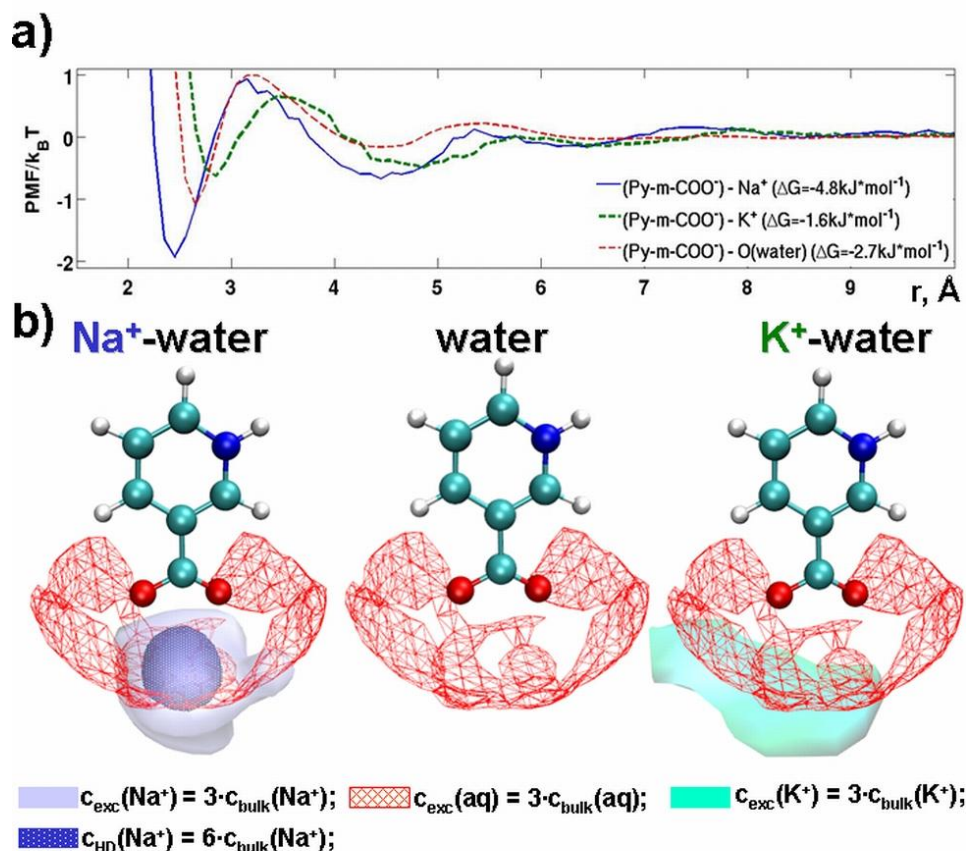


**Figure 4.2** – Water and ions distributions near the carboxylic group of nicotinic acid. a) Potentials of mean force (PMF) between the carboxyl oxygen of nicotinic acid and Na<sup>+</sup>, K<sup>+</sup> and water. The values of the free energies of formation direct contact pairs ( $\Delta G$ ) between the species are given in brackets. The solid blue line is the (Py – m – COO<sup>-</sup>)O – Na<sup>+</sup> PMF; the bold dashed green line is the (Py – m – COO<sup>-</sup>)O – K<sup>+</sup> PMF; the dashed red line is the (Py – m – COO<sup>-</sup>)O – O (water) PMF. b) Water and ions isoconcentration surfaces around the carboxylic group of nicotinic acid. The red mesh as well as the light blue and green surfaces are isosurfaces of local particle concentrations, which are three times higher than the bulk concentrations of water ( $c_{\text{bulk}}(\text{water})$ ), Na<sup>+</sup> ( $c_{\text{bulk}}(\text{Na}^+)$ ) and K<sup>+</sup> ( $c_{\text{bulk}}(\text{K}^+)$ ) correspondingly. The dark blue surface is the isosurface of local Na<sup>+</sup> ion concentration, which is six times higher than the Na<sup>+</sup> concentration in the bulk.

ions preferably interact with the carboxylate via formation of the direct contact pair, which is consistent with the literature data [163, 162, 164, 48]. On the other hand, as it can be seen from figures 4.1 and 4.2, potassium ions have much less potency to make direct contact pairs with the carboxylic group because they cannot compete with water for the first solvation shell of the group. The R – COO<sup>-</sup> group remains fully hydrated as if it were in the bulk water solution. These simulations findings allow to suggest new mechanism of ion effects on complex formation.

### 4.1.3 $\text{Na}^+/\text{K}^+$ specific effects on complex formation. Competition for the guest

Similar to the results reported in the previous sections, differences of sodium and potassium binding to carboxylic acids in water have been studied previously. There are several works where the selective interactions of biologically active cations with carboxylate groups of glycine [163], formate [48, 165], acetate [163, 165, 166],  $\alpha$ -poly-L-glutamic acid [162], and protein anionic side groups [167] have been studied by experimental and theoretical methods. These works demonstrated that  $\text{K}^+$  and  $\text{Na}^+$  cations have different binding affinities to carboxylates. As compared to potassium, much stronger attraction of sodium to carboxylates has been observed. This is consistent with the empirical Law of Matching Water Affinities by Collins [50] (see also section 2.1), according to which the ions with a similar hydration energy form more stable contact ionic pairs. Thus, as discussed in the work of Aziz *et al.* [163], the hydration energies of sodium and carboxylate are very close, and, as a result, these ionic molecular species form rather strong counterion pairs in water.

Complex formation is a form of non-covalent weak intermolecular interaction. Although binding of species in a complex is weak, complex formation is important for many biological and industrial processes. As an example, one could bring a reversible complex formation of oxygen and  $\text{CO}_2$  with haemoglobin which is an essential part of breathing process. Another example of importance of complex formation is its wide employment in the pharmaceutical industry to improve solubility of water-insoluble drug molecules. In this case a soluble molecule, e.g. cyclodextrin, forms a soluble complex with insoluble drug-molecule.

Understanding the principles, governing processes in living organisms, is a key role in more efficient engagement of the complex formation process for the industrial needs as well as better understanding deep biochemical insights of living. Complex formation is a result of interplay of several different forces: van der Waal, hydrophobic, electrostatic, etc. Due to a complex nature of the process of complex formation, this area is a subject of ongoing research for the last century. However, the current understanding of the complex formation is still far from being complete.

The binding constant (stability constant) is a measure of complex stability. The stability constant represents quantitatively an interplay of the intermolecular interactions. Due to ambiguous nature of the complexes, it is not easy to understand the impact of each force on the complex formation. Unfortunately, this force differentiation is not always possible with an experiment. This means, that simulations are an essential part of deep understanding of the complex formation.

Unfortunately, simulations of biomedical related systems presents significant challenges. The most important of them are *i)* low ion concentrations, which force a researcher to increase the size of a simulation cell or prolong the simulation time; *ii)* large numbers of atoms in many biological molecules, e.g. proteins; *iii)* various types of weak interactions, which increase complexity of analysis, etc. Another important restriction is applied on the compounds, which could be considered as biomedical. Although many compounds possess biological activity, one should be aware of toxicity of many compounds just as much as accounting for the compound solubility: an insoluble compound does not possess biological activity. In other words, biological systems consist of very restricted number of compounds, which makes simplified modelling ineffective. The only solvent possible for biological systems is water, which means that one can not use different solvent or even mixtures of solvents to improve a control over processes in biosystems or employ simplified media for simulations. These restrictions bring a new challenge and importance into the task of understanding of selective ion effects on processes of complex formation in biological systems.

Many known biologically active compounds are alkyl or aromatic derivatives of benzene. Benzene is a hydrophobic compound and it is poorly soluble in water (0.02M). The benzene molecule is a symmetrical molecule, and, as a result, it's hydration shell is symmetrical as well. However, once one of the hydrogen atoms in the benzene molecule is substituted, the hydration pattern of the whole molecule changes. Changes in hydration pattern are capable of altering interactions of a molecule with another molecule as well as with an interface, which means altering of interactions of bioactive and drug molecules with a cell membrane, proteins and organelles inside the cell. This is why it is important to understand how a derivation of benzene ring alters the hydration pattern and how these alterations change the interactions of the molecule with a hydrophobic surface.

The review of available literature data, concerning salt effects on binding of CDs with different guests, reveals that in some cases KCl and NaCl act as salting-out agents [168, 169, 170]. Schlenk and Sand [168] experimentally observed the decrease of aqueous solubility of benzoic acid in the presence of KCl. When the salts, displaying salting-out effect, are dissolved in aqueous solution, they are hydrated by water molecules. This process should result in reduction of water available for aromatic carboxylic acids and promote their inclusion into  $\alpha$ -CD cavity. It implies the increase in binding constants, which, as an example, was demonstrated for complexation of  $\beta$ -CD with naphthalene [170], 3-hydroxy-2-naphthoic acid [83], and terfenadine [171]. It should be noted that in all these systems complex formation was driven by hydrophobic effects. However, it has been shown previously [4] that benzoate has pronounced hydrotropic behavior,

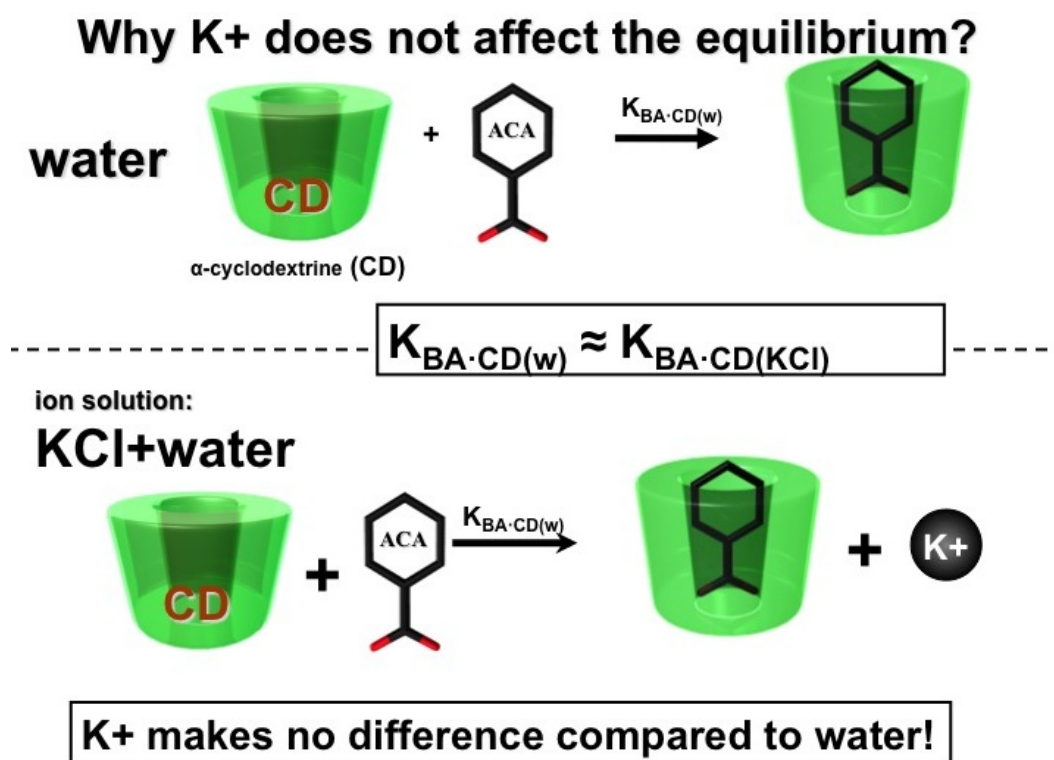


**Figure 4.3** – Scheme of equilibria in the system ACA- $\alpha$ -CD-K<sup>+</sup>. Potassium ion does not participate in formation of ion pairs with benzoate anion (bottom). As a result, the amount of benzoate anions available for interactions with cyclodextrin remains the same compared to pure water (top). As the effective concentration of benzoate anion remains the same in pure water and in a potassium chloride solution, no reduction of apparent binding constant cyclodextrin-acid may be registered.

and we assume that there should be another driving mechanism of CD-ACA binding in addition to hydrophobic interactions. Indeed, the observed in our case decrease in the binding constants indicates that rearrangements in solvent, caused by adding of NaCl and KCl, are not of primary importance, and hydrophobic interactions are not the main driving force in complexation of  $\alpha$ -CD with nicotinic acid and benzoate.

As it was mentioned above, in general, the possible influence of anions should be taken into account for explanation of salt effects. However, in the case of chlorides the formation of ternary complexes between  $\alpha$ -CD, carboxylic acid, and Cl<sup>-</sup> is unlikely. To the best of our knowledge, such ternary complexes formed by Cl<sup>-</sup> were not described in literature. Usually, anions with larger size such as ClO<sub>4</sub><sup>-</sup> or CO<sub>3</sub><sup>2-</sup> interfere with the formation of the complexes. If Cl<sup>-</sup> makes a complex with  $\alpha$ -CD, the competition between chlorides and carboxylic acids for the host cavity should decrease the binding of  $\alpha$ -CD with ACAs. However, interactions of CDs with inorganic anions have been studied in several works [172, 173, 174, 175] where it was shown that Cl<sup>-</sup> and

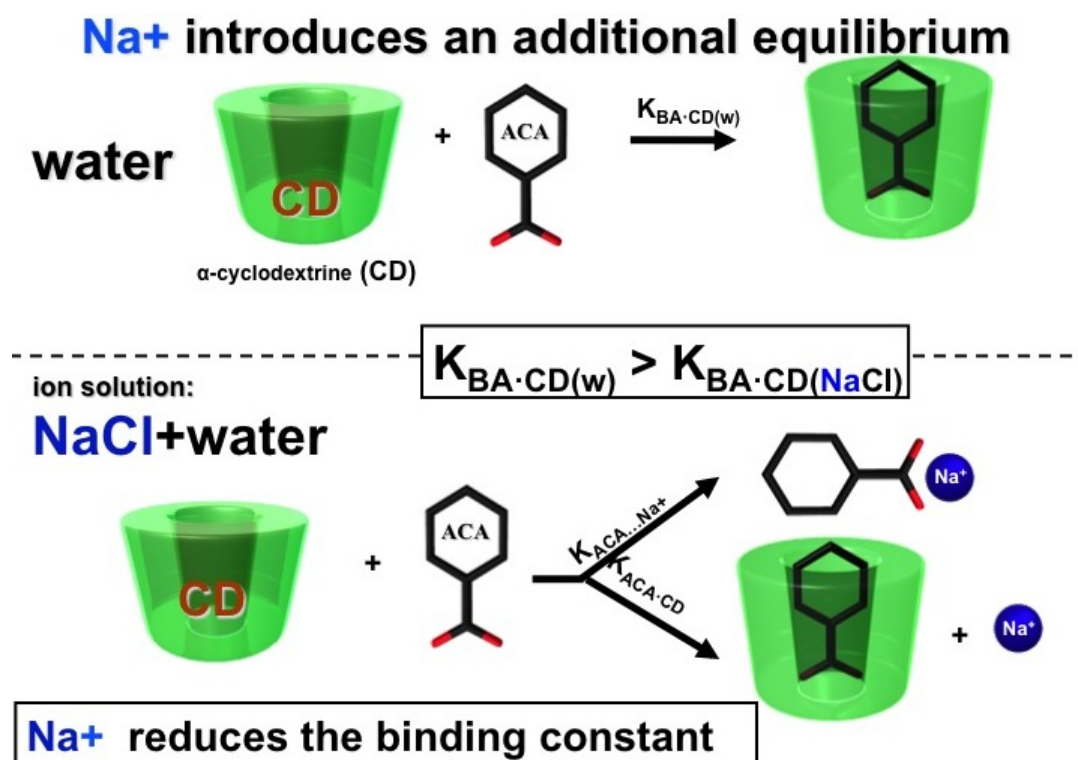
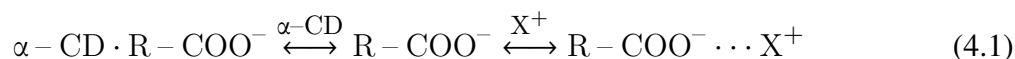


**Figure 4.4** – Scheme of equilibria in the system ACA- $\alpha$ -CD- $\text{Na}^+$ . Sodium ion participates in formation of ion pair with benzoate (bottom) which effectively reduces the amount of benzoate anions available for complex formation with cyclodextrin compare to pure water (top). This reduction of effective benzoic acid concentration leads to reduction of the apparent binding constant cyclodextrin-acid.

$\alpha$ -CD do not form stable complexes. Additionally, a molecular modelling analysis of interactions between  $\alpha$ -CD and  $\text{Cl}^-$  using a 130 ns MD trajectory of  $\alpha$ -CD in KCl and NaCl solutions and found no  $\text{Cl}^-$  ions in the internal  $\alpha$ -CD cavity for any of the MD frames. Thus the literature data as well as the simulations of selective cation effects and CD-benzoate complexation in KOH and NaOH solutions (without the presence of any  $\text{Cl}^-$  ions) suggest that the probability of  $\alpha$ -CD/ $\text{Cl}^-$  complex formation is very low, and, therefore, that can be neglected in our analysis.

The commonly used conceptions in the literature for interpretations of salt effects and the facts discussed above do not explain the different influence of  $\text{Na}^+$  and  $\text{K}^+$  on complex formation between  $\alpha$ -CD and aromatic carboxylic acids. To explain the experimental results, we propose a new mechanism of salt effects on  $\alpha$ -CD complex formation with ionized aromatic carboxylic acids. According to this mechanism,  $\text{Na}^+$  and  $\text{K}^+$  cations compete with  $\alpha$ -CD for the carboxylic acid. In this case, the processes in the solution can be described with the following scheme (see also figures 4.4 and 4.3):



Formation of ionic pairs ( $\text{R} - \text{COO}^- \cdots \text{X}^+$ ), being in competition with complex formation ( $\alpha\text{-CD} \cdot \text{R} - \text{COO}^-$ ), shifts the equilibrium (3.3a) to the left (the direction of complex dissociation). We illustrate this competitive mechanism by the pictorial representation in figures 4.3 and 4.4. Complex formation of  $\alpha\text{-CD}$  with acids under investigation is weak ( $\lg K < 2$ ), and, therefore, it is very sensitive to competitive processes. As a result, we observe the decrease in complex stability.

Selective interactions of  $\text{Na}^+$  and  $\text{K}^+$  with carboxylate have been reported in several experimental and computational studies [48, 163, 162, 164]. These works showed that  $\text{Na}^+$  binds  $\text{R} - \text{COO}^-$  group much stronger than does  $\text{K}^+$ . The MD data also show the preferential binding of  $\text{Na}^+$  to  $\text{R} - \text{COO}^-$  over  $\text{K}^+$ . The revealed preferential direct contact pairing of  $\text{R} - \text{COO}^-$  with  $\text{Na}^+$  determines the difference in the effects of  $\text{Na}^+$  on thermodynamics of  $\alpha\text{-CD-ACA}$  complex formation as compared to  $\text{K}^+$  (tables 3.2 and 3.3).

As the ionic pairing coexists with complex formation, contributions of both these processes are reflected in experimental  $\Delta_c H$  and  $\Delta_c S$  values (table 3.3). The observed in  $\text{NaCl}$  solution decrease of enthalpy and entropy is attributed to increased negative contribution from electrostatic interactions between  $\text{R} - \text{COO}^-$  and  $\text{Na}^+$ .

Presumably, the  $\text{Na}^+$  ion pairing with the anionic carboxylate group of nicotinic acid is responsible for the additional negative contribution to  $\Delta_c H$  due to the favorable electrostatic interactions between the counterions. However, the formation of the sodium-carboxylate contact ion pairs also results in an increase of ordering in the system. Therefore, the favorable enthalpy gain is compensated by the negative entropy term resulting in the overall decrease of the apparent complex stability constant  $K$ .

Generally, the formation of solvent-separated ion pairs [176, 177, 178] in the solution might have some effect on the complex formation changing the equilibrium of the complex formation reaction. However, for the systems studied here, the energy of solvent-separated ion pairing is comparable with the energy of thermal fluctuations  $k_B T$  (see figure 4.1 and the corresponding discussion above). The X-ray absorption results of  $\text{Na} - \text{Cl}$  and  $\text{Na} - \text{OH}$  ion pairing [177, 178] also suggest that the energy of solvent-separated ions pairs is much less than the energy of contact ions pairs. Therefore, we assume that the effects of solvent-separated ion pairs are of secondary importance to the phenomena, considered herein, as compared to the effects of contact pair formation.

It is interesting to note that the opposite influence of NaCl on thermodynamic characteristics of complex formation between hydroxypropyl- $\beta$ -CD (HP- $\beta$ -CD) and 1-butanol in aqueous solution has been detected by Fini and co-workers [179]. The authors showed that in NaCl solution the inclusion complexes are more stable than in water and their stability is increased with rise of NaCl concentration. It was also demonstrated that enthalpy is not changed while the entropy is increased with enhancement of NaCl concentration. Thus, the variance of  $\Delta_c G$  with NaCl concentration is entropy controlled. By comparing the effects of NaCl on  $\alpha$ -CD/nicotinic acid and HP- $\beta$ -CD/butanol binding, we can conclude that influence of NaCl on thermodynamics of complex formation is not the same, and it depends on the solutes nature and driving forces of interaction. In the case of butanol complex formation is realized due to inclusion of apolar moiety of the guest molecule into hydrophobic cavity. The hydrophobic and van der Waals interactions are the main driving forces of HP- $\beta$ -CD binding with butanol. Therefore, the influence of NaCl can be shown as the salting-out effect. On the contrary, the R – COO<sup>-</sup> group of nicotinic acid enters the  $\alpha$ -CD cavity upon binding, and van der Waals interactions as well as hydrogen bonding are responsible for complex formation. The decrease of binding constant, observed in the presence of NaCl, is determined by the partial weakening of interactions of nicotinic acid with  $\alpha$ -CD cavity due to participation of the R – COO<sup>-</sup> group in the ionic pairing with Na<sup>+</sup>.

Generally, it is possible to predict the ion effects theoretically once a true thermodynamic constant of the binding process itself, the list of all possible side processes and all corresponding constants are available. However, the procedure is very complex and in many cases it is practically impossible. That is why it is common to measure conditional binding constants. The disadvantage of conditional (apparent) constants is that they change if the conditions change. On the other hand, this ability of conditional constants allows an easy search of optimal conditions for the particular reaction. It has been mentioned previously that ion effects may manifest themselves indirectly via changes of hydration patterns of solutes in a solution, as well as strength of the hydration. This is why it is important to understand how changes in hydration affect complex formation without ion effects.

#### **Effects of hydration strength on binding constant**

Aromatic carboxylic acids (ACAs) offer rich possibilities to investigate hydration effects on complex formation reactions. First, benzoic acid itself is an amphiphilic compound with a possibility to control hydration properties. Second, the hydration pattern of the molecule can be changed easily by benzoic acid derivation.

**Table 4.1** – Hydration energies of ACAs in different ionization state. Calculated hydration energies of ACAs in a different ionization state, along with the experimentally obtained binding constants.<sup>1</sup> Higher binding constants correspond to less negative free energy of hydration.

complex	ABA ionisation state	Conditions	K, kg/mol	$\Delta_{\text{hydr}}G$
pABA/ $\alpha$ -CD	unionised	water	1492 $\pm$ 42	-53
	anionic, pH 8.5	NaOH <sub>aq</sub>	9 $\pm$ 2	-334
		KOH <sub>aq</sub>	30 $\pm$ 8	
	zwitterionic			-292
mABA/ $\alpha$ -CD	unionised	pH <5		-49
	anionic, pH 8.5	NaOH <sub>aq</sub>	1 $\pm$ 12	-326
		KOH <sub>aq</sub>	4 $\pm$ 1	
		water	59 $\pm$ 1	-276
	zwitterionic	0.2M NaCl	60 $\pm$ 1	
		0.2M KCl	56 $\pm$ 1	
oABA/ $\alpha$ -CD	unionised			-37
	anionic			-261
	zwitterionic			-56



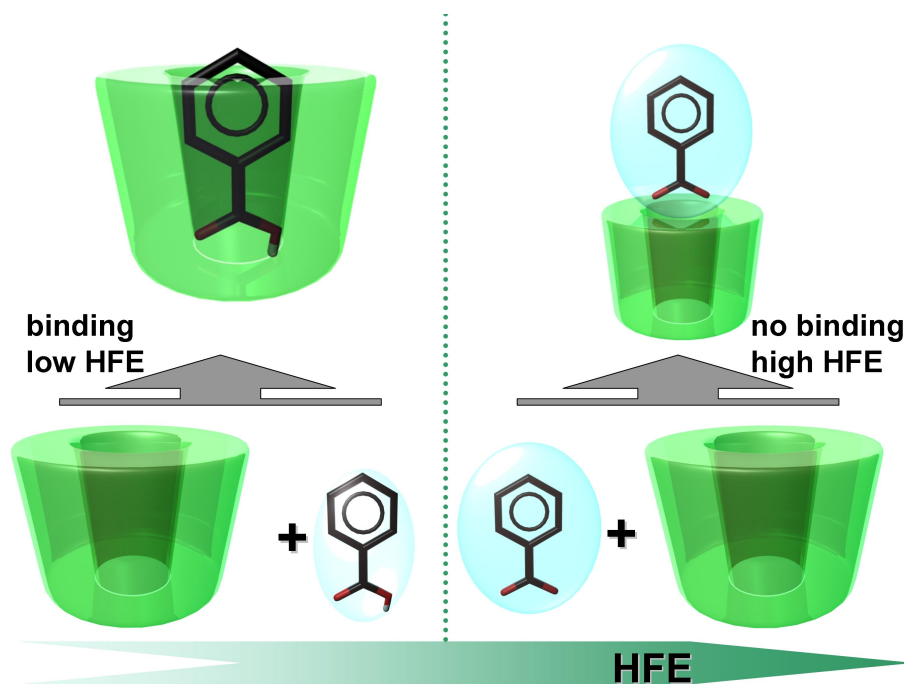


**Figure 4.5** – A pictorial representation of hydration strength effect on ACA-CD complex formation

Complex formation of  $\alpha$ -CD with ACA is not intuitive. It seems that the most probable way to form a complex would be to insert the hydrophobic benzoic ring of the acid into the non-polar cavity of the  $\alpha$ -CD and leave the polar/charged  $-\text{COO}(\text{H})$  group outside to preserve the possibility for H-bond formation with water molecules. However, the work [111] and our results show that the insertion with the carboxylate group takes place.

To explain this phenomenon one should consider, that although the CD cavity is *relatively* non-polar and hydrophobic, it still contains polar OH-groups which could potentially form a hydrogen bond with carboxylic group of the inserted ACA molecule. On the other hand, the hydrophobic benzoic ring is covered from direct water contacts: firstly, it is partially inserted in the CD cavity; secondly, it is partially covered with the CD's OH-groups of the wide rim, which are less polar than water, situated relatively far from the aromatic system, and have a possibility to interact with water molecules outside the cavity; and thirdly, the geometry of the water accessible part of benzene ring is not suitable for efficient interaction. According to this model all possible H-bonds are formed. If the ACA molecule was inserted with the carboxylic group outside the wide rim of the CD it would not be able to form the H-bond due to geometrical mismatches with the CD cavity.

The frequency of possible contacts between ACA molecule and CD molecule in a solution depends on the strength of the molecules hydration. Indeed, as it was discussed in the section 2.4, formation of a complex requires dehydration of the interacting species. The stronger the

hydration, the less probable is the dehydration.

To get some more details of the effects of hydration strengths on the stability of ACA- $\alpha$ -CD complexes, calculations of hydration free energies were performed and compared with experimental data on stability constants. The hydration free energies of ABAs were calculated as the energy difference of the optimised gas-phase molecular structure and the optimised solvated molecular structure. We employed the Poisson-Boltzmann solvation model ( $\epsilon_{\text{water}}=80.37$ , probe sphere radius 1.4 Å) [180, 181]. Both geometry optimisations and energy calculations were performed using the B3LYP/6-31G\*\* level of theory. All calculations were carried on with Jaguar 7.7 from the Schrodinger Suite 2011.

The table 4.1 clearly shows, that highly hydrated ionized forms of the aminobenzoic acid have significantly lower binding constants, compared to neutral forms. It is also interesting to note, that hydration free energy of zwitterionic o-ABA is significantly lower than hydration free energies of other ionized species. This may be explained with a close spatial position of the charged group of this zwitterion. As a result, these two groups neutralize effectively each other's charge. The pictorial representation of the hydration strength effect on the complex formation is demonstrated in figure 4.5.

Cyclodextrin is a relatively hydrophobic large molecule. This molecule plays an important role as a simple model of more complicated macro-molecules, such as proteins. Still, the geometry of the cyclodextrin surface is quite complex, which makes analysis of contacts between cyclodextrin and aromatic carboxylic acids more complicated. In order to better understand, how aromatic carboxylic acids interact with hydrophobic surfaces, one may employ simulations of aromatic carboxylic acids at aqueous solution/vapour interface.

## 4.2 Effects of ions and pH on benzoic acid behaviour at water/vapour interface

The answer to the question how hydration of a solute changes in a solution includes a complex of several inputs on top of the hydration pattern of the molecule: the shape of the interface, affinity of the molecule to the surface, hydrophobicity of the surface, etc. This is why we need to understand how substitution of one hydrogen atom in benzene molecule affects the behaviour of a molecule at a simple interface. In order to understand this we studied behaviour of a mono-substituted benzene (benzoic acid) in different ionization states as well as in the presence

of different ions. Benzoic acid is the most suitable molecule for these studies. First of all, it has a simple and quite rigid structure. Second, benzoic acid is an ionizable molecule, which means that depending on the pH it can be neutral as well as charged (fig. 4.12). It is important to note that the structure of benzoic acid does not change upon ionization. This is why hydration shell changes are easier to understand, which is important for deep understanding of the whole effect.

Benzoic acid has a  $\text{pK}_a^2$  of 4.21 in water, which means that at the pH below this value benzoic acid exists as a neutral molecule (BAH); at the pH values above 4.21 benzoic acid is ionized and exists as benzoate anion ( $\text{BA}^-$ ). The knowledge of the effects of protonation/deprotonation on the molecular structure of the benzoic acid at aqueous solution/vapour interface is important for understanding the molecule's environmental effects, its transport and adsorption properties in technological processes and its photo- and biodegradation in natural and industrial environments [26, 27, 29, 31, 33, 35, 36, 37, 38, 39, 40, 41, 42, 43]. However, there is a lack of understanding of benzoic acid behaviour at the aqueous solution/vapor interface. This lack of understanding makes it impossible to compare the interface behavior of benzoic acid in different protonation states in details.

In this study benzoic acid was considered in neutral (molecular) form as well as in the form of sodium and potassium benzoates. Consideration of both neutral and ionized form of benzoic acid allows us to understand: *i*) general effect of pH (below and above 4.21) and *ii*) effect of counter-ion on the interfacial behaviour of benzoates. Effects of pH may be considered as a type of ion effects. Indeed, hydrogen, despite its special position in the periodic table, is a cation of the first group of the periodic system.

Several forces govern the behaviour of benzoic acid at water-vapour interface. Benzoic acid is an amphiphilic compound with a hydrophobic aromatic ring and a hydrophilic carboxylic group. BAH and  $\text{BA}^-$  differ by the charge state of the carboxylic functional group, which can cause their different behaviour at the aqueous solution/vapour interface. It is known that non-substituted aromatic systems tend to lie flat on the water surface [182, 183, 184, 185]. Substitution of one aromatic proton by a weakly hydrated  $-\text{COOH}$  group apparently does not affect significantly the flat orientation, which is driven by the interaction of the aromatic ring's electronic  $\pi$ -system with the water solvent (the BAH surface orientation is only slightly tilted). However, deprotonation of the carboxylic group may change the balance of hydration energies for the hydrophobic and hydrophilic parts of the molecule drastically. The strongly hydrophilic carboxylate part of  $\text{BA}^-$

---

<sup>2</sup> $\text{pK}_a$  is a negative decimal logarithm of acidity constant (acid dissociation constant). The larger the value of  $\text{pK}_a$ , the stronger is the acid. The physical meaning of  $\text{pK}_a$  may be derived from Henderson-Hasselbach equation for acid-base titration:  $\text{pK}_a$  is a pH at which activity of molecular form of the acid and its conjugated base are equal.

tends to be fully immersed in water because of the high energetic gain upon full hydration of this anionic group. The drastic change of the hydrophobic/hydrophilic balance is also capable of reducing benzoate concentration at the surface, compared to the strongly surface-segregated molecular BAH form. The section 3.3 describes results of an XPS-experiments. Summarizing the experimental results, one may say that molar concentrations of carbon atom of carboxylic group and aromatic carbon atoms are not stochiometric: 7.86 for neutral acid molecule and 10.1 for the benzoate anion. Although the experiment suggests some preferential orientation of the molecular species, it lacks fine molecular level of details. Molecular dynamics simulations is a convenient tool to gain the lacking information and compliment the experiment.

### 4.2.1 Simulation details

#### Productive cell

Fully atomistic molecular dynamics simulation is an essential technique to understand molecular level details of benzoic acid behaviour at interface. This is why we have performed fully atomistic MD simulations of BAH and  $\text{BA}^-$  in a slab of water. Molecular dynamics simulations of separate water solutions of molecular benzoic acid and sodium benzoate were performed using the Gromacs 4.5 package [186, 187, 188, 98, 189]. We used similar methodology as in the previous studies of solvation effects on benzoic acid [11] and an anionic polypeptide with carboxylic groups [49]. Benzoates were neutralized by sodium cations. We used the TIP4P model for water [92] and the OPLSAA force field [151, 152, 153, 154, 155, 156, 157, 158] for organic compounds.  $\text{Na}^+$  ions were described with parameters, developed in [190]. We simulated 20 BAH molecules in a box of 5437  $\text{H}_2\text{O}$  molecules. For  $\text{BA}^-$  simulations we used 87  $\text{BA}^- - \text{Na}^+$  pairs in a box of 4868 water molecules (sodium benzoate is more soluble than the molecular form). A typical simulation cell is represented in the figure 4.6. No restraints were applied on the systems. We note that in simulations we used larger concentrations of BAH and  $\text{BA}^-$  than in experiments because the experimental concentrations are too small (10 mM) for molecular simulations to collect reasonable statistics of molecular distributions at the surface.

Simulations were carried out in two steps for all systems. During the first step we equilibrated the systems in the NPT ensemble for 1 ns. Before the equilibration runs the potential energy of every system was minimized using the energy minimization procedure to avoid sterical clashes between the atoms. Then we performed productive runs in the NVT ensemble at constant temperature ( $T=300$  K) in a slab geometry with PME electrostatics using the Yeh and Berkowitz correction [94, 95] for slab geometry.

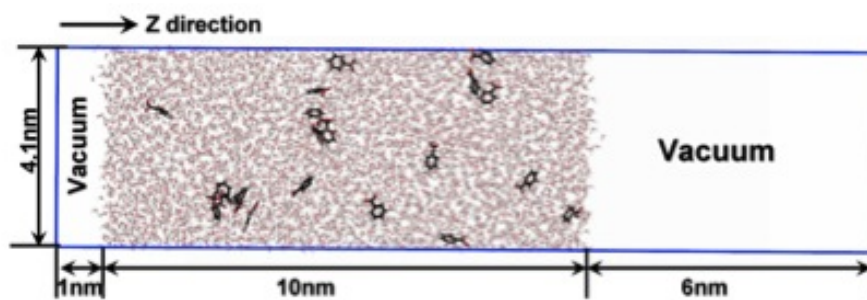


**Figure 4.6** – Simulation cell for simulations of benzoic acid/benzoates at the water/vapour interface.

Experimental technique gives molar concentrations of chemically different carbon atoms. This is why it is important to be able to compare the molar concentrations, available from the experiment with number concentrations, received from molecular dynamics simulations. Photoemission densities may be obtained from the number densities across the Z-direction (direction perpendicular to the water surface) with the following expression:

$$PE_{\text{dens}} = \int_0^{\infty} \rho_A(z) \exp\left(-\frac{1}{\lambda} \int_0^{\infty} \frac{\rho_{\text{tot}}(z')}{\rho_0} dz'\right) dz, \quad (4.2)$$

where  $\rho_A(z)$  is the density profile function for the species A;  $\rho_{\text{tot}}$  is the total sum of densities for all species;  $\rho_0$  is the total density of all components in the bulk [122]. The experimental data describe photoemission densities of the carbon atom of the carboxylic group and an averaged density of all aromatic carbon atoms of the benzene ring. This is why, it is important to obtain number densities of the carbon atoms of the carboxylic groups and an averaged density of aromatic carbon atoms from molecular dynamics simulations. More details on a technique of obtaining density profiles may be found at page 48 in a section Density (Concentration) Profiles. The number density profiles for carbon atoms of carboxylic groups and the number density profiles of aromatic carbon atoms of benzene rings were obtained in this work. To collect sufficient statistics of benzoic acid adsorption we simulated all systems for 30 ns and considered the last 20 ns for analysis. First 10 ns are required for a system to converge (see below). The calculated density profiles are shown in the figure 4.11.

### Definitions of the angles

A rough estimation of the molecular surface orientation can be performed, if the molecular density profiles are known. The comparison of the molecules' linear sizes with the positions of the maxima of the density profiles makes it possible to estimate the molecule's surface orientation. However, this approach has two limitations. First, one could only obtain information about one

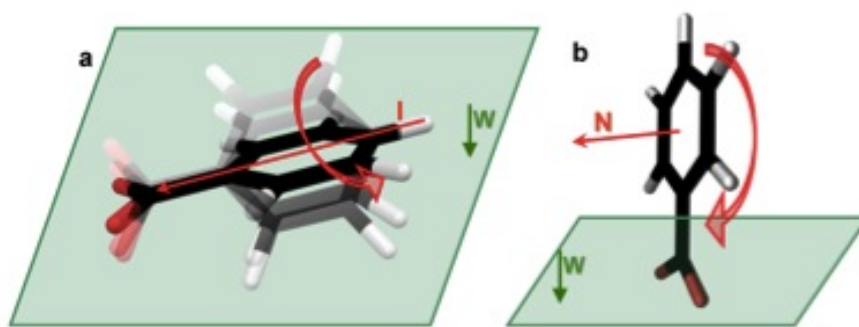


**Figure 4.7** – Definitions of angles used for characterisation of surface orientation of benzoic acid. Two angles are defined to minimize unregistered movements of benzoic acid/benzoates molecules at the interface. Possible unregistered movements of the benzoic acid molecule. a) The angle main molecular axis - surface is known and fixed, which allows rotation along the main molecular axis; b) The angle ring plane - surface is known and fixed, which allows rotation around the molecular center of mass.

angle (between the main molecular axes and the water surface). This analysis is possible due to the approach towards the calculation of the concentration profiles. As all aromatic carbons densities are averaged, the effective density may be attributed to a center of the benzene ring, which is located at the main molecular axis, just as the carbon atom of the carboxylic group. If one assumes that the surface of water is a Gibbs surface, one may find an angle between the main molecular axes and the water surface. However, knowing only one angle would not allow for an authentic description of position of benzoic acid at the interface. The second limitation of the approach is the following: one may not be sure that the particle densities are simple peaks and do not consist of a number of sub-peaks corresponding to distinctly different, co-existing molecular orientations. To overcome these two limitations of the densities profiles, one may employ analysis of angle distribution at the surface.

The orientation of the benzoic acid molecule can not be described fully with a single angle. To describe the orientation of BAH/BA<sup>-</sup> molecule we used a set of two angles. The angle definitions are shown in figure 4.7. As it is seen from the figure 4.7, if one uses only  $\Theta_{I-W}$ , it is impossible to distinguish rotation around the main molecular axis. However, we can see clearly the orientation of the COOH/COO<sup>-</sup> group of the molecule (see figure 4.7a). If we use only  $\Phi_{N-W}$  we can not distinguish a molecule with the COOH/COO<sup>-</sup> pointing to water and a molecule with the COOH/COO<sup>-</sup> pointing to any other direction. However, we can see clearly the orientation of the plane of the aromatic ring (see figure 4.7b). A combination of these two angles describes the molecular orientation completely.

### Jacobian determinant of the angular transformation.

Although description of molecular orientations with an angle or a set of angles presents better control over the molecule compare to density profile, it also presents a challenge: the angle distribution depends on the particular choice of angle. To work around this disadvantage, one should normalize the angle distributions with the Jacobian determinant, as it is suggested in the work [191]. The authors of this work study similar systems and employ angle distribution analysis with one angle (the angle  $\Theta_{I-W}$ ). They normalize the angle distribution with the following Jacobian determinant:  $J = \frac{1}{\sin\Theta}$ .

As this work employed two angles in order to better describe positions of benzoic acid and benzoate molecules, one needs to apply the Jacobian correction to both angles. Vectors used for the angular distribution analysis are orthogonal to each other, meaning that they cannot take any random orientation with respect to each other. Let the vector **I** form an angle  $\Theta$  with the vector **W**. In this case the vector **N** forms an angle  $\Phi$  with the vector **W** such that  $\Theta - 90^\circ < \Phi < \Theta + 90^\circ$ . In other words, for every given value of one angle ( $\Theta$  or  $\Phi$ ) we have a given set of values for the other angle ( $\Phi$  or  $\Theta$ ). Applying the formula for conditioned probabilities, we have an additional member to consider in the Jacobian determinant of the angular transformation:  $\frac{d\Phi}{dx} = \frac{\sqrt{1 - \cos^2\Phi - \cos^2\Theta}}{\sin\Phi}$ , where  $x$  is a parameter for the conditioned set of angles. Implementing this formula to the Jacobian determinant of the angular transformation, we have finally:

$$J = 4\pi \frac{\sqrt{1 - \cos^2\Phi - \cos^2\Theta}}{\sin\Theta \sin\Phi}.$$

### Solubility of the model benzoic acid

The density profiles of neutral benzoic acid (fig. 4.11, panels a)) show a very low concentration of benzoic acid molecules in the bulk. There could be two main reasons for this: *i*) insufficient hydration free energy of benzoic acid model, used in the simulations; and *ii*) insufficient simulation time to reach physical distributions of concentrations of the molecules at the interface and in the bulk water. While the second artefact does not present a significant problem,<sup>3</sup> the first one may affect the behaviour of benzoic acid (and benzoates) at the interface dramatically. This

<sup>3</sup>Benzoic acid is a surface active compound, which means that its concentration in the surface layer should exceed its concentration in the bulk layer. Indeed, in the experiments the signal of benzoic acid measured at the solution surface is approximately 30 times higher compared to bulk solution. This means, that the molecular density of benzoic acid in the surface layer should exceed significantly the molecular density of benzoic acid in the bulk in the simulations.

is why an additional study of hydration free energy of the model of benzoic acid in the model water is required.

Due to a finite size of the simulation box and finite simulation time we are unable to simulate fully the concentration profile in the system: most of benzoic acid molecules spend most of the simulation time in the surface layer. To overcome this difficulty we utilized different simulations techniques, which allows us to obtain the potential of mean forces (PMF) of a benzoic acid molecule, traveling through a water slab. The PMF represents the free energy profile, which can help us understand whether the model of benzoic acid is soluble (see also sec. 3.1.6 for details).

The PMF was obtained as follows. A molecule of benzoic acid was pulled through a slab of water (4 nm thick) with a constant rate of 10 nm/ns. System snapshot (coordinates and velocities) was recorded over equal time intervals (0.02ns). Further, we allowed each of these system snapshots to equilibrate for 1 ns. During this equilibration the benzoic acid molecule was not allowed to move in the Z-direction. Forces, acting in the system, were recorded and averaged over time. To reduce statistical noise we performed 5 independent simulations (replicas). The initial configuration for each replica was generated as follows. We simulated an initial system configuration for 1000 steps at 500K. After the simulation had been finished we assigned new velocities to all particles according to temperature 300K and minimized the energy. A unique random generator seed was used to assign velocities in each system.

This technique of pulling benzoic acid molecule through a water slab has a disadvantage. A benzoic acid molecule in the initial simulation cell does not have microhydration shell. When benzoic acid molecule leaves the water slab, a few water molecules follow it forming a microhydration shell. Microhydration shell changes the free energy of the benzoic acid molecule. Therefore, the parts of the PMF, recorded in vacuum slabs, would not be symmetric. To eliminate this drawback the benzoic acid molecule travelled left to right in all odd replicas, and right to left in all even replicas. By averaging all replicas one obtains a symmetric PMF.

The knowledge of the experimental hydration free energy allows to bridge simulations and experimental data on benzoic acid solvation. The experimental hydration free energy is  $\Delta G_{\text{exp}}^{\text{hyd}} = -15.6 \text{ kJ} \cdot \text{mol}^{-1}$  [192]. As one can see from the figure 4.8, hydration of used model of benzoic acid is somewhat less favourable compare to experimental values, which would result in somewhat smaller solubility compare to the real benzoic acid. It is important that we did not aim to simulate realistic concentration profile, moreover, concentration of benzoic acid molecules in our simulations exceeds real benzoic acid solubility. As our aim was to simulate behaviour of the molecules at water surface we considered the area of water surface available for one benzoic acid molecule as a main criteria of number of benzoic acid molecules in our simulation box.



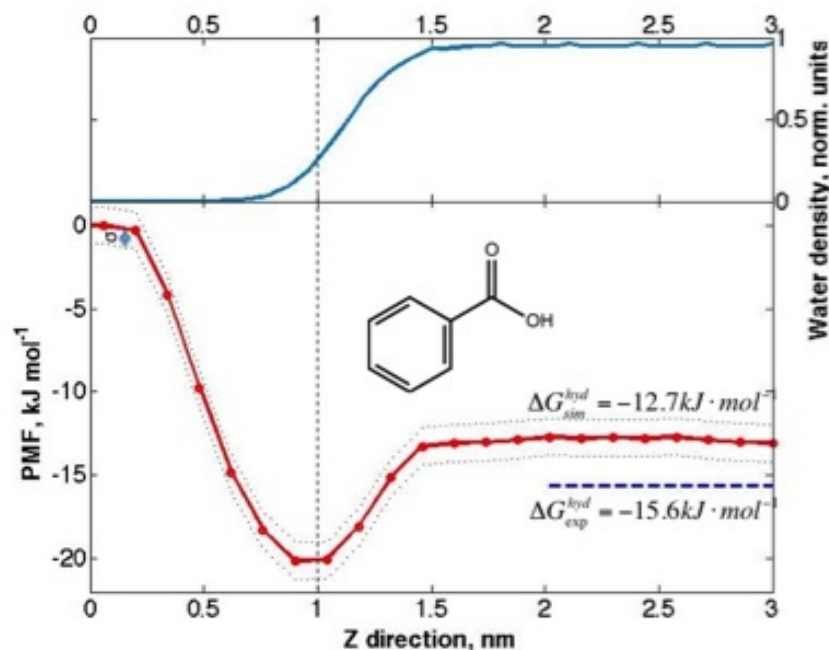


**Figure 4.8** – Free energy profile of benzoic acid along water slab. Water density profile (upper plot) and free energy profile of BAH travelling through the water slab (bottom plot). The value of the free energy in the bulk of the slab corresponds to the hydration free energy. As one may see, the calculated hydration free energy is in a good agreement with the experimental value.

Another important value which we can obtain from the free energy profile is concentration ratios such as vacuum/surface, vacuum/bulk and surface/bulk [193].

$$\frac{c_1}{c_2} = e^{-\frac{\Delta G_{12}}{RT}},$$

where  $c_1$ ,  $c_2$  are compound concentrations in phases 1 and 2;  $\Delta G_{12}$  change of free energy upon transfer of a compound from phase 1 to phase 2;  $R$  - gas constant;  $T$  - temperature (300K). The calculated concentration ratios are shown in the table 4.2. It is worth to highlight here that surface/bulk concentration ratio, obtained from the simulation is in a good qualitative agreement with the experimentally observed enhancement of the surface concentration of benzoic acid.

Comparison of the simulation results and experimental data allows us to conclude the following: *i*) benzoic acid model has water solubility similar to the real benzoic acid; *ii*) the model of benzoic acid represents well surface layer/bulk concentration ratios; *iii*) the model of benzoic acid is capable of representing of molecular orientations at the surface. We can, hence, conclude that the almost zero density of benzoic acid molecules in the water bulk in the figure 4.11a is indeed an artefact, which originates from the finite size of the simulation cell and the finite simulation time. This simulation artefact does not, however, affect the orientation of benzoic acid at water/vapour interface, which is the main subject of this study.

**Table 4.2** – Concentration ratios of benzoic acid in different phases. The ratio surface/bulk is just slightly below the experimentally observed enhancement of the benzoic acid concentration.

Interface	Concentration ratio
Surface/vapour	3500
Bulk/vapour	170
Surface/bulk	20

#### **Effect of the simulation box size on the orientation of benzoic acid at interface**

It has been shown in the previous section, that the model of benzoic acid molecule, used in the simulations, possesses solubility comparable to the real benzoic acid. However, there is still a possibility of simulation artifacts, arising from small simulation box for the amount of benzoic acid molecules used in the simulation. Indeed, at the maximum possible concentration of benzoic acid in water, there are 2780 water molecules per one molecule of benzoic acid. Although the simulation cell was designed to accommodate all benzoic acid molecules with their hydration shells on the surface of the cell, shortage of water molecules may result in some artefacts of the simulation. On the other side, sufficient sampling of benzoic acid orientation at the interface at physically possible concentration is very computationally expensive. To make sure, that the simulations of benzoic acid in smaller simulation cell do not represent artifacts, a short simulation of benzoic acid at the concentration below solubility limit was performed (1 benzoic acid for 2780 water molecules). The methodology of this simulations is just the same, as methodology of simulations of the smaller box, described in the section 4.2.1 with the following difference. The dimensions of the water slab were 13X13X10 nm with 15 nm of vacuum, surrounding the solution from each side. This altered simulation set up allowed to decrease the concentration of benzoic acid down to the solubility limit. It also increased the volume of the simulations cell 10 times, the simulation time was 10 ns, with sampling of the angles during the last 5 ns. Distribution of angles  $\Theta$  and  $\Phi$ , obtained in the short simulation under the concentration limit, is presented in the figure 4.9.

One can see from comparison of the figures 4.9 and 4.11c, that, despite the data noisiness, the main trend of benzoic acid orientation remains the same for both systems. The increased noisiness of the larger cell is due to the following reasons. The sampling of the angle depends on the number of benzoic acid molecules in the cell and on the sampling time. The number of benzoic acid molecules in the cell is 20, the same as in the smaller simulation box. However, the

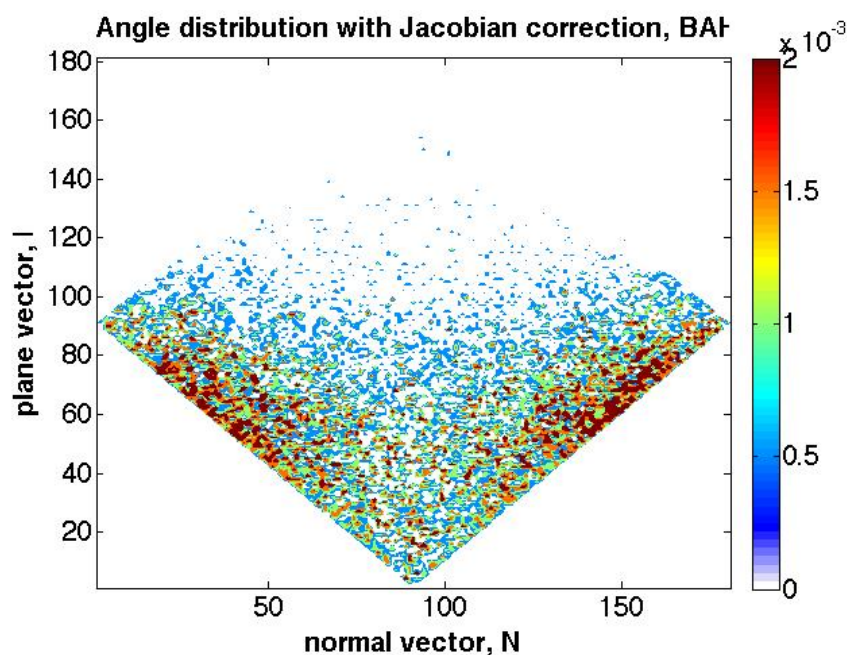
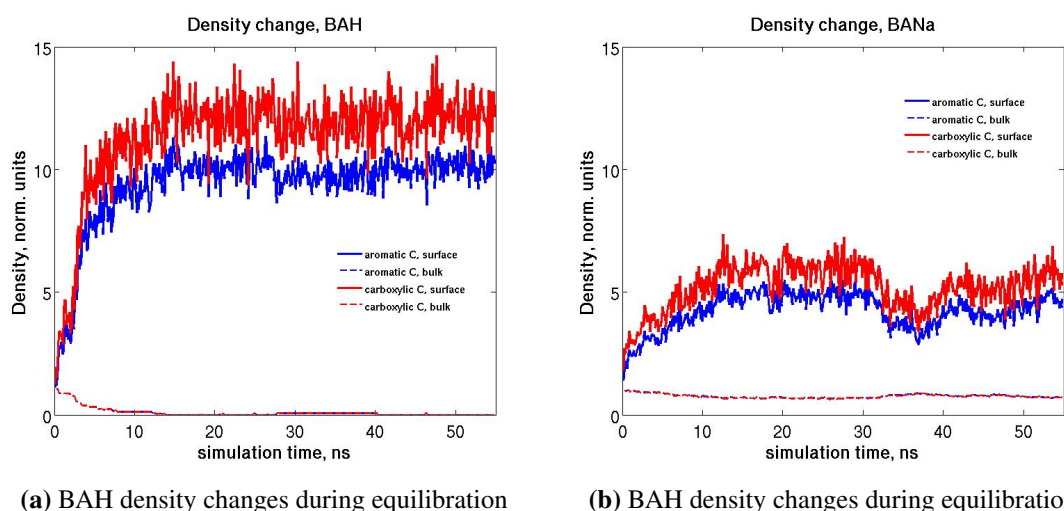


**Figure 4.9** – Benzoic acid orientation under concentration limit. Here the concentration of benzoic acid corresponds to solubility limit of a real benzoic acid. Although the angle distribution is more noisy, compared to the distributions represented in the figure 4.11, the trend is the same, which allows to suggest that simulations in a smaller cell are free from artefacts.

time of the sampling in the larger box is 5 ns compared to 55 ns in the smaller simulation box. That is why the data in the figure 4.9 are more noisy than the data presented in the figure 4.11c.

### Convergence of simulations in slab geometry

The methodology of running productive runs in a slab geometry is different from the bulk productive runs. After introducing a vacuum slab, the system needs some additional time for equilibration. The exact equilibration time depends on the particular system properties. That means that the equilibration time can not be predicted before running the simulations. There are a few possible ways to define whether a system is equilibrated or not. One of the criteria is measuring changes in the surface density during simulation time. We employed this approach here and the results are presented in the figure 4.10. The surface density was registered and averaged every 100 frames. The value was stored, and the procedure was repeated for the next 100 frames. Changes of the surface density over time can be seen in the figure 4.10. As one may see from the figure 4.10, the surface density stops changing at approximately 10 ns after introduction of the vacuum slab into the system. This is why the first 10 ns of the simulations were not considered for analysis.



(a) BAH density changes during equilibration

(b) BANa density changes during equilibration

**Figure 4.10** – BAH and BANa surface density changes during equilibration. The figure shows that both systems require approximately 10 ns to equilibrate.

#### 4.2.2 Effects of pH on benzoic acid behaviour at water/vapour interface

The figure 4.11, panels (a) and (b), shows converged density profiles of the aromatic ring/carboxylic carbons and the water solvent in the water/vapour interface layer, obtained from simulations of benzoic acid (panel a) and sodium benzoate (panel b) in a slab geometry. The respective water, ring carbon and carboxylic/carboxylate carbon density profiles have been normalized so that the unity designates the nominal bulk concentration of the species under ideal mixing.

Consistently with the photoemission data the neutral acid (panel a) is found to be strongly surface segregated in the simulations; the surface concentration of BAH is much higher than in the bulk. We also note that the carboxylic and ring carbon densities to a large extent overlap in the  $z$ -direction, with a slight shift of the ring carbon profile toward the surface, revealing that the molecules have a near flat surface orientation with a weak preference of pointing the carboxylic groups into the aqueous phase. While the benzoate anion (panel b) is also surface enriched, a considerable amount of the molecular anions are found in the interior of the slab. This result is consistent with the drop of the C1s PE signal upon dissociation of benzoic acid (compare figures 3.6 a and b). More importantly the density profiles in the figure 4.11b show a pronounced spatial separation between the aromatic and the carboxylate carbons in the  $Z$ -direction; the latter site ( $R - COO^-$ ) is pointing into the water bulk.

While it is clear from the discussions above that our MD simulations are in good qualitative agreement with the photoemission experiments, the connection can be made more explicit in various ways. We have chosen here to employ a simple attenuation model, as described in the work [122], to simulate the expected PE intensity ratios from the simulated density profiles,

as function of  $\lambda$ ; the electron inelastic mean free path in the aqueous phase. We assume that too small values of  $\lambda$  have to be used ( $<0.2\text{nm}$ ) to reproduce the experimental ring/carboxyl PE ratios. This suggests that the simulations are slightly overemphasising the nearly flat-lying conformers. However, the relative change in the PE ratio upon going from BAH to  $\text{BA}^-$  appears to be in almost quantitative agreement.

Assured that the MD simulations capture important features of the distributions of BAH and  $\text{BA}^-$  at the air-water interface, we move on to a more detailed analysis of the range of surface conformations, present in the respective simulated trajectories. To describe the orientation of a BAH/ $\text{BA}^-$  relative to the water surface we have defined two molecular vectors: The first,  $\mathbf{I}$ , lies in-plane in the direction from the centre of *para*-C atom to the center of  $\text{COOH}/\text{COO}^-$  group carbon atom, while the other,  $\mathbf{N}$ , is normal to the molecular plane. Both vectors are shown graphically in the figure 4.11d together with the normal vector  $\mathbf{W}$  to the water surface. The orientation of an individual molecule can be thus conveniently described in terms of a pair of angles;  $\Theta_{\mathbf{I}-\mathbf{W}}$ , which denotes the angle, formed between  $\mathbf{I}$  and  $\mathbf{W}$ ; and  $\Phi_{\mathbf{N}-\mathbf{W}}$ , which is the angle between  $\mathbf{N}$  and  $\mathbf{W}$ . In other words the angle  $\Theta_{\mathbf{I}-\mathbf{W}}$  describes the  $\text{COOH}/\text{COO}^-$  molecular site orientation and  $\Phi_{\mathbf{N}-\mathbf{W}}$  describes the orientation of the molecular plane with respect to the water surface plane. In terms of these geometrical parameters, the figure 4.11c and e show the angular distribution maps for benzoic acid and benzoate, respectively, near the aqueous solution/vapour interface. Note that, due to the orthogonality of the vectors  $\mathbf{I}$  and  $\mathbf{N}$ , only geometries within a certain quadratic area are allowed. The corners of the quadrangle are situated in centre on the  $\Phi_{\mathbf{N}-\mathbf{W}}$  and  $\Theta_{\mathbf{I}-\mathbf{W}}$  axes. To eliminate the problem with mathematically not uniformed probability distribution of the conformations the distributions in the figure 4.11c and e are normalized with the Jacobian determinant of the angular transformation.

The pronounced differences in surface orientation between BAH and  $\text{BA}^-$  are revealed in great detail in the figure 4.11c and e. As already deduced from the density profiles in the figure 4.11a,b, a considerable amount of the neutral acid molecules are lying nearly flat on the surface with a tendency for the carboxylic group to point into the solution, resulting in considerable intensity peak around  $\Theta_{\mathbf{I}-\mathbf{W}} = 40^\circ$ . Furthermore, most of these configurations have an angle  $\Phi_{\mathbf{N}-\mathbf{W}}$  near the bottom-right/bottom-left edges of the surfaces in the figure 4.11c, which corresponds to a simple tilt of the  $\text{COOH}$ -terminal into the solution, without rotation of the molecule. Configurations around  $\Phi_{\mathbf{N}-\mathbf{W}} = 90^\circ$ , which correspond to the orientation of the aromatic ring perpendicular to the water surface, are much less probable.

A rather detailed picture of the surface orientation of benzoic acid is emerging: The pronounced surface segregation of BAH is driven by hydrophobic interactions. In the surface layer

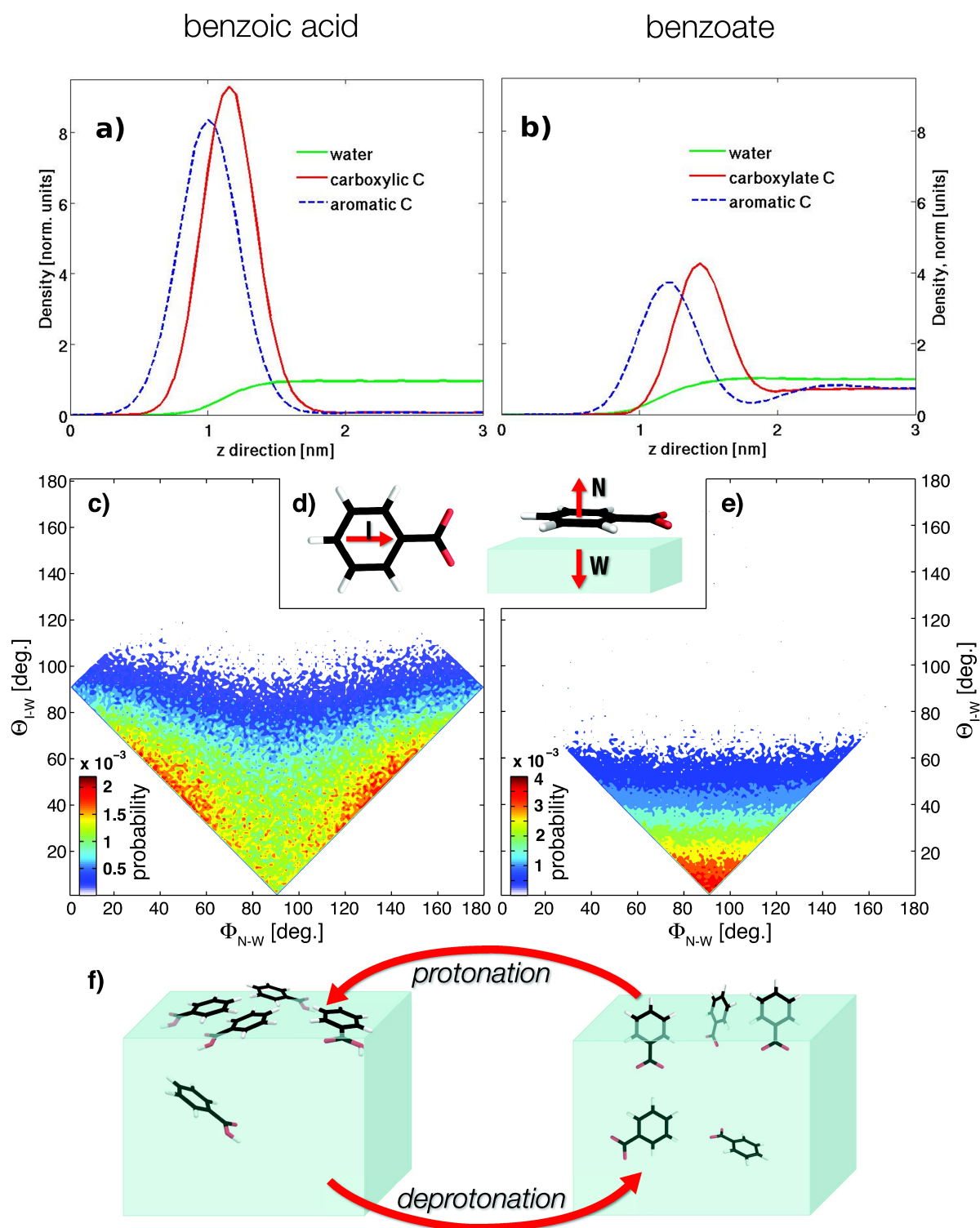


**Figure 4.11** – Molecular orientations in the surface layer of aqueous BAH/BA<sup>-</sup> solutions from MD simulations. a, b) normalized density profiles of the aromatic ring/carboxylic carbons and the water solvent, respectively, in the direction perpendicular to the water surface. c, e) angle distributions of BAH/BA<sup>-</sup> respectively in the surface layer, normalized with the Jacobian determinant of the angular transformation. Insertion d) shows definitions of the molecular orientation vectors **I** and **N**, where **W** is the vector perpendicular to the water surface. f) pictorial representation of the BAH/BA<sup>-</sup> behavior in the surface layer upon protonation/deprotonation.

BAH, however, aligns preferentially the hydrophobic aromatic ring so that its electronic  $\pi$ -system can interact with the polar solvent at one side. This makes parallel orientation favourable, compared to perpendicular one. The carboxylic group, on the other hand, can form somewhat stronger hydrogen donor bonds with the solvent, which is hard to satisfy in a fully parallel geometry with the surface. This represents a driving force for the molecule to tilt into the aqueous phase with the carboxylic group pointing downwards. The angular distribution, shown in the figure 4.11c, is thus the result of balancing these counteracting tendencies in the surface hydration of benzoic acid – see the pictorial representation of the surface layer, given in the figure 4.11f, left part.

In the case of benzoate the maximum of the probability density is centred near  $\Theta_{I-W} = 0^\circ$ ,  $\Phi_{N-W} = 90^\circ$ , i.e. when the  $\text{COO}^-$  groups point directly down into the solution – see pictorial representation in the right part of the figure 4.11f. Furthermore, as it was shown in the figure 4.11b, this also results in increased bulk activity. One can conclude that the carboxylate group of  $\text{BA}^-$  shows a sinker-like behaviour, due to the efficient hydration of the ionic group, while the hydrophobic aromatic ring acts as a buoy, keeping a significant part of the molecular ions close to the interface.

Several studies have shown that the pH level of aqueous benzoic acid solutions (and, hence, the degree of dissociation of the acid) influences the adsorption properties of the molecule at interfaces strongly. For example, Ishikawa *et al.* investigated the adsorption of aromatic carboxylic acids into low-density polyethylene films as a function of pH [35]. They showed that the adsorption level of benzoic acid to the film increased with decreasing of pH. There are also studies of orientation properties of ACAs at interfaces. As an example, the electrochemical studies of benzoic acid behaviour on platinum and gold electrodes by Montilla *et al.* suggest that the aromatic ring of the benzoate anion is oriented preferentially in a perpendicular way to the water-electrode interface [36].

Benzoic acid is an amphiphilic compound with a hydrophobic aromatic ring and a hydrophilic carboxylic group. BAH and  $\text{BA}^-$  differ by the charge state of the carboxylic functional group, which causes their different behaviour at the aqueous solution/vapour interface. It is known that non-substituted aromatic systems tend to lie flat on the water surface [182, 183, 184, 185]. Substitution of one aromatic proton by a weakly hydrated  $-\text{COOH}$  group apparently does not affect significantly the flat orientation, which is driven by the interaction of the aromatic ring's electronic  $\pi$ -system with the water solvent (the BAH surface orientation is only slightly tilted, see figure 4.11). However, deprotonation of the carboxylic group changes the balance of hydration energies for the hydrophobic and hydrophilic parts of the molecule drastically (see figure 4.12).

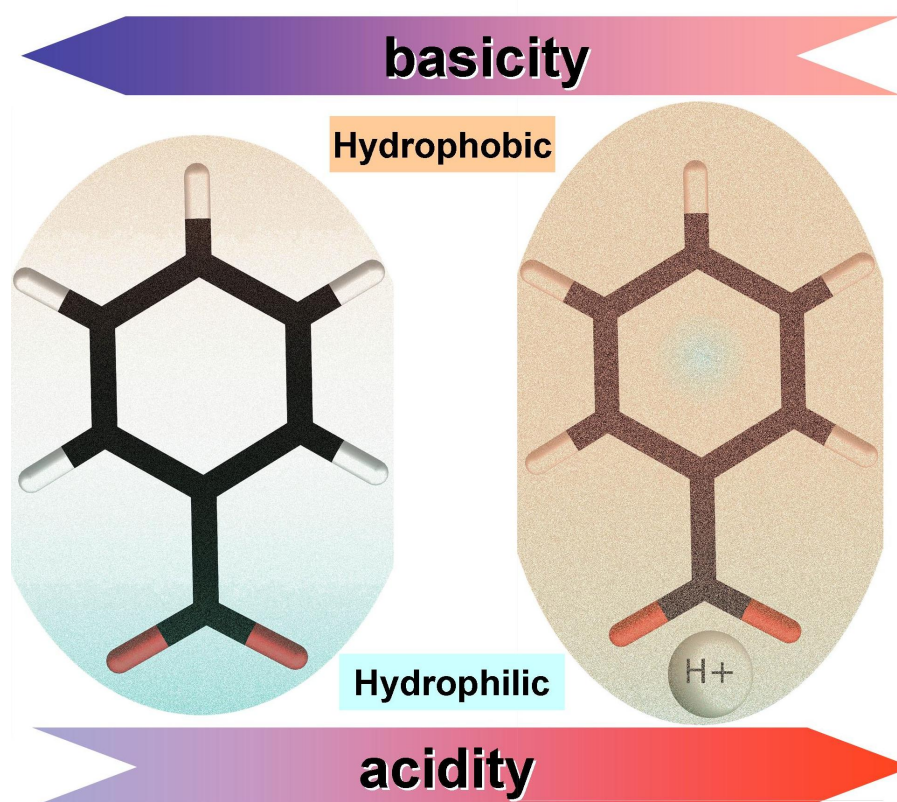


**Figure 4.12** – Pictorial representation of hydrophobic/hydrophilic areas of BAH/BA<sup>-</sup>. Blue-coloured areas represent hydrophilic areas; okra-coloured areas represent hydrophobic areas

The strongly hydrophilic carboxylate part of BA<sup>-</sup> tends to be immersed fully in water because of the high energetic gain upon full hydration of this anionic group. The drastic change of the hydrophobic/hydrophilic balance also leads to a reduced benzoate concentration at the surface, compared to that of the strongly surface segregated molecular BAH form.

The strategy of combining X-ray photoelectron spectroscopy with fully atomistic MD simulations has allowed us to investigate the molecular mechanisms of the adsorption at the water-air interface of benzoic acid in great detail. It was shown that drastic changes in the interface behaviour take place when the acid dissociates into the benzoate anion. The BAH molecules are mainly adsorbed in the interface layer rather than in the bulk with the aromatic rings oriented parallel to the water surface. However, converting the molecule to BA<sup>-</sup> results in a sinker-like behaviour of the carboxylate group, with the aromatic ring becoming perpendicular to the surface and acting as a buoy, keeping the molecule. Moreover, a significant part of the molecules move from the interface layer into the bulk. We attribute the observed differences in interface behaviour of the neutral and dissociated forms of benzoic acid to the changes in the hydration pattern of the carboxylic group upon deprotonation. This changes the balance between the hydrophobic and hydrophilic structural motifs of the amphiphilic molecule resulting in the flip of its interface



orientation.

While the present study only concerned benzoic acid, the most elementary representative of the aromatic acids, the mechanism revealed here is believed to be rather general, at least as a trend, for other molecules in this class. The results presented should thus have important implications in many areas where heterogeneous chemistry of aromatic carboxylic acids is involved, such as surface catalysis, atmospheric and environmental chemistry, pharmacology and food chemistry.

### 4.2.3 Comparison of $\text{Na}^+$ and $\text{K}^+$ effects on surface affinity of benzoate

As we could see before, the pattern of molecular hydration affects preferential surface orientation of benzoic acid. In this section we will understand how changing of benzoate counter-ion influences the details of benzoate behaviour at the water-vapour interface.

What is changed in the benzoate solution when we replace the sodium ( $\text{Na}^+$ ) counter-ion with the potassium ( $\text{K}^+$ )? Although the charge of both cations is the same ( $+1\bar{e}$ ) their radii, and as a result, the ion surface areas, are different. According to [194] the radius of sodium ion varies within the limit of 95 – 102 pm; at the same time radius of potassium varies within the limit 133 – 141 pm, which gives surfaces ratio  $\frac{A(\text{K}^+)}{A(\text{Na}^+)} \sim 1.4$ . This difference, in turn, causes a significant changes in the ion hydration pattern and interactions with the carboxylate group of the benzoate anion.

As it has been shown in the previous works [49, 162], sodium ions have much stronger affinity to carboxylic groups in a solution and, therefore, prefer to stay near the carboxylate group. On the other hand, sodium ions do not show pronounced surface activity and, due to a large energy gain upon hydration, prefer to stay in water bulk [2, 195]. This brings us to the following contradiction: on the one hand, sodium ions tend to stay in bulk water; on the other hand, sodium ions form stable contact pairs with carboxylate ions, which prefer to stay at the water-vapour interface to minimize hydration of the hydrophobic benzoic ring.

For bigger ions (potassium) this contradiction (staying in bulk water solvated, or forming a direct contact pair on the surface) does not exist because these ions have a weaker hydration shell in general, on the one hand, and do not form direct contact pairs with carboxylate. It is known that big ions (with the ion surface area comparable to potassium or greater) show increased surface activity compared to the small ions (with the ion surface area comparable to sodium or smaller).

Which effect could the described difference in the ion hydration have on the surface behavior

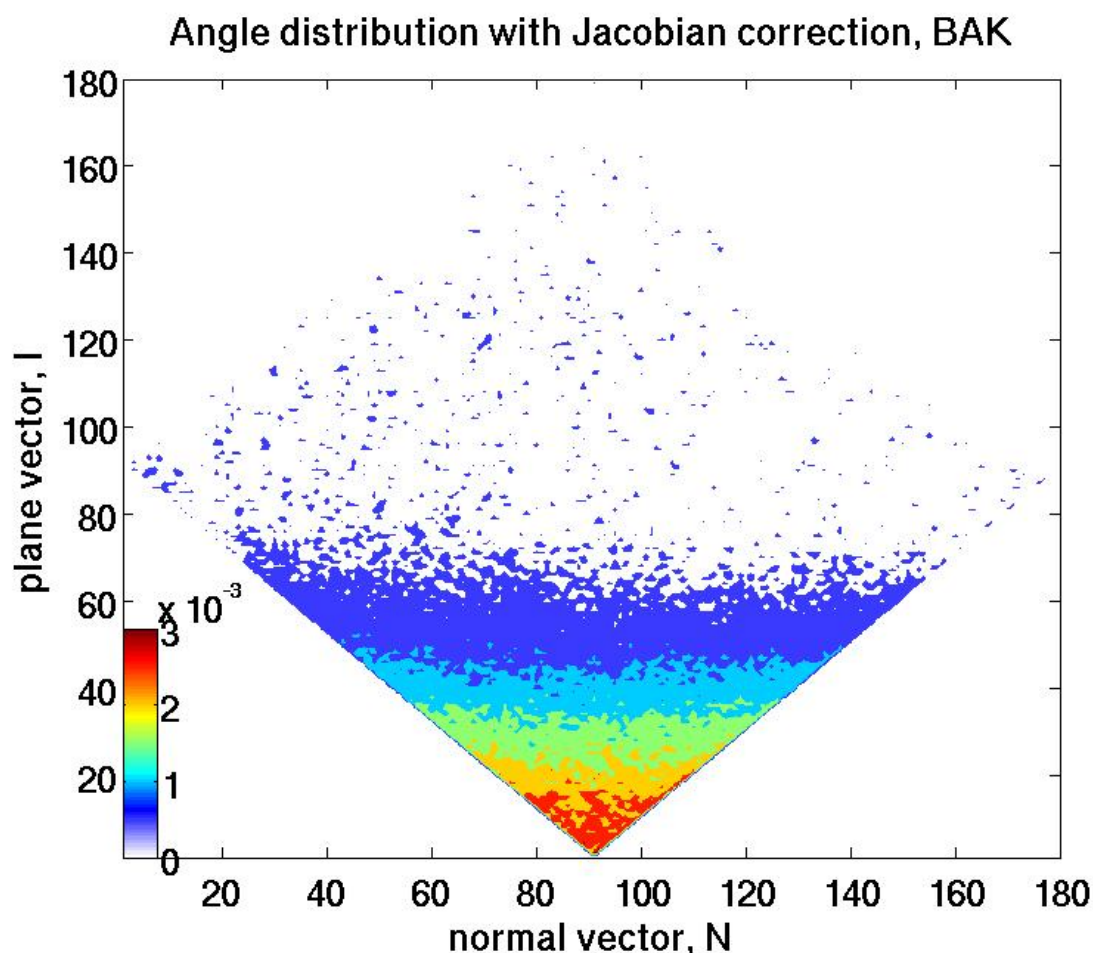


**Figure 4.13** – Angle distribution of BAK at the surface layer. The distribution is similar to the that of sodium benzoate.

of the benzoate ion? On the one hand, strong affinity of sodium ion makes the charge of  $-\text{COO}^-$  group of benzoate screened and, as a result, interactions with water molecules become less pronounced. On the other hand, the orientation of the benzoate ion is similar in both cases (see figures 4.13 and 4.11e).

On the other hand, in the case of potassium benzoate, the cations do not have strong affinity to the carboxylate of benzoic acid. As a result, carboxylate group is open to interactions with water molecules. The absence of charge screening and possibility of direct  $-\text{COO}^- \cdots \text{H}_2\text{O}$  interactions makes the benzoate anion less hydrophobic. And although the change in hydrophobicity is not sufficient to change the pattern of benzoate surface orientation, this decreases noticeably the BAK surface segregation compared to BANa (see figure 4.14).

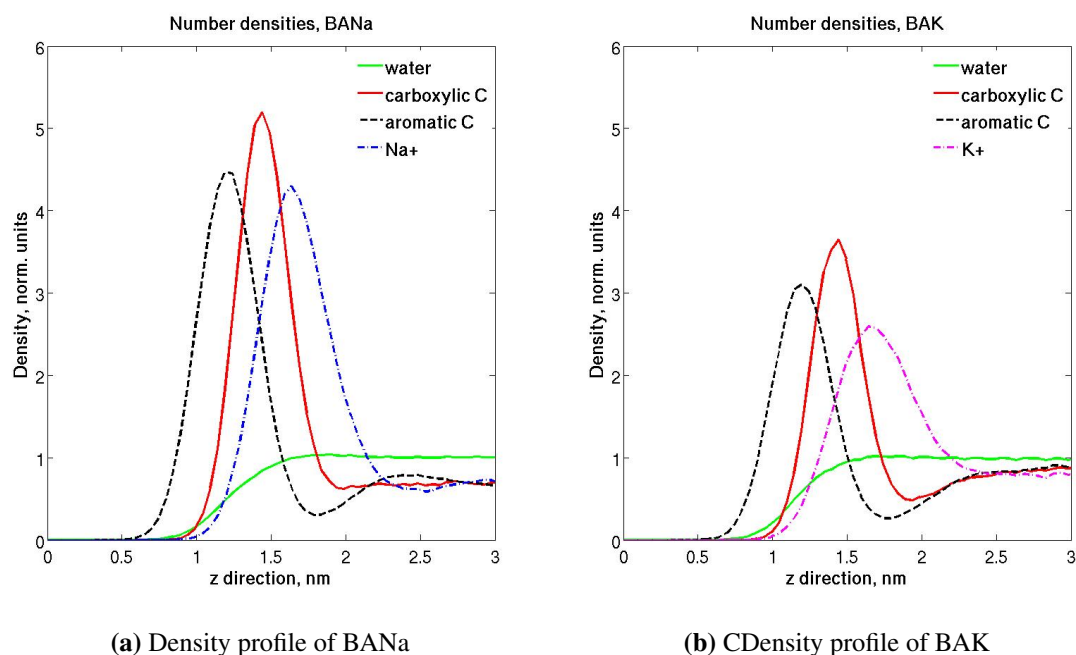


**Figure 4.14** – Relative normalized density profiles of sodium benzoate (BANa) and potassium benzoate (BAK) at the surface layer, obtained from molecular dynamics simulations.

### 4.3 Chapter conclusions

Specific ion effects have been a subject of intensive scientific research for several decades. Nevertheless, there are still many gaps in the understanding of how ions work. This chapter shows the difference between interactions of sodium and potassium with carboxylic acid. Although difference in sodium and potassium effects has been investigated before, see e.g. [162], this work for the first time explores the differences in sodium and potassium interaction as a cause for experimentally observed reduction of binding constant of cyclodextrin with aromatic carboxylic acid. A new mechanism of competition for the guest was suggested in this work. According to this mechanism ions, strongly interacting with a guest molecule, are capable of reduction of the binding constant of this molecule with a cyclodextrin.

The same fundamental difference between sodium and potassium ions interactions with carboxylic group is responsible for differences in surface affinity at the interface water/vapour for sodium and potassium benzoates. Analysis of the orientation of the benzoate molecules at the interface suggested, that both sodium and potassium benzoates tend to be situated perpendicular to the water surface, with carboxylic group fully immersed into water. To accomplish the studies of ion effects on benzoic acid behaviour at the interface it is interesting to understand, how hydrogen ion differ from sodium and/or potassium. It was found that at a low (acidic) pH level, when benzoate is in its neutral form, behaviour of benzoic acid at the interface changes

dramatically. Neutral benzoic acid molecule prefers to lie flat at the surface with just a slight tendency to tilt with its carboxylic group into water. Surface activity of neutral benzoic acid is significantly higher compared to benzoates.

Effects of ions on behaviour of benzoic acid at the interface and on the binding constants of cyclodextrin complexes are manifestations of the same molecular mechanism of ion effects at solvation interfaces.

# 5

## Effects of ions on stability of carbon nanotubes dispersion

### 5.1 Carbon nanotubes in ternary systems

Carbon nanomaterials (CNMs) possess unique properties and can be used in many important applications [196, 197, 198, 199]. Carbon nanotubes, as well as other carbon nanomaterials are strongly hydrophobic [62, 63, 64, 65]. There are two possibilities to increase solubility of carbon nanotubes in water. The first method employs the CNTs surface modification (covalent or non-covalent functionalization) [61, 66]. A great disadvantage of this method is a significant unfavourable change in CNTs properties. The second way to increase carbon nanotubes solubility in water is to shorten the tubes [200]. Unfortunately, this technique can not be employed widely to overcome solvophobicity of carbon nanotubes as many applications of CNTs are very sensitive to the length of CNTs.

Many applications of carbon nanotubes require chiral purity of the material. Currently, carbon nanotubes may be synthesised only as a mixture of chiralities. This is why carbon nanotubes require post synthesis purification and separation of different chiralities into separate fractions. High quality of post synthesis purification and separation of chiralities require dispersion of carbon nanotubes. This is why solvophobicity of carbon nanotubes is an important obstacle on the way to carbon nanotubes applications.

Contrary to water, some organic solvents are capable to disperse significant amounts of carbon nanotubes without surfactants. This is why dispersions of carbon nanotubes in organic solvents attract much of attention today [63]. The use of these dispersions could be particularly useful for

electronic applications of CNMs dispersions (e.g. in photonics and optoelectronics) where it is important to keep the surface of the nanotubes free of chemical or physical modification to avoid changes in their electronic properties [67, 68]. Unfortunately, many organic solvents are toxic and highly volatile which often makes them difficult and dangerous to handle. N-methylpyrrolodone (NMP) proves to be a good compromise: it dissolves CNTs well and it has very a low vapour pressure (1 Torr at 40°C) [201], which reduces potential hazards.

As NMP offers a possibility to disperse carbon nanotubes effectively, it becomes important to understand, how ions affect dispersions of carbon nanotubes in NMP. This understanding is important due to several reasons. First of all, salts are employed widely in organic chemistry and biochemistry to purify and separate compounds. Just the same technique may be potentially used to purify carbon nanotubes and perform chiral separation. Secondly, intercalation with ions allows one to control better electrical properties of carbon nanotubes [202]. Despite importance of understanding the mechanisms of ion effects on carbon nanotubes dispersions, available studies in this area concern mostly surfactant-based aqueous solutions [7]. These studies show fine response of dispersions of carbon nanotubes to addition of salts. The disadvantage of this study is that direct effects of ions on carbon nanotubes in a dispersion coexist with surfactant originating effects, e.g. aggregation of surfactants with increase of ionic strength, which, in turn, may itself reduce the stability of carbon nanotubes dispersion.

NMP is a promising solvent for making stable dispersions of pristine CNTs [63, 73, 74]. It also represents a possibility to study directly ion effects on dispersions of carbon nanotubes without interfering effects of surfactants. Unfortunately, despite its high polarity (the dipole moment of NMP is 4.1 D), many commonly used inorganic salts are poorly soluble in NMP as, for instance, sodium chloride [76]. However, there is a general rule for salt solubility in NMP, which says that the bigger ionic radii of salt ions are the better this salt dissolves in NMP. As an example, sodium iodide salt has relatively good solubility in NMP (~0.2 M) [75]. This is why we have chosen sodium bromide and sodium iodide for our experiments with inorganic ions.

It is worth to mention, that solvent design is an important issue at the current stage of development of carbon nanotube application. The reason for this is as follows. Like with many other solutes, dispersing nanotubes in a solvent followed by change of the conditions is one of the most important technique to alter composition and/or properties of dry carbon nanotubes. Altering of composition and/or bundle structure is required because as-synthesised carbon nanotubes bundles are not suitable for applications, either because of insufficient chiral purity or density. As a example one could quote the work [203], which suggests a technique to increase bundle density by employing solvophobicity of carbon nanotubes.

In principle, the bundle formation can be achieved by dispersing CNTs in various liquid solutions, provided that the dispersion process leads to CNTs bundles with predefined structures. Unfortunately, this approach presents a lot of difficulties in controlling the process by standard methods [71]. Preparation of CNT dispersions is an important step in CNT bundle engineering. Preparation of CNTs bundles from CNT dispersions represents all advantages of bottom-up approach of fabrication of nanostructures, e.g. possibility to fine tune the structure of the resulting bundles. The bundle engineering is very important in ultrafast photonics and bio-medical applications [67, 69, 70].

Despite rapid progress in the area of solvent engineering for CNT dispersions, the main physical-chemical mechanisms of solvent effects on CNTs have not been sufficiently explored. Even less studied have been the effects of other solution/dispersion components, such as salts and water (osmotic active compounds). However, osmotic active compound may have significant effects on dispersion stability as well as on electronic properties of nanotube materials [72]. It has been shown recently that salts can regulate dispersing properties of CNTs in aqueous solutions stabilized by surfactants [7, 8]. Unfortunately, in the multi-component CNT-surfactant aqueous dispersions the salt effects on CNTs interfere with the salt effects on the surfactant molecules. Thus it is important to see whether salts produce any effects on CNT dispersions in organic solvents, where the direct effects of salts on pristine CNTs are not masked by the effects of dispersing agents.

Ion effects on carbon nanotubes dispersion may be described with a solution theory of Kirkwood-Buff [204, 205]. This theory follows a more general approach of the Gibbs-Duhem theory, which uses the chemical potential of a solute. According to this theory the change in the chemical potential of a solute molecule (S), dissolved in a solvent (V), upon addition of a cosolvent (X) may be written as

$$\Delta\mu_S \approx -\Gamma_{SX}\Delta\mu_X,$$

where  $\Delta\mu_S$  is the change in the chemical potential of solute,  $\Delta\mu_X$  is change of chemical potential of the cosolute (ion),  $\Gamma_{SX}$  is the solute - cosolute preferential interaction coefficient (deficit or excess of the number of cosolvent molecules around a solute molecule, compared to the same volume of the bulk solution). This is an approximate relationship because differentials are approximated by the finite differences. Ions are considered here as cosolvents. According to this relationship absorption of ions will decrease chemical potential of the nanotube surface. Consequently this enhances stability of the dispersion. Depletion of ions from the tube surface, in turn, increases the chemical potential of the surface. As an increase of chemical potential of

the surface corresponds to an increase in the free energy of the solvation interface tube-salty NMP, tube will tend to decrease the surface area available for interactions with NMP. To reduce surface area, available for interactions with NMP, carbon nanotubes should associate with each other, forming bundles and larger aggregates, which lowers stability of the dispersion. Based on this theory, one may suggest two hypotheses of how ions may affect stability of carbon nanotubes dispersions: *i*) as ions are charged, they should be repelled from hydrophobic surface of carbon nanotubes. This, according to the Kirkwood-Buff theory, should decrease stability of the dispersion; *ii*) if ions are repelled selectively from nanotubes of different chiralities, this will lead to a selective increase in the chemical potential. This would mean selective precipitation of tubes from the dispersion.

## 5.2 Effects of aqueous impurities on carbon nanotubes dispersion stability

The Kirkwood-Buff theory is a quite general theory and it is capable of description of interactions in many ternary systems. Ideas, described in the previous chapter, may be applied to ternary systems NMP-CNT-water. Similar to ions, water molecules avoid contacts with the carbon nanotube surface, while NMP forms a thick solvation layer around the CNT. This non-uniform distribution of the solvent and cosolvent around carbon nanotube leads potentially to reduction of stability of NMP based dispersions of carbon nanotubes in the presence of water admixtures.

Organic solvents like NMP are capable to dissolve carbon nanotubes in relatively high concentrations. However, all organic solvents possess one common disadvantage: they are *always contaminated with water* unless specially designed techniques are employed. These techniques are quite complicated and expensive because the sample handling in dried inert gas and preliminary solvent drying are indispensable parts of them. Additionally, a moisture sensitive technique represents more challenges in scaling from the laboratory to industrial production. On the other hand, it is known that aqueous contamination of non-aqueous solvents is capable of changing solubility of solutes dramatically. The reason for this is that once an organic solvent is contaminated with water, it becomes a mixed solvent. Properties of mixed solvents are different from properties of pure solvents. A good example to illustrate the difference between pure organic solvents and water contaminated solvents is a general organic chemistry practice to precipitate the products of a synthesis from non-aqueous solutions by adding water to organic solvent. It is important to highlight here, that effects of water on solubility of different solutes



depends on the interplay of mutual forces acting between solute, solvent and cosolvent.

This study aims to understand effects of very small amounts of organic and inorganic salts on carbon nanotube bundles formation in organic solvents. Previously, water effects were studied in the work [206]. However, the authors of this study did not consider the dilution of the carbon nanotubes dispersion. Spectrophotometric titration was performed in order to understand the effect more in details. As accurate description of bundle formation is important, it is critical to understand how and to which extent water affects bundle formation. Effects of water on stability of the NMP-based dispersions of carbon nanotubes may be studied effectively with spectrophotometric titration of the NMP-based dispersion with water. The general approach of the experiment involved controlled addition of water into the dry CNT-NMP dispersions. Although maximum realistic estimation of water content in the CNT-NMP dispersion is 4%<sup>1</sup>, we started from the 1%<sub>V</sub> concentration of water in the dispersions and finished with 70 %<sub>V</sub> of water content in CNT-NMP.<sup>2</sup> This wide range of water concentrations allowed us to get answers to the following questions: *i*) whether water effect is smooth over a wide range of concentrations; *ii*) whether water effects have a saturation point; *iii*) whether water influences stability of carbon nanotubes in NMP.

## 5.2.1 Spectrophotometric titration

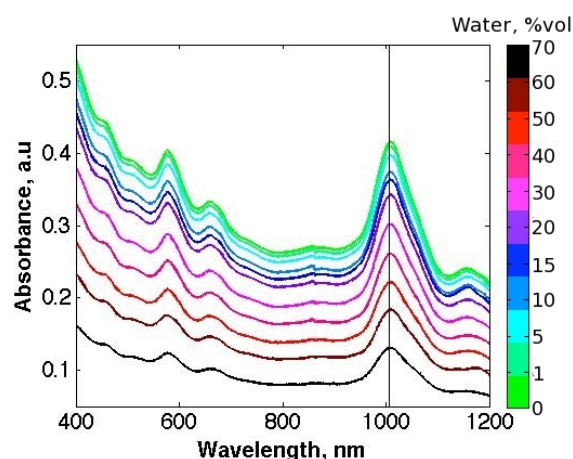
### Sample preparation

UV-vis-NIR light absorbance is a powerful tool to analyse overall concentration of CNTs in a dispersion as well as their chirality distribution. This is why in order to understand effects of water on stability of carbon nanotubes dispersion in NMP spectrophotometric titration was performed. The main idea of the method is to record changes of intensity upon addition of the titrant (in this case – water). This allows to measure effectiveness of admixtures quantitatively. The challenges of the spectrophotometric titration of carbon nanotubes originate in problems of authentic decomposition of carbon nanotube spectra (discussed in section the 3.4). Despite these challenges, spectrophotometric titration is capable of reliable determination of *overall* concentration of carbon nanotubes upon increasing of water concentration. As the main objective of this study was to determine water effects on *overall* stability of carbon nanotubes dispersion, spectrophotometric titration was considered as suitable for this study.

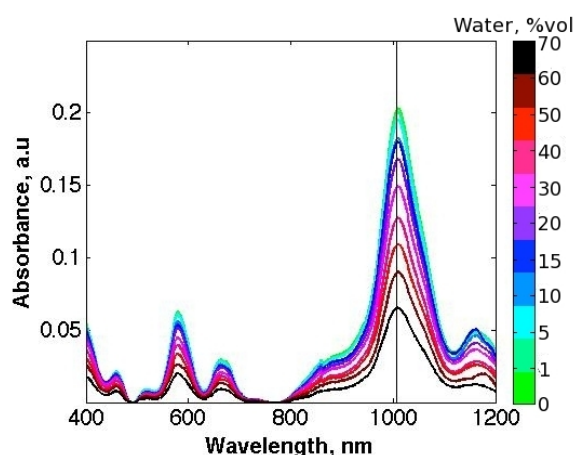
---

<sup>1</sup>In the future in this work we focus on water content 4%<sub>wt</sub> as maximum realistic concentration of water in CNT-NMP dispersions in a laboratory environment.

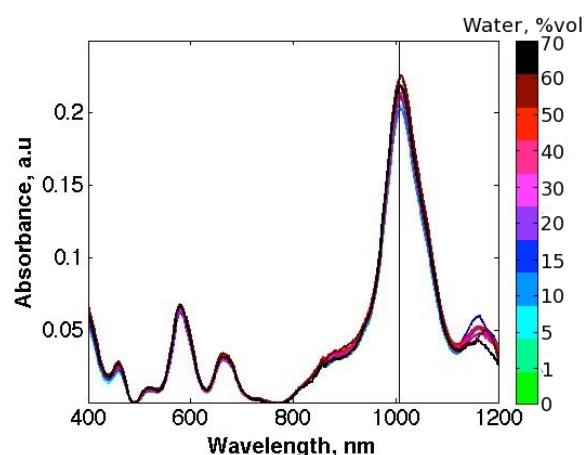
<sup>2</sup>For this experiment we used dry NMP.



(a) Spectrophotometric titration. Original results.



(b) Spectrophotometric titration. Baseline corrected.



(c) Spectrophotometric titration. Baseline corrected and normalised to dilution.

**Figure 5.1** – Spectrophotometric titration of NMP based dispersions of carbon nanotubes with water. Original spectra, as well as spectra corrected to the baseline, show a significant drop in concentration. This drop is associated solely with dilution of the sample. The spectra normalized to dilution do not show decrease of concentration of carbon nanotubes.

The samples for spectrophotometric titration were prepared as follows. The CNTs (cat. # 704148, lot MKBG5771V, >50% CNTs are 6,5 chirality) were dispersed in neat N-methyl-2-pyrrolidone (anhydrous, 99.5%, Sigma-Aldrich 328634) via ultrasonication (24 kHz; 240 W; pulse mode: 0.5 sec active - 0.5 sec passive; 45 min active) with a Branson S450-D digital sonifier ultrasonic processor or with analogues settings with Hielscher ultrasonic processor UP400S at the 60% amplitude. The dispersion was subjected to centrifugation (5 h; 20 000 rpm). The dispersion and water were mixed into samples of 2.5 ml in proportions, corresponding to 0, 1, 5, 10 15, 20, 30, 40, 50, 60 and 70 %<sub>v</sub> of water. The samples were sealed immediately with parafilm. Absorbance spectrum of each sample was recorded (see fig. 5.1a).

CNTs absorb in a wide wavelength interval, therefore, one needs to make sure that one obtains pure CNT spectra with no contribution from a solvent (NMP) or a cosolvent (water). All CNT spectra were treated identically. Spectra were recorded on spectrophotometer PerkinElmer Lambda 950 and PerkinElmer Lambda 2 (the later spectrophotometer has a smaller wavelength range and is capable of recording spectra only up to 1100 nm). These spectrophotometers are two beam spectrophotometer, which allows one to automatically subtract absorption of the solvent (reference). Mixture of water with NMP with water concentration, corresponding to the water concentration in the sample, was used as a reference for each sample.

In order to bring more clarity into the spectrophotometric titration results obtained spectra were processed further. The wavelengths were transferred to an energy domain (eV), where the baseline is linear. A linear baseline, such that the baseline slope repeats the slope of the spectrum, was subtracted from each spectrum. The resulting spectra are represented in the figure 5.1b. The procedure of the titration involves a significant dilution of the carbon nanotubes dispersions. This dilution according to Lambert-Beer law leads to spectra intensity reduction. To account for this effect, each sample was normalized to the original concentration of carbon nanotubes (see fig. 5.1c).

## Results and discussion

Upon addition of water, no visible aggregates were detected. Original results of the spectrophotometric titration are represented in the figure 5.1a. The spectra reveal a significant reduction of carbon nanotubes concentration. The same trend remains after subtraction of the baseline.<sup>3</sup> However, this visible reduction of absorption intensity may be associated with dilution of carbon nanotubes rather than with their precipitation. To account for dilution, the spectra intensity was normalised to the concentration of the nanotubes in the original sample (figure 5.1c). As one may see, normalised spectra with subtracted baseline do not reveal any significant reduction of the concentration, compared to the original sample.

As one can see from the figure 5.1, dilution corrected concentration of CNTs in the dispersion stays constant upon addition of water. Constant CNTs concentration upon increasing water concentration suggests that water, added to prepared CNT dispersions,<sup>4</sup> does not affect stability

---

<sup>3</sup>The spectra were transferred into an energy domain (wavelengths measure in eV), where the baseline becomes linear. A linear baseline was then subtracted from the original spectrum and the resulting spectral curve was transferred back to the nanometres wavelengths measure.

<sup>4</sup>Qualitative analysis shows that 4%<sub>wt</sub> of water in NMP *before* preparation of CNT-NMP dispersion, does not affect the ability of the solvent to disperse CNTs.

of carbon nanotubes dispersion in NMP. As water does not affect the dispersion stability, we may work with CNT-NMP dispersions without special facilities, like dry boxes. These findings are in a good agreement with the findings in [206].

However, as one may notice from the figure 5.1c, the absorbance does not stay constant. These changes may be noted at the main absorbance peak, which corresponds to nanotubes of chirality 6,5, as well as in the longer wavelengths region of the spectrum. The maximum deviation of the peak height is less than 12%. These changes may originate in restructuring of water-NMP mixture as well as in possible artifacts of the baseline correction. It is important to note here that spectral lines of carbon nanotubes broaden upon bundle formation. Subtraction of linear baseline in the energy domain is, in principle, capable of partial removing of this contribution into the spectra. Partial removal of the spectra features, associated with bundle formation, may lead to small differences in the resulting spectra.

### 5.2.2 Transmission electron microscopy

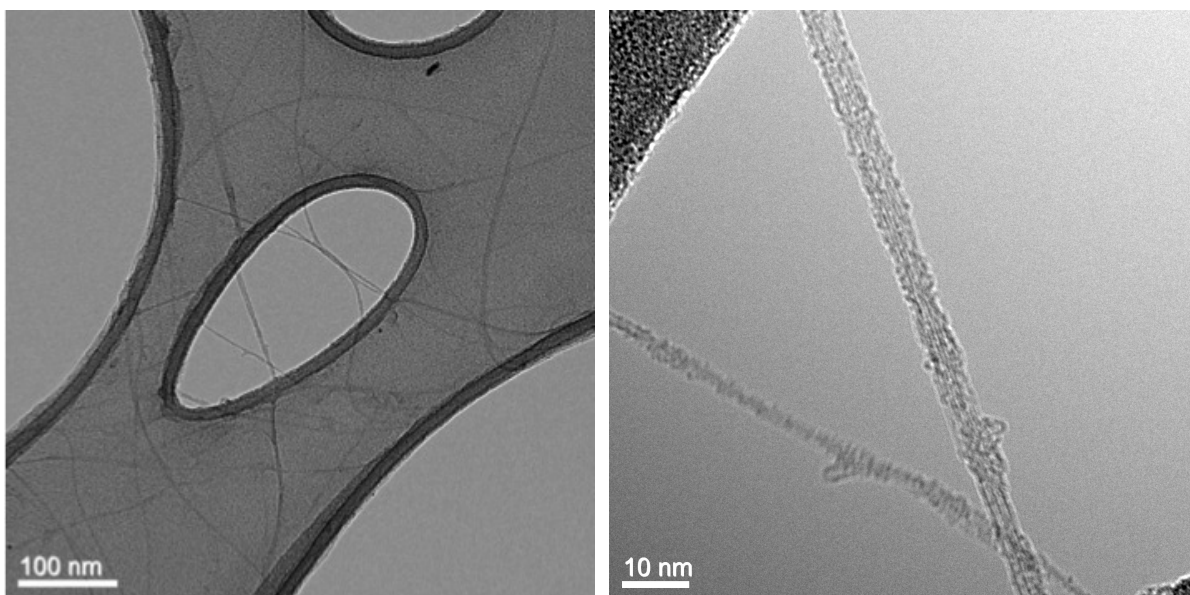
Although water admixtures do not significantly affect general stability of CNT-NMP dispersions, it could still make changes on molecular level, e.g. clusters of water-NMP molecules could have been attached to the surface. To understand, whether an effect of water molecules takes place at a molecular level, we performed transmission electron microscopy of a reference CNT-NMP dried dispersion and CNT-NMP dispersion with water additions before drying.

The figure 5.2 shows micrographs of reference pure CNT-NMP dispersion (5.9a) and CNT-NMP dispersion with 4 %<sub>wt</sub> (5.2a) at magnification  $\sim 30$  KX. Magnification of 30 KX is relatively low magnification for a transmission electron microscope. On the one hand, this magnification does not allow us to see real molecular level details of bundle structure. On the other hand, it allows us to see the general distribution of carbon nanotubes in the relatively high area and estimate the average length of single CNTs and their bundles. Additionally, it is already possible to make a rough estimation of the number of CNTs in bundles.

To understand more details about how CNT bundles are structured at a molecular level, we made micrographs with higher magnification ( $\sim 200$  KX). The results are represented in the figure 5.2 and in the table 5.1. As one can see, the linear length distribution<sup>5</sup> in the sample with water is similar to that of the reference sample. On the other hand, the CNT surface contains somewhat more residues of solvent. Comparing reference micrographs and micrographs of the sample with water in the figures 5.9 and 5.2 one can conclude that bundle structures do not

---

<sup>5</sup>see page 124 for details.



(a) TEM of CNT-NMP dispersion with 4%<sub>wt</sub> of water. 30 KX

(b) TEM of CNT-NMP dispersion with 4%<sub>wt</sub> of water. 200 KX

**Figure 5.2** – Characteric transmission electron microscopy images of CNT-NMP dispersion with water content in the dispersion 4%<sub>wt</sub>. 4%<sub>wt</sub> is an estimation of maximum realistic water amount absorbed by the CNT-NMP dispersion during work. Lacey carbon.

change significantly upon addition of water.

Visual inspection of micrographs as well as analysis of bundle structures observed under TEM suggests that water in small concentrations does not affect CNT bundle formation. Therefore, we did not use special moisture protection techniques to keep our CNT-NMP dispersions dry. We assume that a thick layer of NMP molecules acts as a surfactant and isolates a tube from water molecules. Unlike the surfactant NMP can evaporate, leaving the carbon nanotube surface pristine.

## 5.3 Effects of iodide and bromide

### 5.3.1 Spectrophotometric titration and photoluminescence control

#### Sample preparation

The methodology of spectrophotometric titration with sodium iodide and bromide is similar to spectrophotometric titration with water. The CNT dispersion was prepared analogically. The prepared CNT-NMP dispersion was divided into samples 2.5 ml each. A small volume of concentrated salt solution in NMP was added to the dispersion, such that the resulting salt

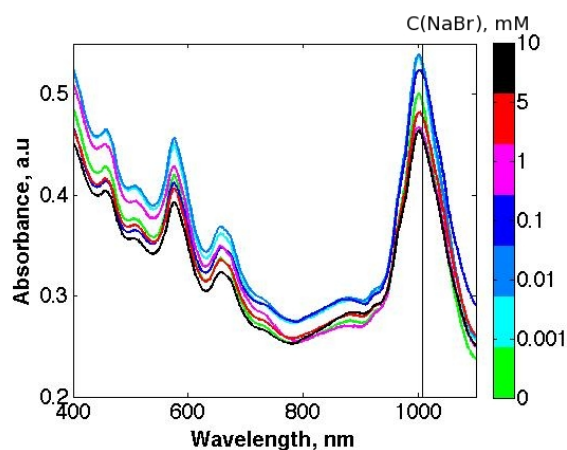
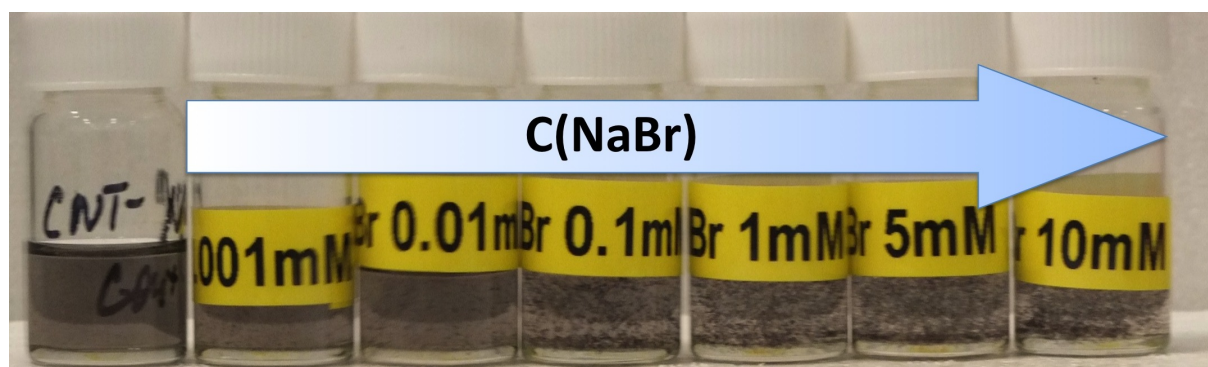
concentration would be 0.001, 0.01, 0.1, 1, 5 and 10 mM. The samples were mixed throughout on a shaker at 300 rpm for an hour. All CNT spectra were treated identically. Carbon nanotubes were obtained from Sigma (cat. # 704148, lot MKBG5771V). More than 50% CNTs in the CNT mixture of the sample have the 6,5 chirality. NMP was purchased from Sigma (anhydrous, 328634). Salts were purchased from Sigma (NaBr: cat # 02119, lot SZBB1170V; NaI: cat. # 383112, lot MKBK2320V) and used without further purification.

The spectra were recorded on the PerkinElmer Lambda 2 spectrophotometer. This spectrophotometer is two beam spectrophotometer, which allows one to automatically subtract absorption of the solvent (reference). The NMP solution of a salt with the salt concentration, corresponding to the concentration of the salt in the sample, was used as a reference for each sample. Original results of the spectrophotometric titration with sodium bromide are shown in the figure 5.3b and the original results of the titration with sodium iodide are can be seen in the figure 5.4b. As the dilution of the original dispersion was minor, its effect may be omitted. The baseline correction of the spectra was analogous to the baseline correction for the spectrophotometric titration with water. However, unlike with water addition of salts produce a significant amount of well visible bundles (see figures 5.3a, 5.4a). These bundles contribute to the measured spectra and, therefore, have to be removed. Removal of the bundles was done by mild centrifugation at 10000 rpm in a fixed angle rotor for 30 minutes. The spectra of the dispersions after separation of the bundles are specified in the figures 5.3d and 5.4d.

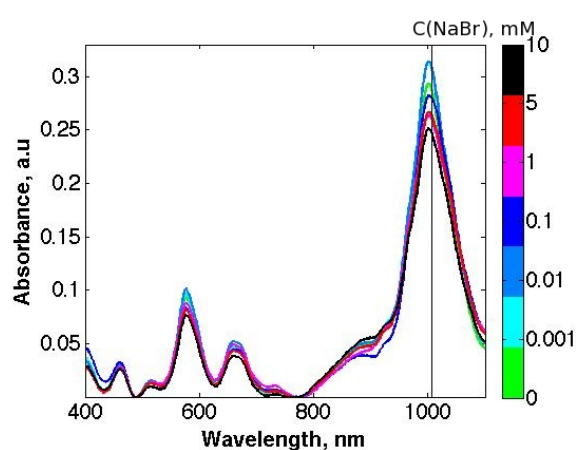
## Results and discussion

Significant amount of carbon nanotube aggregates are visible to the bare eye after addition of salts to the CNT-NMP dispersion (see figures 5.3a, 5.4a). Amount of these aggregates increases with an increase of salt concentration. Qualitatively salt effects may be registered spectroscopically for both sodium iodide and sodium bromide. However, these effects do not show a significant dependence on the salt concentration (figures 5.3b and 5.4b). The reason for this is the presence of aggregated nanotubes in the sample. These tubes interfere with the dispersed nanotubes, partially absorbing the light and partially increasing the scattering. Mild centrifugation is the best tool to separate the precipitate from the dispersion as it introduces only minimal additional clustering of the tubes.

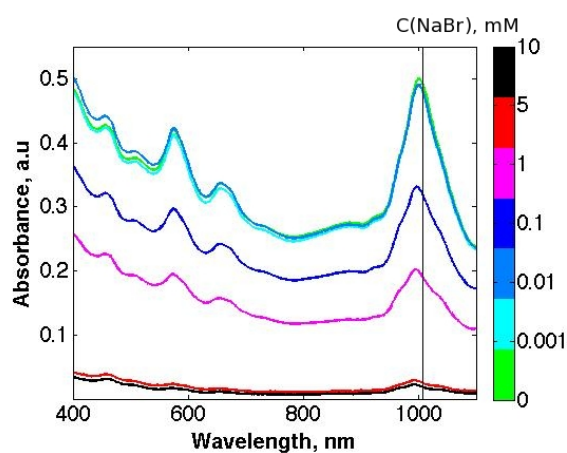
After a mild centrifugation both systems (NaBr and NaI) show a gradual reduction of the concentration of carbon nanotubes in the dispersion with increase of salt concentration (see figures 5.3e, 5.3e, 5.4e, 5.4e). The lowest concentration (0.001mM) almost does not affect the



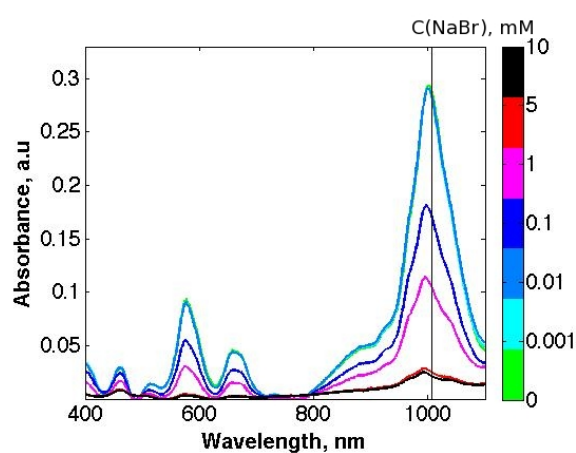
(b) Original spectra of spectrophotometric titration of CNT-NMP dispersion with NaBr before centrifugation



(c) Baseline corrected spectra of spectrophotometric titration of CNT-NMP dispersion with NaBr before centrifugation

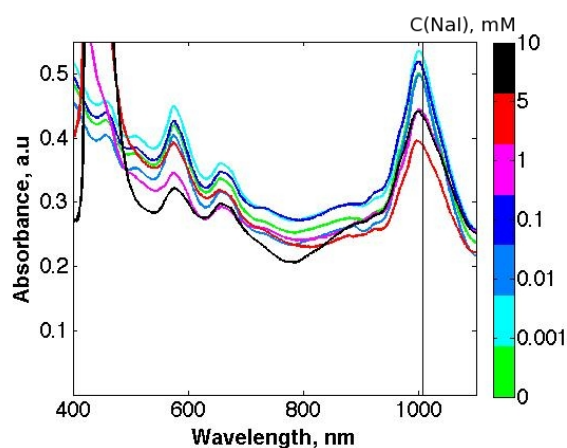
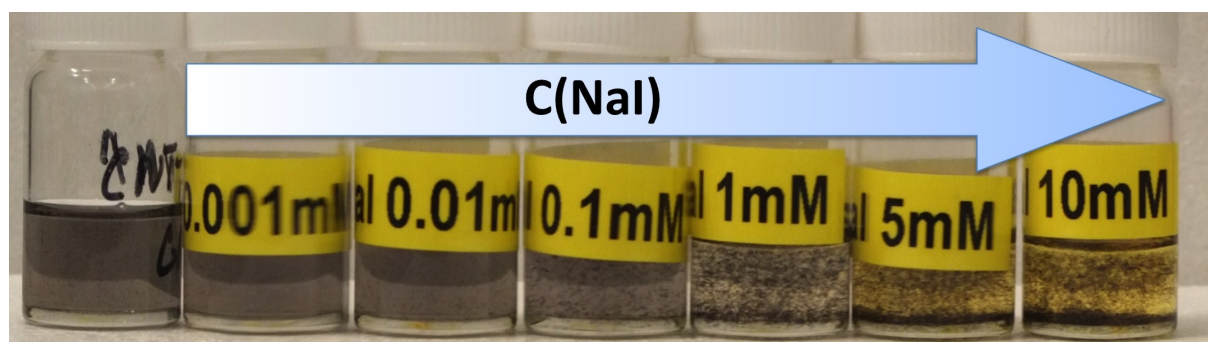


(d) Original spectra of spectrophotometric titration of CNT-NMP dispersion with NaBr after centrifugation

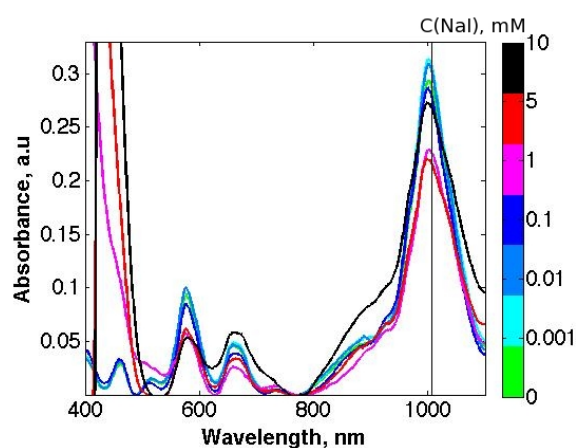


(e) Baseline corrected spectra of spectrophotometric titration of CNT-NMP dispersion with NaBr after centrifugation

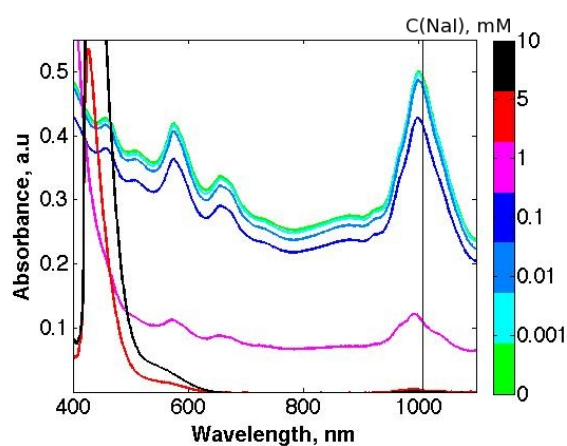
**Figure 5.3** – Spectrophotometric titration of CNT-NMP dispersion with NaBr



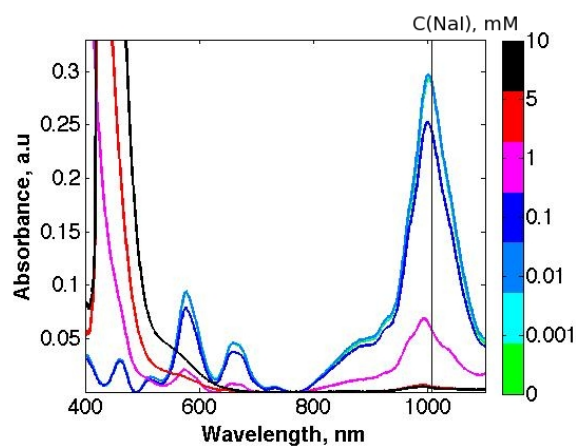
(b) Original spectra of spectrophotometric titration of CNT-NMP dispersion with NaI before centrifugation



(c) Baseline corrected spectra of spectrophotometric titration of CNT-NMP dispersion with NaI before centrifugation



(d) Original spectra of spectrophotometric titration of CNT-NMP dispersion with NaI after centrifugation



(e) Baseline corrected spectra of spectrophotometric titration of CNT-NMP dispersion with NaI after centrifugation

**Figure 5.4** – Spectrophotometric titration of CNT-NMP dispersion with NaI



stability of the dispersion. Higher salt concentrations (5 and 10 mM) precipitate almost all nanotubes from the dispersion. Although the main trend remains the same for both sodium iodide and sodium bromide (reduction of the CNT concentration with increase of salt concentration), there are some differences in the behaviour of the systems at the intermediate concentrations (0.01, 0.1).

At the intermediate concentrations (0.01 and 0.1 mM) sodium bromide shows higher ability of precipitating carbon nanotubes compared to sodium iodide. According to the Kirkwood-Buff theory and in line with the discussions in the chapter 4 and based on lower solubility of sodium bromide in NMP, compared to sodium iodide, one may suggest the following explanation for the observed behaviour. The surface charge density of sodium ion is closer to the surface charge density of bromide ions, compared to iodide ions. This leads to higher tendency of sodium ions to form direct ion pairs with bromide ions, compared to iodide ions in NMP. As NMP is a polar solvent, ions and ionic pairs are solvated strongly in the solution. These ionic pairs are also more depleted from neutral carbon nanotube surface, compared to more polarizable iodide ions. As a result, one may expect a more pronounced depletion of bromide ions from a carbon nanotube wall compared to iodide ions. This increased depletion of bromide ions, compared to iodide ions, leads to a more pronounced increase in the free energy of the carbon nanotube surface in solution of sodium bromide.

Interestingly, this trend does not hold true for salt concentration 1mM. The following mechanism may be suggested to explain this deviation from the theory. As one may see from the figures 5.4, an intense band starts to emerge in shorter wavelengths. In principle, there are two possible sources for this band: *i*) it is an artefact of incorrect subtraction of a very intense band of sodium iodide, which goes out of the absorbance range of the spectrophotometer; and *ii*) it is an intense iodine band, which also goes above the measurement range. An iodide ion has a small redox potential (-0.54 Volt),<sup>6</sup> which allows iodide ions to oxidise easily on air. Possibly, oxidation of iodine goes more effectively in the presence of carbon nanotubes, e.g. on wall defects of the tubes. Probably, this molecular iodine alters the mechanism of CNT precipitation.

### Photoluminescence control

Photoluminescence spectroscopy<sup>7</sup> was used as a tool for monitoring the presence of isolated CNTs and small bundles in the dispersions [207, 208, 209]. We assume that the concentration of nanotubes within the sample correlates with the intensity of the PL bands and optical absorbance

---

<sup>6</sup>vs. standard hydrogen electrode

<sup>7</sup>PL spectra were recorded only for titration with sodium iodide

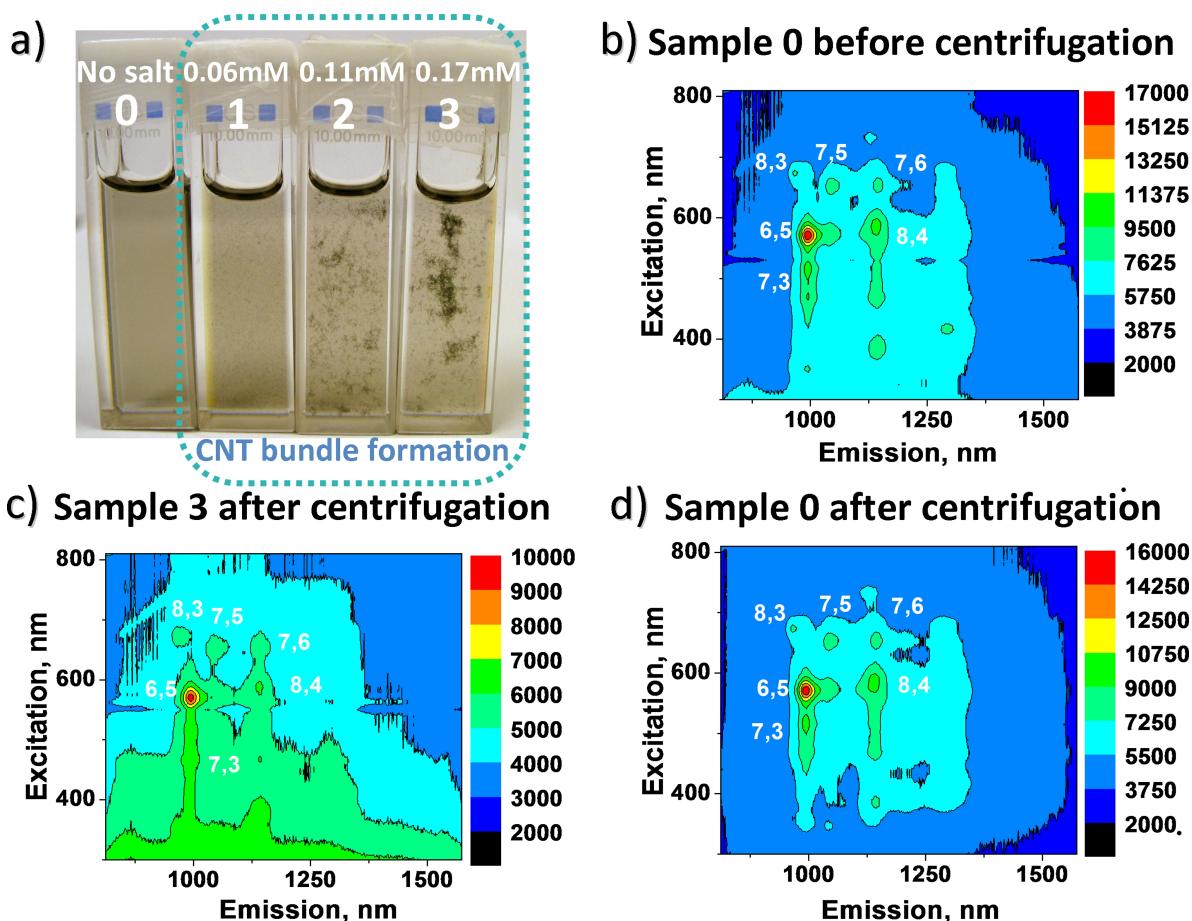


**Figure 5.5** – Photoluminescence evidence of CNT bundle formation in the presence of NaI. a) Samples of the CNT-NMP dispersions after addition of different amounts of salt (NaI) and aging for 15 minutes. The left sample (0) is the control CNT-NMP dispersion with no salt. In the samples 1-3 there are visible aggregates, formed by self-assembled nanotubes, which appeared after addition of the salt. The size of the aggregates increases with the increase in salt concentration. b) Photoluminescence (PL) map of the control CNT-NMP dispersion sample (no salt) before centrifugation. The map shows the presence of single wall CNTs of different chiralities, which are indicated on the map; c) PL map of the CNT-NMP dispersion sample at 0.17 mM concentration of NaI salt after centrifugation (sample 3). The map shows that isolated CNTs and small CNT bundles remain in the dispersion. However, the overall PL intensity drops down significantly as compared to the control sample before (b) and after centrifugation (d); d) PL map of the control sample (sample 0) after centrifugation. The map is very similar to the PL map of the control sample before centrifugation, showing only a minor decrease in the overall intensity, as compared to the PL map of the sample 0 before centrifugation (b).

for corresponding CNT chiralities. That allows us to make quantitative analysis of changes in the dispersions upon additions of salt.

Addition of NaI into the CNT-NMP dispersions results in sedimentation of CNTs. The nanotubes self-assemble into bundles, which later form CNT aggregates in the samples, visible

to the bare eye. The effect is taking place for the following salt concentrations: 0.06, 0.11 and 0.17 mM (figure 5.5a). This picture shows photography of the samples of CNT-NMP dispersion with different salt concentrations in comparison to the control sample.

Photoluminescence intensities of CNTs were recorded before and after centrifugation of the dispersions. It was found that addition of salt decreases markedly the PL intensity as well as the optical absorbance for CNTs of all chiralities in the dispersions, as compared to the control sample. The decrease in PL intensity and the optical absorbance correlate with the salt concentration in the samples as illustrated by the Figure 5.5. The figure shows that larger concentrations of salt cause a larger decrease in the intensity. These changes in spectra intensities were attributed to a significant decrease in concentration of isolated nanotubes and small CNTs bundles in these dispersions after centrifugation. The addition of NaI salt stimulates the CNTs self-assembly into large aggregates (see Figure 5.5a), which can be simply extracted from the dispersions by centrifugation. On the contrary, centrifugation of the initial (control) dispersion makes a much smaller effect on the PL intensity and optical absorbance of CNTs, indicating a high stability of the control dispersion. This could serve as an additional confirmation that the observed self-assembly of CNTs is stimulated by salt rather than by ageing of the CNT dispersions. The observed phenomenon is attributed to the so-called "salting-out effect", which is defined as a decrease of solvency of non-polar species in polar solvents upon addition of salts. This effect is widely used in biochemistry for precipitation, separation and coagulation of biomolecules from their aqueous solutions [210, 211, 212, 213].

An explanation of the observed phenomena in CNT-NMP dispersions was proposed, which is inspired by the interpretation of salting-out effects in water solutions demonstrated in works [210, 211] We assume that it is reasonable to extrapolate the qualitative explanations of the effect from water to NMP solutions. Indeed similar to water, NMP is a highly polar solvent, where the solvent molecules interact strongly with dissolved ions due to the charge-dipole interactions and thus form distinctive ion solvation shells [214]. Therefore, ions in the CNT-NMP dispersion tend to interact mostly with the polar NMP molecules rather than with the CNTs non-polar surface. On another side, the ions in the vicinity of the CNT surface have less NMP molecules to interact with, as compared to the ions in the bulk solution because of the sterical restraints, caused by the surface. When contacting the CNTs surface, ions undergo partial desolvation, which should be energetically unfavorable in a highly polar solvent like water or NMP [215]. Overall, this should result in formation of an ion depletion area around the non-polar CNTs, where the ion concentration is significantly lower than in the bulk. This gradient of the ion concentration produces osmotic stress, a thermodynamic force which tends to compensate the

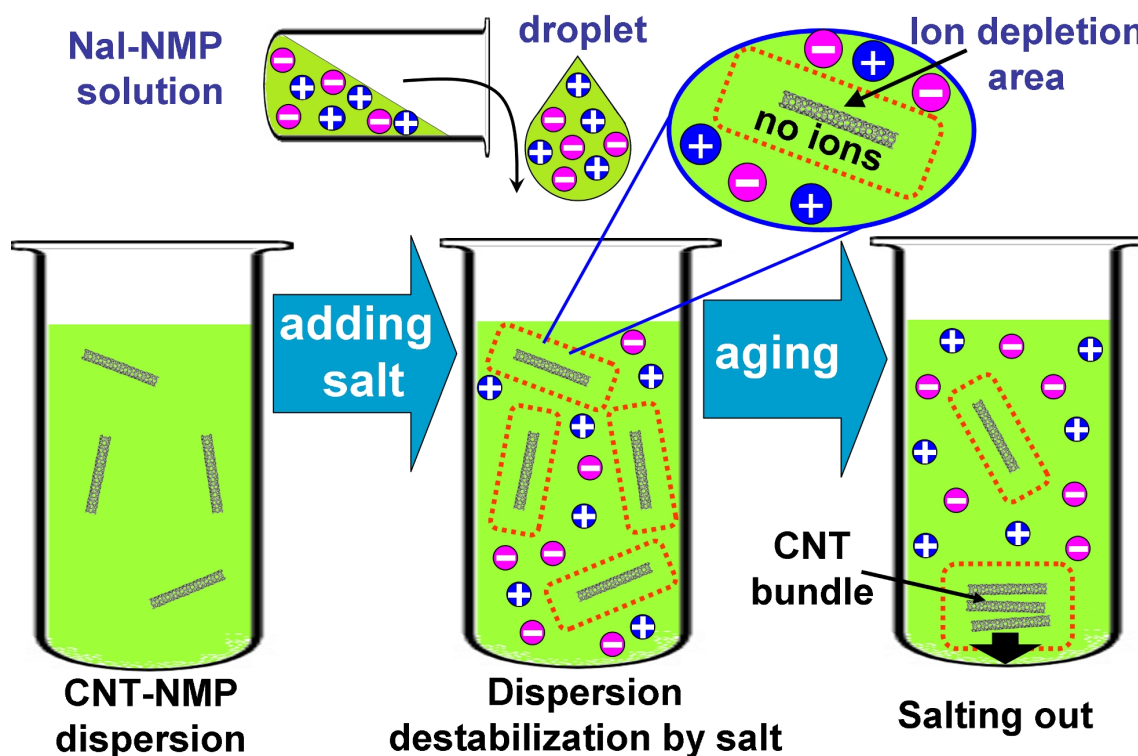


**Figure 5.6** – A pictorial illustration of the nanotube self-assembly, directed by the salting out effect. The addition of salt stimulates the self-assembly of nanotubes in bundles because ions are depleted from the nanotube surface. This results in an osmotic stress, which increases the strength of solvophobic forces, acting on the nanotubes. Consequently, the CNTs interact preferentially with each other, forming bundles. Reproduced from ref. [9]

depletion of ions from the nanotube. The osmotic stress makes the CNTs more solvophobic and, as the result, the CNTs more preferentially interact with each other due to the increasing strength of solvophobic interactions. This leads to self-assembling of nanotubes into bundles because CNTs in bundles have much less overall solvent accessible surface. Hence, after addition of salt, some numbers of CNTs assemble into large aggregates, which can be separated from the dispersion by centrifugation. We illustrate the suggested mechanism of the observed salt effects on CNT-NMP dispersions with a pictorial presentation in the figure 5.6. It was shown that ions have significant impact on CNT bundle formation in NMP. Addition of salt into the nanotube dispersion leads to self-assembly of nanotubes and formation of large CNT bundles, which can be extracted from the solution by centrifugation. The overall effect of salt increases with an increase of the salt concentration.

### 5.3.2 Transmission electron microscopy

Transmission electron microscopy is a convenient experimental tool to study substances at the molecular level. This is why this technique supplements the spectrophotometric study.

A standard procedure to prepare a TEM sample is as follows. Three droplets of the dispersion are placed on a TEM grid (Cu mesh 300/400, lacey carbon/ lacey carbon on a thin carbon film) situated on a filter paper. The grid dries in air in a covered dish for at least 24 hours. Afterwards, the grids are collected into a marked TEM grid sample box and stored in a desiccator. This sample preparation technique ensures that TEM sample grids represent best the bulk of the material and the specimen is electron transparent at the same time. With this method of TEM sample grid preparation we expect that salts stay on the TEM sample-grid. Therefore, these structures could interfere with the structure of CNT bundles. Another open question here is how we characterize changes in bundle structures upon addition of cosolutes. To address these two issues we performed a series of reference measurements. The details of the reference studies are represented below.

#### **Reference studies. Microscopic behaviour of NaI, NaBr and pristine carbon nanotubes.**

In order to understand how cosolutes such as water or salts affect bundle structures of carbon nanotubes, we need to study carefully every component of the system separately. This study provides an important information on structures formed by carbon nanotubes and salts individually. Here we assume that the solvent evaporates fully, this is why we did not study reference grids of water-NMP mixtures without CNTs.

The first reference grids, which we studied, are the most simple grids with salts on them. We prepared a salt-NMP solution with a salt concentration of 0.1, 0.5, 1.0 and 10mM. Further, TEM grids were prepared with the standard technique, described above. Salt does not evaporate and stays on the grid. This is why we are able to analyse a typical pattern created by salt on a TEM grid.

Let us start with a typical pattern, created by NaBr of a TEM grid. The figure 5.7 shows a typical structure, formed by NaBr on a grid: a dense uniform film. Although sodium iodide is a closely related salt to sodium bromide, it may form completely different structures during solution evaporation. This is why we continued our reference studies with NaI reference. The figure 5.8 depicts a typical pattern created by NaI. As one can see, NaI produces electron dense droplet-like aggregates. This behaviour is very different from sodium bromide behaviour and suggests that NaI forms soot-like aggregates on the grid surface. Fortunately, these aggregates

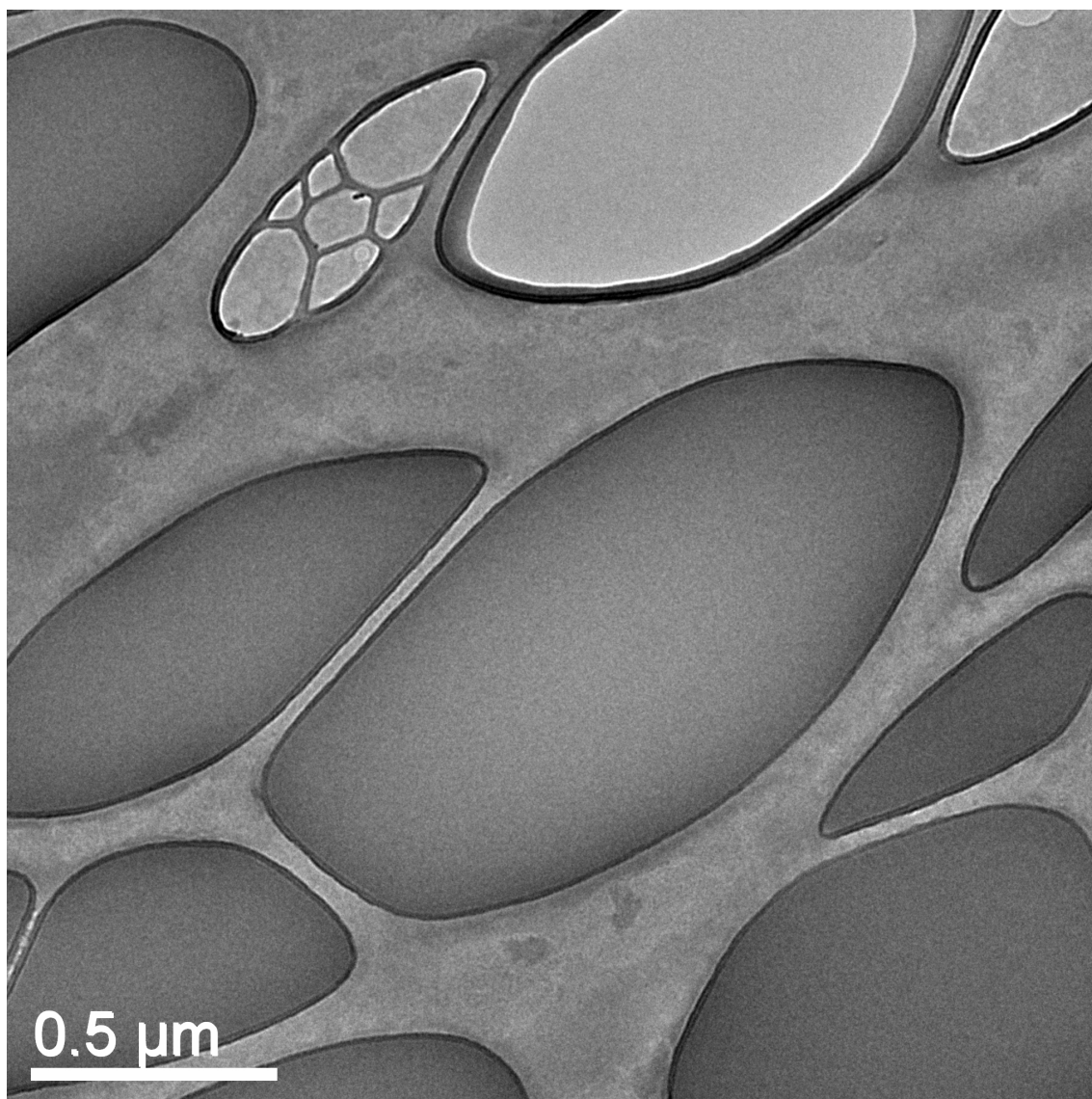
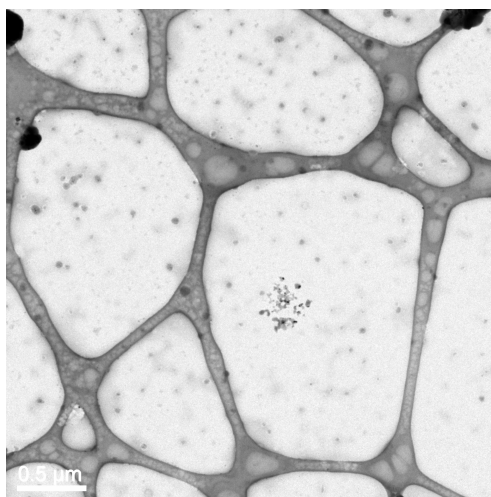


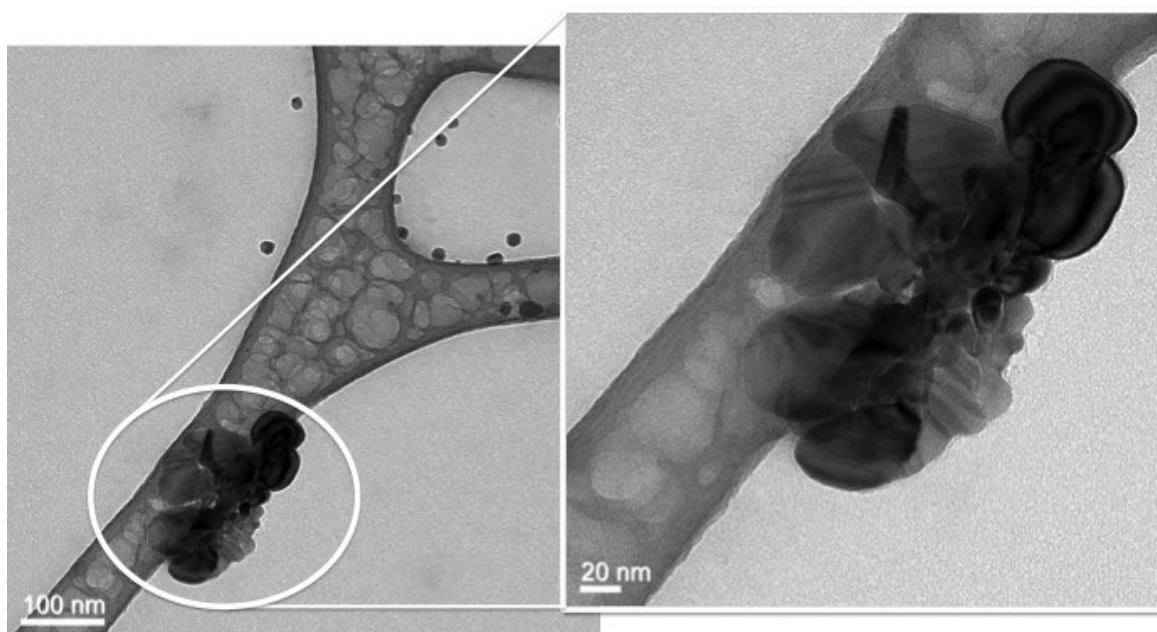
**Figure 5.7** – TEM image of a typical structure formed by NaBr: a dense uniform film, covering the whole hole on lacey carbon film.

can be well differentiated from the carbon nanotubes.

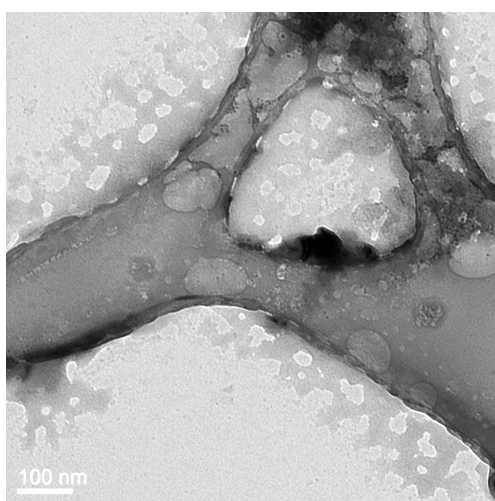
The study of reference grids would not be complete without the study of CNT bundles in a pure NMP solvent. This also allows to account for possible hydrocarbon contaminations [141]. The figure 5.9 shows a typical structure, formed for a pure CNT-NMP dispersion. As one can see, the bundle structure (5.9b) at the reference grid suggests, that tubes are well aligned in a bundle and there are just minor solvent residues on the tube's surface. Hydrocarbon contaminations, described in the work [141] were not found on the CNT-NMP reference grid. Unfortunately, micrographs, although very detailed, do not allow a quantitative characterisation of the tubes in the bundles. To eliminate this disadvantage of TEM, we sampled over several regions at several identical grids. Detailed procedure of the analysis is described below. Although electron microscopy represents a unique possibility to get molecular level details directly from an



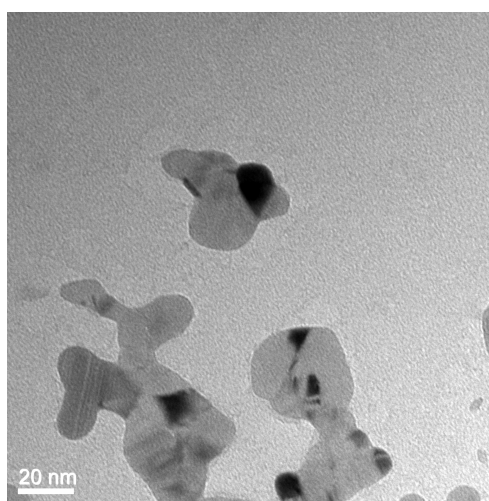
(a) TEM image of a NaI reference grid



(b) TEM image of NaI cluster.



(c) NaI discontinuous films



(d) NaI film in more details

**Figure 5.8** – TEM images of typical structures formed by NaI. Lacey carbon on ultra-thin carbon.

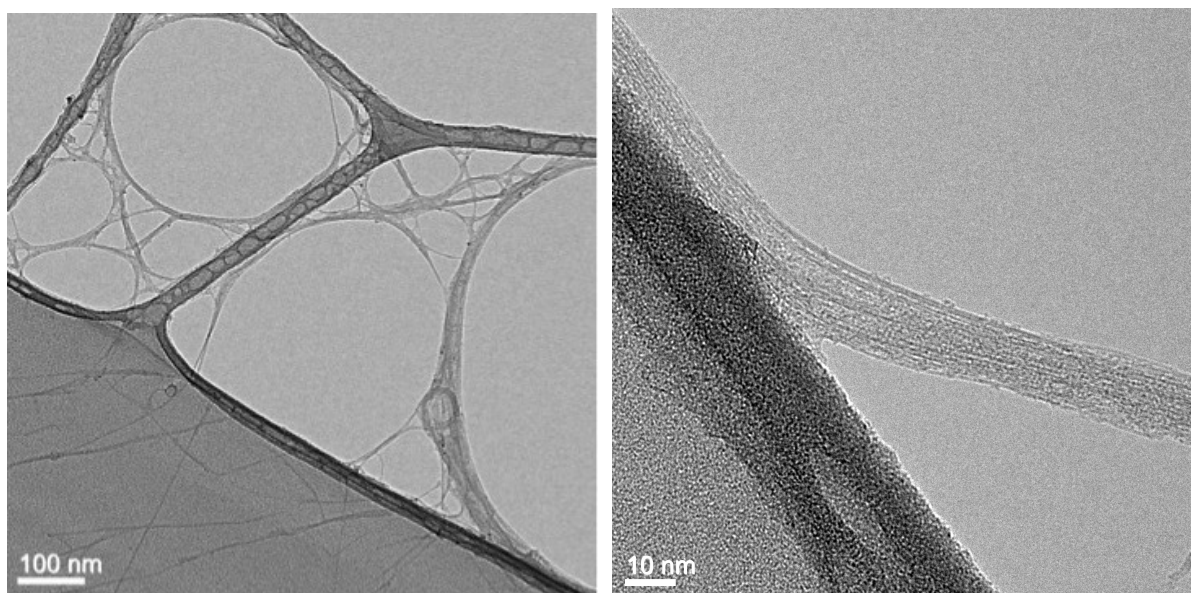
experiment, it has two major disadvantages. Firstly, as it has already been mentioned, sampling is all the time an issue because micrographs cover only small areas. Secondly, micrographs on their own do not provide any quantitative data. This is why here we developed a semi-quantitative criteria to compare micrographs of different systems.

**The semi-quantitative criteria to assess micrographs** is as follows: *i*) linear length of tubes/bundles; *ii*) width distribution of bundles. As these criteria are not strict, they require an additional formalisation. First, let us consider the linear length. A real carbon nanotube is not a rigid molecule. This is why linear lengths vary from just a few nanometres to hundreds of nanometres. This means that averages of the linear length have enormous standard deviation. This is why we used frequency distribution of lengths rather than the average length as a criterion of linearity of CNT bundles.

The second criterion we consider is the size distribution of CNT bundles. We note that salt films reduce contrast of CNTs, because the salt films are more electron dense, compared to CNTs. This means that we are not able to distinguish clearly individual tubes in bundles. To analyse bundle size using the same criterion for all studied systems, we employ bundle width as a main criterion of bundle size rather than number of tubes in the bundle. Unfortunately, bundle width range is wider for lower magnifications. This is why we performed bundle width analyses only at micrographs with magnification larger than 80 KX (magnification 80 000 times). We do not consider two tubes crossing each other in one point as a bundle. Similarly, two bundles, which form a cross with one intersection, are not considered as a joined bundle. The results of analysis of reference grid with CNT-NMP dispersion are shown in the table 5.1.

As one can see from the distribution of linear lengths for a reference micrographs of CNTs, obtained from pure NMP dispersion, the most probable linear length for a bundle is about 50 nm. There are several factors, which affect the linear length distribution. First of all, a tube naturally tends to sustain linear conformation. The reason for this is the native geometry of  $sp^2$  hybridisation of carbon atoms, forming the tube. Several studies of the persistent length of carbon nanotubes in dispersions, e.g. [216, 217], have revealed, that a relaxed persistent length of carbon nanotubes vary from 26 to 138  $\mu\text{m}$ , depending on the tube diameter. On the other hand, in the process of drying on a TEM grid, multiple capillary forces act on the tube, which forces the tube to bend. The interplay of these forces makes partial input into the obtained distribution of the linear lengths 5.1. It is also important to mention here, that there are two possible regimes of the bundle formation: thermodynamic and kinetic. Thermodynamically driven bundle formation of carbon nanotubes should result in well aligned tubes, while kinetically driven process may result in chaotically bended tubes. The later structure is not thermodynamically stable, still, it





(a) TEM of CNT-NMP reference dispersion. 30 KX

(b) TEM of CNT-NMP reference dispersion. 200 KX

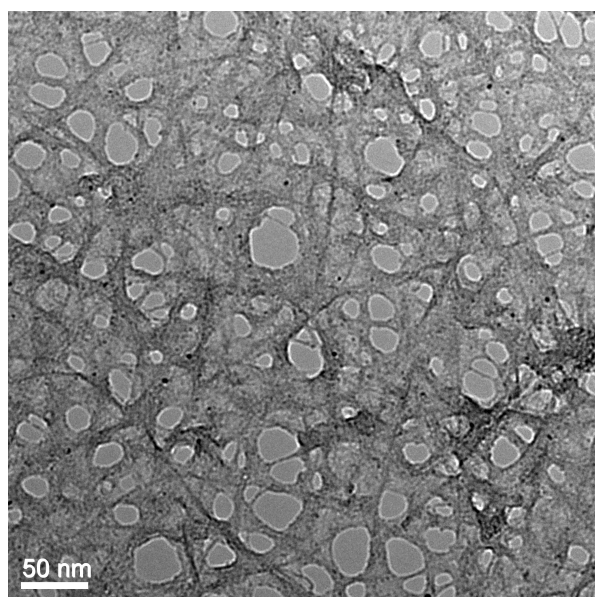
**Figure 5.9** – TEM image of typical structures observed in reference CNT-NMP dispersion. Lacey carbon.

may possess a significant kinetic stability, if, for example, the bundles are constrained with salts.

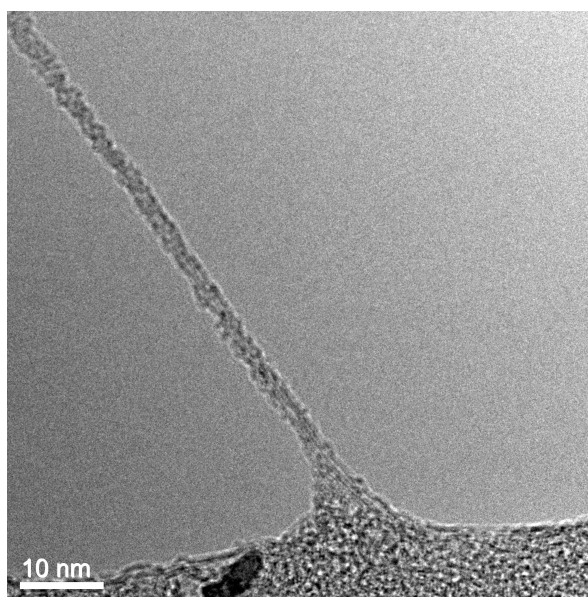
Another important property of the CNTs, obtained from the reference CNT-NMP dispersion, is the fact that the tube's surfaces are smooth and contain only minor residues of solvent. This suggests, that in the case of pure CNT-NMP dispersion, the solvent evaporates completely under normal conditions, leaving the surface of the tubes clean.

In the section 5.3.1 it was shown that salts can be used to regulate the CNT concentration in the carbon nanotubes dispersion, as illustrated by the observed changes in the intensities of PL and absorbance spectra of the samples at different salt concentrations. The self-assembly of nanotubes can be initiated by even small amounts (0.1 mM) of salts and the effect is reproducible with different types of carbon nanotubes (SWeNt CG100, Lot # 000-0012 and 6.5 chirality, 704148 Aldrich). This provides an easy, robust and safe route to form bundles of pristine carbon nanotubes. Unfortunately, spectrophotometry does not answer the question, whether the bundle structure is affected by salts. To gain this knowledge we performed transmission electron microscopy and collected statistics on how bundles are structured. The technique of semi-quantitative analysis of micrographs is the same as in the section 5.3.2, page 124.

Visual inspection of micrographs reveals that, unlike the smooth and clear surface of the carbon nanotubes, obtained from the reference CNT-NMP dispersion, the surface of carbon nanotubes, obtained after additions of salts, is very rough. This roughness of the surface suggests

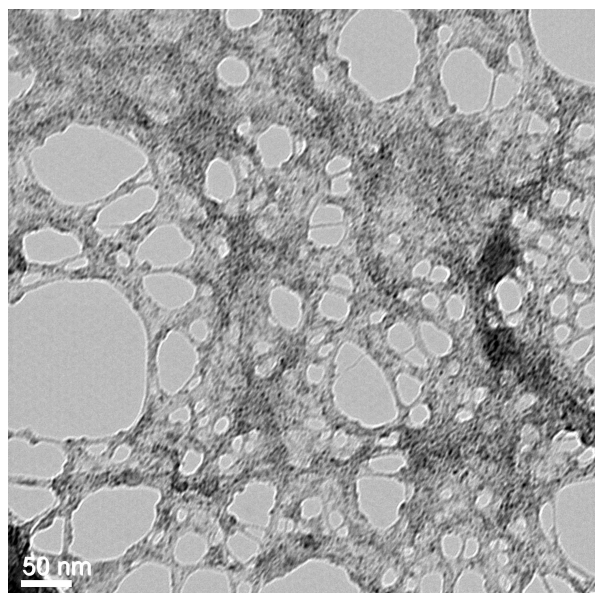


(a) TEM of CNT-NMP after addition of 0.1 mM of NaBr. Magnification 40 KX.

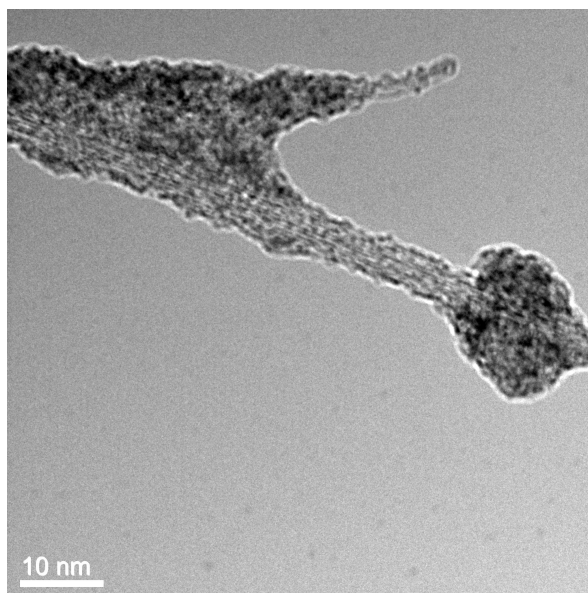


(b) TEM of CNT-NMP after addition of 0.1 mM of NaBr. Magnification 250 KX.

**Figure 5.10** – TEM micrographs of CNT-NMP dispersion after addition of 0.1 mM of NaBr



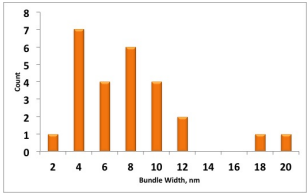
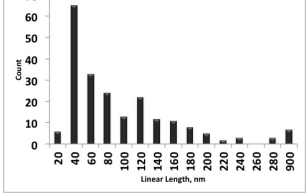
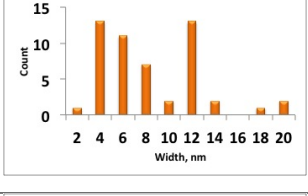
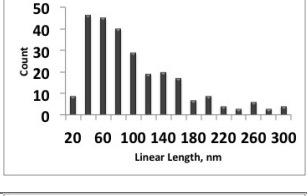
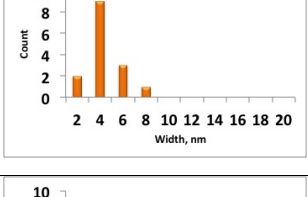
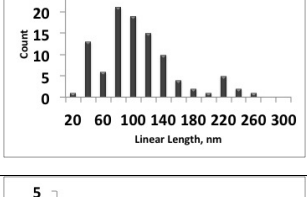
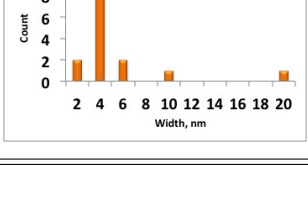
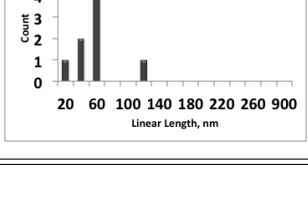
(a) TEM of CNT-NMP after addition of 0.1 mM of NaI. Magnification 35 KX.



(b) TEM of CNT-NMP after addition of 0.1 mM of NaI. Magnification 250 KX.

**Figure 5.11** – TEM micrographs of CNT-NMP dispersion after addition of 0.1 mM of NaI

**Table 5.1** – Semi-quantitative analysis of characteristics of CNT bundles obtained with TEM

	Bundle width	average linear length, nm
CNT-NMP dispersion		
CNT-NMP-water dispersion		
CNT-NMP NaBr 0.1 mM		
CNT-NMP NaBr 0.5 mM		

that remaining salt solvates covers the carbon nanotubes surface. We explain the presence of the salt solvates as follows. The energetic barrier to remove NMP molecule from solvation shell of the carbon nanotube is higher compared to energy of a molecule at the room temperature. Furthermore, this dense NMP layer attracts ions, which form an ionic shell around the NMP shell. Our findings suggest that this layered structure remains untouched upon evaporation of the bulk NMP from the dispersion (see fig. 5.12). Results of the previous work [10] suggest, that NMP molecules are oriented around a CNT in such a way that their positively charged dipole site is located on the outer surface of the solvation shell. This small excessive positive charge attracts anions ( $I^-$  or  $Br^-$ ) (see fig. 5.12), and they concentrate in the second solvation shell of the carbon nanotube. This excessive ion concentration may prevent NMP evaporation of NMP molecules from the first solvation shell. In other words, NMP molecules and ions form a shell around a carbon nanotube, which does not evaporate (see fig. 5.12). This solvent-ion layer makes a tube more rigid, compared to a tube in pure NMP. This increased rigidity of carbon nanotubes results in a slightly higher most probable linear length of tubes and bundles (see table 5.1).

The study of microscopical aggregates, formed by NaI and NaBr (see section 5.3.2, page

## How NMP-NaI solution solvates CNT?

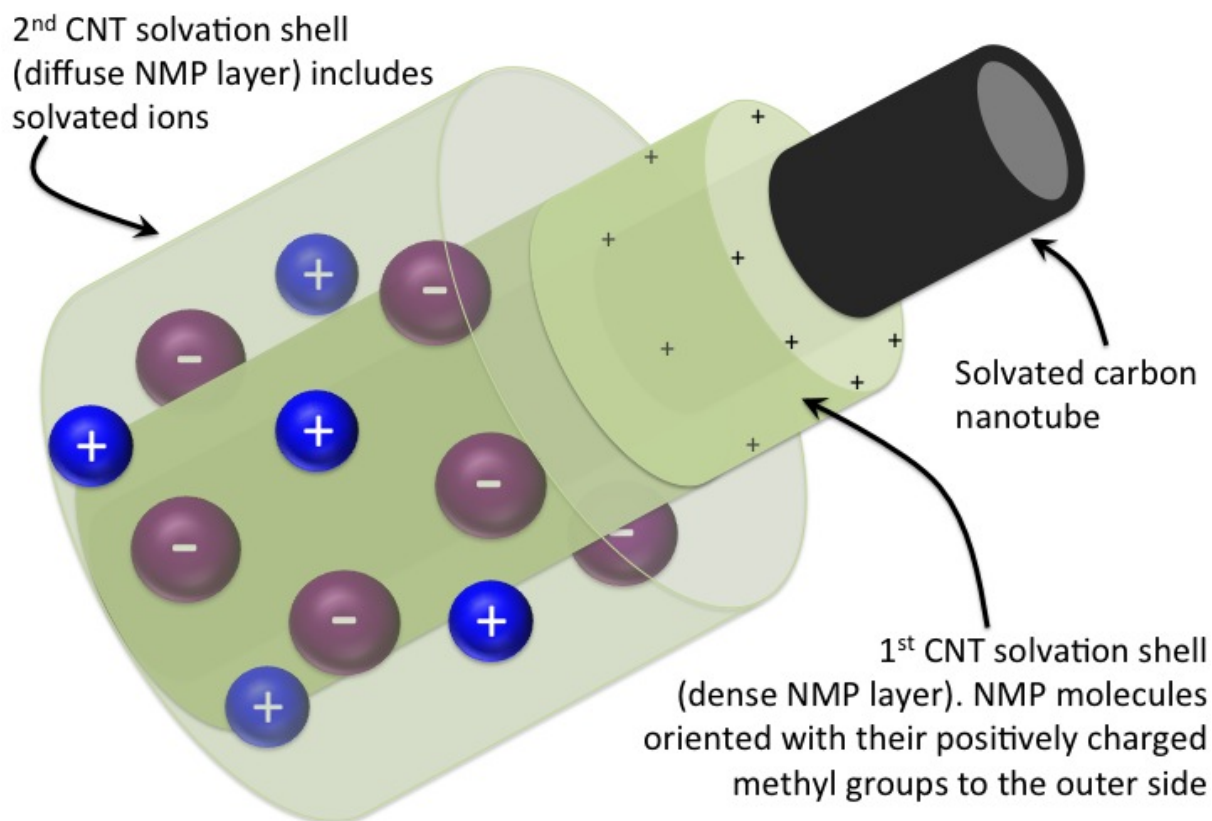


**Figure 5.12** – Pictorial illustration of the CNT-NMP-salt crystallosolvate after evaporation of bulk NMP. Salts do not evaporate with the solvent, which results in an "ionic shell" around a CNT and prevents evaporation of the NMP molecules from a CNT solvation shell.

121), shows that sodium bromide tends to form smoother films while sodium iodide tends to form clustered aggregates. This pattern of salt behaviour remains the same in the presence of carbon nanotubes. As one can see from the figure 5.10a sodium bromide forms a thick film on the grid holes even in the presence of carbon nanotubes, which are incorporated in the film and do not define its overall structure. This film is very similar to the sodium bromide film in the absence of the tubes (fig. 5.7). At higher magnification (fig. 5.10b) one can see that sodium bromide forms quite smooth thick coating around a carbon nanotube. Unlike sodium bromide, sodium iodide does not tend to form thick films. As one can see from figure 5.11a, carbon nanotubes form a frame, filled with discontinuous NaI film. At higher magnifications one can see the salt clustering on the nanotube (fig. 5.11b), similar to the salt clustering without the nanotube (fig. 5.8b). There are several possible explanations to the observed difference between sodium iodide and sodium bromide.

1. NMP changes its color from colorless to orange upon addition of sodium iodide. As we

know from the simulations [10], the iodide ion is strongly solvated. This allows us to suggest that its solvation shell is strong enough to withstand drying at normal conditions. In other words, iodine may form crystallo-solvates similar to  $\text{CuSO}_4 \cdot 5\text{H}_2\text{O}$ . This would mean, that the observable aggregates are large aggregates of NMP molecules and iodide ions. If the interactions between bromide ions and NMP molecules are weaker than similar interactions between iodide ions and NMP molecules, then it may explain the observed difference in microscopic behaviour of these two salts. This hypothesis may be checked by analysing the sodium iodide crystals, obtained from NMP solution, as well as by detailed computational study of energy of interactions between NMP and bromine.

2. The change of NMP color to orange upon dissolution of sodium iodide, also suggests, that a redox reaction may take place with iodine as one of the reaction products. In this case, an  $\text{I}_3^-$  ion may be formed, which would be detected by TEM as a very electron dense aggregate. To check this hypothesis we would need to analyse the sodium iodide solution for the presence of iodine.

## 5.4 Chapter conclusions

Controllable bundle formation of carbon nanotubes is important for many areas of applications, e.g. ultrafast photonics and biomedical applications [67, 70, 69]. Bottom-up approach to carbon nanotubes bundle construction, in principle, is more flexible and allows more fine-tuning, compared to top-down approach. Unfortunately, bottom up approach also represents significant challenges, including low solubility of carbon nanotubes, poor general purity of carbon nanotubes samples, and, particularly, poor chiral purity of carbon nanotubes samples. This is why it is important to study molecular mechanisms of bundle formation of carbon nanotubes.

Controllable precipitation of carbon nanotubes from a dispersion has a great potential to controllable bundle formation. As one may vary concentrations as well as composition of the precipitating agents, this approach allows fine control over the precipitation process. Unfortunately, studies in this field are insufficient.

Biochemistry and organic chemistry utilise ion effects to separate and purify proteins and some synthetic products. This approach was applied here to the NMP-based carbon nanotubes dispersion. Spectrophotometric titration helped one understand how salts (NaI and NaBr) affect overall concentration of carbon nanotubes. In both cases the concentration of dispersed carbon nanotubes was reduced upon addition of a salt. The concentration of the nanotubes in the

dispersions was decreasing with the increase of salt concentration in the dispersion. This effect was explained with a theory of solutions, proposed by Kirkwood and Buff. According to the theory, co-solvent/co-solute, depleted from the solvation interface, is capable of increasing free energy of the interface. As a result, the carbon nanotubes tend to aggregate with each other. Unfortunately, although spectrophotometric titration is a convenient tool to estimate concentration of carbon nanotubes, it gives little understanding of molecular level details of the formation of carbon nanotubes aggregates.

The van der Waals interactions govern formation of carbon nanotubes bundles. These interactions may be altered by a solvent or co-solvent/co-solute. As a result, molecular structure of bundles may be altered. There are two principal possibilities for a carbon nanotubes to form a bundle. The first possibility is formation of smooth ordered bundles, where carbon nanotubes are bonded by the van der Waals interactions and  $\pi - \pi$ -interactions over long distances. This happens when the process is thermodynamically controlled i.e., when a bundle is formed slowly. This may result in dense bundles, with no materials between the tubes, as well as bundles of smaller density, with surfactants, solvents, or ions between the tubes, depending on the bundling conditions. Second possibility is formation of disordered carbon nanotubes aggregates, where the tubes are bent. This is possible when the process is kinetically driven, i.e. the process is fast. In this case bending of carbon nanotubes should correspond roughly to their bending in solution.

The structure of the carbon nanotubes bundles, formed upon addition of salt to the NMP-based dispersions, was studied with a method of transmission electron microscopy. This microscopic study suggests several results. Firstly, salt was found in the direct proximity of carbon nanotubes. This finding seemingly contradicts to the conclusions, based on the Kirkwood-buff theory. However, a model was proposed, according to which ions may be attracted to the second solvation shells of carbon nanotubes, while being depleted from the first solvation shell. Secondly, carbon nanotubes were found to be incorporated into salt-NMP aggregates. These incorporated nanotubes are bent, which suggests that the precipitation process is kinetically controlled.

These findings may be further used in the areas of research, devoted to controlled carbon nanotubes bundle formation, environmental control of carbon nanomaterials and carbon nanotube doping with ions.

# 6

## Conclusions

1. Using a combination of experimental and computational tools, we studied the effects of ions on association processes of different solutes in polar solvents: effects of inorganic and organic ions on the stability of carbon nanotube dispersions in neat NMP, and inorganic ion effects on the stability of complexes of aromatic carboxylic acids with  $\alpha$ -cyclodextrin in water. To explain the observed effects of ions on association processes, we suggest mechanisms of specific and non-specific interactions of ions with these solutes, based on a balance between multiple interactions between ions, solvent and solute.
2. It was found experimentally that presence of sodium ions in a solution reduces effectively the binding constants of benzoic and nicotinic acids with  $\alpha$ -cyclodextrin. Unlike the presence of sodium, presence of potassium ions affects the binding constant only insignificantly within the error limits. To explain the difference in sodium and potassium effects, we propose a molecular mechanism, based on our molecular dynamics simulations. According to this mechanism, sodium ions form a stable ion pair with benzoate or nicotinate anions, which reduces effective concentration of the acid available for binding with  $\alpha$ -cyclodextrin.
3. We studied ion effects on the orientation of benzoic acid at liquid-vapour interface by molecular dynamics simulations and compared our results with direct X-ray photoemission spectroscopic results. We have found, that the nature of the ions affects dramatically the hydration pattern of benzoic acid. As a result of ion-induced changes in hydration pattern, the molecule changes its orientation at the interface as well as its affinity to the interface. Neutral molecules of benzoic acid tend to lie flat on the surface and show high surface affinity. Unlike neutral acid molecules, benzoates tend to stay perpendicular to the water-vapour interface. Surface affinity of benzoates is significantly reduced, compared to a

neutral acid.

4. We found experimentally (UV-vis-NIR absorbance and photoluminescence spectroscopy), that inorganic ions reduce the stability of carbon nanotube dispersions in N-methylpyrrolodone, which leads to aggregation of nanotubes into large bundles. Comparing our experimental findings with molecular dynamics simulations, we suggest a mechanism, which describes carbon nanotubes aggregation. It was shown, that inorganic ions avoid direct contact with the carbon nanotube, which leads to the formation of an ion depletion area around the nanotube. According to Kirkwood-Buff theory, formation of an ion depletion area around a carbon nanotube increases the free energy of nanotube surfaces in direct contact with a salt solution. Following the principle of minimum free energy, carbon nanotubes tend to reduce their surface areas in direct contact with the solution, forming large bundles, which can be easily separated from solution.
5. Small salt concentrations of inorganic salts are capable of precipitating carbon nanotubes from their dispersions. By means of transmission electron microscopy we confirmed that salt can be fully removed from the precipitate by simple washing out with water. This finding may be useful in nanotube bundle engineering as well as in development of environmental friendly techniques of carbon nanoparticles recycling.



# 7

## Future work

In this work an issue of ion effects on different association processes has been addressed. Studies of ion effects have attracted significant attention since the end of the 19<sup>th</sup> century. Still the detailed mechanism of how ions affect association processes in a solution is not clear. This work deepens the understanding of molecular level details of ions, acting at solvation interface and shows, that ion association with each other as well as with other species in a solution is capable of significant alteration of association process in a solution. However, there are some important issues which have not been addressed in this work or which arise from this work. These issues should be studied more in details in future.

1. **Ion interactions in NMP.** NMP is a popular solvent to disperse carbon nanotubes, because it is capable of dispersing significant amount of tubes without any surfactants. Even more, dispersions of carbon nanotubes in NMP show some signs of real solutions, e.g. they are stable in time. Unfortunately, the knowledge of how ions interact with each other and with other species in a solution are far from complete. Solubility, solvation energies, structure of solvation shells of the ions require a systematic investigation. This would help to rationalize the search of controllable bottom-up self aggregation of carbon nanotubes.
2. **Kinetics of CNT precipitation.** This work has shown, that bundle formation and aggregation of carbon nanotubes is a fast, kinetically controlled process. Despite massive research in the field of carbon nanotubes, studies of kinetics of carbon nanotubes bundling have been rare. On the other hand, organic chemistry suggests, that controlling the kinetics of a process may help in control of the products. This is why studies of kinetics and pathways of carbon nanotubes bundling and aggregation has a potential to increase the level of control of bundle formation.

3. **Spectral characteristics of CNTs in NMP.** The spectral characteristics of carbon nanotubes in aqueous dispersions have been studied in details. In fact, although the decomposition of carbon nanotubes is still a laborious and require some modelling, today it is possible to determine composition of carbon nanotubes sample, based on absorption spectrum of a dispersion. Unfortunately, this is not the case for non-aqueous dispersions. The data, obtained for aqueous dispersions of carbon nanotubes, unfortunately, can not be easily transferred to non-aqueous dispersions. The reason for this is that peak position changes with change of the solvent. These changes may be different for different chiralities of nanotubes. As a result, taking into account challenges of spectral decomposition of carbon nanotubes, at the moment it is impossible to decompose authentically an absorption spectrum of a carbon nanotubes dispersion. This is why it seems important to study structure of carbon nanotubes spectra in non-aqueous dispersions, including NMP-based dispersions.
  
4. **Effects of organic ions on carbon nanotubes dispersions.** This work has shown that inorganic ions, depleted from the carbon nanotubes surface, are capable of significant reduction of stability of NMP-base carbon nanotubes dispersion. Charged inorganic ions are depleted from the neutral CNT surface and prefer to stay solvated in the NMP bulk. This behaviour of ions may change significantly, if one changes inorganic ions to organic ones. Organic ions may be attracted to the carbon nanotubes surface, which, in turn, may enhance stability of carbon nanotubes dispersion. Moreover, affinity of inorganic ions may vary for different carbon nanotubes chiralities. This, in turn, may become a starting point of rationalization selective self-assembly of carbon nanotubes.

# 8

## Bibliography

- [1] W. Kunz, J. Henle, and B.W. Ninham. 'Zur Lehre Von Der Wirkung Der Salze' (About The Science Of The Effect Of Salts): Franz Hofmeister's Historical Papers. *Current Opinion In Colloid And Interface Science*, 9(1-2):19–37, 2004.
- [2] P. Jungwirth and D.J. Tobias. Molecular Structure Of Salt Solutions: A New View Of The Interface With Implications For Heterogeneous Atmospheric Chemistry. *The Journal Of Physical Chemistry B*, 105(43):10468–10472, 2001.
- [3] P. Jungwirth and D.J. Tobias. Specific ion effects at the air/water interface. *Chemical Reviews*, 106(4):1259–1281, 2006.
- [4] B. Minofar, P. Jungwirth, M. R. Das, W. Kunz, and S. Mahiuddin. Propensity Of Formate, Acetate, Benzoate, And Phenolate For The Aqueous Solution/Vapor Interface: Surface Tension Measurements And Molecular Dynamics Simulations. *The Journal Of Physical Chemistry C*, 111(23):8242–8247, 2007.
- [5] C. L. Henry and V. S. J. Craig. The link between ion specific bubble coalescence and Hofmeister effects is the partitioning of ions within the interface. *Langmuir*, 26(9):6478–6483, 2010.
- [6] J.K. Angarska, K.D. Tachev, P.A. Kralchevsky, A. Mehreteab, and G. Broze. Effects of counterions and co-ions on the drainage and stability of liquid films and foams. *Journal of Colloid and Interface Science*, 200(1):31 – 45, 1998.
- [7] S. Niyogi, S. Boukhalfa, S. B. Chikkannanavar, T. J. McDonald, M. J. Heben, and S. K. Doorn. Selective Aggregation Of Single-Walled Carbon Nanotubes Via Salt Addition. *The Journal Of The American Chemical Society*, 129(7):1898, 2007.

- [8] S. Niyogi, C. G. Densmore, and S. K. Doom. Electrolyte Tuning Of Surfactant Interfacial Behavior For Enhanced Density-Based Separations Of Single-Walled Carbon Nanotubes. *The Journal Of The American Chemical Society*, 131(3):1144–1153, 2009.
- [9] M. V. Fedorov, R. N. Arif, A. I. Frolov, M. Kolar, A. O. Romanova, and A. G. Rozhin. Salting Out In Organic Solvents: A New Route To Carbon Nanotube Bundle Engineering. *Physical Chemistry Chemical Physics*, 13(27):12399–12402, 2011.
- [10] A. I. Frolov, R. N. Arif, M. Kolar, A. O. Romanova, M. V. Fedorov, and A. G. Rozhin. Molecular Mechanisms Of Salt Effects On Carbon Nanotube Dispersions In An Organic Solvent (N-Methyl-2-Pyrrolidone). *Chemical Science*, 3(2):541–548, 2012.
- [11] I. V. Terekhova, A. O. Romanova, R. S. Kumeev, and M. V. Fedorov. Selective  $\text{Na}^+/\text{K}^+$  effects on the formation of  $\alpha$ -cyclodextrin complexes with aromatic carboxylic acids: Competition for the guest. *The Journal Of Physical Chemistry B*, 114(39):12607–12613, 2010.
- [12] M. G. Cacace, E. M. Landau, and J. J. Ramsden. The Hofmeister series: salt and solvent effects on interfacial phenomena. *Quarterly Reviews of Biophysics*, 30:241–277, 1997.
- [13] G. Marrucci and L. Nicodemo. Coalescence of gas bubbles in aqueous solutions of inorganic electrolytes. *Chemical Engineering Science*, 22(9):1257, 1967.
- [14] H.K. Christenson and V.V. Yaminsky. Solute effects on bubble coalescence. *Journal of Physical Chemistry*, 99(25):10420, 1995.
- [15] C. L. Henry, L. Parkinson, J. R. Ralston, and V. S. J. Craig. A mobile gas-water interface in electrolyte solutions. *Journal of Physical Chemistry C*, 112(39):15094–15097, 2008.
- [16] K. B. Lehman. Most recent investigations on the determination, preservative action and admissibility of the use of benzoic acid. *Science*, 35:577 – 585, 1912.
- [17] J. H. Long. The physiological significance of some substances used in the preservation of food. *Science*, 37(950):395–404, 1913.
- [18] S. Brul and P. Coote. Preservative agents in foods: Mode of action and microbial resistance mechanisms. *The International Journal Of Food Microbiology*, 50(1-2):1 – 17, 1999.
- [19] B. Nair. Final report on the safety assessment of benzyl alcohol, benzoic acid, and sodium benzoate. *The International Journal Of Toxicology*, 20:23 – 50, 2001.

- [20] I. Izumi, F.-R. F. Fan, and A. J. Bard. The heterogeneous photocatalytic decomposition of benzoic acid and adipic acid on platinized TiO<sub>2</sub> powder. the photo-kolbe decarboxylative route to the breakdown of the benzene ring and to the production to butane. *The Journal Of Physical Chemistry*, 85:218 – 223, 1981.
- [21] M. Tokunaga, J. F. Larrow, F. Kakiuchi, and E. N. Jacobsen. Asymmetric catalysis with water: Efficient kinetic resolution of terminal epoxides by means of catalytic hydrolysis. *Science*, 277(5328):936–938, 1997.
- [22] H. A. Chiong, Q.-N. Pham, and O. Daugulis. Two methods for direct ortho-arylation of benzoic acids. *The Journal Of The American Chemical Society*, 129(32):9879–9884, 2007.
- [23] L. W. Gibbons, V. Gonzalez, N. Gordon, and S. Grundy. The prevalence of side effects with regular and sustained-release nicotinic acid. *The American Journal Of Medicine*, 99(4):378 – 385, 1995.
- [24] R. H. Stern. The role of nicotinic acid metabolites in flushing and hepatotoxicity. *The Journal Of Clinical Lipidology*, 1(3):191 – 193, 2007.
- [25] D. S. Corrigan and M. J. Weaver. Adsorption and oxidation of benzoic acid, benzoate, and cyanate at gold and platinum electrodes as probed by potential-difference infrared spectroscopy. *Langmuir*, 4(3):599–606, 1988.
- [26] R. Méndez-Román and N. Cardona-Martínez. Relationship between the formation of surface species and catalyst deactivation during the gas-phase photocatalytic oxidation of toluene. *Catalysis Today*, 40(4):353 – 365, 1998.
- [27] V. Augugliaro, S. Coluccia, V. Loddo, L. Marchese, G. Martra, L. Palmisano, and M. Schiavello. Photocatalytic oxidation of gaseous toluene on anatase TiO<sub>2</sub> catalyst: Mechanistic aspects and ft-ir investigation. *Applied Catalysis B: Environmental*, 20(1):15 – 27, 1999.
- [28] T. M. Mccollom, J. S. Seewald, and B. R. T. Simoneit. Reactivity of monocyclic aromatic compounds under hydrothermal conditions. *Geochimica Et Cosmochimica Acta*, 65(3):455 – 468, 2001.
- [29] J. He, W. Ma, W. Song, J. Zhao, X. Qian, S. Zhang, and J. C. Yu. Photoreaction of aromatic compounds at [Alpha]-FeOOH/H<sub>2</sub>O interface in the presence of H<sub>2</sub>O<sub>2</sub>: Evidence for organic-goethite surface complex formation. *Water Research*, 39(1):119 – 128, 2005.

- [30] C. Verduyn, E. Postma, W. A. Scheffers, and J. P. Van Dijken. Effect of benzoic acid on metabolic fluxes in yeasts: A continuous-culture study on the regulation of respiration and alcoholic fermentation. *Yeast*, 8(7):501–517, 1992.
- [31] F. Natella, M. Nardini, M. Di Felice, and C. Scaccini. Benzoic and cinnamic acid derivatives as antioxidants: Structure-activity relation. *The Journal Of Agricultural And Food Chemistry*, 47(4):1453–1459, 1999.
- [32] Q. Chen and N. V. Richardson. Surface facetting induced by adsorbates. *Progress In Surface Science*, 73:59 – 77, 2003.
- [33] M. A. De Jesus, K. S. Giesfeldt, and M. J. Sepaniak. Factors affecting the sorption of model environmental pollutants onto silver polydimethylsiloxane nanocomposite raman substrates. *Applied Spectroscopy*, 58:1157–1164(8), 2004.
- [34] B. Han, Z. Li, and T. Wandlowski. Adsorption And Self-Assembly Of Aromatic Carboxylic Acids On Au/Electrolyte Interfaces. *Analytical And Bioanalytical Chemistry*, 388:121–129, 2007.
- [35] H. Ishikawa, T. Matsui, T. Ohtsu, K.-I. Watanabe, K. Matsumoto, and K. Matsumoto. pH Of Solution Greatly Affects Sorption Of Ionizable Compounds Into Low-Density Polyethylene Film. *The Journal Of Agricultural And Food Chemistry*, 53(9):3488–3492, 2005.
- [36] F. Montilla, E. Morallón, and J. L. Vázquez. Electrochemical behaviour of benzoic acid on platinum and gold electrodes. *Langmuir*, 19(24):10241–10246, 2003.
- [37] H. Oda, M. Kishida, and C. Yokokawa. Adsorption of benzoic acid and phenol from aqueous solution by activated carbons – effect of surface acidity. *Carbon*, 19(4):243 – 248, 1981.
- [38] J. K. Nicholson and I. D. Wilson. Understanding 'global' systems biology: Metabonomics and the continuum of metabolism. *Nature Reviews Drug Discovery*, 2:668 – 676, 2003.
- [39] Franz, H. A. Arafat, and N. G. Pinto. Effect of chemical surface heterogeneity on the adsorption mechanism of dissolved aromatics on activated carbon. *Carbon*, 38(13):1807 – 1819, 2000.
- [40] I. Kuzmenko, M. Kindermann, K. Kjaer, P. B. Howes, J. Als-Nielsen, R. Granek, G. V. Kiedrowski, L. Leiserowitz, and M. Lahav. Crystalline films of interdigitated structures

- formed via amidinium-carboxylate interactions at the air-water interface. *The Journal Of The American Chemical Society*, 123(16):3771–3783, 2001.
- [41] A. Natan, L. Kronik, H. Haick, and R. T. Tung. Electrostatic properties of ideal and non-ideal polar organic monolayers: Implications for electronic devices. *Advanced Materials*, 19(23):4103–4117, 2007.
- [42] G. L. Perlovich, T. V. Volkova, A. N. Manin, and A. Bauer-Brandl. Extent and mechanism of solvation and partitioning of isomers of substituted benzoic acids: A thermodynamic study in the solid state and in solution. *The Journal Of Pharmaceutical Sciences*, 97(9):3883–3896, 2008.
- [43] W. C. Qina, L. M. Sua, X. J. Zhanga, H. W. Qina, Y. Wena, Z. Guoa, F. T. Suna, L. X. Shenga, Y. H. Zhaoa, and M. H. Abraham. Toxicity of organic pollutants to seven aquatic organisms: Effect of polarity and ionization. *SAR And QSAR In Environmental Research*, 21:398 – 401, 2010.
- [44] T. Loftsson and D. Duchéne. Cyclodextrins and their pharmaceutical applications. *The International Journal Of Pharmaceutics*, 329(1 - 2):1 – 11, 2007.
- [45] T. Loftsson, P. Jarho, M. Másson, and T. Järvinen. Cyclodextrins in drug delivery. *Expert Opinion On Drug Delivery*, 2(2):335–351, 2005.
- [46] R. Challa, A. Ahuja, J. Ali, and R. Khar. Cyclodextrins in drug delivery: An updated review. *AAPS PharmSciTech*, 6:E329–E357, 2005.
- [47] S. Gould and R. C. Scott. 2-hydroxypropyl- $\beta$ -cyclodextrin (hp- $\beta$ -cd): A toxicology review. *Food and Chemical Toxicology*, 43(10):1451 – 1459, 2005.
- [48] B. Jagoda-Cwiklik, R. Vácha, M. Lund, M. Srebro, and P. Jungwirth. Ion pairing as a possible clue for discriminating between sodium and potassium in biological and other complex environments. *The Journal Of Physical Chemistry B*, 111(51):14077–14079, 2007.
- [49] M. V. Fedorov, J. M. Goodman, and S. Schumm. The effect of sodium chloride on poly-L-glutamate conformation. *Chemical Communications*, pages 896 – 898, 2009.
- [50] K.D. Collins. Charge density-dependent strength of hydration and biological structure. *Biophysical Journal*, 72(1):65 – 76, 1997.

- [51] N. Hennrich and F. Cramer. Inclusion compounds. XVIII.1 the catalysis of the fission of pyrophosphates by cyclodextrin. a model reaction for the mechanism of enzymes. *The Journal Of The American Chemical Society*, 87(5):1121–1126, 1965.
- [52] E. Norkus. Metal ion complexes with native cyclodextrins. An overview. *Journal of Inclusion Phenomena and Macrocyclic Chemistry*, 65:237–248, 2009.
- [53] Fullerene (chemical compound) – britannica online encyclopedia. <http://www.britannica.com/EBchecked/topic/221916/fullerene>. Accessed: 10 Jan 2013.
- [54] M. Monthieux and V. L. Kuznetsov. Who should be given the credit for the discovery of carbon nanotubes? *Carbon*, 44(9):1621–1623, 2006.
- [55] K. S. Novoselov, A. K. Geim, S. V. Morozov, D. Jiang, Y. Zhang, S. V. Dubonos, I. V. Grigorieva, and A. A. Firsov. Electric field effect in atomically thin carbon films. *Science*, 306(5696):666–669, 2004.
- [56] B. Peng, Y. Yao, and J. Zhang. Effect of the reynolds and richardson numbers on the growth of well-aligned ultralong single-walled carbon nanotubes. *The Journal Of Physical Chemistry C*, 114(30):12960–12965, 2010.
- [57] Q. Wen, R. Zhang, W. Qian, Y. Wang, P. Tan, J. Nie, and F. Wei. Growing 20 cm long dwnts/twnts at a rapid growth rate of 80-90 m/s. *Chemistry Of Materials*, 22(4):1294–1296, 2010.
- [58] X. Wang, Q. Li, J. Xie, Zh. Jin, J. Wang, Y. Li, K. Jiang, and Sh. Fan. Fabrication of ultralong and electrically uniform single-walled carbon nanotubes on clean substrates. *Nano Letters*, 9(9):3137–3141, 2009.
- [59] R. Jansen and P. Wallis. Manufacturing, characterization and use of single walled carbon nanotubes. *Material Matters*, 4(1):23–27.
- [60] V. N. Popov. Carbon nanotubes: properties and application. *Materials Science and Engineering: Reports*, 43(3):61 – 102, 2004.
- [61] R.H. Baughman, A.A. Zakhidov, and W.A. De Heer. Carbon Nanotubes – The Route Toward Applications. *Science*, 297(5582):787 – 792, 2002.



- [62] J. Chen, M.A. Hamon, H. Hu, Y.S. Chen, A.M. Rao, P.C. Eklund, and R.C. Haddon. Solution Properties Of Single-Walled Carbon Nanotubes. *Science*, 282(5386):95–98, 1998.
- [63] S. Giordani, S. D. Bergin, V. Nicolosi, S. Lebedkin, M. M. Kappes, W. J. Blau, and J. N. Coleman. Debundling Of Single-Walled Nanotubes By Dilution: Observation Of Large Populations Of Individual Nanotubes In Amide Solvent Dispersions. *The Journal Of Physical Chemistry B*, 110(32):15708–15718, 2006.
- [64] D. Mattia and Y. Gogotsi. Review: Static And Dynamic Behavior Of Liquids Inside Carbon Nanotubes. *Microfluidics And Nanofluidics*, 5(3):289–305, 2008.
- [65] Y. Hernandez, V. Nicolosi, M. Lotya, F. M. Blighe, Z. Sun, S. De, I. T. McGovern, B. Holland, M. Byrne, Y. K. Gun'ko, J. J. Boland, P. Niraj, G. Duesberg, S. Krishnamurthy, R. Goodhue, J. Hutchison, V. Scardaci, A. C. Ferrari, and J. N. Coleman. High-Yield Production Of Graphene By Liquid-Phase Exfoliation Of Graphite. *Nature Nanotechnology*, 3(9):563–568, 2008.
- [66] A. Hirsch. Functionalization Of Single-Walled Carbon Nanotubes. *Angewandte Chemie-International Edition*, 41(11):1853–1859, 2002.
- [67] T. Hasan, Z. Sun, F. Wang, F. Bonaccorso, P. Heng Tan, A. G. Rozhin, and A. C. Ferrari. Nanotube-Polymer Composites For Ultrafast Photonics. *Advanced Materials*, 21(38-39):3874–3899, 2009.
- [68] F. Bonaccorso, Z. Sun, T. Hasan, and A. C. Ferrari. Graphene Photonics And Optoelectronics. *Nature Photonics*, 4(9):611–622, 2010.
- [69] T. R. Fadel, E. R. Steenblock, E. Stern, N. Li, X. Wang, G. L. Haller, L. D. Pfefferle, and T. M. Fahmy. Enhanced Cellular Activation With Single Walled Carbon Nanotube Bundles Presenting Antibody Stimuli. *Nano Letters*, 8(7):2070–2076, 2008.
- [70] T. R. Fadel, M. Look, P. A. Staffier, G. L. Haller, L. D. Pfefferle, and T. M. Fahmy. Clustering Of Stimuli On Single-Walled Carbon Nanotube Bundles Enhances Cellular Activation. *Langmuir*, 26(8):5645–5654, 2010.
- [71] D. Tasis, N. Tagmatarchis, A. Bianco, and M. Prato. Chemistry Of Carbon Nanotubes. *Chemical Reviews*, 106(3):1105–1136, 2006.

- [72] J. J. Brege, C. Gallaway, and A. R. Barron. Fluorescence Quenching Of Single-Walled Carbon Nanotubes In Sdbs Surfactant Suspension By Metal Ions: Quenching Efficiency As A Function Of Metal And Nanotube Identity. *The Journal Of Physical Chemistry C*, 111(48):17812–17820, 2007.
- [73] D. Mac Kernan and W. J. Blau. Exploring The Mechanisms Of Carbon-Nanotube Dispersion Aggregation In A Highly Polar Solvent. *EPL*, 83(6), 2008.
- [74] K.D. Ausman, R. Piner, O. Lourie, R.S. Ruoff, and M. Korobov. Organic Solvent Dispersions Of Single-Walled Carbon Nanotubes: Toward Solutions Of Pristine Nanotubes. *The Journal Of Physical Chemistry B*, 104(38):8911–8915, 2000.
- [75] A. Domard, M. Rinaudo, and C. Terrassin. New Method For The Quaternization Of Chitosan. *The International Journal Of Biological Macromolecules*, 8(2):105–107, 1986.
- [76] W.E. Willy, D.R. Mckean, and B.A. Garcia. Conversion of alkylchlorides to bromides, selective reactions of mixed bromochloroalkanes, and halogen exchange. *Bulletin Of The Chemical Society Of Japan*, 49(7):1989–1995, 1976.
- [77] CRCnetBASE . Handbook of chemistry and physics. [www.hbcnetbase.com](http://www.hbcnetbase.com). Accessed: 23 Apr 2013.
- [78] M. V. Fedorov and A. A. Kornyshev. Unravelling the solvent response to neutral and charged solutes. *Molecular Physics*, 105(1):1–16, 2007.
- [79] G. Wypych, editor. *Handbook Of Solvents*. William Andrew Publishing And ChemTec Publishing, Toronto, New York, 2001.
- [80] J.-C. Bradley, C. Neylon, R. Guha, A. Williams, B. Hooker, A. Lang, T. Bohinski, D. Bulger, M. Federici, J. Hale, J. Mancinelli, K. Mirza, M. Moritz, D. Rein, C. Tchakounte, and H. Truong. *Open Notebook Science Challenge: Solubilities Of Organic Compounds In Organic Solvents* . Available From Nature Precedings, 2010. Accessed: 7 Dec 2012.
- [81] N.V. Avramenko, A.L. Mirakyan, and M.V. Korobov. Thermal behaviour of the crystals formed in the buckminsterfullerene-toluene, o-xylene and bromobenzene systems. *Thermochimica Acta*, 299(1-2):141–144, 1997.
- [82] F. Cramer, W. Saenger, and H.-Ch. Spatz. Inclusion compounds. XIX.1a The formation of inclusion compounds of  $\alpha$ -cyclodextrin in aqueous solutions. Thermodynamics and kinetics. *The Journal of the American Chemical Society*, 89(1):14–20, 1967.

- [83] Z.P. Yi, C.C. Zhao, Z.Z. Huang, H.L. Chen, and J.S. Yu. Investigation of buffer-cyclodextrin systems. *Physical Chemistry Chemical Physics*, 1(3):441–444, 1999.
- [84] The prospects for using of carbon nanomaterials as hydrogen storage systems. *International Journal of Hydrogen Energy*, 27(10):1063 – 1069, 2002.
- [85] M. V. Fedorov, J. M. Goodman, and S. Schumm. Solvent effects and hydration of a tripeptide in sodium halide aqueous solutions: An in silico study. *Physical Chemistry Chemical Physics*, 9(40):5423–5435, 2007.
- [86] S. D. Bergin, V. Nicolosi, Ph. V. Streich, S. Giordani, Zh. Sun and A. H. Windle, P. Ryan, N. P. P. Niraj, Zh.-T. T. Wang, L. Carpenter, W. J. Blau, J. J. Boland, J. P. Hamilton, and J. N. Coleman. Towards solutions of single-walled carbon nanotubes in common solvents. *Advanced Materials*, 20(10):1876–1881, 2008.
- [87] M. J. Hughes, D. Aherne, S. D. Bergin, A. O’Neill, P. V. Streich, J. P. Hamilton, and J. N. Coleman. Using solution thermodynamics to describe the dispersion of rod-like solutes: application to dispersions of carbon nanotubes in organic solvents. *Nanotechnology*, 23(26):265604, 2012.
- [88] S. Niyogi, S. Boukhalfa, S. B. Chikkannanavar, T. J. McDonald, M. J. Heben, and S. K. Doorn. Selective aggregation of single-walled carbon nanotubes via salt addition. *Journal of the American Chemical Society*, 129(7):1898–1899, 2007.
- [89] S. Niyogi, C. G. Densmore, and S. K. Doorn. Electrolyte tuning of surfactant interfacial behavior for enhanced density-based separations of single-walled carbon nanotubes. *Journal of the American Chemical Society*, 131(3):1144–1153, 2009.
- [90] D. Frenkel and B. Smit. *Understanding Molecular Simulation: From Algorithms to Applications*. Academic Press, 2001.
- [91] W. L. Jorgensen and J. D. Madura. Temperature and size dependence for Monte Carlo simulations of TIP4P water. *Molecular Physics: An International Journal At The Interface Between Chemistry And Physics*, 56:1381–1392, 1985.
- [92] W. L. Jorgensen, J. Chandrasekhar, J. D. Madura, R. W. Impey, and M. L. Klein. Comparison of simple potential functions for simulating liquid water. *Journal of Chemical Physics*, 79:926–935, 1983.

- [93] S. W. Rick and S. J. Stuart. *Potentials and Algorithms for Incorporating Polarizability in Computer Simulations*, pages 89–146. John Wiley & Sons, Inc., 2003.
- [94] Y.-C. Yeh and M. L. Berkowitz. Ewald summation for systems with slab geometry. *The Journal of Chemical Physics*, 111:3155–3162, 1999.
- [95] Y.-C. Yeh and M. L. Berkowitz. Effects of the polarizability and water density constraint on the structure of water near charged surfaces: Molecular dynamics simulations. *The Journal of Chemical Physics*, 112:10491–10495, 2000.
- [96] H. J. C. Berendsen, J. P. M. Postma, W. F. van Gunsteren, A. DiNola, and J. R. Haak. Molecular dynamics with coupling to an external bath. *The Journal of Chemical Physics*, 81(8):3684–3690, 1984.
- [97] Stephen C. Harvey, Robert K.-Z. Tan, and Thomas E. Cheatham. The flying ice cube: Velocity rescaling in molecular dynamics leads to violation of energy equipartition. *Journal of Computational Chemistry*, 19(7):726 – 740, 1998.
- [98] D. Van Der Spoel, E. Lindahl, B. Hess, G. Groenhof, A. E. Mark, and H.J. Berendsen. Gromacs: Fast, flexible and free. *Journal of Computer Chemistry*, 26:1701–1718, 2005.
- [99] K.J. Bowers, E. Chow, H. Xu, R.O. Dror, M.P. Eastwood, B.A. Gregersen, J.L. Klepeis, I. Kolossvary, M.A. Moraes, F.D. Sacerdoti, J.K. Salmon, Y. Shan, and D.E. Shaw. Scalable Algorithms For Molecular Dynamics Simulations On Commodity Clusters. In *2006 Proceedings Supercomputing 2006*, page 13 Pp., Los Alamitos, CA, USA, 2006. IEEE Comput. Soc.; ACM Sigarch, IEEE Comput. Soc. SC 2006 Proceedings Supercomputing 2006, 11-17 November 2006, Tampa, FL, USA.
- [100] Z. Guo, U. Mohanty, J. Noehre, T. K. Sawyer, W. Sherman, and G. Krilov. Probing the  $\alpha$ -helical structural stability of stapled p53 peptides: Molecular dynamics simulations and analysis. *Chemical Biology & Drug Design*, 75(4):348–359, 2010.
- [101] D. Shivakumar, J. Williams, Y. Wu, W. Damm, J. Shelley, and W. Sherman. Prediction of absolute solvation free energies using molecular dynamics free energy perturbation and the OPLS force field. *Journal of Chemical Theory and Computation*, 6(5):1509–1519, 2010.
- [102] S. Plimpton. Fast parallel algorithms for short-range molecular dynamics. *Journal of Computational Physics*, 117(1):1–19, 1995.

- [103] LAMMPS. <http://lammmps.sandia.gov>. Accessed: 30 Apr 2013.
- [104] AMBER. <http://ambermd.org/>. Accessed: 21 May 2013.
- [105] T. L. Hill. *Statistical Mechanics: Principles And Selected Applications*. Dover Publications, 1987.
- [106] I. Terekhova, R. Kumeev, and G. Alper. NMR and calorimetric study on binding ability of cyclodextrins to isomeric pyridinecarboxylic acids in aqueous solution. *The Journal Of Inclusion Phenomena And Macrocyclic Chemistry*, 62:363–370, 2008.
- [107] I. Terekhova and N. Obukhova. Thermodynamics of nicotinic acid interactions with some saccharides. *The Journal Of Solution Chemistry*, 34:1273–1282, 2005.
- [108] I. Terekhova, R. De Lisi, G.Lazzara, S. Milioto, and N. Muratore. Volume and heat capacity studies to evidence interactions between cyclodextrins and nicotinic acid in water. *The Journal Of Thermal Analysis And Calorimetry*, 92:285–290, 2008.
- [109] I. V. Terekhova. *Selective Interactions Of Native And Modified Cyclodextrins With Some B-Vitamins In Aqueous Solution. Thermodynamic Study*, pages 93 – 115. Nova Science Publishers, New York, 2008.
- [110] M. V. Rekharsky and Y. Inoue. Complexation thermodynamics of cyclodextrins. *Chemical Reviews*, 98(5):1875–1918, 1998.
- [111] R. J. Bergeron, M. A. Channing, and K. A. Mcgovern. Dependence of cycloamylose-substrate binding on charge. *The Journal Of The American Chemical Society*, 100(9):2878–2883, 1978.
- [112] S. Simova and H.-J. Schneider. NMR analyses of cyclodextrin complexes with substituted benzoic acids and benzoate anions. *Journal of the Chemical Society, Perkin Transactions 2*, pages 1717–1722, 2000.
- [113] K. A. Connors, S.-F. Lin, and A. B. Wong. Potentiometric study of molecular complexes of weak acids and bases applied to complexes of  $\alpha$ -cyclodextrin with para-substituted benzoic acids. *The Journal Of Pharmaceutical Sciences*, 71(2):217–222, 1982.
- [114] K. Harata. Structure of cyclodextrin complex. 5. Crystal-structures of alpha-cyclodextrin complexes with para-nitrophenol and para-hydroxybenzoic acid. *Bulletin Of The Chemical Society Of Japan*, 50:1416 – 1424, 1977.

- [115] R. I. Gelb, L. M. Schwartz, B. Cardelino, and D. A. Laufer. The complexation chemistry of cycloamyloses: Equilibrium constants by novel spectrophotometric methods. *Analytical Biochemistry*, 103(2):362 – 368, 1980.
- [116] R. L. Vanetten, J. F. Sebastian, G.A. Clowes, and M. L. Bender. Acceleration of phenyl ester cleavage by cycloamyloses. a model for enzymic specificity. *The Journal Of The American Chemical Society*, 89(13):3242–3253, 1967.
- [117] P. G. Laye, S. B. Warrington, Thermal Methods Group, G. R. Heal, D. M. Price, and R. Wilson. *Principles of Thermal Analysis and Calorimetry*. RSC Paperbacks. The Royal Society of Chemistry, 2002.
- [118] S. Hüfner. *Photoelectron Spectroscopy*. Springer-Verlag Berlin Heidelberg, 1995.
- [119] A. Nilsson. Applications of core level spectroscopy to adsorbates. *Journal of Electron Spectroscopy and Related Phenomena*, 126:3–42, 2002.
- [120] M. Faubel, B. Steiner, and J. P. Toennies. Applications of core level spectroscopy to adsorbates. *The Journal Of Chemical Physics*, 106:9013–9031, 1997.
- [121] N. Ottosson, A. Romanova, J. Söderström, O. Björneholm, G. Öhrwall, and M. V. Fedorov. Molecular sinkers: X-ray photoemission and atomistic simulations of benzoic acid and benzoate at the aqueous Solution/Vapor interface. *The Journal of Physical Chemistry B*, 116(43):13017–13023, 2012.
- [122] N. Ottosson, M. Faubel, S. E. Bradforth, P. Jungwirth, and B. Winter. Photoelectron spectroscopy of liquid water and aqueous solution: Electron effective attenuation lengths and emission-angle anisotropy. *Journal of Electron Spectroscopy and Related Phenomena*, 177:60–70, 2010.
- [123] S. Lunell, S. Svensson, P.-A. Malmqvist, U. Gelius, E. Basilier, and K. Siegbahn. A theoretical and experimental study of the carbon 1s shake-up structure of benzene. *Chemical Physics Letters*, 54:420–424, 1978.
- [124] M. P. Keane, A. N. De Brito, N. Correia, S. Svensson, and S. Lunell. Experimental and theoretical study of the N1s and C1s shake-up satellites in pyridine and aniline. *Chemical Physics*, 155:379, 1991.

- [125] S. M. Bachilo, M. S. Strano, C. Kittrell, R. H. Hauge, R. E. Smalley, and B. R. Weisman. Structure-assigned optical spectra of single-walled carbon nanotubes. *Science*, 298(5602):2361–2366, 2002.
- [126] N. Nair, M. L. Usrey, W.-J. Kim, R. D. Braatz, and M. S. Strano. Estimation of the (n,m) concentration distribution of single-walled carbon nanotubes from photoabsorption spectra. *Analytical Chemistry*, 78(22):7689–7696, 2006.
- [127] Y. Tian, H. Jiang, J. von Pfaler, Z. Zhu, A. G. Nasibulin, T. Nikitin, B. Aitchison, L. Khriachtchev, D. P. Brown, and E. I. Kauppinen. Analysis of the Size Distribution of Single-Walled Carbon Nanotubes Using Optical Absorption Spectroscopy. *Journal of Physical Chemistry Letters*, 1(7):1143–1148, 2010.
- [128] A. V. Naumov, S. Ghosh, D. A. Tsyboulski, S. M. Bachilo, and R. B. Weisman. Analyzing absorption backgrounds in single-walled carbon nanotube spectra. *ACS Nano*, 5(3):1639–1648, 2011.
- [129] M. E. Itkis, D. E. Perea, S. Niyogi, S. M. Rickard, M. A. Hamon, H. Hu, B. Zhao, and R. C. Haddon. Purity evaluation of as-prepared single-walled carbon nanotube soot by use of solution-phase near-IR spectroscopy. *Nano Letters*, 3(3):309–314, 2003.
- [130] K. L. Day and D. R. Huffman. Measured extinction efficiency of graphite smoke in the region 1200 – 6000 Å. *Nature*, 243(125):50–51, 1973.
- [131] Y. Zhang and L. Zheng. Towards chirality-pure carbon nanotubes. *Nanoscale*, 2(10):1919–1929, 2010.
- [132] H. Ozawa, T. Fujigaya, Y. Niidome, N. Hotta, M. Fujiki, and N. Nakashima. Rational concept to Recognize/Extract single-walled carbon nanotubes with a specific chirality. *The Journal of the American Chemical Society*, 133(8):2651–2657, 2011.
- [133] L. Zhang, X. Tu, K. Welsher, X. Wang, M. Zheng, and H. Dai. Optical characterizations and electronic devices of nearly pure (10,5) single-walled carbon nanotubes. *the Journal of the American Chemical Society*, 131(7):2454–2455, 2009.
- [134] L. Oudjedi, A. N. G. Parra-Vasquez, A. G. Godin, L. Cognet, and B. Lounis. Metrological investigation of the (6,5) carbon nanotube absorption cross section. *The Journal of Physical Chemistry Letters*, 4(9):1460–1464, 2013.

- [135] S. Ohmori, T. Saito, M. Tange, B. Shukla, T. Okazaki, M. Yumura, and S. Iijima. Fundamental importance of background analysis in precise characterization of single-walled carbon nanotubes by optical absorption spectroscopy. *The Journal of Physical Chemistry C*, 114(22):10077–10081, 2010.
- [136] D. B. Williams and C. B. Carter. *Transmission Electron Microscopy. A textbook for materials science*. Springer, 2009.
- [137] J. Ayache. Transmission electron microscopy (TEM): sample preparation guide. [http://temsamprep.in2p3.fr/guides\\_methodologiques.php?lang=eng](http://temsamprep.in2p3.fr/guides_methodologiques.php?lang=eng). Accessed: 24 Jul 2012.
- [138] J. Ayache, L. Beaunier, J. Boumendil, G. Ehret, and D. Laub. *Sample Preparation Handbook for Transmission Electron Microscopy. Vol. 1: Methodology; Vol. 2: Techniques*. Springer, 2011.
- [139] P.J.F. Harris. Carbonaceous contaminants on support films for transmission electron microscopy. *Carbon*, 39(6):909–913, 2001.
- [140] R.F. Klie, D. Ciuparu, L. Pfefferle, and Y. Zhu. Multi-walled carbon nanotubes on amorphous carbon films. *Carbon*, 42(10):1953–1957, 2004.
- [141] C. M. McGilvery, A. E. Goode, M. S. P. Shaffer, and D. W. McComb. Contamination of holey/lacey carbon films in STEM. *Micron*, 43(2-3):450–455, 2012.
- [142] J. Buchner and T. Kiefhaber. *Alcohol- And Salt-Induced Partially Folded Intermediates*, pages 884 – 915. Wiley-VCH Verlag Gmbh, Weinheim, 2008.
- [143] J.-Y. Suh, Ch. Tang, and G. M. Clore. Role of electrostatic interactions in transient encounter complexes in protein-protein association investigated by paramagnetic relaxation enhancement. *The Journal Of The American Chemical Society*, 129(43):12954 – 12955, 2007.
- [144] S. Milev, H. R. Bosshard, and I. Jelesarov. Enthalpic and entropic effects of salt and polyol osmolytes on site-specific protein-DNA association: The integrase Tn916-DNA complex. *Biochemistry*, 44(1):285 – 293, 2005.
- [145] M. Sitohy, J.-M. Chobert, and T. Haertle. Study of the formation of complexes between DNA and esterified dairy proteins. *International Dairy Journal*, 11(11-12):873 – 883, 2001.



- [146] Y. Goto and Y. Hagihara. Mechanism of the conformational transition of melittin. *Biochemistry*, 31(3):732–738, 1992.
- [147] Y. Goto and A. L. Fink. Acid-induced folding of heme proteins. *Methods In Enzymology*, 232:3–15, 1994.
- [148] T. Matsuda and M. Annaka. Salt effect on complex formation of neutral/polyelectrolyte block copolymers and oppositely charged surfactants. *Langmuir*, 24(11):5707–5713, 2008.
- [149] X. Wang, Y. Li, J. Li, J. Wang, Y. Wang, Z. Guo, and H. Yan. Salt effect on the complex formation between polyelectrolyte and oppositely charged surfactant in aqueous solution. *The Journal Of Physical Chemistry B*, 109(21):10807–10812, 2005.
- [150] M. W. Mahoney and W. L. Jorgensen. A five-site model for liquid water and the reproduction of the density anomaly by rigid, nonpolarizable potential functions. *The Journal Of Chemical Physics*, 112(20):8910–8922, 2000.
- [151] W. L. Jorgensen, D. S. Maxwell, and J. Tirado-Rives. Development and testing of the OPLS all-atom force field on conformational energetics and properties of organic liquids. *The Journal Of American Chemical Society*, 118:11225–11236, 1996.
- [152] W. Damm, A. Frontera, J. Tirado-Rives, and W. L. Jorgensen. OPLS all-atom force field for carbohydrates. *Journal of Computer Chemistry*, 18:1955–1970, 1997.
- [153] W. L. Jorgensen and N. A. McDonald. Development of an all-atom force field for heterocycles. Properties of liquid pyridine and diazenes. *Journal of Molecular Structure*, 424:145–155, 1998.
- [154] N. A. McDonald and W. L. Jorgensen. Development of an all-atom force field for heterocycles. Properties of liquid pyrrole, furan, diazoles, and oxazoles. *The Journal Of Physical Chemistry*, 102:8049–8059, 1998.
- [155] R. C. Rizzo and W. L. Jorgensen. OPLS all-atom model for amines: Resolution of the amine hydration problem. *The Journal Of American Chemical Society*, 121:4827–4836, 1999.
- [156] E. K. Watkins and W. L. Jorgensen. Perfluoroalkanes: Conformational analysis and liquid-state properties from *Ab Initio* and Monte Carlo calculations. *The Journal Of Physical Chemistry*, 105:4118–4125, 2001.

- [157] J. Tirado-Rives G. A. Kaminski, R. A. Friesner and W. L. Jorgensen. Evaluation and reparametrization of the OPLS-AA force field for proteins via comparison with accurate quantum chemical calculations on peptides. *The Journal Of Physical Chemistry B*, 105:6474–6487, 2001.
- [158] R. A. Friesner M. P. Jacobson, G. A. Kaminski and C. S. Rapp. Force field validation using protein side chain prediction. *The Journal Of Physical Chemistry B*, 106:11673–11680, 2002.
- [159] U. Essmann, L. Perera, M. L. Berkowitz, T. Darden, H. Lee, and L. G. Pedersen. A smooth particle mesh ewald method. *The Journal Of Chemical Physics*, 103:8577–8593, 1995.
- [160] D. A. Fletcher, R. F. Mcmeeking, and D. Parkin. The United Kingdom Chemical Database Service. *The Journal Of Chemical Information And Computer Sciences*, 36(4):746–749, 1996.
- [161] W. Humphrey, A. Dalke, and K. Schulten. VMD: Visual Molecular Dynamics. *The Journal Of Molecular Graphics*, 14(1):33–38, 1996.
- [162] M. V. Fedorov, J. M. Goodman, and S. Schumm. To switch or not to switch: The effects of potassium and sodium ions on  $\alpha$ -poly-l-glutamate conformations in aqueous solutions. *The Journal Of The American Chemical Society*, 131(31):10854 – 10856, 2009.
- [163] E. F. Aziz, N. Ottosson, S. Eisebitt, W. Eberhardt, B. Jagoda-Cwiklik, R. Vácha, P. Jungwirth, and B. Winter. Cation-specific interactions with carboxylate in amino acid and acetate aqueous solutions: X-ray absorption and ab initio calculations. *The Journal Of Physical Chemistry B*, 112(40):12567–12570, 2008.
- [164] P.B. Petersen and R.J. Saykally. Adsorption Of Ions To The Surface Of Dilute Electrolyte Solutions: The Jones-Ray Effect Revisited. *The Journal Of The American Chemical Society*, 127(44):15446–15452, 2005.
- [165] J. S. Uejio, C. P. Schwartz, A. M. Duffin, W. S. Drisdell, R. C. Cohen, and R. J. Saykally. Characterization of selective binding of alkali cations with carboxylate by X-ray absorption spectroscopy of liquid microjets. *Proceedings Of The National Academy Of Sciences*, 105(19):6809–6812, 2008.

- [166] N. Vlachy, B. Jagoda-Cwiklik, R. Vácha, D. Touraud, P. Jungwirth, and W. Kunz. Hofmeister series and specific interactions of charged headgroups with aqueous ions. *Advances In Colloid And Interface Science*, 146(1-2):42 – 47, 2009.
- [167] L. Vrbka, J. Vondrá, B. Jagoda-Cwiklik, R.T. Vácha, and P. Jungwirth. Quantification and rationalization of the higher affinity of sodium over potassium to protein surfaces. *Proceedings Of The National Academy Of Sciences*, 103(42):15440–15444, 2006.
- [168] D. M. Sand and Hermann Schlenk. Acylated cyclodextrins as polar stationary phases for gas-liquid chromatography. *Analytical Chemistry*, 33(11):1624–1625, 1961.
- [169] R. Breslow. Hydrophobic effects on simple organic reactions in water. *Accounts Of Chemical Research*, 24(6):159–164, 1991.
- [170] S. Sau, B. Solanki, R. Orprecio, J. Van Stam, and C.H. Evans. Higher-Order Cyclodextrin Complexes: The Naphthalene System. *The Journal Of Inclusion Phenomena And Macrocyclic Chemistry*, 48(3-4):173–180, 2004.
- [171] M. Al Omari, M. Zughul, J. Davies, and A. Badwan. Effect of buffer species on the complexation of basic drug terfenadine with  $\beta$ -cyclodextrin. *The Journal Of Inclusion Phenomena And Macrocyclic Chemistry*, 58:227–235, 2007.
- [172] J.F. Wojcik and R.P. Rohrbach. Small Anion Binding To Cycloamylose - Equilibrium-Constants. *The Journal Of Physical Chemistry*, 79(21):2251–2253, 1975.
- [173] J.N. Spencer, Q. He, X.M. Ke, Z.Q. Wu, and E. Fetter. Complexation Of Inorganic Anions And Small Organic Molecules With Alpha-Cyclodextrin In Water. *The Journal Of Solution Chemistry*, 27(11):1009–1019, 1998.
- [174] R.I. Gelb, L.M. Schwartz, C.T. Murray, and D.A. Laufer. Complexation of 4-biphenylcarboxylate by cyclohexaamylose - conductometric and C-13 nuclear magnetic-resonance spectrometric analysis. *The Journal Of The American Chemical Society*, 100(11):3553–3559, 1978.
- [175] R.P. Rohrbach, L.J. Rodriguez, E.M. Eyring, and J.F. Wojcik. Equilibrium And Kinetic Investigation Of Salt-Cycloamylose Complexes. *The Journal Of Physical Chemistry*, 81(10):944–948, 1977.

- [176] S. Koneshan and J.C. Rasaiah. Computer Simulation Studies Of Aqueous Sodium Chloride Solutions At 298 K And 683 K. *The Journal Of Chemical Physics*, 113(18):8125–8137, 2000.
- [177] E.F. Aziz, A. Zimina, M. Freiwald, S. Eisebitt, and W. Eberhardt. Molecular And Electronic Structure In NaCl Electrolytes Of Varying Concentration: Identification Of Spectral Fingerprints. *The Journal Of Chemical Physics*, 124(11), 2006.
- [178] E. F. Aziz, S. Eisebitt, W. Eberhardt, L. Cwiklik, and P. Jungwirth. Existence Of Oriented Ion-Hydroxide Clusters In Concentrated Aqueous NaCl Solution At pH 13. *The Journal Of Physical Chemistry B*, 112(4):1262–1266, 2008.
- [179] P. Fini, M. Castagnolo, L. Catucci, P. Cosma, and A. Agostiano. The Effects Of Increasing NaCl Concentration On The Stability Of Inclusion Complexes In Aqueous Solution. *The Journal Of Thermal Analysis And Calorimetry*, 73(2):653–659, 2003. Phandta 6 Symposium, Monte Verita, Switzerland, 2002.
- [180] D. J. Tannor., B. Marten, R. Murphy, R. A. Friesner, D. Sitkoff, A. Nicholls, B. Honig, M. Ringnalda, and W. A. Goddard. Accurate first principles calculation of molecular charge distributions and solvation energies from ab initio quantum mechanics and continuum dielectric theory. *The Journal of the American Chemical Society*, 116(26):11875–11882, 1994.
- [181] B. Marten, K. Kim, C. Cortis, R. A. Friesner, R. B. Murphy, M. N. Ringnalda, D. Sitkoff, and B. Honig. New model for calculation of solvation free energies: Correction of self-consistent reaction field continuum dielectric theory for short-range hydrogen-bonding effects. *The Journal of Physical Chemistry*, 100(28):11775–11788, 1996.
- [182] A. Pohorille and I. Benjamin. Molecular dynamics of phenol at the liquid-vapour interface of water. *Journal of Physical Chemistry*, 94:5599–5605, 1991.
- [183] A. Pohorille and I. Benjamin. Structure and energetics of model amphiphilic molecules at the water liquid-vapor interface. *Journal of Physical Chemistry*, 97:2664–2670, 1993.
- [184] I. Benjamin. Chemical reactions and solvation at liquid interfaces: A microscopic perspective. *Chemical Reviews*, 96:1449–1475, 1996.

- [185] R. Vacha, L. Cwiklik, J. Rezac, P. Hobza, P. Jungwirth, K. Valsaraj, S. Bahr, and V. Kempter. Adsorption of hydrocarbons and ozone at environmental aqueous surfaces. *Journal of Physical Chemistry A*, 112:4942–4950, 2008.
- [186] H. Bekker. *Photoelectron Spectroscopy*. World Scientific, 1993.
- [187] H. J. C. Berendsen, D. Van Der Spoel, and R. Van Drunen. Gromacs: A message-passing parallel molecular dynamics implementation. *Computer Physics Communications*, 91:43–56, 1995.
- [188] E. Lindahl, B. Hess, B., and D. Van Der Spoel. Gromacs 3.0: A package for molecular simulation and trajectory analysis. *Journal of Molecular Modelling*, 7:306–317, 2001.
- [189] B. Hess, C. Kutzner, D. Van Der Spoel, and E. Lindahl. Gromacs 4: Algorithms for highly efficient, load-balanced, and scalable molecular simulation. *Journal of Chemical Theory and Computation*, 435:435–447, 2005.
- [190] K. P. Jensen and W.L. Jorgensen. Halide, ammonium, and alkali metal ion parameters for modeling aqueous solutions. *Journal of Chemical Theory and Computation*, 2:1499–1509, 2006.
- [191] R. Vácha, L. Cwiklik, J. Rezac, P. Hobza, P. Jungwirth, K. Valsaraj, S. Bahr, and V. Kempter. Adsorption of aromatic hydrocarbons and ozone at environmental aqueous surfaces. *The Journal of Physical Chemistry A*, 112(22):4942–4950, 2008.
- [192] G. L. Perlovich, S. V. Kurkov, A. N. Kinchin, and A. Bauer-Brandl. Thermodynamics of solutions III: comparison of the solvation of (+)-naproxen with other nsoids. *European Journal of Pharmaceutics and Biopharmaceutics*, 57:411–420, 2004.
- [193] R. Vacha, P. Jungwirth, and J. Chen. Adsorption of polycyclic aromatic hydrocarbons at the air-water interface: Molecular dynamics simulations and experimental atmospheric observations. *Physical Chemistry Chemical Physics*, 8:4461 – 4467, 2006.
- [194] Y. Marcus. *Ion Properties*. Marcel Dekker, Inc, 1997.
- [195] M. Mucha, T. Frigato, L.M. Levering, H.C. Allen, D.J. Tobias, L.X. Dang, and P. Jungwirth. Unified Molecular Picture Of The Surfaces Of Aqueous Acid, Base, And Salt Solutions. *The Journal Of Physical Chemistry B*, 109(16):7617–7623, 2005.

- [196] S. Park and R. S. Ruoff. Chemical Methods For The Production Of Graphenes. *Nature Nanotechnology*, 5(4):309, 2010.
- [197] S. Stankovich, D.A. Dikin, G. H. B. Dommett, K. M. Kohlhaas, E. J. Zimney, E. A. Stach, R. D. Piner, S. T. Nguyen, and R. S. Ruoff. Graphene-Based Composite Materials. *Nature*, 442(7100):282–286, 2006.
- [198] T. Ramanathan, A. A. Abdala, S. Stankovich, D. A. Dikin, M. Herrera-Alonso, R. D. Piner, D. H. Adamson, H. C. Schniepp, X. Chen, R. S. Ruoff, S. T. Nguyen, I. A. Aksay, R. K. Prudhomme, and L. C. Brinson. Functionalized Graphene Sheets For Polymer Nanocomposites. *Nature Nanotechnology*, 3(6):327–331, 2008.
- [199] W.J. Blau and A.J. Fleming. Materials Science - Designer Nanotubes By Molecular Self-Assembly. *Science*, 304(5676):1457–1458, 2004.
- [200] D. H. Marsh, G. A. Rance, M. H. Zaka, R. J. Whitby, and A. N. Khlobystov. Comparison of the stability of multiwalled carbon nanotube dispersions in water. *Physical Chemistry Chemical Physics*, 9:5490–5496, 2007.
- [201] NMP physical properties. [http://www2.basf.us/diols/bcdiolsnmp\\_properties.html](http://www2.basf.us/diols/bcdiolsnmp_properties.html). Accessed: 24 September 2012.
- [202] L. Duclaux. Review of the doping of carbon nanotubes (multiwalled and single-walled). *Carbon*, 40(10):1751–1764, 2002.
- [203] Z. Liu, N. Bajwa, L. Ci, S.H. Lee, S. Kar, P.M. Ajayan, and J. Q Lu. Densification of carbon nanotube bundles for interconnect application. In *International Interconnect Technology Conference, IEEE 2007*, pages 201–203, 2007.
- [204] J. G. Kirkwood and F. P. Buff. The statistical mechanical theory of solutions. I. *The Journal Of Chemical Physics*, 19(6):774–777, 1951.
- [205] J. M. Schurr, D. P. Rangel, and S. R. Aragon. A contribution to the theory of preferential interaction coefficients. *Biophysical Journal*, 89(4):2258 – 2276, 2005.
- [206] Zh. Sun, I. O’Connor, S. D. Bergin, and J. N. Coleman. Effects of ambient conditions on Solvent-Nanotube dispersions: Exposure to water and temperature variation. *The Journal of Physical Chemistry C*, 113(4):1260–1266, 2009.

- [207] M.J. O'Connell, S.M. Bachilo, C.B. Huffman, V.C. Moore, M.S. Strano, E.H. Haroz, K.L. Rialon, P.J. Boul, W.H. Noon, C. Kittrell, J.P. Ma, R.H. Hauge, R.B. Weisman, and R.E. Smalley. Band Gap Fluorescence From Individual Single-Walled Carbon Nanotubes. *Science*, 297(5581):593–596, 2002.
- [208] P. H. Tan, A. G. Rozhin, T. Hasan, P. Hu, V. Scardaci, W. I. Milne, and A. C. Ferrari. Photoluminescence Spectroscopy Of Carbon Nanotube Bundles: Evidence For Exciton Energy Transfer. *Physical Review Letters*, 99(13), 2007.
- [209] L. Lacerda, G. Pastorin, W. Wu, M. Prato, A. Bianco, and K. Kostarelos. Luminescence Of Functionalized Carbon Nanotubes As A Tool To Monitor Bundle Formation And Dissociation In Water: The Effect Of Plasmid-DNA Complexation. *Advanced Functional Materials*, 16(14):1839–1846, 2006.
- [210] V.A. Parsegian, R.P. Rand, and D.C. Rau. Osmotic Stress, Crowding, Preferential Hydration, And Binding: A Comparison Of Perspectives. *Proceedings Of The National Academy Of Sciences Of The United States Of America*, 97(8):3987–3992, 2000.
- [211] K.D. Collins and M.W. Washabaugh. The Hofmeister Effect And The Behavior Of Water At Interfaces. *Quarterly Reviews Of Biophysics*, 18(4):323–422, 1985.
- [212] J. Porath, L. Sundberg, N. Fornsted, and I. Olsson. Salting-Out In Amphiphilic Gels As A New Approach To Hydrophobic Adsorption. *Nature*, 245(5426):465–466, 1973.
- [213] S.A. Miller, D.D. Dykes, and H.F. Polesky. A Simple Salting Out Procedure For Extracting DNA From Human Nucleated Cells. *Nucleic Acids Research*, 16(3):1215, 1988.
- [214] Y. Marcus. *Ion Solvation*. John Wiley & Sons, 1985.
- [215] A. I. Frolov, A. G. Rozhin, and M. V. Fedorov. Ion Interactions With The Carbon Nanotube Surface In Aqueous Solutions: Understanding The Molecular Mechanisms. *ChemPhysChem*, 11(12):2612–2616, 2010.
- [216] N. Fakhri, D. A. Tsyboulski, L. Cognet, R. B. Weisman, and M. Pasquali. Diameter-dependent bending dynamics of single-walled carbon nanotubes in liquids. *Proceedings of the National Academy of Sciences*, 106(34):14219–14223, 2009.
- [217] B. I. Yakobson. and L. S. Couchman. Persistence length and nanomechanics of random bundles of nanotubes. *The Journal of Nanoparticle Research*, 8(1):105–110, 2006.

- [218] P. Atkins. *Concepts On Physical Chemistry*. W. H. Freeman And Company, New York, 1995.



# **Appendix A**

## **Experimental details**

### **A.1 Force field parameters**

**Table A.1** – Parameters used in MD for pH dependency

Atom type	$\sigma$ , Å	$\epsilon$ , kJ/mol	$q$ , $\bar{e}$
Molecular benzoic acid			
C4a	3.55	0.29288	-0.12
H6a	2.42	0.12552	0.12
C2a	3.75	0.43932	0.64
O4a	3.00	0.71128	-0.53
O2a	3.96	0.87864	-0.44
H8a	0.50	0.12552	0.45
Molecular benzoic acid			
C4a	3.55	0.29288	-0.12
H6a	2.42	0.12552	0.12
C2a	3.75	0.43932	0.71
O2a	3.96	0.87864	-0.80
Water			
OW	3.16	0.64852	0.00
HW	0.00	0.000	0.52
PSEUDO(MW)	0.00	0.000	-1.04
Ions			
Na <sup>+</sup>	4.070	0.002093	1

**Table A.2** – MD parameters for simulations of CD-ACAs

Atom type	$\sigma$ , Å	$\epsilon$ , kJ/mol	$q$ , $\bar{e}$
Nicotinic acid			
N7	3.25	0.71128	-0.24450
H5	10 <sup>-5</sup>	0.0000	0.36810
C4	3.55	0.29288	0.13260
C4	3.55	0.29288	-0.15070
C4	3.55	0.29288	0.15960
C4	3.55	0.29288	-0.24080
Continued on next page			

Table A.2 – continued from previous page

Atom type	$\sigma$ , Å	$\epsilon$ , kcal/mol	$q$ , $e$
H6	2.42	0.12552	0.18270
H6	2.42	0.12552	0.15760
H6	2.42	0.12552	0.20510
C2	3.75	0.43932	0.71500
O2	2.96	0.87864	0.80000
Benzoic acid			
C4	3.55	0.29288	-0.11500
H6	2.42	0.12552	0.11500
C2	3.75	0.43932	0.71500
O2	2.96	0.87864	-0.80000
$\alpha$ -cyclodextrin			
C1	3.5	0.27614	0.30000
C1	3.5	0.27614	0.20500
C1	3.5	0.27614	0.17000
C1	3.5	0.27614	0.15400
O3	3.12	0.71128	-0.68300
O1	2.9	0.58576	-0.40000
H1	2.5	0.12552	0.10000
H1	2.5	0.12552	0.06000
H1	2.5	0.12552	0.03000
H1	2.5	0.12552	0.41800
Water			
OW	3.15365	0.64852	0.00
H5	$10^{-5}$	0.000	0.52422
PSEUDO(MT1)	0.00	0.000	-1.04844
Ions			
Na <sup>+</sup>	4.070	0.002092	1
Cl <sup>-</sup>	4.02	2.97064	-1
K <sup>+</sup>	5.17	0.002092	1

## A.2 Equipment characteristics

**Table A.3** – Technical characteristics of electron microscope JEOL JEM 1400

Resolution	
Lattice Image	0.20 nm
Point Image	0.38 nm
Accelerating Voltage	
Steps (5)	40 - 120 KeV
Variable Steps	30 V min, step
stability	$2 \times 10^{-6}$
Magnification	
Mag Mode	x200-x120000
Low Mag Mode	x50-x1000
SA Mag Mode	x2000-x300000
Specimen Chamber	
Specimen Tilt Angle (X-axis)	$\pm 25$ degrees ( $\pm 70$ degrees with optional holder)
Condenser lens	
lens system	2 stages (first and second condenser lenses)
aperture material	Mo foil
aperture size	100, 200 and 300 $\mu\text{m}$
Objective lens	
lens system	2 stage (objective lens, high performance objective mini-lens)
aperture material	Mo foil
aperture size	20, 40, 60 and 120 $\mu\text{m}$

## Appendix B

# Example of a spectrum correction

Absorbance spectroscopy is a powerful tool to determine concentrations of dissolved/dispersed species compounds. On top of this, absorbance spectroscopy is a relatively cheap, express technique, which can be applicable to many of compounds. This is why absorbance spectroscopy facilities are available in most of laboratories world-wide. And this is why we have chosen this technique as the major technique to study carbon nanotubes dispersion.

Measuring of the absorbance spectrum, as in the case of many others technique, requires some preparative research as well as post-measurement processing in order to reveal information about solution/dispersion composition. Preparation for measuring of the absorbance spectrum includes:

1. **Define the area of maximum absorbance of the target compound.** The maximum should be well defined and distinguishable from other absorbance maxima of the same compound and/or from absorbance maxima of other compounds in the mixture. Preferably, that absorbance maximum of the interest should be well distinguishable from the absorbance maximum of the solvent. The narrow incentive absorbance maximum of the target compound in the area where other compounds of the mixture are transparent is an ideal candidate for measuring the concentration of the target compound. Characteristic peaks of many known compounds are available in the literature. If the data are not available for the target compound, one should define the characteristic peak along with the extinction coefficient.
2. **Define the material of a cell to measure the absorbance.** Quality of the resulting spectrum depends dramatically on the transparency of the cell material. Ideally, the material of the cell should be nearly 100% transparent (nearly zero absorbance) in the

whole required wavelength interval, and it should be free from any significant and sharp absorbance peaks. Also the material should be chemically resistant to all components of the measured sample and be rigid enough to ensure constant width during the whole process of spectrum recording. In practice there are few materials, which meet the requirements, e.g. "Suprazil" quartz. As a rule, cells made of these materials are quite expensive. To solve this problem one can use less transparent materials, e.g. graded plastics, which ensure constant low absorbance with no sharp peaks.

3. **Recording references for base-line corrections.** Absorbance spectra only rarely show one sharp peak, situated on zero level. Usually, especially if the spectrum has been recorded in a graded plastic cell, the target peak is situated on a broad peak or a plateau. This wide peak or a plateau is usually called a base-line. The base-line often has several sources: the equipment background level, solvent and co-solvents absorbance and intrinsic background absorbance of the target compound. Approaches to eliminate different kinds of base-lines are different.

The equipment originated base-line is the difference between registered light emission and detected light intensity. This difference could originate in non-precise measurement of emitted and detected light amount, and in the light scattering on the working surfaces of the equipment e.g. due to non-ideal lenses. In the modern spectrophotometers this error is usually eliminated by the software control of the equipment (base-line correction).

Background or peaks, induced by a solvent or co-solvents, are essentially absorbance spectra of the solvent or co-solvents. As an example, let us consider a spectrum of pure NMP. According to visual inspection NMP is colourless and transparent. Let us assume, that we are interested to use it as a dispersant for CNTs to record absorbance spectrum of the CNTs in the wavelength region of 400-1100 nm, which corresponds to UV-vis-NIR region. However, UV-vis-NIR spectral region covers not only visible wavelength range. This is why it is not enough to ensure transparency and colourlessness of NMP in the visible region. To ensure its transparency in the 400-1100 wavelength region, we need to record a spectrum of pure NMP (see upper spectrum in the fig. B.1) .

As one can see from the fig. B.1, NMP shows high background absorbance as well as a few small peaks. This absorbance is a part of extremely broad absorbance peak, found for many aromatic compounds. If one needs to correct the target compound spectrum with respect to NMP induced base-line, one should use this spectrum of NMP as a correction. If it is required to show a spectrum of NMP, it is quite common to remove this base-line

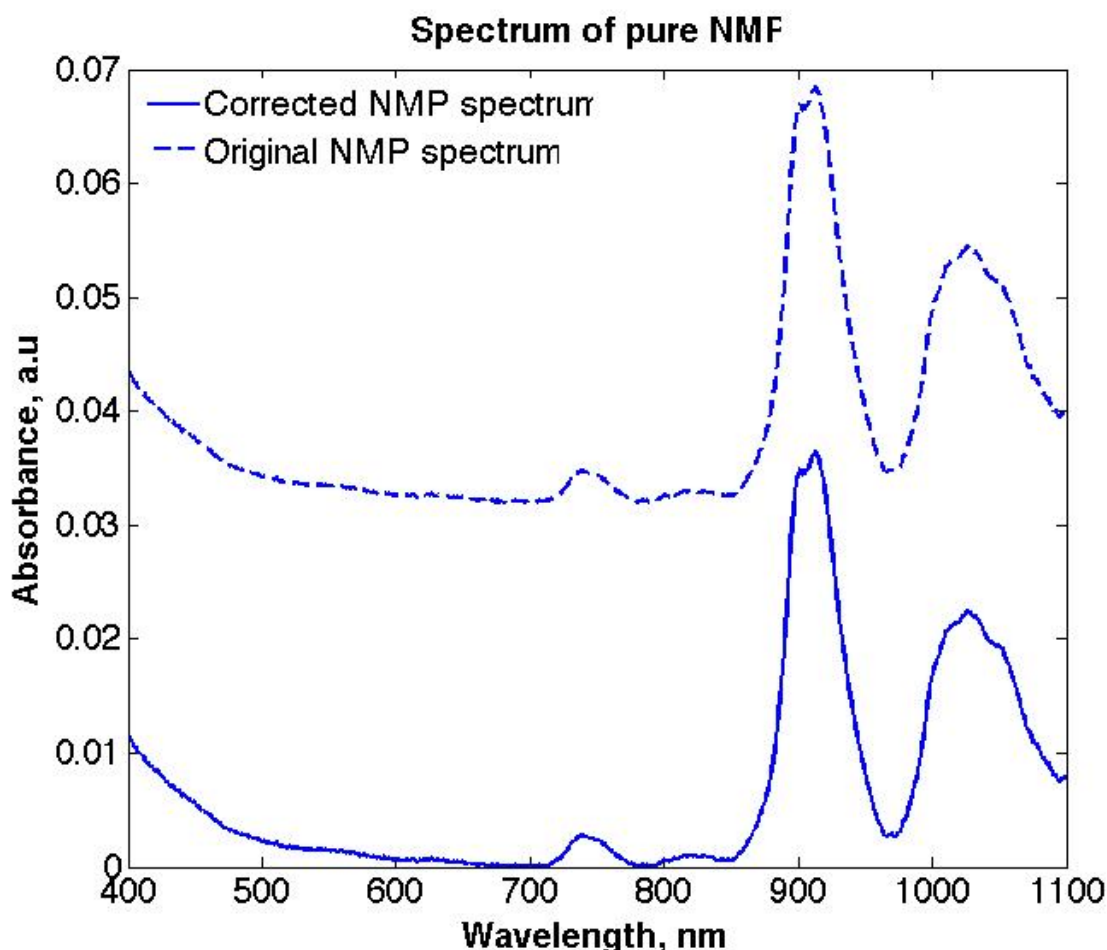


**Figure B.1** – Original (upper) and zero-corrected (bottom) spectrum of pure NMP. Original spectrum shows relatively high background absorbance due to broad peak, revealed by many aromatic compounds. If required, the whole spectrum can be moved down to zero-level (background removal)

linearly or by fitting a wing of broad Gaussian to it (see fig B.1, bottom spectrum). In this case the spectrum becomes easier to read.

Another type of a background absorbance is intrinsic absorbance of target compound, which could, for example, originate in  $\pi$ -shake up for aromatic carbon-based compounds. Usually, this type of background should not be excluded from spectra processing and can well be described with a Gaussian. This issue will be addressed later in the text.

These several above mentioned points summarize the preparation required for an absorbance spectra recording. The next step in the analysis is to record a spectrum of the sample. There are two principle schemes of spectrophotometers available in laboratories: with one or with two beams. Usually, one-beam spectrophotometers provide high speeds of recording spectra. On the other hand, two-beam spectrophotometers possess greater reliability, smaller errors and are capable of automatic spectra correction to the solvent induced base-line. Due to these reasons

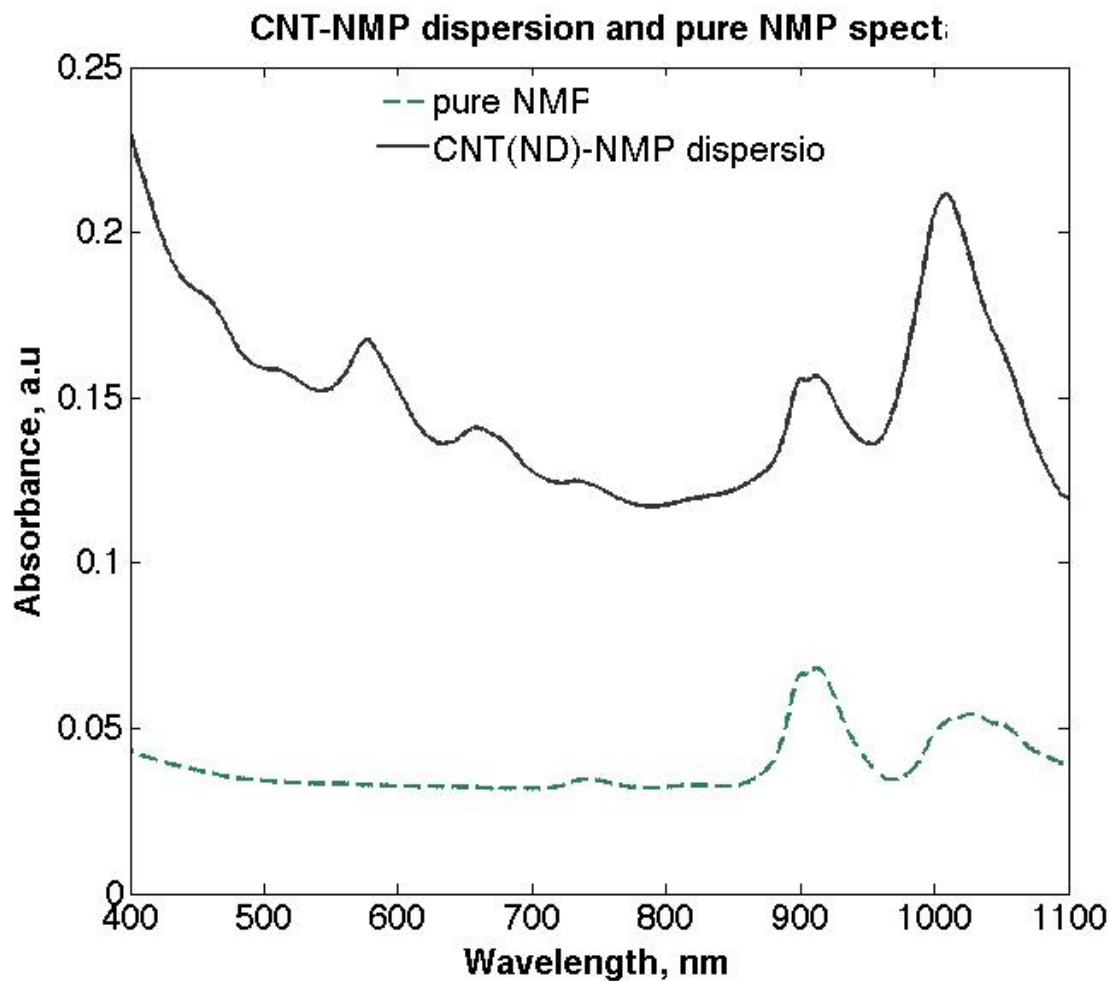


**Figure B.2** – Uncorrected spectrum of pure CNT-NMP dispersion in comparison with spectrum of pure NMP. It is clear, that NMP contributes significantly to absorption of CNT-NMP dispersion. NMP is not transparent in the region of interest.

two-beam spectrophotometers are somewhat more popular in laboratories.

Although modern two-beam spectrophotometers are capable of performing much of routine work automatically, it is important to know the initial and intermediate spectra just for the case of software failure. Let us have a closer look at the spectrum processing. A row spectrum of CNT-NMP dispersion is shown in the figure B.2 (upper spectrum). A spectrum of CNT-NMP dispersion is superimposed to the spectrum of pure NMP (solvent, bottom spectrum). As one can see, the solvent (NMP) has quite distinct spectral features in the area of 900-1100 nm. Additionally, this spectrum shows base-line related features: general non-zero absorbance, which increases somewhat in a shorter wavelength interval.

Due to the principle of spectral superposition, one can obtain a pure spectrum of carbon nanotubes by subtracting the spectrum of NMP from the spectrum of CNT-NMP dispersion (figure B.3). This is how we can obtain spectrum of *pure* CNTs in the CNT-NMP dispersion. This



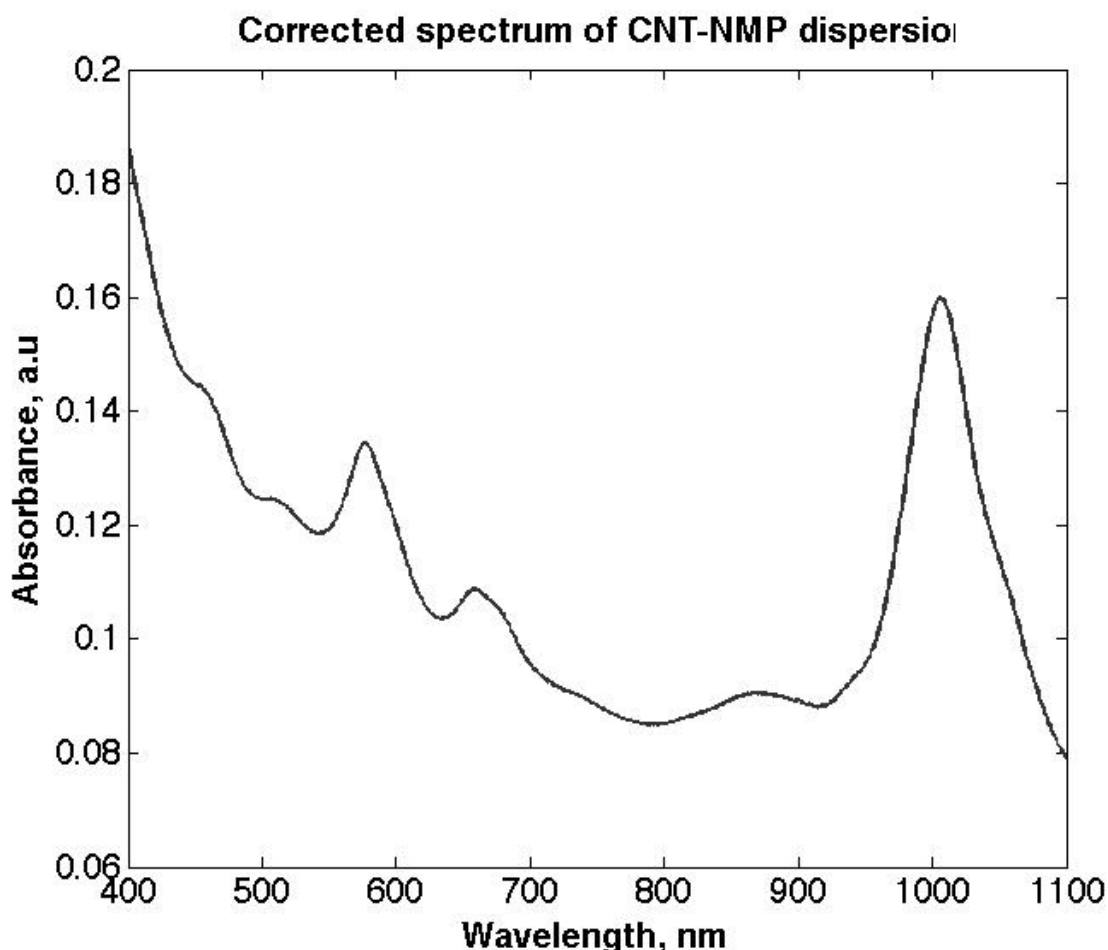


**Figure B.3** – Corrected spectrum of CNTs in CNT-NMP dispersion. This spectrum shows CNTs in the CNT-NMP dispersions as if there were no solvent in the mixture.

spectrum is shown in the figure B.3. The corrected spectrum of CNTs in CNT-NMP dispersion represents CNTs in assumption that there is no solvent (solvent input is removed). The same spectrum can be obtained with the two-beam spectrophotometer if the dispersion is inserted into the test beam and the solvent is inserted into the correction beam. On the other hand, the CNT spectrum was recorded in the presence of the solvent, therefore, the obtained corrected spectrum can not be considered as spectrum of pure CNTs. Although this point is quite confusing, it is extremely important to understand it.

A spectrum of pure substance can be obtained only if two conditions are fulfilled: the substance does not interact with anything and the substance is pure. In other words, a spectrum of pure compound can be obtained if the spectrum is recorded in vacuum, using very pure chemicals. For most of practical tasks this technique is not used, due to its cost and complexity. On the other hand, once we dissolve/disperse a solute in a solvent, weak intermolecular interactions between solute and solvent start to take place. Often these interactions are capable of changing

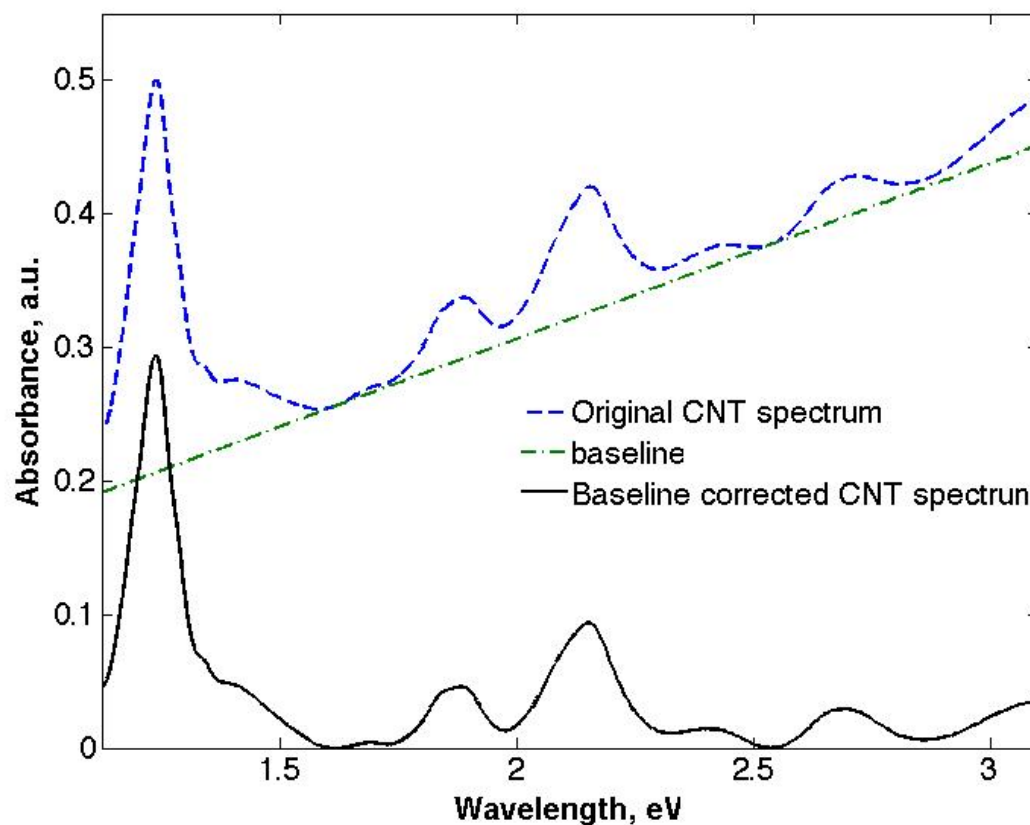


**Figure B.4** – Example of linear baseline subtraction (energy domain). The technique was employed in the chapter 5. See the chapter text for details.

the spectrum of the solute significantly: shift positions of absorbance maxima, change relative intensities of different maxima as well as their shape. When we subtract spectrum of solvent from the spectrum of solution/dispersion, we obtain a spectrum of the solute/dispersed compound, altered by solvation. This property allows one to investigate interactions of solute with solvent.

The chapter 5 employs a technique of subtracting linear baseline from CNT spectra in energy domain. An example of this subtraction is shown in the figure B.4.

## Appendix C

# List of Peer-Reviewed Journal Papers

1. A. O. Romanova, E. Chibunova, R. S. Kumeev, M. V. Fedorov, I. V. Terekhova,  $\alpha$ -Cyclodextrin/aminobenzoic acid binding in salt solutions at different pH: Dependence on guest structure. *Int. J. Biol. Macromol.*, vol. 57, pp. 255-258.
2. N. Ottosson, A. O. Romanova, J. Söderström, O. Björneholm, G. Öhrwall, and M. V. Fedorov, "Molecular Sinkers: X-ray Photoemission and Atomistic Simulations of Benzoic Acid and Benzoate at the Aqueous Solution/Vapor Interface", *J. Phys. Chem. B*, vol. 116, no. 43, pp. 13017-13023, Nov. 2012.
3. A. I. Frolov, R. N. Arif, M. Kolar, A. O. Romanova, M. V. Fedorov, and A. G. Rozhin, "Molecular mechanisms of salt effects on carbon nanotube dispersions in an organic solvent (N-methyl-2-pyrrolidone)", *Chemical Science*, vol. 3, no. 2, p. 541, 2012.
4. M. V. Fedorov, R. N. Arif, A. I. Frolov, M. Kolar, A. O. Romanova, and A. G. Rozhin, "Salting out in organic solvents: a new route to carbon nanotube bundle engineering", *Phys. Chem. Chem. Phys.*, vol. 13, no. 27, pp. 12399-12402, Jun. 2011.
5. I.V. Terekhova, A.O. Romanova, R.S. Kumeev, M.V. Fedorov (2010). "Selective  $\text{Na}^+/\text{K}^+$  effects on the formation of  $\alpha$ -Cyclodextrin Complexes with aromatic carboxylic acids: competition for the guest", *J. Phys. Chem. B* 114(39) 12607 -12613

# Appendix D

## Contributions to the work

The significant part of this work is based on publications, which would not be possible without contributions from the collaborators. This chapter helps to the reader understand, which contribution to this work is made by the author, and which one belongs to the collaborators.

The chapter 4 combines the papers *N. Ottosson, A. O. Romanova, J. Söderström, O. Björnehölm, G. Öhrwall, and M. V. Fedorov, "Molecular Sinkers: X-ray Photoemission and Atomistic Simulations of Benzoic Acid and Benzoate at the Aqueous Solution/Vapor Interface", J. Phys. Chem. B, vol. 116, no. 43, pp. 13017-13023, Nov. 2012., I.V. Terekhova, A.O. Romanova, R.S. Kumeev, M.V. Fedorov (2010)."Selective Na<sup>+</sup>/K<sup>+</sup> effects on the formation of  $\alpha$ -Cyclodextrin Complexes with aromatic carboxylic acids: competition for the guest", J. Phys. Chem. B 114(39) 12607 -12613 and A. O. Romanova, E. Chibunova, R. S. Kumeev, M. V. Fedorov, I. V. Terekhova,  $\alpha$ -Cyclodextrin/aminobenzoic acid binding in salt solutions at different pH: Dependence on guest structure. Intl. J. Biol. Macromol., vol. 57, pp. 255-258.* The experimental part of these works was done by E. Chibunova, R. S. Kumeev and I. V. Terekhova (Institute of Solution Chemistry of the Russian Academy of Sciences). The simulations, included into the papers as well as their analyses (calculations of PMF,  $g(r)$ , density profiles, angle distributions, other connected routines), were performed by A. Romanova. A. Romanova participated in preparation of the papers by compiling and writing all simulations-connected materials of the papers as well as reviewing the drafts and preparing them for publications.

The chapter 5 is based on the papers *M. V. Fedorov, R. N. Arif, A. I. Frolov, M. Kolar, A. O. Romanova, and A. G. Rozhin, "Salting out in organic solvents: a new route to carbon nanotube bundle engineering", Phys. Chem. Chem. Phys., vol. 13, no. 27, pp. 12399-12402, Jun. 2011. and A. I. Frolov, R. N. Arif, M. Kolar, A. O. Romanova, M. V. Fedorov, and A. G. Rozhin, "Molecular mechanisms of salt effects on carbon nanotube dispersions in an organic*

*solvent (N-methyl-2-pyrrolidone)*”, *Chemical Science*, vol. 3, no. 2, p. 541, 2012. A. Romanova participated in designing and performing of experimental parts of papers. Processing of the original spectral data was performed by A. Romanova. A. Romanova participated in preparation of the papers by compilation and writing all experiment-connected materials of the papers as well as reviewing the drafts and preparing them for publication. All unpublished materials from the chapter 5 (transmission electron microscopy, spectrophotometric titration with sodium bromide) were obtained and analysed by A. Romanova.

# Glossary

**1-4 interactions** interactions between atoms in the same molecule if the more than three covalent bonds separate the atoms.

**allotrope** different structural modifications of an element.

**bonded interactions** interactions between atoms in the same molecule if the atoms are separated by three or less covalent bonds.

**calorimetry** the measurement of the heat changes which occur during a process.

**chaotrope** ions which weakly bind water in their hydration shells. Water in hydration shells of chaotropes has more entropy compare to bulk.

**chemical shift** nuclei of a particular element that are in different chemical environments within the same molecule generally experience slightly different applied magnetic field strength due to the shielding and deshielding effects of nearby electrons. As a result, their resonance frequencies differ, and each is defined by a characteristic chemical shift value.

**chirality** the geometric property of a rigid object (or spatial arrangement of points or atoms) of being non-superposable on its mirror image; such an object has no symmetry elements of the second kind (a mirror plane, a centre of inversion, a rotation-reflection axis). If the object is superposable on its mirror image the object is described as being achiral.

**classical molecular dynamics simulations** a technique for computing the equilibrium and transport properties of a mechanic N-particle system, where dynamics of particles obey the laws of classical mechanics. Adapted from [90].

**colloidal dispersion** a system in which particles of colloidal size of any nature (e.g. solid, liquid or gas) are dispersed in a continuous phase of a different composition (or state).

**complex** a molecular entity formed by loose association involving two or more component molecular entities (ionic or uncharged), or the corresponding chemical species. The bonding between the components is normally weaker than in a covalent bond.

**dissolution** the mixing of two phases with the formation of one new homogeneous phase (i.e. the solution).

**ensemble** a collection of imaginary replications of the actual system (statistical thermodynamics) [218].

**Ewald summation method** a method for computing the interaction energies of periodic systems (e.g. crystals), particularly electrostatic energies.

**flying ice cube effect** a numerical integration artifact in which the energy of high-frequency fundamental modes is drained into low-frequency modes, particularly into zero-frequency motions such as overall translation and rotation of the system.

**force field** a consistent set of atomic parameters used in a computer experiment, such as molecular dynamics.

**Gibbs surface** a geometrical surface chosen parallel to the interface and used to define the volumes of the bulk phases in the calculation of the extent of adsorption, and of other surface excess properties.

**hydration** the term "hydration" replaces the term "solvation" if the solvent is water.

**ion** charged molecular species. Structurally ions are separated into simple ions (mono-atomic species) and multi-atomic ions.

**kosmotrope** ions which strongly bind water in their hydration shells. Water in hydration shells of kosmotropes has less entropy compare to bulk.

**Lagrangian** a function that summarizes the dynamics of the system.

**molecular site** approximate representation of atoms (groups of atoms) as a single unit.

**NMR** see "nuclear magnetic resonance".

**non-bonded interactions** interactions between atoms which do not belong to the same molecule.

**nuclear magnetic resonance** a spectroscopic technique which make use of electromagnetic radiation with frequencies  $\sim 10^8$  Hz (radio frequencies region of electromagnetic spectrum).

**osmotic active compound** cosolutes or cosolvents which are capable to change osmotic pressure of a solution, e.g. salts, water admixtures in organic solvents.

**potential of mean force** a potential acting on a molecule  $j$  at distance  $r$  from the molecule  $i$  and including an average forces acting on these two molecules from all other molecules in the system.

**real solution** real solution is homogeneous (single phase) thermodynamically stable mixture of two or more substances. Solutes in real solution have dimensions less than 1 nm in any direction.

**salting-out effect** reduction of solubility of non-electrolyte upon addition of an electrolyte to the solution (dispersion).

**short-range forces** forces, which decay within a few atomic distances.

**solute** the minor component of a solution which is regarded as having been dissolved by the solvent. Generally, any dissolved compound is a solute. In this work we use this term in less rigorous and more narrow meaning: solute is a *major dissolved compound*, which can not be considered as "background compound" for keeping ionic strength or pH of a solution.

**solution** liquid or solid phase containing more than one substance, when for convenience one (or more) substance, which is called the solvent, is treated differently from the other substances, which are called solutes. When, as is often but not necessarily the case, the sum of the mole fractions of solutes is small compared with unity, the solution is called a dilute solution. A superscript attached to the  $\infty$  symbol for a property of a solution denotes the property in the limit of infinite dilution. Solution is a system in a dynamic equilibrium.

**solvation** is any stabilizing interaction of a solute (or solute moiety) and the solvent or a similar interaction of solvent with groups of an insoluble material. Such interactions generally involve electrostatic forces and van der Waals forces, as well as chemically more specific effects such as hydrogen bond formation.



**solvation interface** solvation interface is a molecular level interface between a solute molecule and solvent.

**solvation shell** solvent molecules in direct vicinity of a solute. These molecules are different from solvent molecule in the bulk: i) their relative orientation to each-other is different compare to solvent molecules around other solvent molecules; ii) residence time of solvent molecules near a solute is different compare to residence time of solvent molecules around other solvent molecules (In the bulk).

**solvent** the major component of a solution which solvates solute. Conventionally, solvent does not change its state upon formation of a solution.

3D 3 dimensional

*m*ABA *meta*-aminobenzoic acid

*o*ABA *ortho*-aminobenzoic acid

*p*ABA *para*-aminobenzoic acid

ABA aminobenzoic acid

ACA aromatic carboxylic acid

BA<sup>-</sup> benzoate anion

BAH benzoic acid

BAK potassium benzoate

BANa sodium benzoate

BE binding energies

CD cyclodextrin

CNT carbon nanotube

DC dissolved compound

EM electron microscopy

HFE hydration free energy

HP-β-CD hydroxypropyl-β-cyclodextrin

LJ potential Lennard-Jones potential

MD molecular dynamics

NIR near infra red

NMP N-Methyl-2-pyrrolidone

NMR nuclear magnetic resonance

OPLS-AA all-atom optimized molecular potential for liquid simulation

PBC periodic boundary condition

PE photoemission

PL photoluminescence

PMF potential of mean force

STEM scanning mode of transmission electron microscope

SWCNT single walled carbon nanotube

TEM transmission electron microscopy (or microscope)

TIP4P four-point transferable intermolecular potential

UV ultra violet

Vis. visible

XPS X-ray photoelectron spectroscopy